Pyrolysis and gasification of coal residues derived from tetralin liquefaction of South African density separated coal

RC Uwaoma

orcid.org/ 0000-0002-3306-9878

Thesis accepted in fulfilment of the requirements for the degree *Doctor of Philosophy in Science with Chemistry* at the North-West University

Promoter:	Prof CA Strydom
Co-promoter:	Dr RH Matjie
Assistant Promoter:	Prof JR Bunt

Graduation July 2020

25452622

DEDICATION

This Thesis is gratefully dedicated to the loving memory of my late father who died on 8th June, 2020

Mr Romanus Uwaoma (Snr).

May his gentle soul rest in perfect peace!

"Aim for success, not perfection. Never give up your right to be wrong, because then you will lose the ability to learn new things and move forward with your life. Remember that fear always lurks behind perfectionism."

David M. Burns

DECLARATION

I, R.C Uwaoma, hereby declare that this thesis entitled: "**Pyrolysis and gasification of coal residues derived from tetralin liquefaction of South African density separated coal**", submitted in fulfilment of the requirements for the degree Doctor of Philosophy in Chemistry at the North-West University is my own work and has not been submitted to any other university in whole or in part. Written consent from authors had been obtained for publications where co-authors have been involved.

Signed at Potchefstroom on the……..11th……..of …….July……...2020

R.C Uwaoma

PREFACE

Thesis format:

The format of this thesis is in accordance with the academic rules of the North-West University, where rule **A.5.4.2.7** states: “Where a candidate is permitted to submit a thesis in the form of a published research article or articles, or as an unpublished manuscript or manuscripts in article format and more than one such article or manuscript is used, the thesis must still be presented as a unit, supplemented with an inclusive problem statement, a focused literature analysis, and integration and with a synoptic conclusion, and the guidelines of the journal concerned must also be included.”

Rule **A.5.4.2.8** states: “Where any research article or manuscript and/or internationally examined patent is used for the purpose of a thesis in article format to which other authors and/or inventors than the candidate contributed, the candidate must obtain a written statement from each co-author and/or co-inventor in which it is stated that such co-author and/or co-inventor grants permission that the research article or manuscript and/or patent may be used for the stated purpose and in which it is further indicated what each co-author's and/or co-inventor's share in the relevant research article or manuscript and/or patent was.”

Rule **A.5.4.2.9** states: “Where co-authors or co-inventors as referred to in **A.5.4.2.8** above were involved, the candidate must mention that fact in the preface and must include the statement of each co-author or co-inventor in the thesis immediately following the preface.”

Format of numbering and referencing: The formatting, referencing style, numbering of tables and figures, and general outline of the manuscripts or chapters were changed to ensure uniformity throughout the thesis. The format of manuscripts which have been submitted and/or published adheres to the author guidelines as stipulated by the editor of each journal. The headings and original technical content of the manuscripts were not changed from the submitted and/or published scripts, and minor spelling and typographical errors were corrected therein.

STATEMENT FROM CO-AUTHORS

Letter of consent

To whom it may concern, the listed co-authors hereby give consent that **RC Uwaoma** may submit the following papers and manuscript as part of his thesis, entitled: **Pyrolysis and gasification of coal residues derived from tetralin liquefaction of South African density separated coal**, for the degree Philosophiae Doctor in Chemistry, at the North-West University:

Uwaoma RC, Strydom CA, Matjie RH. Gasification of chars from tetralin liquefaction of <1.5 g/cm^3 carbon-rich residues derived from waste coal fines in South Africa. Journal of Thermal Analysis and Calorimetry, **submitted for publication**, 2020 (Manuscript number: JTAC-D-20-00049)

Uwaoma RC, Strydom CA, Matjie RH, Bunt JR. Influence of density separation of selected South African coal fines on the products obtained during liquefaction using tetralin as a solvent. Energy & Fuels. **2019**, 33(3):1837-49.

Uwaoma RC, Strydom CA, Matjie RH, Bunt JR, Okolo GN, Brand DJ. Pyrolysis of tetralin liquefaction derived residues from lighter density fractions of waste coals taken from waste coal disposal sites in South Africa. Energy & Fuels. **2019**, 33(9):9074-86.

(This letter of consent complies with rules **A5.4.2.8 and A.5.4.2.9** of the academic rules, as specified by the North-West University)

Signed at Potchefstroom

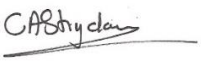

Christien A. Strydom — 04th March 2020 Date

John R. Bunt — 04th March 2020 Date

Henry R. Matjie — 04th March 2020 Date

Gregory Okolo — 04th March 2020 Date

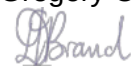

DJ Brand — 04th March 2020 Date

LIST OF PUBLICATIONS

Journal articles

Uwaoma RC, Strydom CA, Matjie RH, Bunt JR. Influence of density separation of selected South African coal fines on the products obtained during liquefaction using tetralin as a solvent. Energy & Fuels. **2019**, 33(3):1837-49.

Uwaoma RC, Strydom CA, Matjie RH, Bunt JR, Okolo GN, Brand DJ. Pyrolysis of tetralin liquefaction derived residues from lighter density fractions of waste coals taken from waste coal disposal sites in South Africa. Energy & Fuels. **2019**, 33(9):9074-86.

Uwaoma RC, Strydom CA, Bunt JR, Okolo GN, Matjie RH. The catalytic effect of Benfield waste salt on CO_2 gasification of a typical South African Highveld coal. Journal of Thermal Analysis and Calorimetry. **2019**, 135(5):2723-32.

Uwaoma RC, Strydom CA, Matjie RH, Bunt JR, Van Dyk JC. The influence of the roof and floor geological structures on the ash composition produced from coal at UCG temperatures. International Journal of Coal Preparation and Utilization. 2018 Jun 22:1-9.

Tsemane MM, Matjie RH, Bunt JR, Neomagus HW, Strydom CA, Waanders FB, Van Alphen C, **Uwaoma RC**. Mineralogy and Petrology of Chars Produced by South African Caking Coals and Density-Separated Fractions during Pyrolysis and Their Effects on Caking Propensity. Energy & Fuels. **2019**, 33(8):7645-58.

Matjie RH, Lesufi JM, Bunt JR, Strydom CA, Schobert HH, **Uwaoma RC**. In situ capturing and absorption of sulfur gases formed during thermal treatment of South African coals. ACS Omega. **2018**, 3(10):14201-12.

Conference Presentation

R.C Uwaoma, C.A. Strydom, R.H. Matjie, J.R. Bunt. Direct Liquefaction of 2 South African bituminous coals and their beneficiated float fractions presented at 10th Int'l Conference on Advances in Science, Engineering, Technology & Waste Management (ASETWM-18) Cape Town, South Africa (oral presentation).

JC van Dyk, **R.C. Uwaoma**, C.A. Strydom, R.H. Matjie, J.R. Bunt. The Effect of the Roof and Floor Geological Structures on the Mineralogical Composition of Ash Produced from Coal at UCG Operating Temperatures presented at 34th Annual energy, environmental and sustainable conference International Pittsburgh coal conference USA (oral presentation).

R.C Uwaoma, Strydom CA, Bunt JR, Okolo GN, Matjie RH. The catalytic effect of Benfield Waste salt on CO_2 gasification of a typical South African Highveld coal presented at 8th International Symposium on Calorimetry and Thermal Analysis (CATS-2017), Fukuoka, Japan (oral presentation).

R.C Uwaoma, C.A. Strydom, R.H. Matjie, J.R. Bunt. Gasification of the Residues Derived from Tetralin Liquefaction of Beneficiated Products Produced from South African Discard Fine Coal presented at 17th International Conference on Science, Engineering, Technology and Waste Management (SETWM-19) Johannesburg, South Africa (oral presentation).

R.C Uwaoma, C.A. Strydom, R.H. Matjie, J.R. Bunt. Pyrolysis of residues from tetralin solvent extraction of the float fractions from density separated South African coal fines presented at 17th International Conference on Coal Science & Technology (ICCS&T2019) Poland (oral presentation).

ACKNOWLEDGEMENTS

The author, at this moment, wishes to acknowledge and thank all individuals and institutions for their contribution, assistance, help and guidance during this study; a special appreciation and words of gratitude go to the following:

- ✓ First and foremost I would like to dedicate this work to my heavenly father for His spiritual guidance, encouragement in a time of weakness, good health in mind, soul and body, blessing, unconditional love and mercy upon my life that aided me to preserve to the end of this investigation.
- ✓ To my supervisors, Prof C.A. Strydom, Dr R.H. Matjie and Prof J.R. Bunt for their benevolence, excellent foresight, expert guidance, criticisms, fruitful deliberations during meetings, invaluable suggestions and brilliant contributions without which this study would not have been a success. I am eternally grateful to you all.
- ✓ The NRF and SARChI coal research chair (Grant no. UID 85632) for their financial support with regards to this investigation.
- ✓ Dr Gregory Okolo for his help with the surface area analysis and his advice, suggestions and discussions on the gasification experiments.
- ✓ Dr D.J. Brand for his help with the solid and liquid state NMR analysis on the oil, tar and char.
- ✓ Mrs Belinda Venter for her assistance with XRD and XRF analyses.
- ✓ Dr Roelf Venter for his help with the training on the liquefaction setup and guidance during the liquefaction test.
- ✓ Dr Kgutso Mokoena for his help with the GC-MS analysis on the oil and tar samples.
- ✓ Bureau Veritas Testing and Inspections and SGS inspection, verification, testing, and laboratories for assisting with the analytical methods.
- ✓ Mr Jan Kroeze, Mr Adrian Brok and Mr Elias Mofokeng for their assistance with the pyrolysis and liquefaction setup and other issues relating to the equipment used during this investigation.
- ✓ South African power stations (Highveld and Waterberg) for the supply of the discards coal fines that was used for this investigation.
- ✓ Colleagues and friends from the coal chemistry, Chemical and Resource Beneficiation, and Centre of Excellence in Carbon-based fuels for their support, friendliness and contributions.
- ✓ To my amiable friends whom I hold dearly to heart: Prof Damina Onwudiwe, Dr Obinna Ezeokoli, Dr Nneka Umeroah, Dr Boitumelo Mogwase, Emmanuel, Chris, Charity Sphiri, Nnandi and wife, Ifeanyi and his wife and others who in one way or the other contributed

to the successful completion of this study: thanks for supporting me through the good and bad times.

- ✓ My mum and dad, uncle daddy Engr. Mike Uwaoma and his wife, my siblings (Vincent, Marykate, Edith and Michael) and Uncle Charles and family. I thank you all for the financial and moral support, prayers, love, patience, encouragements during the down moments; you are the cornerstone on which my life house is built; without you people, nothing would have been possible.

ABSTRACT

The South African coal mining industry produced approximately 307 million tons of low-rank bituminous coal in 2007. The local thermo-chemical processes utilise this coal for oils, petrochemicals and steam generation. South African coal mines and power stations in Secunda Synfuels Operations produce more than 10 million tons of coal fine discards (an unavoidable by-product) per year. This study focuses on the beneficiation of these discards, using the float-sink density separation method and investigates the possible utilisation of the float fractions in thermochemical processes. This investigation was divided into three phases; namely, the density separation and liquefaction phase, pyrolysis of the residues derived from the liquefaction and gasification of the char residues.

The first stage of this investigation aimed at beneficiation of two South African coal fine discards using float-sink density separation techniques, followed by liquefaction and analyses of the different products generated from the liquefaction of the float fraction and the discarded coal fines' samples. The direct liquefaction of South African coal fine discards and their density separated (float) fractions were carried out under moderate conditions in a laboratory autoclave. The liquefaction temperature ranged between 380 and 420 $^{\circ}$C, using tetralin as a solvent and an initial nitrogen gas pressure of 3 MPa. Results from the liquefaction tests show that the carbon conversion and oil yields are higher for the float fractions when compared to the coal fine discards. Waterberg and Highveld coal float fractions achieved a high carbon conversion of 50.7 wt.% daf and 52.7 wt.% daf respectively, compared with < 42 wt.% daf carbon conversion for the coal fines wastes. The efficiency of the liquefaction carbon conversion was correlated with the reactive macerals and the surface areas of the individual samples. It was observed that the density separated coal fractions, which have higher surface areas, higher vitrinite contents and higher reactive macerals contents achieved higher extraction efficiencies. The residues and extracts generated during the liquefaction were characterised using nuclear magnetic resonance spectroscopy, proximate and ultimate analyses. The analytical results indicated that the residues showed slight decreases in calorific values and aliphatic components, with lower H/C ratios and higher ash yields. Also, the results showed that using the float fractions of South African coal fine discards at moderate liquefaction temperatures could be beneficial in the production of liquid fuel.

The second phase, which was one of the primary aims of this investigation, involved the use of the liquefaction residues (waste) generated from the first stage for pyrolysis experiments. In this phase, float fractions produced from two South African discard coal fines samples and their liquefaction residues generated from phase one were used as feedstock for pyrolysis experiments. Analysis of the pyrolytic products from the liquefaction residues and float fractions

was reported. Pyrolysis was carried out in a modified Fischer Assay setup at 750˚C and 920˚C under an argon atmosphere. Tar samples were analysed using gas chromatography-mass spectrometry (GC-MS), nuclear magnetic resonance (NMR) spectroscopy, and Fourier-transform infrared (FTIR) spectroscopy. The chars produced were analysed using proximate and ultimate analyses, solid-state ^{13}C NMR and CO_2 low-pressure gas adsorption (CO_2-LPGA). Results obtained from the pyrolysis experiments showed that the liquefaction residues produced higher char and gas yields when compared to the coal fine discards float fractions. The pyrolysis char yields of the solvent extraction residues ranged from 74–76% and that of float fractions from coal fine discards ranged between 67.0% and 71.5%. Gas pyrolysis yields ranged from 16.0–20.0% (daf) for the residues and 14.5–18.4% for pyrolysis gas yields produced from the coal fines fractions, whilst the pyrolytic water and the tar yields of the coal float fractions were slightly higher compared to that of the liquefaction extraction residues. Proton NMR analysis of the tars produced from the liquefaction residues showed a higher amount of aromatic protons, ranging from 60.5–62.0 ppm, in comparison to < 56.0 ppm for the float fractions of the coal fine discards. The amounts of aliphatic protons of the tars obtained from the float fractions from the coal fine discards were higher when compared to those of the solvent extraction residues. The chars produced after pyrolysis of the liquefaction residues showed a higher porosity when compared to those of chars produced during the pyrolysis of the float fractions from the coal fine discards. The porosity values of the chars produced from the liquefaction residues ranged from 15.5–16.3%, in comparison to < 14% after pyrolysis of the float fractions. The differences in the porosity values were attributed to the opening of pores and extraction of some of the molecular structures from the coal matrix during liquefaction. Further analysis of the pyrolysis products showed that the residues generated after liquefaction of the float fractions from South African bituminous coal fines samples may be utilised for pyrolysis and may offer a means of using some of the liquefaction waste material.

The final stage of this investigation was the use of the liquefaction residue chars generated from the pyrolysis of the liquefaction residues for gasification. The char residues generated from tetralin liquefaction of density separated coal float fractions of the coal fines waste products and the coal float fractions, were subjected to CO_2 gasification tests. CO_2 gasification was investigated using a thermogravimetric analyser by heating the samples at isothermal temperatures between 880 and 940˚C. Results from the gasification studies showed that the liquefaction residues' char reactivities values (R_i, R_s, R_{tf}, $R_{t/0.5}$, $R_{t/0.9}$) were higher when compared to the reactivity values from the float fraction chars. The higher reactivities of the liquefaction residues were attributed to opening up of pores in the structure of the residues' chars, after tetralin liquefaction. It was observed that the initial reactivities of the liquefaction residues were doubled compared to that obtained from the coal float fraction chars. The increases in the number of pores, caused by liquefaction, accelerated the reaction process and aided in the reduction of the activation energies

needed for the residues' char gasification reactions. The activation energies of the float fraction chars were found to be 190.5 kJ·mol^{-1} and 236.7 kJ·mol^{-1} for the two float fractions samples produced from South African coal fine discards. The activation energies for the liquefaction residues from the same two float fraction samples from the coal fine discards were 145.3 kJ·mol^{-1} and 196.0 kJ·mol^{-1}. These results showed that tetralin liquefaction affected the coal matrix and aided in enhancing the gasification reactivities of the residues. Gasification of residues (waste material) generated after liquefaction of float fractions produced from density separation of South African coal fines (also waste products) has the potential to be utilised in the gasification process.

Keywords: discarded coal fines, density separation, float fraction, residues, liquefaction, pyrolysis, gasification

TABLE OF CONTENTS

DEDICATION ..... **I**

DECLARATION ..... **II**

PREFACE ..... **III**

STATEMENT FROM CO-AUTHORS ..... **IV**

LIST OF PUBLICATIONS ..... **V**

ACKNOWLEDGEMENTS ..... **VII**

ABSTRACT ..... **IX**

NOMENCLATURE ..... **XXIV**

ACRONYMS/ABBREVIATIONS ..... **XXV**

CHAPTER 1 INTRODUCTION **1**

1.1 Background **2**

1.2 Problem statement **5**

1.3 Research objectives **8**

1.4 Study hypothesis **9**

1.5 Significance of the research **9**

1.6 Outline of the study **10**

1.7 Scope of the thesis **13**

1.8 Chapter 1 references **15**

CHAPTER 2 LITERATURE REVIEW **18**

2.1 Coal composition **19**

2.1.1 Organic components of coal 19

2.1.2 Coal mineral matter 20

2.2 Coal classification 22

2.3 Thermochemical utilisation of coal 22

2.3.1 Coal pyrolysis 22

2.3.2 Coal gasification 24

2.3.3 Coal combustion 25

2.3.4 Coal liquefaction 25

2.3.4.1 History of liquefaction 26

2.3.4.2 Types of liquefaction 27

2.3.4.3 Factors affecting direct coal liquefaction 30

2.3.5 Products from direct coal liquefaction 38

2.4 The utilisation of liquefaction derived residues in thermochemical conversion processes 43

2.4.1 Summary of previous studies on the use of liquefaction residues for pyrolysis 43

2.4.2 Summary of previous studies on the use of liquefaction residues for gasification. 45

2.5 Chapter 2 references 48

CHAPTER 3: INFLUENCE OF DENSITY SEPERATION OF SELECTED SOUTH AFRICAN COAL FINES ON THE PRODUCTS OBTAINED DURING LIQUEFACTION USING TETRALIN AS A SOLVENT. 65

3.1 Introduction 67

3.2 Experimental procedures 69

3.2.1 Materials 69

3.2.2 Density separation 69

3.2.3 Liquefaction experiments 69

3.2.4 Analysis of coal fines, float fractions and extracted products after the liquefaction 71

3.2.4.1 Coal fines discard, float fractions and extracted products compositions 71

3.2.4.2 CO_2 low-pressure gas adsorption analysis 71

3.2.4.3 Petrographic analyses 72

3.2.4.4 X-ray diffraction (XRD) and X-ray fluorescence (XRF) analyses 72

3.2.4.5 Inductively coupled plasma-optical emission spectrometry (ICP-OES) analysis 72

3.2.4.6 Gas chromatography-mass spectrometry (GC-MS) analyses 73

3.2.4.7 Nuclear magnetic resonance (NMR) of HS products 73

3.2.4.8 Solid-state ^{13}C NMR analyses 73

3.3 Results and discussion 74

3.3.1 Coal composition 74

3.3.2 CO_2 low-pressure gas adsorption analysis 77

3.3.3 Petrographic analyses 77

3.3.4 XRF analysis results 78

3.3.5 XRD analysis results 79

3.4 Effect of coal maceral composition on liquefaction 80

3.5 Effect of temperature on the product distribution 83

3.5.1 Effect of temperature on carbon conversion 83

3.5.2 Effect of temperature on products yields during the liquefaction tests 83

3.6 Analysis of liquefaction products 84

3.6.1 Proximate, ultimate and ICP-OES analyses of residues, PAA and oils extracts 84

3.6.2 GC-MS analyses of the oily (HS) part of the liquefaction product 88

3.6.3 ^{1}H nuclear magnetic resonance analysis results of oily (HS) liquefaction products 90

3.6.4 Solid-state ^{13}C nuclear magnetic resonance results 92

3.7 Conclusions 95

3.8 Chapter 3 references 98

CHAPTER 4: PYROLYSIS OF TETRALIN LIQUEFACTION DERIVED RESIDUES FROM LIGHTER DENSITY FRACTIONS PRODUCED OF WASTE COALS TAKEN FROM WASTE COAL DISPOSAL SITES IN SOUTH AFRICA. 102

4.1 Introduction 104

4.2 Experimental procedures and analytical methods 105

4.2.1 Material 105

4.2.2 Pyrolysis 105

4.2.2.1 Thermogravimetric analyses 105

4.2.2.2 Fisher Assay analyses 105

4.3 Analysis of pyrolysis products 106

4.3.1 Tar analysis 106

4.3.2 Char composition 107

4.4 Results and discussion 108

4.4.1 TGA of coal float fractions and their liquefaction residues 108

4.4.2 Distribution of pyrolytic products 110

4.4.3 Tar analysis results 114

4.4.3.1 GC-MS analysis of tar samples 114

4.4.3.2 NMR results of tar 116

4.4.3.3 FTIR results of tar produced during pyrolysis at 750°C from coal lighter density fractions and their liquefaction residues. 120

4.4.4 Chars composition 123

4.4.4.1 Proximate and elemental analyses 123

4.4.4.2 ^{13}C NMR analysis of the char produced during pyrolysis. 126

4.4.4.3 Surface area analysis of samples 128

4.5 Conclusions 131

4.6 Chapter 4 references 133

CHAPTER 5: GASIFICATION OF CHARS FROM TETRALIN LIQUEFACTION OF <1.5 G/CM^3 CARBON-RICH RESIDUES DERIVED FROM WASTE COAL FINES IN SOUTH AFRICA. 138

5.1 Introduction 140

5.2 Experimental procedures and analytical methods 141

5.2.1 Materials and sample preparation for experiments and analyses 141

5.2.2 Demineralisation of liquefaction residue chars 141

5.2.3 Composition of the chars of the <1.5 g/cm^3 coal and its liquefaction residue samples 142

5.2.4 Char CO_2 gasification reactivity experiments. 142

5.2.5 Char CO_2 gasification kinetics 143

5.3 Results and discussion 145

5.3.1 Char analysis results 145

5.3.1.1 The compositions of the <1.5 g/cm^3 density fraction and liquefaction residue chars 145

5.3.1.2 XRD analysis 148

5.3.1.3 XRF analysis 149

5.4 Char-CO_2 gasification results 150

5.5 Effect of temperature on the gasification conversion 152

5.6 CO_2 gasification reactivity of the chars 152

5.7 Effect of porosity on gasification reactivity of <1.5 g/cm^3 density fraction and carbon-rich residue chars 154

5.8 Influence of mineral matter on gasification reactivity of lighter density fraction and residue chars 155

5.9 Kinetic modelling using the random pore model volumetric reaction model 156

5.10 Determination of activation energy and pre-exponential factor 159

5.11 Conclusions 161

5.12 Chapter 5 references 164

CHAPTER 6 CONCLUSIONS AND RECOMMENDATIONS 168

6.1 Introduction 169

6.2 Conclusions regarding the objectives of the study 169

6.3 Conclusions regarding the hypotheses of the study 172

6.4 General contributions of the study 174

6.5 Recommendations for future research 175

LIST OF TABLES

Table 2-1: Operating conditions, coal types, solvents used, carbon conversion, and oil yields during direct coal liquefaction. 39

Table 2-2: Summary of reported proximate and ultimate analyses results and H/C atomic ratios of coal liquefaction residues 42

Table 3-1: Proximate, ultimate, calorific value, H/C, O/C, mass, and density separation yield results of coal fines and their density separated fractions 76

Table 3-2: CO_2 low-pressure gas adsorption analysis results of coal fines and their float fractions..... 77

Table 3-3: Petrographic analysis results of the HR and WR, and their float fractions (%vol., mmb)..... 78

Table 3-4: Normalised XRF analysis results based on loss on ignition and B/A (base/acid) ratios for the HR and WR and their density separated float fractions (%wt.) 79

Table 3-5: XRD results of the coal fines and their float fraction (as % crystalline and amorphous phases) (%wt.) 80

Table 3-6: Percentages products distribution of coal fine discards and float fractions at 380°C, 400°C, 420°C, and coal conversion..... 82

Table 3-7: Proximate and the ultimate analyses results of DCL products (HS, PAAs and residues) 85

Table 3-8: Trace and lighter elements contents as determined by ICP-OES analyses in the float fractions, and their liquefaction products: PAAs and residues 87

Table 3-9: The GC-MS analysis results for the oil samples derived from HR, HF WR and WF at 420°C..... 89

Table 3-10: Proton NMR results of the oil samples derived from HR, HF, WR and WF at 420°C (ppm) 91

Table 3-11: Structural parameters from solid-state ^{13}C CP-NMR for the coal fines, float fractions and their liquefaction products: residues and PAAs..... 94

Table 4-1: Normalised pyrolytic products distribution of coal float fractions and their corresponding liquefaction residues at 750 and 920°C (%wt.)..... 112

Table 4-2: Proportion of amorphous and total crystalline mineral phases of the float fractions, residues and their char samples from XRD analysis (%wt.). 114

Table 4-3: The GC-MS analysis results of the tar samples generated from the pyrolysis of lighter density fractions and their corresponding liquefaction residues at 750°C (tetralin free basis) 115

Table 4-4: The liquid-state ((^{1}H) and ^{13}C) NMR analysis results obtained from the pyrolysis of lighter density fractions and their liquefaction residues at 750°C (ppm). Integral areas in the NMR spectra are all normalised to 100 and thus expressed as a percentage of all integral areas within each NMR spectra. 118

Table 4-5: Proximate, ultimate, H/C, O/C, S/C analyses results of the lighter density fractions, liquefaction residues and char samples generated from the pyrolysis of coal float fractions and liquefaction residues at 750 and 920°C..... 125

Table 4-6: Structural and lattice results of ^{13}C NMR of the lighter density fraction, their residues and pyrolysis char samples (produced at 920°C) 127

Table 4-7: CO_2 low-pressure gas adsorption analysis results of the lighter density fractions, their corresponding liquefaction residues and chars samples generated from the pyrolysis of coal float fractions and their corresponding residues at 750 and 920°C charring temperature..... 130

Table 5-1: Proximate and ultimate analyses results of the chars generated at 920°C from the <1.5 g/cm^3 coal samples, their liquefaction carbon-rich residues, and the demineralised samples 147

Table 5-2: XRD analysis results of the chars generated at 920°C of the <1.5 g/cm^3 coal samples, their liquefaction carbon-rich residues, and the demineralised samples (%wt.) 149

Table 5-3: XRF results of the ash samples of coal density fractions of <1.5 g/cm^3 and their liquefaction carbon-rich residue chars on LOI free basis (%wt. lfb)..... 149

Table 5-4: Gasification reactivities of the char samples from the <1.5 g/cm^3 coal density fractions and their liquefaction carbon-rich residue samples 154

Table 5-5 RPM and VRM determined time factors, $t_{f,}$ structural parameter, ψ, quality of fit, and error sum of squares..... 158

Table 5-6 Activation energies (kJ/mol) and lumped pre-exponential factors (min^{-1}) for CO_2 gasification as determined from the various reaction reactivity models 160

LIST OF FIGURES

Figure 1-1: Global primary energy consumption by fuel type in 2016. Source: BP Statistical Review of World Energy.[8] 3

Figure 1-2: South African coal production and consumption in 2016. Source: BP Statistical Review of World Energy.[9] 4

Figure 1-3: South Africa's primary energy consumption in 2016. Source: BP Statistical Review of World Energy.[9] 5

Figure 1-4: South Africa's energy importation by country of origin in 2014 (Adapted from Global Trade Information).[24] 6

Figure 1-5: Schematic of sample preparation and analysis. 10

Figure 1-6: Schematic of the liquefaction experiment. 11

Figure 1-7: Schematic of the liquefaction product analysis. 12

Figure 1-8: Schematic of the pyrolysis and char-CO_2 gasification experiment. 13

Figure 2-1: Schematic representation of a fixed-bed gasifier showing the four zones of reactivity (adapted from Hebden and Stroud[81]) 25

Figure 2-2: Scheme of the Indirect Coal liquefaction (ICL) process to produce transportation fuels using Fischer-Tropsch synthesis (adapted from Spath and Dayton, [90]). 28

Figure 2-3: Direct coal liquefaction route to transport fuel (adapted from Deutsche Bank [98]) 30

Figure 3-1: Percentage products distribution of coal fines and density separation fractions at (a) 380°C, (b) 400°C, (c) 420°C, (d) Coal conversion at different temperatures. Note: HR= Highveld coal fines, HF<1.5= Highveld float fraction, WR= Waterberg coal fines, WF<1.5= Waterberg float fraction. 81

Figure 3-2: Correlation of (a) surface area vs carbon conversion, (b) Total reactive macerals vs conversion Note: HR= Highveld coal fines, HF<1.5=

Highveld float fraction, WR= Waterberg coal fines, WF<1.5= Waterberg float fraction 82

Figure 3-3: ^{13}C CP NMR spectrum of the float fractions and their liquefaction products: residues and PAAs 93

Figure 4-1: The Fisher Assay setup (adapted from Roet et al.[8]) 106

Figure 4-2: DTG and TG curves of (a) Highveld float fraction and residue in N_2; (b) Waterberg float fraction and residue in N_2; (c) Highveld float fraction and residue in air; (d) Waterberg float fraction and residue in air. HF N_2 = Highveld float under nitrogen; WF N_2 = Waterberg float under nitrogen; HF-R 420°C N_2 = Highveld float residue under nitrogen; WF-R 420°C N_2 = Waterberg float residue under nitrogen; HF Air = Highveld float under air; WF Air = Waterberg float under air; HF-R 420°C Air = Highveld float residue under air; WF-R 420°C Air = Waterberg float residue under air. 110

Figure 4-3: ^{1}H and ^{13}C NMR spectra of tars produced from lighter density fraction and their residues at 750°C pyrolysis temperature: (a) ^{1}H spectra, (b) ^{13}C spectra (The y-axis in all cases is Signal Intensity (Arbitrary units)) 120

Figure 4-4: FTIR spectra of tars samples produced from the pyrolysis of lighter density fractions and liquefaction residues at 750°C charring temperature..... 122

Figure 4-5: ^{13}C CP NMR spectra at 12 kHz MAS of the lighter density fractions, residues, and their corresponding char samples 128

Figure 5-1: Char-CO_2 isothermal gasification mass loss results for the char samples at 940°C..... 151

Figure 5-2: Normalised gasification fractional carbon conversion curve of the char–CO_2 gasification experiments at 940°C for WF, HF, and their liquefaction carbon-rich residues..... 151

Figure 5-3: Effect of temperature on fractional conversion for: (a) Highveld coal density fractions <1.5 g/cm^3, (b) Highveld liquefaction carbon-rich residue, (c) Waterberg coal density fractions <1.5 g/cm^3, (d) Waterberg liquefaction carbon-rich residue sample 152

Figure 5-4: Comparison of the reactivities of the four samples: *dX/dt* as a function of carbon conversion at 940°C 153

Figure 5-5: Influence of some surface parameters on the initial reactivity of the samples: (a) Influence of porosity; (b) Influence of micropore surface area. (WF= Waterberg float char, HF= Highveld float char, WF-R= Waterberg float residue char, HF-R= Highveld float residue char 155

Figure 5-6: Mass loss and carbon conversion of the chars from the liquefaction residues and demineralised liquefaction residues during CO_2 gasification at 880°C 156

Figure 5-7: RPM and VRM fitting to experimental data of (a) Highveld <1.5 g/cm^3 density fraction, (b) Highveld <1.5 g/cm^3 density fraction residue, (c) Waterberg carbon-rich residue, (d) Waterberg carbon-rich residue sample 159

Figure 5-8: Carbon fractional conversions as a function of reduced time for chars from (a) Highveld <1.5 g/cm^3 density fraction, (b) Highveld residue, (c) Waterberg <1.5 g/cm^3 density fraction, (b) Waterberg residue 161

NOMENCLATURE

Symbol	Description	Unit
A_o	Final ash yield of coal or char after demineralisation	%wt.
A_d	Original ash yield of coal or char before demineralisation	%wt.
CV	Calorific value MJ·kg-1	$MJ \cdot kg^{-1}$
d_p	Average diameter of coal or char particles	µm, mm
D_p	Pore diameter / average pore diameter	Å
E	Activation energy	$kJ \cdot mol^{-1}$
E_d	Effectiveness of demineralisation	%
f_a	Carbon aromaticity	-
H_a	Hydrogen aromaticity	-
H_{al}	Hydrogen aliphatic	-
k'_{so}	Lumped pre-exponential factor	$min^{-1} \cdot bar^{-m}$
R_i,R_s,$R_{0.5}$	Reaction rate constant	min^{-1}
m_{ash}	Mass of ash	mg
MI	Maceral index	-
m_o	Initial mass of char	mg
m_t	Mass of char at time, t	mg
RMI	Reactive maceral index	-
Rr	Mean random vitrinite reflectance	%
T	Temperature	°C
t	Time	min
$t_{0.5}$	Time for fractional carbon conversion of 50%	min
$t_{0.9}$	Time for fractional carbon conversion of 90%	min
t_f	Time factor	min^{-1}
X	Fractional conversion of carbon	-

ACRONYMS/ABBREVIATIONS

Acronym / Abbreviation	Meaning
adb	Air dry basis
Afrox	African Oxygen
ASTM	American Society for Testing Materials
Ave.	Average value
BET	Brunauer-Emmett-Teller Method
CCT	Clean coal technology
CGS	Council for Geosciences
CLR	Coal liquefaction residue
CP-MAS	Cross-polarization and magnetic angle spinning
CTL	Coal to liquid
daf	Dry ash-free basis
DCL	Direct coal liquefaction
d-$CDCL_3$	Deuterated chloroform
Demin	Demineralised coal or char sample
dmmb	Dry mineral matter basis
D-R	Dubinin-Radushkevich method
DTG	Derivative thermogravimetric analyser
ESKOM	South African Electricity Supply Commission
ESS	Error sum of squares
FC	Fixed carbon
FT	Fischer-Tropsch synthesis
FTIR	Fourier transform infrared
GC-FID	Gas chromatography-flame ionisation detection.
GC-MS	Gas chromatography-mass spectroscopy
GTIS	Global trade information
H/C	Hydrogen-carbon atomic ratio
HCl	Hydrochloric acid
HF	Hydrofluoric acid
H-K	Horvath-Kawazoe method
HI	Hexane insoluble

Acronym / Abbreviation	**Meaning**
HS	Hexane soluble
ICL	Indirect coal liquefaction
ICP-OES	Inductive coupled plasma-optical emission spectrometry
ID	Identity
ISO	International Standard Organisation
LPGA	Low-pressure gas adsorption
MAS	Magic angle spinning
mmb	Visible mineral matter basis
MPa	Mega pascal
MSD	Mass selective detector
NIST	National Institute of Standard and Technology
NMR	Nuclear magnetic resonance
NWU	North-West University
O/C	Oxygen-carbon atomic ratio
OECD	Organisation for Economic Co-operation and Development
OPEC	Organisation of Petroleum Exporting Countries
rpm	Revolutions per minute
RPM	Random pore model
SA	South Africa
SABS	South African Bureau of Standards
SCM	Shrinking core model
SSL	Single-stage liquefaction
TBE	Tetrabromoethane
THFI	Tetrahydrofuran insoluble
THFS	Tetrahydrofuran soluble
TGA	Thermogravimetric analyser
TPL	Temperature-programmed liquefaction
TSL	Temperature stage liquefaction
VM	Volatile matter content
Vol.%	Volume percent
VRM	Volumetric reaction model
wt.%	Weight percent
XRD	X-ray diffraction
XRF	X-ray fluorescence
˚C/min	Degree Celsius per minute

CHAPTER 1 INTRODUCTION

In Chapter 1, the motivation for the investigation into the beneficiation of the discard coal fines, the direct liquefaction of the float fraction obtained from the density separation and subsequent utilisation of the liquefaction residues are presented. This chapter is subdivided into six sections: background of coal utilisation globally and in South Africa, research problem statement, research aims and objectives of the study, research hypothesis, significance of the study, outline of the research and the scope of the thesis.

1.1 Background

The economic development of any country is highly dependent on the availability of energy. Energy can be considered as the driving force in every growing and developed economy in the world. Globally, the three most extensively used energy sources are crude oil, coal and natural gas.[1] Coal is arguably one of the most economical and abundant fossil fuels. Even though the world interest is drifting towards renewable energy, coal will remain an integral part of the energy supply.[2,3] Coal boosts economic development via providing a reliable and cheap power source desired to meet the high demand for electricity. The significant problem encountered globally is the increasing population, which translates to an increase in energy demand. Therefore, the utilisation of coal plays an essential role in driving sustainable energy growth and development in the world at large. Regardless of the environmental worries related to the usage of coal, it has continued to gain more grounds as energy source choice for power generation and other utilisation processes. The development of clean coal technologies (CCTs) has helped to minimise the unwanted emissions of CO_2, SO_2, NO_x and particulate matter linked with coal usage. The use of CCTs will continue to play a vital part in reducing the environmental impact associated with the utilisation of coal as an energy source. Studies have revealed that the use of coal globally accounts for about 64% of the total energy demand by source, with natural gas contributing 17%, and oil accounting for 19% of energy sources in the world.[4]

The International Energy Agency (IEA)[1] has reported that the global need for coal will still increase by about 2% each year until 2020. Globally, coal is the second-largest provider of energy after petroleum. The use of coal accounts for approximately 27% of the global energy need. This is after 33% contributed by petroleum, natural gas providing 21%, and the rest is distributed between nuclear, hydro, combustible renewable, waste and others as illustrated in Figure 1.1.[8] Renewable energy technology is currently facing some constraint with regards to usage and storage. Even though the South African government is facilitating the use of biofuels to increase the growth of renewable energy sources, there are controversies around the use of biofuels globally, due to increased food demand and deforestation. This factor will invariably affect the energy system negatively because more energy is used to generate more fuel than being produced. The chance of having a solar energy plant is high in South Africa due to the high intensity of solar radiation.

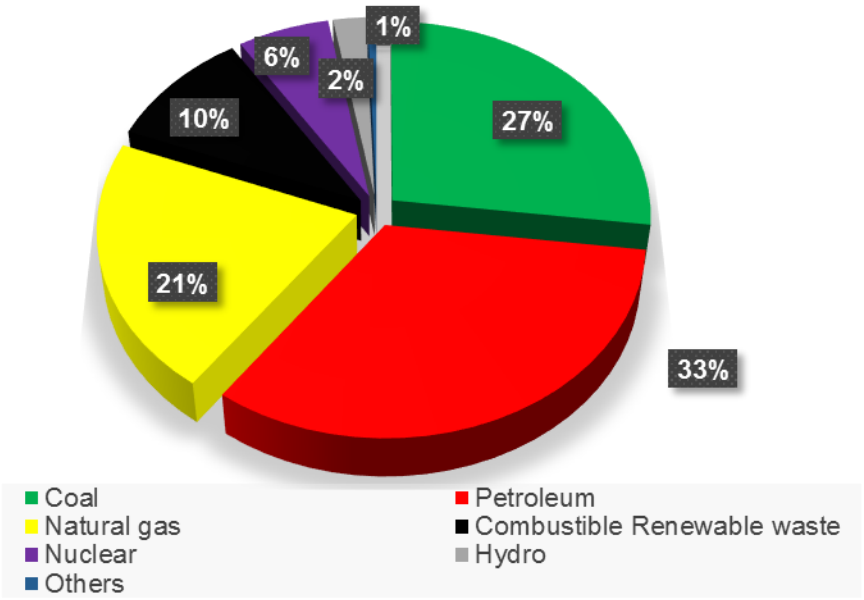

Figure 1-1: Global primary energy consumption by fuel type in 2016. Source: BP Statistical Review of World Energy.[8]

Studies have shown that South African coal production is the sixth biggest globally, and the sales from coal in South Africa contributes about 20% of mineral sales to South Africa's revenues.[5,6] The Eskom annual report[7], has shown that South Africa has a projected 53 billion tonnes of coal reserves, and based on this prediction, it is estimated that these coal reserves will last up to 200 years.[7] In South Africa, coal production is the country's second-largest mining activity.[7] According to a Fossil Fuel Foundation (FFF) report[8], approximately 307 million tonnes of coal are produced annually in South Africa; 22% of these are exported, and the rest is utilised locally for various thermochemical industrial processes.[8] With this production rate, South Africa is ranked as the fifth-highest exporter of coal behind countries such as Colombia, Russia, Indonesia and Australia[8], with annual exportation of about 67 Mt in 2015.[8,9]

During the process of mining and utilisation of South African coals, coal fines of <1 mm particle sizes are generated. These coal fines accumulate over the years and increase as mining continues.[10] With the current rate of production of these coal fines, it has been reported that as of 2014, South Africa has generated about a billion tonnes of discarded coal fines.[11] Annually approximately 60 million tonnes of coal fines are generated and discarded; the coal fines are the by-products obtained from mining, beneficiation, and utilisation of coal in South Africa.[9] Studies by Reddick et al.[12] and Matjie et al.[13] have shown that the chemical and mineralogical properties of these discarded coal fines are similar to those of South African feed coals used during thermochemical processes.[12,13] These coal fines are generally

regarded as low-rank coals, exhibiting relatively high ash yields with inferior quality in comparison to high-rank coals. The costs associated with the handling and discarding of the waste coal surpasses the market fuel values of these waste coals.[12] The coal fines also impact the environment negatively. These negative impacts include acid mine drainage, dust and spontaneous combustion of coal fines, pollution, etc. Due to these problems, there is a need to develop a method to use the discarded coal fines, which in most cases are regarded as waste.

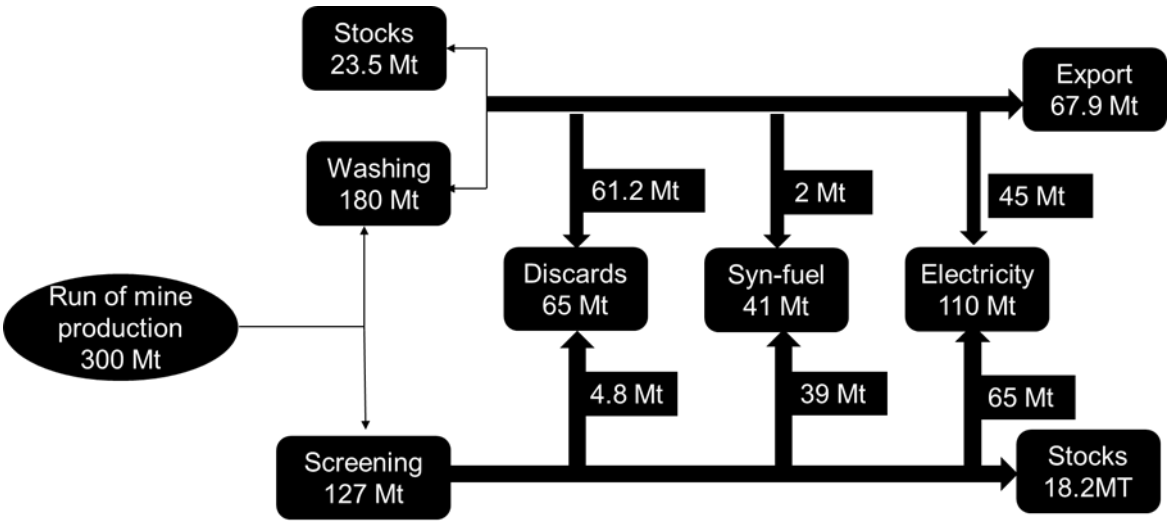

Figure 1-2: South African coal production and consumption in 2016. Source: BP Statistical Review of World Energy.[9]

Approximately 96% of the coal reserves in South Africa are made up of bituminous coal, 2% is metallurgical coal, and the balance is anthracite.[14] Sasol gasifies about 33% (50 million tonnes per year) of South Africa's low-grade coals into high-quality synthetic fuels, transportation fuel and petrochemicals, using the Fischer-Tropsch process. Sasol uses coal to liquid (CTL) technology and is the sole manufacturer of synthetic fuel in South Africa. Eskom uses about 53% of coal in South Africa in the production of electricity, while metallurgical industries and domestic uses account for 12% and 2%, respectively (Figure 1.3).[7,9]

The mining of coal in South Africa is done in different provinces, based on the enrichment of this natural resource. The mining areas include Mpumalanga, Limpopo, KwaZulu-Natal and the boundary area with Botswana in the North-West Province.[15,16] The coals in South Africa are found in different coalfields, such as Waterberg, Highveld, Ermelo and the Witbank coalfields in the Mpumalanga area, while the Klip River coalfields are located in the KwaZulu-Natal Province.[15,16] The Witbank, Highveld and the Klip River coalfields make up approximately 83% of coalfields in South Africa.[17] The Witbank coalfield is the largest in South

Africa followed by the Highveld coalfield. Sasol predominantly mines the Highveld coalfields and utilises the mined coals in the production of petrochemicals and synthetic fuel.[15,18] The Highveld coal seams are usually mined for export, and a small amount is used locally. The Waterberg coalfield is estimated to be the best source of mineable coal in the near future.[15] A report by Cairncross[17] has predicted that the Waterberg coalfield would be an essential source of mined coal in the near future, while the Klip River coalfield is the smallest in South Africa and produces anthracite and some of the coking coal.

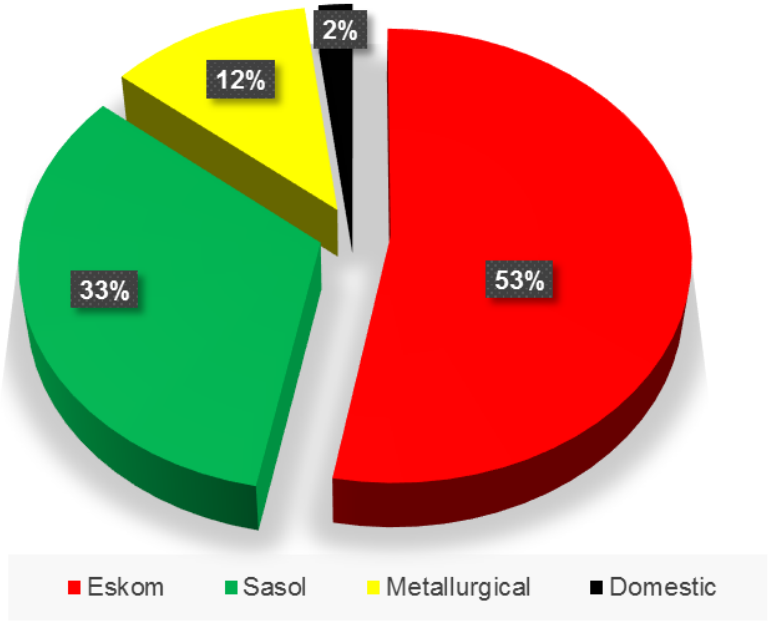

Figure 1-3: South Africa's primary energy consumption in 2016. Source: BP Statistical Review of World Energy.[9]

1.2 Problem statement

South Africa has abundant coal reserves but falls short of gas and oil reserves. Hence, South Africa depends on its vast coal resources to meet its energy needs. The utilisation of coal in South Africa accounts for about 72% of its entire energy utilisation.[15] It is estimated that South Africa has a crude oil reserve shortfall of approximately 15 million barrels per year[19], especially, when compared with other African countries like Nigeria, Angola, and Algeria.[20] The dependence of South Africa on the importation of crude oil is high. [21-23] A report published by the South African Revenue Service in 2015 shows that South Africa imports about 425,000 barrels per day (bbl/d) of crude oil.[24] South Africa imports the majority of the crude oil used domestically from the Organization of Petroleum Exporting Countries (OPEC), with import

percentages for Saudi Arabia being 38%, Nigeria 31%, Angola 12%, and the deficit is distributed between other African countries, Central South America, Europe and other Middle-Eastern Countries (Figure 1.4).

Since South Africa generates a substantial amount of coal fine discards annually, there is an opportunity to beneficiate the coal fine discards via density separation, and subsequently, use it for the development of a coal-based fuel for transportation to meet local demand for transportation fuel and thus be less dependent on imported fuel.

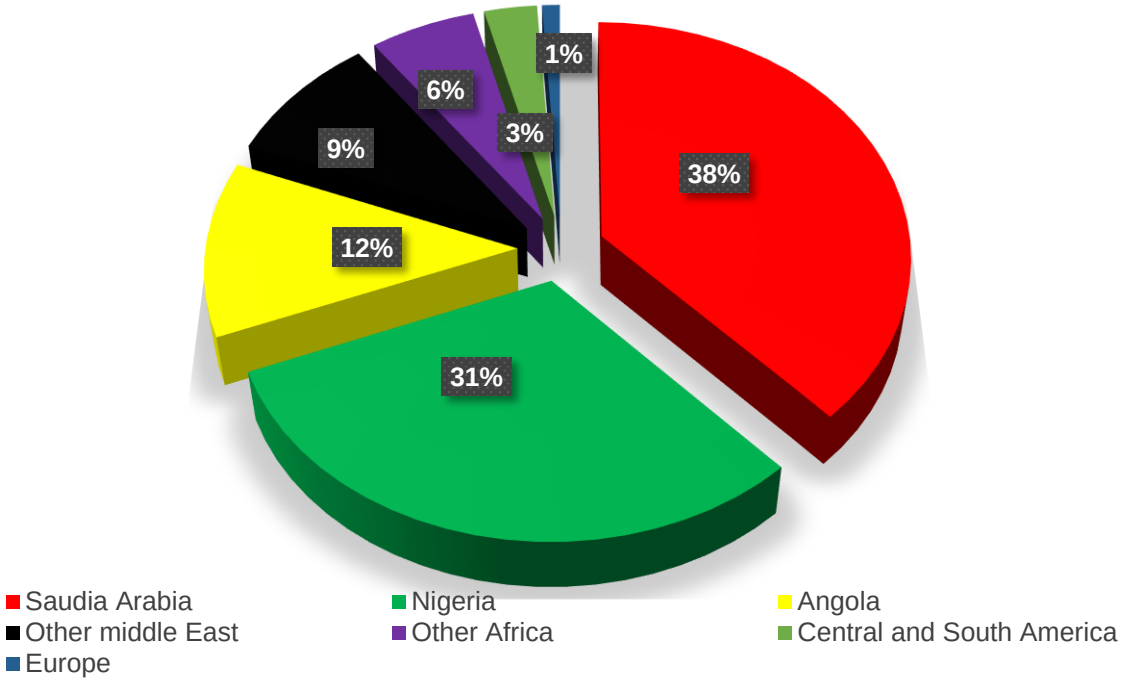

Figure 1-4: South Africa's energy importation by country of origin in 2014 (Adapted from Global Trade Information).[24]

The density separation method may be a better way of beneficiating these coal fine discards and subsequently using the cleaned coal obtained from the density separation experiment for other thermochemical coal utilisation processes. The density separation of coal fine discards involves their beneficiation by decreasing the yield and increasing the reactive macerals' content. Petrographic analysis has shown that liptinite and vitrinite are the predominant macerals in the lighter fraction (float), and the heavy components (sink) are inertinite-rich and mineral matter-rich, depending on the maceral content of the feed material before density separation.[25-29] If the coal has a high vitrinite content, it may be possible to transform the coal into useful products by liquefaction due to its high reactivity. Studies have shown that coals rich in vitrinite and liptinite give better yields during liquefaction than coal abundant in inertinite.[29,30]

Thermo-chemical conversion of coal fines and their density separated fraction (float) to liquid hydrocarbons will be a better way to use this float fraction. This can be achieved through the following: pyrolysis, solvent extraction, direct coal liquefaction (DCL), gasification and indirect coal liquefaction.[31,32] Liquefaction is the direct conversion of coal to liquids by the dissolution of coal in a hydrogen donor solvent in the presence of a catalyst under mild temperature and pressure conditions.[31-34] Products obtained during direct coal liquefaction are gases, mixed oils and coal residue. Khare and Dell'Amico[34] reported that approximately 60% of mixed oils, 15% of gases and 35% of residue could be produced during direct coal liquefaction depending on the temperature and the solvent used. During coal liquefaction, the thermal disintegration of the coal structure generates organic free radicals, which combine with hydrogen supplied by either the solvent, the coal itself, or externally supplied hydrogen. This process produces oil fractions, gases, pre-asphaltenes, and asphaltenes as intermediates, together with a solid residue, that may be further processed into char or semi-coke. Residual solids can also be used for gasification processes. The optimisation of the liquefaction process with different operating parameters such as coal particle sizes and temperatures under inert atmosphere and the usability of the residue (solid faction) produced after liquefaction needs to be investigated.

A mixture of oils is the dominant product obtained from liquefaction, which is usually referred to as synthetic crude oil, and it can be further processed by fractional distillation using different boiling points to produce transportation fuels, such as gasoline, kerosene, naphtha and diesel. The gaseous component can also be processed to produce hydrogen, which may be recycled back into the process; while the coal liquefaction residue may be used as a precursor for gasification due to the high fixed carbon content and some mineral matter, which could catalyse the gasification process. Studies by various researchers have shown that the chemical properties such as elemental composition (C, H, N, O) and calorific values of coal-derived liquefaction residues are comparable to the feed coal used during the liquefaction process.[35-36] However, the direct use of the coal liquefaction residue could be a problem, due to its high mineral matter content.

Presently, South Africa relies heavily on indirect coal liquefaction, i.e. coal gasification for the production of synthetic gas and the Fischer-Tropsch synthesis to produce liquid fuels, augmenting the petroleum supply. However, this process involves high production costs and poses a negative impact on the environment, such as unwanted gaseous emissions (e.g. carbon dioxide and nitrogen oxides), and a significant amount of coal ash. This investigation will not only seek for the optimised utilisation of waste coal, but it will also assist in improving liquefaction technology by using the residue (waste) generated from liquefaction in thermochemical conversion processes.

1.3 Research objectives

This study aims to investigate the products (gaseous, liquid and solid) produced from the liquefaction of float fractions (<1.5 g/cm^3) generated from density separation of South African coal fines, and subsequent pyrolysis and gasification of the produced liquefaction coal residues, to evaluate the suitability of coal residues for use in a coal gasification process.

Specific objectives of this study include the following:

- Determine the physical, chemical and structural properties of the coal and its density-separated fractions, and subsequently evaluate the suitability of this feedstock for the coal liquefaction experiment.
- Estimate the influence of the liquefaction operating temperature on the efficiency of the process using tetralin as a solvent.
- Determine the chemical composition of the liquid products from tetralin coal liquefaction using different conventional and advanced analytical methods.
- Determine the composition of the tetralin liquefaction residue produced from the coal fines and the float fraction after density-separation.
- Compare the liquefaction products of the coal fine discards and its low density-separated fractions.
- Investigate and compare the different product yields from the float fraction samples, and their liquefaction derived residues.
- Determine and compare the chemical, physical and structural changes of the subsequent chars after pyrolysis.
- Conduct CO_2 gasification reactivity experiments on the produced char samples on a laboratory scale under temperatures similar to fluidised bed operating conditions.
- Investigate the influence of the chemical, physical and structural changes of the chars on the observed CO_2 gasification reactivity of the density-separated (float fractions) char samples and the liquefaction residue char samples.
- Fit the resulting gasification experimental data to existing gasification kinetic models.

1.4 Study hypothesis

The following hypotheses were formulated for this study:

- Density separation of the coal fines will assist in beneficiation of the coal fines, and the float fraction will be enriched with more reactive macerals and lower ash yields.
- During liquefaction of coal fines and their density separated fractions (float fractions), organic species may dissolve in the selected solvent at different temperatures.
- Higher extraction efficiencies may be achieved from the float fraction after density separation in comparison to the coal fines samples that were not density separated.
- The oil yield produced during liquefaction can be improved by using the density-separation method to increase the percentage of reactive macerals in the starting material.
- During liquefaction, the coal matrix undergoes dredging, which could lead to an increase in porosity – the larger porosity of the residues will influence the gasification reactions.
- Coal liquefaction residues that contain relatively high contents of fixed carbon and hydrogen and relatively high calorific values may be used for coal gasification processes.
- The liquefaction process of coal may improve the reactivity of the coal residues and may have an impact on the activation energy of the gasification reactions.

1.5 Significance of the research

- Based on the available literature, there are limited studies on the analysis of different density separated fractions of South African coal fine discards using conventional and advanced analytical methods. This study is unique, as it will be conducted on different density-separated fractions from South African discarded coal fines to be used in coal liquefaction.
- Some investigators have studied the liquefaction of South African coal, but limited studies have been conducted using different density-separated float fractions generated from South African discarded coal fines.
- This study will also be useful to understand the application of liquefaction residues.
- The study will also focus on the influence of liquefaction on the char produced from the residue and its applicability and effectiveness during gasification. This is to understand the suitability of the liquefaction residues produced from different density-separated coal fractions in the thermochemical processes (gasification and pyrolysis).

1.6 Outline of the study

This investigation is divided into four phases:

Phase I: Sample preparation and characterisation study

Samples of bituminous coals from Waterberg and Highveld coal fine discards were collected and used in the study. The coal fine discards were subjected to a density-separation method to produce float (<1.5 g/cm^3), middlings (between >1.5 and <1.9 g/cm^3), and sink (>1.9 g/cm^3) fractions. The characterisation study of the coal fines and their different density separated fractions was performed using various analytical techniques, as shown in Figure 1.5. The characterisation study of the samples was conducted to determine the suitability of the different fractions for utilisation in the liquefaction process.

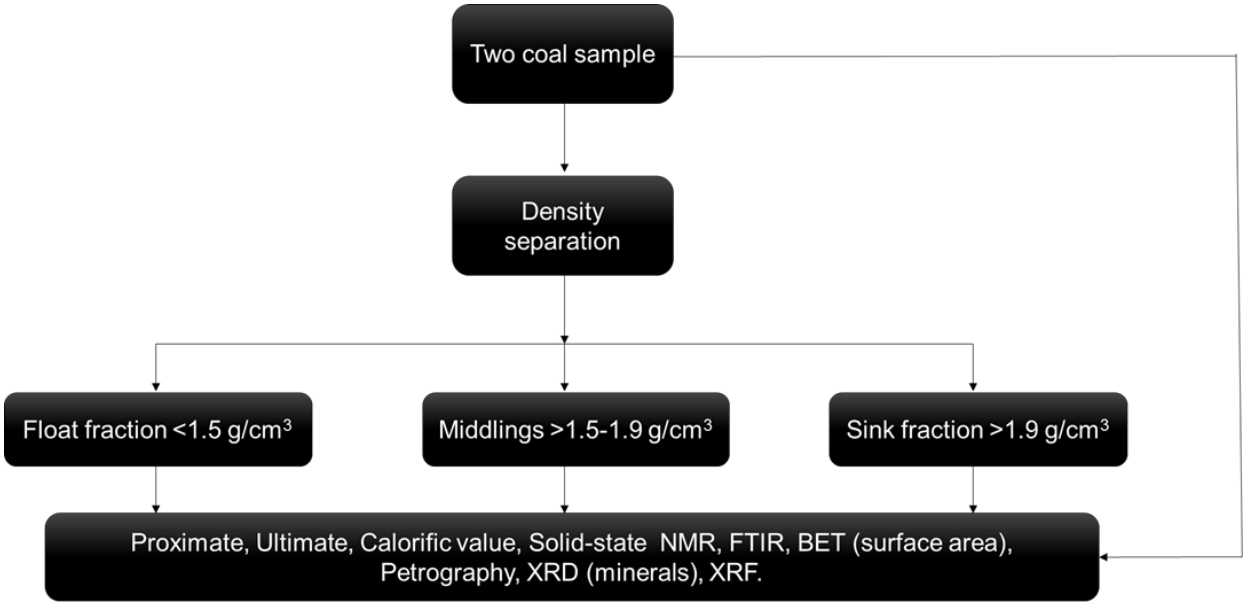

Figure 1-5: Schematic of sample preparation and analysis.

Phase II: Coal liquefaction experiments

After the suitability of the density-separated fractions was asserted, the preferred fraction and the coal fines were used for the liquefaction experiments. The liquefaction experiments were carried out in an ASS316 high-pressure stainless steel autoclave (90 mm diameter, 150 mm height, and 950 mL capacity) under N_2 atmosphere. The detailed schematic of Phase II of this investigation is shown in Figure 1.6, and the different liquefaction products were separated in this phase. The middling and the sink fractions of the density-separated coal fine discards

were not subjected to a liquefaction test in this investigation due to the relatively high proportion of ash yield, low carbon content values and calorific values.

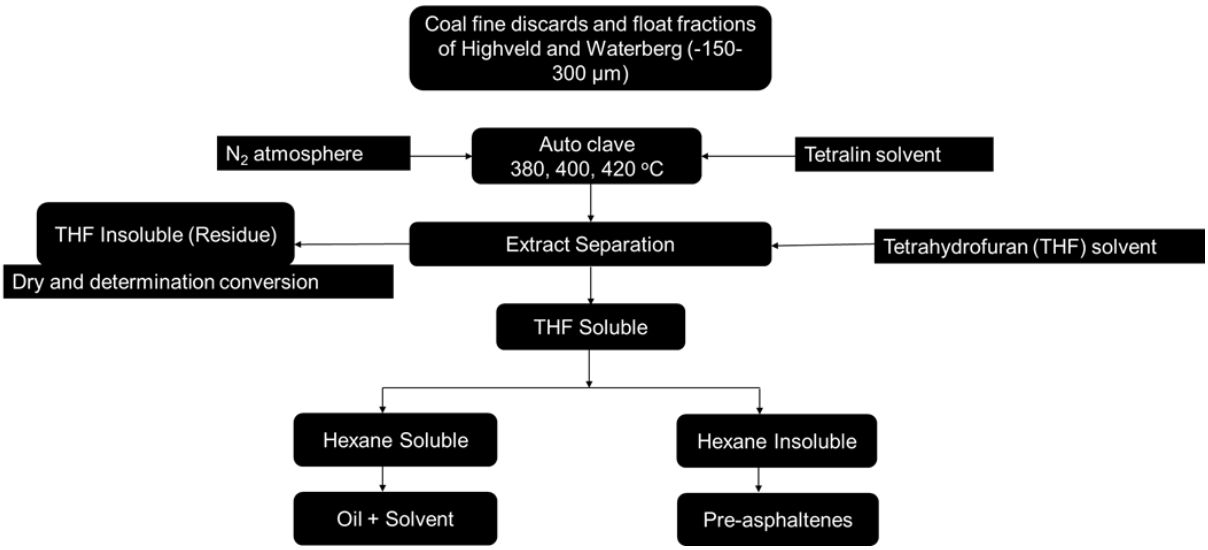

Figure 1-6: Schematic of the liquefaction experiment.

Phase III: Determination of organic species in the organic liquids/extracts, including solvents, and analysis of the residual solids

The third stage of this investigation involves the characterisation study of the different liquefaction products (extracts and the residues) using different conventional and advanced analytical techniques. The products obtained from the liquefaction experiments were characterised using the following analytical methods: proximate and ultimate analysis, solid- and liquid-state nuclear magnetic resonance (^{13}C NMR), gas chromatography-mass spectrometry (GC-MS), calorific value and Fourier-transform infrared spectroscopy (FTIR) analyses. These are illustrated in Figure 1.7. These analytical techniques were all used to determine the concentrations of organic species in the organic liquids and concentrations of elements in the solid (PAA and residues) products. The processing, statistical analysis, and interpretation of obtained results were conducted in this phase of the investigation.

Figure 1-7: Schematic of the liquefaction product analysis.

Phase IV: Gasification of the residues produced from the liquefied products

The liquefaction residue from the preferred density-separated fractions based on the amount of fixed carbon was gasified using CO_2, to determine the suitability of the liquefaction residue (char) produced from the different density-separated fractions in the char-CO_2 gasification process. Firstly, the float fractions and its liquefaction residues were pyrolysed at 750 and 920°C to produce chars that were used for the CO_2 gasification tests. The resulting pyrolysis products (char and tars) were analysed using conventional and advanced analytical methods. Further gasification experiments were carried out on the pyrolytic char at different gasification temperatures: 880, 900, 920, and 940°C under CO_2 atmosphere. The data obtained from the gasification experiments were analysed using different gasification reactivity and kinetic models. The schematic of the Phase IV investigation is presented in Figure 1.8.

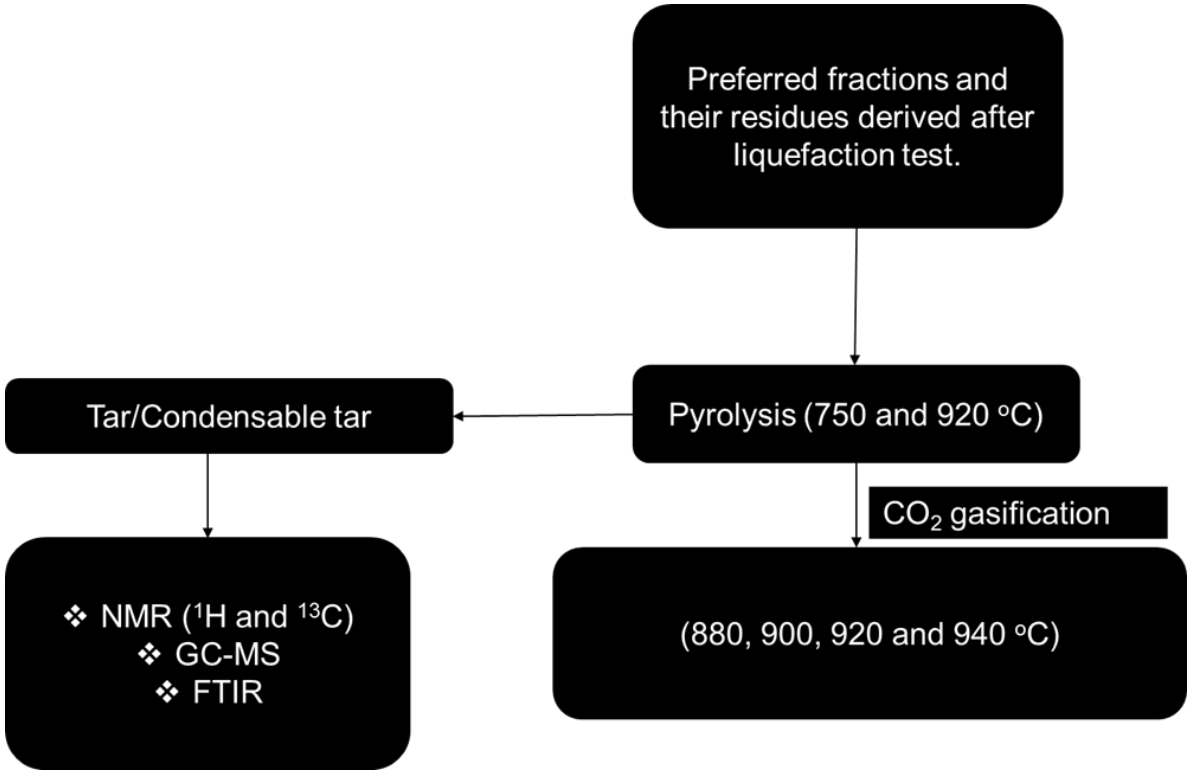

Figure 1-8: Schematic of the pyrolysis and char-CO_2 gasification experiment.

1.7 Scope of the thesis

Chapter 1 – Introduction

The aims and objectives, problem statement and hypotheses are discussed in this chapter.

Chapter 2 – Literature review

This chapter contains a summary of previous work based on the available literature, research and publications related to coal utilisation. Literature regarding coal properties, formation, and composition is discussed, and different coal utilisation processes are explained in detail. This section also highlights already existing studies on liquefaction of coals from different countries and gasification of coal liquefaction residue chars.

Chapters 3, 4, and 5 – Results and discussion

These chapters are in the form of published papers and manuscripts. Results obtained from the experimental work are divided into three sections.

Chapter 3: Influence of density separation of selected South African coal fines on the products obtained during direct liquefaction

In this paper, the analyses of the coal fines, the density-separated fractions, liquefaction of coal fines and different density-separated South African coal samples were discussed. After the liquefaction test, a comparison of the different liquefaction products derived from the coal fine discards and the float fractions is given. The analyses of all the liquefaction products are reported.

Chapter 4: Pyrolysis of tetralin liquefaction derived residues from lighter density fractions produced from waste coals taken from waste coal disposal sites in South Africa

In this paper, the pyrolytic products obtained from the float density separated coal fines fractions, and their liquefaction residues are described via detailed characterisation of the different pyrolytic products (tar and chars) using various analytical methods.

Chapter 5: Gasification of chars from tetralin liquefaction of <1.5 g/cm^3 carbon-rich residues derived from waste coal fines in South Africa

Gasification of coal residues (chars) produced from liquefaction of coal and the density-separated coal fractions are reported in this paper. Gasification experiments were done on the coal residues produced during liquefaction tests. The suitability and the influence of the liquefaction residues during gasification experiments were investigated and are reported on in Chapter 5.

Chapter 6: Conclusions and recommendations

This chapter is a summary of the most relevant results, confirming or rejecting the initial hypotheses. Future work to be done in this area of research covering any shortcomings during this study is highlighted in Chapter 6.

1.8 Chapter 1 references

1. US Energy Information Administration. *South Africa: Analysis*. 2017. https://www.eia.gov/beta/international/analysis.php?iso=ZAF (accessed May 16, 2017).
2. Kleiner, K. Nuclear energy: Assessing emissions. *Nature Climate Change*. **2008,** *1*, 130–131.
3. Ye, R.; Xiang, C.; Lin, J.; Peng, Z.; Huang, K.; Yan, Z.; Cook, N.P.; Samuel, E.L.; Hwang, C.C.; Ruan, G.; Ceriotti G. Coal as an abundant source of graphene Quantum Dots. *Nature Communications*. **2013,** *4*, 2943.
4. International Energy Agency. *Working Paper 2012: The Global Value of Coal.* http://www.desmogblog.com/sites/beta.desmogblog.com/files/global_value_of_coal.pdf (accessed July 20, 2017).
5. Energy Information Administration. *South Africa*. 2015. https://www.connaissancedesenergies.org/sites/default/files/pdf-pt-vue/south_africa.pdf (accessed April 12, 2017).
6. Gupta, R.P. Coal Research in Newcastle: Past, present and future. *Fuel.* [Online] **2005,** *84* (10), 1176–1188. https://www.researchgate.net/publication/223826325_Coal_research_in_Newcastle_-_Past_present_and_future (accessed July 20, 2017).
7. Eskom. *Eskom Factsheet: Coal in South Africa*. 2017. http://www.eskom.co.za/AboutElectricity/FactsFigures/Documents/CO0007CoalSARev14.pdf (accessed 21 March, 2018).
8. Fossil Fuel Foundation. *The Value of the Continued Use of Coal in the Energy Plan for South Africa*. 2017. http://www.fossilfuel.co.za/wp-content/uploads/2017/06/FFF-response-to-IRP2016_Rev-5-003.pdf (accessed June 2, 2017).
9. BP. *Statistical Review of World Energy*. 2017. http://www.bp.com/statisticalreview (accessed June 2018).
10. Mangena, S.J.; De Korte, G.J.; McCrindle, R.I.; Morgan, D.L. The amenability of some Witbank bituminous ultra-fine coals to binderless briquetting. *Fuel Process Technol*. **2004,** *85*, 1647–62.
11. ESI Africa. *The Economic Possibilities of South Africa's Coal Fines*. 2014. https://www.esi-africa.com/news/the-economic-possibilities-of-south-africas-coal-fines/ (Accessed June 23, 2017).
12. Reddick, J.F.; Von Blottnitz, H.; Kothuis, B. A Cleaner Production Assessment of the Ultra-Fine Coal Waste Generated in South Africa. *J. Southern Afr. Inst. Min. Metall*. **2007,** *107*, 811–16.

13. Matjie, R.H.; Li, Z., Ward, C.R.; Kosasi, J.; Bunt, J.B.; Strydom, C.A. Mineralogy of Furnace Deposit Produced by South African Coals During Pulverized-Fuel Combustion Tests. *Energy Fuels***. 2015**, 29, 8226–8238.
14. Baruya, P. Supply Costs for Internationally Traded Coal. 2007. https://www.researchgate.net/publication/324389732_Supply_costs_for_internationally_traded_coal (accessed June 9, 2017).
15. Jeffrey, L.S. Characterization of the Coal Resources of South Africa. *J. Southern Afr. Inst. Min. Metall.*. **2005**,*105*, 95–102.
16. Keaton Energy. About SA coalfields. 2009. https://web.archive.org/web/20090614092534/http://www.keatonenergy.co.za/cm/sa_coal.asp (accessed June 9, 2017).
17. Cairncross B. An Overview of the Permian (Karoo) Coal Deposits of Southern Africa. *J Afr Earth Sci*. **2001**, *33*, 529–562.
18. Pinetown, K.L.; Ward, C.R.; Van der Westhuizen, W.A. Quantitative Evaluation of Minerals in Coal Deposits in The Witbank and Highveld Coalfields, and the Potential Impact on Acid Mine Drainage. *Inter. J. Coal Geol*. **2007**, *70*,166–83.
19. US Energy Information Administration. *Total Petroleum and Other Liquids Production*. 2014. https://www.eia.gov/beta/international/rankings/#?prodact=53-1&cy=2014 (accessed March 03, 2017).
20. Oil & Gas Journal. *Worldwide look at Reserves and Production*. 2015. http://www.ogj.com/articles/print/volume-112/issue-1/drilling-production/worldwidelook-at-reserves-and-production.html (accessed May 25, 2017).
21. Fletcher, J.; Sun, Q.; Bajura, R.; Zhang, Y.; Ren, X. Coal to Clean Fuel: The Shenhua Investment in Direct Coal Liquefaction. In *21st Annual International Pittsburgh Coal Conference, September 13–17, Osaka, Japan*, 2004.
22. Nolan, P.; Shipman, A.; Rui, H. Coal Liquefaction, Shenhua Group, and China's Energy Security. *European Management Journal*. **2004**, *22*,150–64.
23. Zhao, L.; Gallagher, K.S. Research, Development, Demonstration, and Early Deployment Policies for Advanced-Coal Technology in China. *Energy Policy***. 2007**, *35*, 6467–77.
24. US Energy Information Administration. *South Africa: Analysis*. 2016. https://www.eia.gov/beta/international/analysis.php?iso=ZAF (accessed January 4, 2017).
25. Cloke, M.; Clift, D.A.; Gilfillan, A.J.; Miles, N.J.; Rhodes, D. Liquefaction of Density Separated Coal Fractions. *Fuel Process Technol*. **1994,** *38*,153–63.

26. Cloke, M.; Barraza, J.; Miles, N.J. Pilot-Scale Studies Using a Hydrocyclone and Froth Flotation for the Production of Beneficiated Coal Fractions for Improved Coal Liquefaction. *Fuel*. **1997**, *76*, 1217–23.
27. Kawashima, H.; Yamashita, Y.; Saito, I. Studies on Structural Changes of Coal Density-Separated Components During Pyrolysis By Means of Solid-State 13C NMR Spectra. *J. Anal. Appl. Pyrol*. **2000**, *53*, 35–50.
28. Joseph, J.T.; Fisher, R.B.; Masin, C.A.; Dyrkacz, G.R.; Bloomquist, C.A.; Winans, R.E. Coal Maceral Chemistry. 1. Liquefaction Behavior. *Energy Fuels*. **1991**, *5*, 724–729.
29. Davis, A.; Mitchell, G.D.; Derbyshire, F.J.; Rathbone, R.F.; Lin, R. Optical properties of coals and liquefaction residues as indicators of reactivity. *Fuel*. **1991**, *70*, 352–360.
30. Keogh, R.A.; Taulbee, D.N.; Hower, J.C.; Chawla, B.; Davis, B.H. Liquefaction Characteristics of the Three Major Maceral Groups Separated from a Single Coal. *Energy Fuels* **1992**, *6*, 614–618.
31. Akash, B.A. Thermochemical Liquefaction of Coal. *Inter. J. Therm. Environ. Eng*. **2013**, *1*, 51–60.
32. Mochida, I.; Okuma, O. and Yoon, S.H. Chemicals from Direct Coal Liquefaction. *Chemical Reviews*. **2013,** *114*, 1637–1672.
33. Miura, K.; Shimada, M.; Mae, K.; Sock, H.Y. Extraction of Coal Below 350°C in Flowing Non-Polar Solvent. *Fuels.* **2001,** *80*, 1573–1582.
34. Khare, S.; Dell'Amico, M. An Overview of Conversion of Residues from Coal Liquefaction Processes. *The Cana. J. Chem. Eng*. **2013**, *91*,1660–1670.
35. Cui, H.; Yang, J.; Liu, Z.; Bi, J. Characteristics of Residues from Thermal and Catalytic Coal Hydroliquefaction. *Fuels.* **2003**, *82*, 1549–1556.
36. Yan, J.; Bai, Z.; Li, W.; Bai, J. Direct Liquefaction of Chinese Brown Coal and CO_2 Gasification of the Residues. *Fuel*. **2014**;*136*, 280–286.
37. Burgess, C.E.; Schobert, H.H. Direct Liquefaction for Production of High Yields of Feedstocks for Speciality Chemicals or Thermally Stable Jet Fuels. *Fuel Processing Technology*. **2000**, *64*, 57–72.
38. Fox, E.B.; Liu, Z.W.; Liu, Z.T. Ultraclean Fuels Production and Utilisation for the Twenty-First Century: Advances Toward Sustainable Transportation Fuels. *Energy Fuels*. **2013,** *27*, 6335–6338.

CHAPTER 2 LITERATURE REVIEW

An overview of coal properties (maceral and mineral matter) and composition are presented in this chapter. This is followed by the different thermochemical processes used for coal conversion to synthetic fuel and chemicals with a focus on liquefaction of coal, using direct liquefaction technology. The utilisation of liquefaction residues for pyrolysis and gasification will also be discussed.

2.1 Coal composition

Coal is an organic sedimentary rock material which originates from seam deposits. Coal is formed through the coalification process via the process of physical and chemical transformation of plant materials.[1-5] Coal consists of high proportions of organic matter (macerals) and mineral matter (minerals and non-mineral inorganic elements). The organic components in coal contain a high carbon content, with small proportions of hydrogen, oxygen, organic sulphur and nitrogen.[6,7] The organic part of coal consists of two structures, namely (a) the insoluble molecular phase, which is usually made up of condensed aromatic structures and hydrocarbon structures; and (b) the soluble phase or molecular phase. The latter phase is the fraction of coal that is soluble in a solvent. The soluble phase is made up of low molecular mass compounds, which usually comprise aliphatic hydrocarbons, polycyclic aromatic hydrocarbons (PAH), hydroxylated polycyclic aromatic compounds and heterocyclic compounds.[8,9] The amount of aromatics in coal increases as the rank of coal increases, with anthracite having the highest aromaticity for coal. The number of side chains connecting the main macro-molecules in coal decreases as the coal rank increases.

The inorganic components consist of compounds that form ash during thermal coal processing.[10] The amount of mineral matter in coal is usually used to grade coal and partly determines the quality of coal.

2.1.1 Organic components of coal

The organic fraction of coal is generally referred to as macerals. These macerals originate from the physical and chemical modifications of organic matter, deposited during coal formation. Macerals have different structural and chemical properties, depending on the specific organic matter that they were formed from. Different macerals in coal will behave differently with regards to reactivity, char structure, swelling propensity, and amount of volatiles liberated.[11] The components of different macerals in coal assist in the estimation of the chemical, physical and optical properties of coal.[12,13] Coal is a heterogeneous mixture which contains three different classes of macerals, namely inertinite, vitrinite and liptinite.

Inertinites are maceral groups, which have a high reflectance when compared to other maceral groups. Inertinite macerals can be subdivided into different sub-macerals, namely semifusinite, fusinite, macrinite, funginite, and micrinite.[14] Inertinite is generally known to be carbon-rich, very aromatic and contains a lower amount of volatile matter and hydrogen than the other types of macerals. During thermochemical utilisation, inertinite macerals are relatively unreactive (inert); hence they are less suitable for liquefaction processes than other macerals.

Vitrinites are maceral groups which are made up of brightly coloured constituents known as vitrain. They are mostly regarded as the most reactive macerals.[15] However, it has been established that all vitrinites are not reactive; and not all inertinites are inert.[16,17] Vitrinite macerals are subdivided into different sub-macerals, namely vitrodetrinite, corpogelinite, telovitrinite, detrovitrinite, collotelinite, gelovitrinite, gelinite and collodetrinite.[18] Vitrinite macerals consist of a moderate amount of hydrogen and volatile matter. These properties render vitrinite macerals suitable for hydrogenation and liquefaction processes.

Liptinites are one of the maceral groups which are formed from non-humic plant material.[19] They are characterised by a high hydrogen content and low reflectance, compared to other maceral groups. Liptinite macerals are further subdivided into sub-macerals, such as cutinite, resinite, alginate, bituminate, subernite, litodetrinite and exsudatinite.[20] Liptinite macerals contain a higher fraction of aliphatic carbons, and a higher amount of hydrogen and volatile matter than most other macerals, and are readily oxidised during thermochemical utilisation processes. Considering the higher amounts of aliphatics, hydrogen and volatile matter, liptinites are generally considered to be the most appropriate for the liquefaction process.

The macerals differ in chemical, structural and physical properties. The macerals' properties are essential in determining the behaviour of coal during utilisation processes. During coal solvent extraction, observations from previous studies have shown that vitrinite and liptinite abundant coals provide higher carbon conversion than coals that are inertinite-rich.[21] The influence of maceral groups during thermochemical processes have been investigated by different researchers.[22-25] Dyrka and Horwitz,[22] and Choi et al.,[23] found that liptinite is richer in aliphatic carbons than other macerals and vitrinite macerals are rich in phenolic compounds, while inertinite is rich in aromatic carbon. By density separation, it is estimated that liptinite predominates in the lighter fractions (float) and contains less mineral matter than in the higher density-separated fractions. Other researchers have also shown that where the coal contains different macerals after density separation, liptinite and vitrinite macerals are concentrated in the float fractions of the coal, while inertinite concentrates to a greater extent in the heavier fractions.[17] The sink fraction usually contains a high concentration of the mineral matter of the coal.[22]

2.1.2 Coal mineral matter

Mineral matter in coal is categorised into three different forms, namely inherent (included) minerals, extraneous (excluded or discrete particles) minerals, and non-mineral inorganic elements (organically associated inorganic components, such as salts of carboxylic acid, inorganic element ions and water-soluble inorganic salts).[26-29] For low-rank coal, the number of different inorganic element carboxylates (organically associated inorganic elements) may

be directly related to the amount of organic carbons and inorganic components in the coal.[4] Mineral matter, and inorganic elements are detected by mineralogical and chemical analytical techniques such as XRD, QEMSCAN and XRF spectroscopy.[6,30.31]

The inorganic species in higher rank coals are in the form of minerals, with a smaller percentage of carboxylic acid salts than in lower rank coal.[4] The percentages of organically associated inorganic constituents vary with rank of coal, as with reducing coal rank, the fraction of organically associated inorganic components increases.

The inorganic part of coal may contain over 125 minerals, mostly in microgram per gram quantities.[32,33] Mineral matter and macerals in coal are transformed or decomposed at elevated temperatures during the thermochemical utilisation of coal.[34-41] Coarse coal feedstock fed to commercial gasifiers, for example, consists of rock fragments (sandstone, siltstone and mudstone particles) and carbon-rich particles. These rocks contaminate the carbon-rich particles through intra-seam bands, floor or roof layers. Some of the rock material can be liberated from the organic carbon particles during sample preparation using crushers and grinders.[42-45] Mineral matter in coal has been shown to have a substantial influence during coal utilisation processes. The chemical structure of the mineral products is influenced by heat treatment.[30,46,47]

Some minerals in coal have been shown to enhance the gasification process by serving as catalysts during coal utilisation processes.[48-53] The addition of alkaline metallic compounds, such as Li, Na, K, Ca and Ba carbonates, oxides and hydroxides, has been used to enhance gasification. The catalytic reaction occurs through chemical and electronic interaction with the carbon matrix.[48] The catalytic performance of these metallic compounds was shown to be dependent on various parameters, such as the concentration of the catalyst, the method of catalytic dispersion, and chemical form. Previous studies on South African coal have shown that K_2CO_3 addition enhances the gasification process.[49] Wang et al.[50] studied the catalytic behaviour of a blend of calcium hydroxide and potassium carbonate salts during gasification. They observed from their study that the addition of minerals to the char improved the gasification reactivity of the chars. In an investigation conducted by Zhang et al.[51] on the reactivity of coal char using a Ca and Na doped catalyst, it was observed that the catalysed samples showed higher reactivities during steam gasification when compared to parent coal samples. Sakawa et al.[52]; Ye et al.[53] and Hattingh et al.[54] used the alkali index to examine the relationship between mineral matter content and reactivity. Results from their experiments showed that gasification reactivity increased with increasing alkali index.

2.2 Coal classification

The degree of coalification or metamorphosis of coal from peat to graphite-like material is known as the rank of coal.[12] The percentage of carbon content is usually used to evaluate the rank of coal and also used to evaluate the level of maturity of coal.[55] There are different factors to be considered in identifying different ranks of coal; these factors include the heating value of the coal and the behavioural pattern of coal during the utilisation processes. Coal is generally categorised into different ranks namely: brown, lignite, sub-bituminous, bituminous and anthracite coal, with anthracite regarded as the highest rank coal and brown coal the lowest-rank coal.[11,12] Higher rank coal can be differentiated by the following parameters: vitrinite reflectance and fixed carbon content; whereas, lower rank coal can be distinguished based on the amount of moisture, mineral matter content and calorific values of the coal.[56] In practice, when a coal sample has a high ash yield and inherent moisture content, the heating value of such coal is low. Since anthracite is high-rank coal, it has a higher heating value when compared to the lower rank lignite coal.[55] As the coal matures due to the loss of some organic components of coal, such as hydroxyl and carbonyl groups, the oxygen and moisture contents of the coal decrease. The elemental hydrogen content also reduces with increasing coal rank, and the elemental carbon content of coal increases as the maturity or rank of coal increases.[57]

As coal ages, the carbon content, molecular cluster sizes, and aromaticity of the coal increase, with a considerable reduction in the volatile matter and moisture contents.[58] The abstraction of aliphatic and the acyclic moieties of coal during coalification is attributed to the increase in aromaticity of higher rank coal.[57-61] The organic part of coal contains carbon (70-95 wt. %), hydrogen (3-6 wt. %), oxygen (5-25 wt. %), and small percentages of sulphur and nitrogen.[52] The percentages of organic matter in coal depend on the coal rank.

2.3 Thermochemical utilisation of coal

Thermochemical processing of coal is the thermal degradation of organic components of coal to yield various products, which can be used as fuel or can be further processed to be used as fuel or chemicals. Thermochemical processes can be subdivided into four main categories depending on the operating conditions used. These are pyrolysis, gasification, combustion and liquefaction.

2.3.1 Coal pyrolysis

Pyrolysis is a thermochemical process which is conducted in a temperature range of 400–950°C in an inert atmosphere. During pyrolysis, carbonaceous material called char is produced. The temperature at which pyrolysis occurs is low when compared to the gasification

temperature. The products obtained during pyrolysis are gases, tars, water and chars. Pyrolysis involves the thermal disintegration of coal in an inert atmosphere such as N_2, Ar, or He. Pyrolytic processes are complex and involve different reactions taking place; each of the reactions leads to the generation of different pyrolytic products. Products generated during pyrolysis include reactive solid (chars), liquids (water and tar), as well as gaseous compounds.[62,63] The aromatic and hydro-aromatic units are the primary building blocks of coal and are held together by elements and functional groups such as oxygen, sulphur and methylene.[64] During pyrolysis, the thermally labile compounds, which are weakly bonded to the coal matrix are liberated in the form of volatiles; the crosslink bridges rupture; and the building blocks in coal (aromatic and hydro-aromatic) are transformed into aromatic blocks.[62,63]

Tars are generated during coal pyrolysis. The composition of the tar is influenced by factors such as the rank of coal, particle size, and mineral matter in the coal.[65,66] The tars are estimated to make up approximately 50–80% of the total mass loss during pyrolysis of low-rank coal samples.[67] Light compounds in the tar comprise mainly benzene, xylene, toluene, cyclohexane, alkanes, olefins and some aromatic compounds.[5,65] The heavy compounds in tars, which are regarded as the most valuable products, comprise mainly pyridine, cresols, naphthalene, phenanthrene, phenol, pyrene and biphenyl.[5,66,68,69] These tar compounds need to be upgraded before they can be used commercially.[5,46,70]

The gaseous products generated during pyrolysis of coal usually contain gases such as CO, CO_2, CH_4, H_2, C_2H_6, and C_2H_4. These products can be upgraded using methanation to produce syngas that are used in the industry for the production of liquid fuel. [65,71,72,73]

The char, which is the main product generated during pyrolysis, primarily contains carbon, ash and a small percentage of hydrogen. These chars can be used in the gasification process owing to their high reactivity. [5,73-75] Conditions of the pyrolysis process determine, among other factors, the char reactivity during gasification. Studies have also shown that the char produced during pyrolysis can be used in the metallurgical industry as a reductant, in the production of carbon molecular sieves and activated carbon which are used in water treatment processes, gas separation and food processing.[74,75] The structure of the char, char yield, and reactivity are dependent on parameters such as coal rank and grade, heating value, particle size, and residence time used during pyrolysis.

Most studies have focused on the influence of pyrolysis conditions and analysis of products from South African coals.[76-78]

2.3.2 Coal gasification

Gasification is the process whereby coal reacts under atmospheres such as air, CO_2, steam, oxygen or a combination of these gases to produce synthetic gas (a mixture of CO and H_2), that is used as fuel or feedstocks during chemical synthesis. The composition of gases generated during gasification depends on the gasifying agent, coal rank and its composition, the operating conditions and all these control the gasification reactivity.[79] Entrain flow gasification and plasma gasification are conducted at temperatures exceeding 1500°C and 2000°C respectively under controlled pressure. The products generated (mainly syngas) may be used directly in the production of electricity, or the production of chemicals.[79] Gasification is sometimes referred to as incomplete or partial combustion because during gasification CO, and H_2 are produced as compared to CO_2 and H_2O that are produced during combustion.[80]

As an example of the industrial gasification process, a schematic presentation of the Sasol-Lurgi fixed bed gasifier is given in Figure 2.1. Sasol uses a Sasol-Lurgi fixed bed dry bottom (FBDB) gasifier for the production of synthesis gas (syngas). The Sasol-Lurgi gasifier uses a variety of coal feedstock, such as high ash and high melting point mineral matter coal for the production of a H_2/CO syngas.[42] Coals fed from the top of the gasifier at a pressure of 30 bar in the presence of steam and oxygen as gasifying agents. From Figure 2.1, different reaction zones are observed from the top of the gasifier to the bottom. The different reaction zones are: (1) the drying zone, where moisture is released; (2) the devolatilisation zone, where pyrolysis occurs as the volatiles in coal are liberated; (3) the reduction zone, where the endothermic syngas producing reactions take place; and (4) the combustion zone, where oxidation reactions (exothermic) occur. The dry ash is discharged from the bottom of the gasifier.

For this investigation, the gasification process is simulated on a laboratory scale by producing a char from the starting material under pyrolysis conditions and then subjecting the produced char to heat treatment in a CO_2 atmosphere.

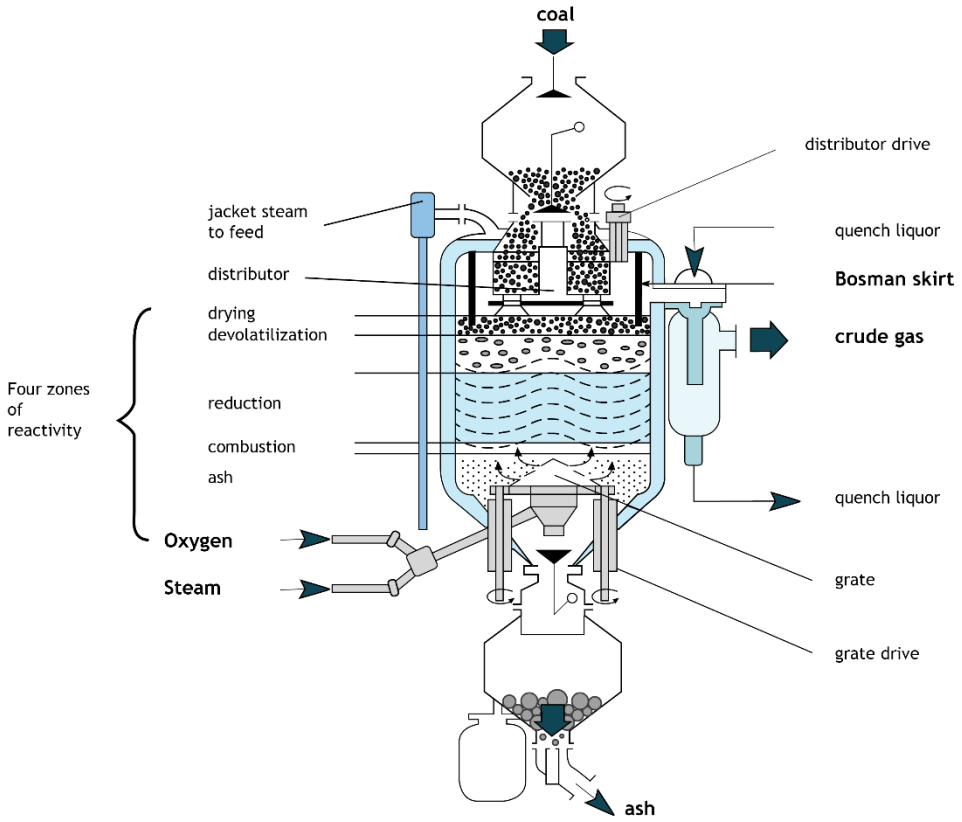

Figure 2-1: Schematic representation of a fixed-bed gasifier showing the four zones of reactivity (adapted from Hebden and Stroud[81]).

2.3.3 Coal combustion

Coal combustion is a process used in the production of electricity by the ignition of coal in a furnace.[80] The reactant gases for combustion are air and/or oxygen. Coal combustion involves the breaking down of chemical bonds in coal to form mainly CO_2 and H_2O to liberate energy. Combustion is usually done at atmospheric pressure and high temperature (above 800˚C).

2.3.4 Coal liquefaction

Transportation fuels currently in use are obtained from crude oil, which contains double the amount of hydrogen as coal. In order to obtain transportation fuels from coal, the coal needs to be converted to liquids. The process whereby liquids are extracted from coal is liquefaction. The process to produce transportation fuels must thus make provision for the conversion or extraction of liquids from coal to have a similar hydrogen content and properties to crude oil before it can substitute for crude oil. During the liquefaction process, carbon is removed from coal using a hydrogen-rich solvent.[82] Liquefaction is performed under mild pressure and temperature conditions.

Coal has atomic hydrogen to carbon ratio ranging between 0.7–0.95, petroleum's (crude oil) H/C ratio is approximately 1.5, and natural gas' ratio is 4.[83] One of the advantages of coal liquefaction is the production of liquid fuels with atomic H/C ratios ranging from 1.8–2.5. Hydrogen is added during liquefaction to obtain the higher H/C ratio, and in the process, some oxygen and carbon are removed from the coal matrix. The smaller liquid hydrocarbons formed during the liquefaction process concentrate in the liquid and gas phases.

2.3.4.1 History of liquefaction

Coal to liquid (CTL) industrial technology has been in existence for a long time.[84] CTL technology was developed by a German scientist Friedrich K.R. Bergius in 1913. Indirect coal liquefaction technology was first employed by the Germans during World War II, due to the relative abundance of coal in Germany.[83] The motivation for the development of CTL was the high demand for transportation fuels for military aeroplanes, tanks, and warships. The use of CTL met about 92% of Germany aviation fuel and some fraction of the petroleum needs during World War II. The initial stage of production generated up to 127,000 barrels of fuel per day from about 25 CTL plants.[84] Direct coal liquefaction (DCL) has also been developed in other countries such as the United Kingdom, United States of America, Japan and China. A Synthetic Liquid Fuels Act was passed in 1944 by the United States for the production of fuel using CTL technology. The law was promulgated because of the oil shortage facing the US during the war. The passed Act promoted the manufacturing of liquid fuels from coal and other organic materials for five years.[86] Nonetheless, excessive cheap oil after the war reduced attention to CTL. However, numerous developmental programmes continued in operation in the US and other countries.

South Africa is one of the countries, which has implemented commercial CTL technology after the Second World War era. In the early 1950s, South Africa started supporting CTL technology development. The commencement of CTL technology in South Africa was partly due to fear that the importation of oil to South Africa may be sanctioned, because of policies carried out during the apartheid regime. At present, Sasol has more than 50 years of experience in the use of CTL technology to produce synthetic fuels. Approximately 40% of the gasoline consumed in South Africa is obtained from liquefied coal.[86] Sasol uses CTL technology to produce gasoline, diesel, jet fuel and chemicals. This initiative was as an effect of the restriction placed on South Africa on the importation of oil from other countries by international arrangements. The oil shocks of the 1970s led to new attention to the process in the US, Japan and some of the countries that depend on the importation of crude oil. Still, again the accessibility of large amounts of cheap oil made the utilisation of large-scale CTL technology unsuccessful and unappealing. During the past ten years, the prices and the demand for

energy have astronomically increased, and CTL technology has returned to the global energy discourse. In 2009, a Chinese company Shenhua Energy Co. LTD developed the first commercial direct coal liquefaction plant.[87]

2.3.4.2 Types of liquefaction

Coal liquefaction is divided into direct coal liquefaction (DCL), solvent extraction and indirect coal liquefaction (ICL). The types of liquefaction differ from each other with regards to their operating conditions. A more detailed description of the different liquefaction processes will be given in this section.

- **Indirect coal liquefaction (ICL)**

Indirect coal liquefaction processes mostly involve gasification of coal to generate synthesis gas, a mixture of CO and H_2 (syngas). This mixture is converted to liquid hydrocarbons by the Fisher-Tropsch process. The ICL process refers to coal that is not transformed directly into a liquid but has to undergo other processes before it is converted to liquids. ICL involves the gasification process, in which coal reacts with gasifying agents such as CO_2, O_2 and steam, or a combination of these gases, at a moderately elevated temperature (>1000 ˚C) to generate hydrocarbon and synthetic gases.[88,89] The indirect liquefaction process as a first step thus deals with the direct breakdown of the coal macromolecular structure. Since the products obtained from indirect coal liquefaction and direct coal liquefaction have lower hydrogen to carbon ratio than those needed for liquid fuels, a hydrogenation process is required. Figure 2.2 shows a typical pathway in which gasoline and other chemicals are produced using Fischer-Tropsch technology. This study focused on the direct liquefaction of coal, which will be described in more detail.

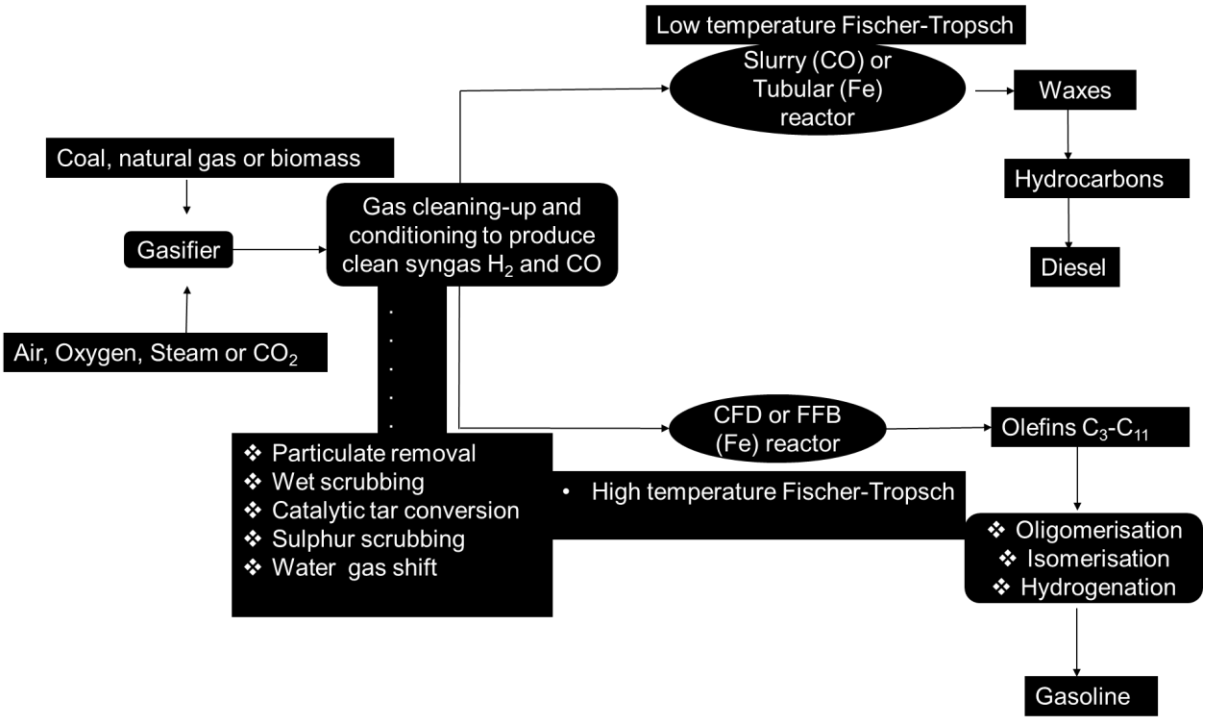

Figure 2-2: Scheme of the Indirect Coal liquefaction (ICL) process to produce transportation fuels using Fischer-Tropsch synthesis (adapted from Spath and Dayton, [90]).

Solvent extraction.

The solvent extraction process involves the heating of coal in the presence of a non-reactive organic solvent. Solvent extraction differs from DCL, as for solvent extraction, a hydrogen-rich solvent is not required, and the temperature used for solvent extraction can range from 150–400˚C. This temperature range is subject to the boiling point of the solvent employed in the process.

The solvents used in solvent extraction have been categorised into two classes.[4] The first class of solvents can extract only about 10% of coal and includes acetone, chloroform, diethyl ether and benzene. The second class of solvents can dissolve about 40% of coal. Solvents such as pyridine, 1,2-diaminoethane and quinolone fall in this category. Studies have shown that at temperatures above 300˚C, solvents such as phenol, anthracene, 2-naphthol and phenanthrene are useful for the extraction of up to 50% of coal depending on the coal type.[4,91] Different solvents used with the same coal can have different extraction yields and products. The extraction efficiency is also influenced by coal rank. With increasing coal rank, the effective solvent extraction decreases. Anthracite coals give a low yield irrespective of the solvent used in the process. The extraction yield also depends on other factors such as coal macerals, temperature and particle size of the coal.[91] Higher carbon extraction efficiency can be obtained from coal containing higher amounts of vitrinite and liptinite, and lower extraction

yields are derived from coal with higher amounts of inertinite. When using the same solvent and coal type, extraction yields can be improved by elevating the liquefaction temperature and also by reducing the particle size of the coal used in the process.[91]

- **Direct coal liquefaction (DCL)**

DCL is a process that involves the treatment of coal with a hydrogen-rich solvent, with or without a catalyst, under a pressurised atmosphere at a moderate heating rate and final temperatures between 300–450°C.[92] The solvent is essential because it also assists in mass transfer during chemical reactions. During DCL, the thermal disintegration of the coal generates free organic radicals, which react with hydrogen provided by the solvent, or externally supplied hydrogen gas (when hydrogen is used as atmosphere). The organic radicals react to assist in the production of different hydrocarbons ranging from lighter aliphatic to aromatic compounds. The hydrogen provided by the solvent helps in the thermal disintegration of aromatic rings in coal into smaller molecules or large paraffin hydrocarbons similar to those in crude oil. Carbon and oxygen are removed in the form of H_2O, CO_2 or CO during the liquefaction process. The DCL process produces oil fractions, gases, pre-asphaltenes, and asphaltenes as intermediates, together with a residue that becomes further condensed into char or semi-coke. The residual solids from the process may be further used in gasification processes.[92-96] The majority of solvents used during DCL include phenanthrene, methylnaphthalene, tetrahydrofuran, benzene, diethyl ether, pyridine, quinolone, 1,2-diaminoethane, tetralin and cresol.

DCL has been used by various researchers to investigate the liquefaction product distribution yields and carbon conversion efficiency.[92-96] Many challenges and problems are associated with DCL technology, and these difficulties include unclear reaction mechanisms and kinetics that are associated with the liquefaction process.[97] Direct liquefaction is needed by countries with shortages in crude oil reserves and dependency on coal, especially South Africa.

The significant difference between DCL and ICL is that during the DCL process, the majority of the macro-structural components of the coal matrix remain unaltered, whereas, in the ICL process, the organic components of coal are broken down to generate a mixture of light gases such as CO, H_2, CO_2 and CH_4.

The dominant products generated from DCL are mixed oils, gases and a small quantity of solid residue, depending on the chemical, physical and petrographic properties of the coal and the solvents used. The mixed oils produced by the DCL process have to be upgraded before they can be used as transportation fuels. Upgrading is done through catalytic cracking and heating of the oil to generate different products such as vacuum gas oil, kerosene, naphtha,

and diesel. Products generated from the upgrading of DCL oil are similar to those of crude petroleum oil. The oil obtained during DCL is the most wanted product and influences the economy of the liquefaction process. A good quality coal or density-separated fractions of coal that will give high oil yields are vital for commercialisation of the liquefaction technology. The DCL process has the following benefits: the production of a variety of hydrocarbons; similarity of the oil product to that of crude oil; an increase in the economy of the country; and finally, some environmental benefits.

Direct coal liquefaction is performed in three stages: (1) coal is first digested with a solvent rich in hydrogen, which also serves as a carrier; (2) coal is thermally dissolved under mild temperature and pressure; and (3) hydrogen is transferred to dissolve coal products. The schematic route for the DCL process is given in Figure 2.3.

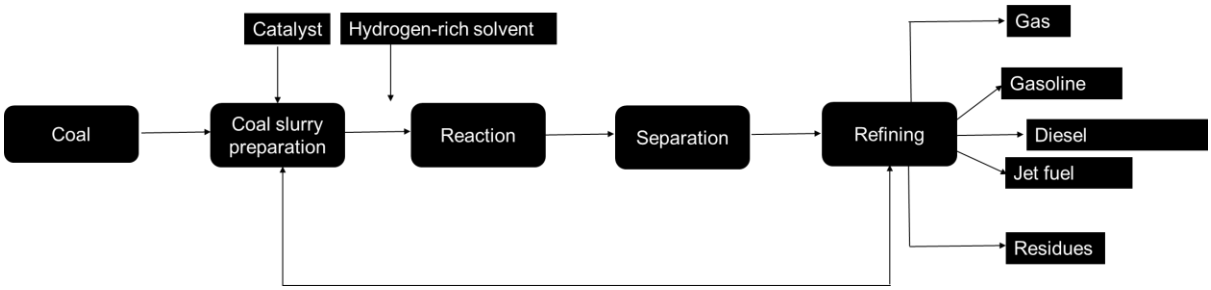

Figure 2-3: Direct coal liquefaction route to transport fuel (adapted from Deutsche Bank [98])

2.3.4.3 Factors affecting direct coal liquefaction

Various factors that influence the yield of the different products during the direct liquefaction of coal have been pointed out by researchers. These factors are listed and discussed below.

- **Temperature**

Temperature is one of the main factors during liquefaction that affect the formation of free radicals and afterwards influence free radical reactions. DCL involves, firstly, the dissolution of coal in a hydrogen-rich solvent, and secondly, the disintegration of the macromolecular components of coal into different radicals under mild temperature conditions. These compounds (radicals) are stabilised and hydrogenated to produce components with low molecular weights at temperatures between 350–450˚C.[92,99-101] Temperature helps in the thermal breakdown of the C-C bonds in the coal molecule and further increases the reaction rate. Elevated temperatures also assist in intensifying the natural breakdown of coal macromolecules into liquids. A further increase in temperature could disintegrate the macromolecular structure of coal, which will favour the formation of gases.

Several investigators have studied the influence of temperature during DCL.[99--104] Flatman-Fairs and Harrison[100] studied the DCL of UK bituminous coal, Spanish lignite and a blend of both coals at 380–420˚C. Their results showed that an increase in the liquefaction temperature from 380 to 400˚C favoured the production of oil by increasing secondary cleavage reactions. They also found that a further rise in liquefaction temperature to 450˚C favoured the formation of coke. Recently, Cai et al.[101] studied liquefaction of lignite from China in a tube reactor under a CH_4 atmosphere, at a temperature ranging from 400–800˚C with a variation in residence time from 4.5 to 11.2 s and pressure from 10 to15 MPa without a catalyst. They observed that as temperature increased, the effectiveness of the DCL process increased. Their reported conversions were found to increase from 4.8% at 400˚C to 25.4% at 750˚C at a pressure of 10 MPa CH_4, with a residence time of 10.0 s. A decrease in the oil yield was observed when the temperature was increased from 750˚C to 800°C. They concluded that temperature and residence time are important factors affecting the carbon conversion of coal and product distribution during the liquefaction process. In a similar investigation by De Marco et al.[103] into the behaviour of Spanish sub-bituminous coal during liquefaction, using tetralin as a solvent, at temperatures ranging from 400 to 475°C, the authors found that an increase in liquefaction temperature led to an increase in the formation of free radicals. The optimal temperature for a high oil yield using the specific coal sample and conditions was found to be 420°C.

- **Solvent**

The efficiency of selective liquefaction depends not only on the rank of coal but also on the solvent types.[105,106] The solvents used in coal liquefaction can be generally classified into four types depending on their effects on coal macromolecular structure. They are reactive, degrading, specific and non-specific solvents.

Reactive solvents are those that can react with the coal matrix during the liquefaction process. The reactive solvents can be subdivided into two groups: non-donor solvents and donor solvents. Examples of a non-donor solvent include decalin, pyrene, and fluoranthene, while common donor solvents are tetralin, tetrahydrofluoranthene and dihydroanthracene.

Degrading solvents are those solvents that decompose and produce hydrogen free radicals that react with the fragments from the coal matrix. Degrading solvents can extract up to 90% of the available liquid part of coal at temperatures higher than 200°C. Degrading solvents are unique and different from other solvents because of the high percentage recovery of the solvent after liquefaction. Some commonly used degrading solvents include phenanthridine and anthracene. Liquefaction using reactive and degrading solvents are mainly performed at high temperatures.

Specific solvents can react with the coal macromolecular structure at low temperatures. These solvents include pyridine and n-methyl-2-pyrrolidone. Specific solvents can dissolve about 20–40% of coal at 200°C.

Non-specific solvents can dissolve coal structures at lower temperatures compared to specific solvents. Examples of non-specific solvents include alcohol, benzene, chloroform, and acetone. Both specific and non-specific solvents are electron donors, and both can dissolve coal macromolecular structures at low temperature.

Some researchers have studied the effect of solvents during coal liquefaction.[107-115] Sakata et al.[114] investigated the role of non-donor solvents in the transfer of hydrogen during the liquefaction process using Australian brown coal. Three polycondensed aromatic hydrogen-carbon solvents (pyrene, fluoranthene, and anthracene) were used in their study in combination with tetrahydrofluoranthene. Results from their research showed that non-donor solvents, pyrene and fluoranthene, gave a lower yield when compared to the yield achieved with tetrahydrofluoranthene, which is a donor solvent. A higher yield was achieved when the non-donor and donor solvents were mixed, i.e. a mixture of tetrahydrofluoranthene with pyrene or fluoranthene. Sakata et al.[114] concluded from their study that the higher yield obtained from the mixture of the two solvents could be a result of the non-donor solvent assisting in the swelling of the coal matrix, which would in turn aid in the distribution of hydrogen donor solvents into the coal and further dissolve the coal macromolecular structure.

Similar research has also demonstrated some synergistic effects through the use of donor and non-donor solvents.[106-109] Chiba et al.[110] studied liquefaction of Yallourn coal using a binary system solvent. The two solvents used in their study were tetralin and a polynuclear aromatic compound (phenanthrene). From their study, they demonstrated that the addition of phenanthrene facilitated the hydrogen transfer reaction from tetralin to the coal fragments. Kuznetsov et al.[108] studied the synergistic behaviour between a reactive donor solvent (tetralin) and a non-specific solvent (alcohol) using Ashinsk brown coal. They found that there were synergistic properties when the two solvents (tetralin and methanol) were mixed during liquefaction. They attributed the synergistic behaviour to the ability of the alcohol solvent to cause swelling of the coal structure, thereby enhancing the reactivity of the coal fragment to the reactive hydrogen donor, tetralin.

Mochida et al.[112] studied the role of donor solvents during liquefaction of Australian coal under 1 MPa pressure and N_2 atmosphere with poly-hydrogenated condensed aromatics using tetrahydrofluoranthene, octahydroanthracene, hexahydroanthracene, and dodecaherotriphenylene. Results from their study showed that the yield of oils and asphaltenes at 450 °C with a 5 min residence time and a liquid to solid ratio of 1:1 were

hexahydroanthracene, 35%; dodecaherotriphenylene, 40%; octahydroanthracene, 50%; and tetrahydrofluoranthene, 40%. In a similar study by Mochida et al.[113], synergistic effects between solvents were investigated using Australian brown coal and a mixture of tetrahydrofluoranthene and octahydroanthracene.

Non-donor solvents have been shown by Sakanishi et al.[107] to be suitable during liquefaction. They investigated the liquefaction of brown coal and sub-bituminous coal using a NiMo sulphide catalyst. Tetralin (donor) and anthracene (non-donor) were used as solvents during the process. They found that the non-donor solvent achieved a higher conversion when compared to the donor solvent in the presence of the catalyst. Water has been proven by other investigators to be useful as a co-solvent during liquefaction and could assist in catalyst dispersion during the liquefaction process.[115-117]

Tetralin has been proven as a useful solvent to convert high-mineral matter bituminous coal into useful products via liquefaction. However, most of these investigations were performed on a laboratory scale.[92,96] Tetralin is an organic solvent, which serves as a hydrogen donor during liquefaction. It has high thermal stability and good hydrogen donor capabilities.

The hydrogen that is donated by the solvent during the liquefaction process stimulates the liquefaction process through the stabilisation of the free radicals that are produced by the thermal cracking process.[118] The solvent thus acts as a means of transferring hydrogen to coal during the liquefaction process.[119]

- **Pressure and atmosphere**

A high pressure during the coal liquefaction process has a significant influence because maintaining the pressure above the optimum pressure of the process will aid the dissolution and hydrolysis of the coal macromolecule. High pressures, however, assist in keeping the solvents and products in the liquid phase, preventing the accumulation of coke on the walls of the reactor, and facilitate hydrogenation reactions. The density of the solvent may be increased at higher pressures, and this can aid in an even penetration and distribution of the solvent in the coal structure, thereby facilitating a better extraction efficiency. Some researchers have shown that when an appropriate solvent with a high boiling point and a catalyst are used during liquefaction, high pressures may be required.[120-123]

Although an increase in pressure will favour the conversion of coal to liquid products, investigators have demonstrated that optimum pressure exists above which no further increase in the production of oil is observed.[101,113,124] In a study by Mochida et al.[113] on the role of donor solvents during liquefaction of brown coal from Australia, where they varied the operating pressure from 17.4 to 26.1 MPa, no changes in the oil yield and carbon conversion

were observed. In a similar study by Cai et al.[101] on the rapid liquefaction of lignite coal between 10 and 15 MPa without a catalyst, they found that the oil yield at 10 MPa was 25.4% and 26.1% at 15 MPa.

Different atmospheres (N_2, H_2, CO, CO-H_2 mixtures, H_2-H_2O, CH_4, CH_4-H_2 and syngas-H_2O) can be used during DCL.[113,124-129] Mochida et al.[113] found in their study that the use of a N_2 atmosphere in the presence of a suitable solvent could achieve high oil yields and conversions. However, most DCL processes are carried out in a high-pressure hydrogen atmosphere. Hydrogen is a good capping agent that can aid in preventing coke formation and assist in radical and fragment conversion to liquid products during liquefaction. The hydrogen bond in molecular hydrogen is very stable and can only break under severe conditions and in the presence of a catalyst. The H_2 molecule can decompose into reactive atomic hydrogen using specific catalysts and conditions.[127] Hata et al.[125] studied the effect of a $FeSO_4$ catalyst using syngas-water as a hydrogen source during liquefaction of low-rank coal. Results from their study demonstrated that a high product yield was achieved when a syngas-water mixture was used as a solvent in the presence of a catalyst.

Water vapour used as an atmosphere during the liquefaction process has gained considerable interest, although some researchers have demonstrated that water could have an undesirable influence. This could be as a result of water being problematic to catalytic activity and further enhancing the formation of CO_2. However, other researchers have disagreed and showed that water could be a suitable solvent during the DCL process.[129] Watanabe et al.[129] studied coal liquefaction in a syngas-water system in the presence of a synthetic pyrite catalyst. Results obtained from their study showed that a high carbon conversion could be achieved at lower liquefaction temperatures (375°C). They attributed the higher carbon conversion to the formation of hydrogen by the water shift gas reaction, where the hydrogen generated in-situ had a better reactivity for coal liquefaction when compared to the pressurised hydrogen.[127-129] Recently, Shui et al.[127] studied the influence of different atmospheres on the liquefaction of lignite. They found that a high carbon conversion was achieved when water was used as solvent under CO atmosphere. Nonetheless, the conversion was low when compared to the results obtained when tetralin was used as solvent under N_2 atmosphere.

Methane has been established to be a useful atmosphere during coal liquefaction processes.[42] The co-presence of hydrogen can improve the utilisation of CH_4 as a gas during liquefaction.[130] Yan et al. [130] studied the reaction of coal with methane and a mixture of CH_4-H_2 as atmospheres in the presence of a catalyst. Results from their study showed that a 43% carbon conversion was achieved when CH_4 was used, and 51.5% carbon conversion was achieved when the CH_4 was mixed with hydrogen.

- **Catalyst**

The investigation of catalysts with high activity is vital for the development of DCL technology. Most inorganic elements in the periodic table have been studied and have shown to be active catalysts in the DCL process.[131] Pyrite and other Fe-containing minerals in coal could catalyse the coal liquefaction process. Iron-containing catalysts (pyrite (FeS), troilite (FeS), pyrrhotite ($Fe_{1-x}S$), iron oxides, iron sulphate, and iron hydroxide) have been widely used due to their lower environmental impact and low cost.[96] The catalyst facilitates the production of active hydrogen atoms and promotes the circulation of hydrogen atoms during the liquefaction process.[114] One of the factors influencing the activity of a catalyst is the coal particle size. Various investigators[131,132-134] claimed that higher catalytic activity is achieved by finer particles, which leads to a better dispersion of the catalyst.

Researchers have conducted studies on the effectiveness of catalysts on coal liquefaction.[115,116,131,132,134-139] Ikenaga et al.[131] investigated coal hydro-liquefaction using a highly dispersed catalyst, namely, organometallic carbonyl compounds: $Fe(CO)_5$-S, $Mo(CO)_6$-S and $Ru_3(CO)_{12}$. Results from their investigation showed that higher conversions and oil yields were achieved when catalysts were used as compared to the un-catalysed process. Liu et al.[133] investigated in-situ impregnation of the iron-based catalyst during the DCL process. In their study, the coal was mixed with a Na_2S and $FeCl_3$ solution. This step was accompanied by washing, filtration, and drying. Results obtained from their study showed that catalysed samples had higher conversions and high oil yields relative to un-catalysed reactions.

Kaneko et al. [136] studied the transformation of iron catalysts into an active phase during coal liquefaction. They used five different iron-based catalysts (α-FeCOOH, γ-FeCOOH, ferrihydrite, limonite, and pyrite) that were transformed into pyrrhotite. From their study, they observed that γ-FeCOOH showed high catalytic activity and could transform into pyrrhotite with small crystalline sizes under the conditions used during the liquefaction process.

Song et al.[115] studied the dispersion of a bimetallic catalyst obtained from $Mo_2Co_2S_4(Cp)_2(CO)_2$ (Cp=cyclopentadiene), also known as MoCo-TC2. Results obtained from their study indicated that the bimetallic catalyst produced from MoCo-TC2 had a higher activity when compared to those obtained from a mixture of metallic carbonyl compounds ($Mo(CO)_6$ + $Co_2(CO)_8$) and sulphur. Song et al.[115] concluded that the bonding between Mo, Co, and S could result in the bimetallic catalyst having a good catalytic activity.

Hulston et al.[137] studied the effectivity of a nickel molybdate catalyst on the hydrogenation of brown coal without solvent addition. They observed that pre-impregnation of aqueous nickel acetate and ammonium heptamolybdate into brown coal produced a high conversion of

approximately 92% at 400˚C. They claimed that the catalysts could have a synergistic effect during coal liquefaction, leading to higher conversions and oil yields when used in combination. Similar studies have shown some synergistic effects between two catalysts such as SO_4^{2-}/Fe_2O_3 and SO_4^{2-}/ZrO_2 during coal liquefaction.[138,139] Wang et al.[139] studied the catalytic behaviour of a SO_4^{2-}/ZrO_2 superacid catalyst. Liquefaction experiments were conducted at 400˚C, 30 min of residence time with an initial pressure of 4 MPa. Their results showed that a carbon conversion of 76.3% and oil yield of 32.9% was achieved.[138]

- **Heating rate**

The production of liquid products during the liquefaction process also depends on the heating rate. Song et al.[102] conducted a study on the effect of heating rate using the temperature-programmed liquefaction (TPL) on lignite and sub-bituminous coal samples. The TPL process investigated involved soaking of the sample in the solvent at 200˚C with a holding time of 15 min, a slow heating rate of 7°C/min until the final temperature (300–425°C). The reaction mixture was held for 30 min at the final temperature. The main reason the authors used the TPL soaking method was to allow the solvent to penetrate the coal matrix before it was applied as a hydrogen donor. Results of their study showed that the conversion for the TPL process was 77.8–81% at 400°C for the lower heating rate, compared to the conversion of 71–72.5% obtained from fast heating.[102] Song et al.[102] concluded in their study that by using a lower heating rate for the TPL process, the coal efficiently liquefied and they attributed this to the rate at which the weaker bonds were cleaved while crosslinking of the free radicals were reduced.

Huang and Schobert[104] conducted a study using three methods, namely temperature-programmed liquefaction (TPL), single-stage liquefaction (SSL), and temperature stage liquefaction (TSL), with ammonium tetrathiomolybdate as a catalyst with a non-reactive solvent. Results from their study showed that the TPL method achieved the highest conversion of 90.9%, while TSL and SSL had conversions of 89.5% and 84.4%, respectively.

- **Mineral matter in coal**

Mineral matter as an inherent part of coal has been recognised by various researchers to play an active role during DCL, by acting as catalysts for the transformation of organic matter.[140,141] Gray[142] studied the effect of inherent mineral matter during hydrogenation of coal at 450°C in an autoclave at a hydrogen pressure of 10 MPa. Results of his study showed that mineral matter in the coal could facilitate the reduction in coal particle agglomeration, and subsequently facilitate diffusion of hydrogen to the areas of bond ruptures. In a similar study by Barraza et al.[142] on the liquefaction of beneficiated (reduction of mineral matter

concentration) coal samples from Colombia, South America, they observed that there was a remarkable reduction in several liquefaction products (total conversion and oil yield) from the beneficiated coal in comparison to the parent coal sample. They attributed the decrease in the product yields to the removal of mineral matter by coal beneficiation.

Mineral matter has been shown to play a useful role during DCL.[142,144,145] Pyrite in coal could catalyse the DCL process. Gözmen et al.[145] studied the effect of pyrite on coal samples that were demineralised with HNO_3. They observed that the treated samples showed lower carbon conversion and oil yields when compared to the untreated coal samples. Their findings strongly support the catalytic effect of pyrite during the DCL process. Mukherjee and Chowdhury[144] conducted a study to demonstrate the catalytic influence of mineral matter in coal during hydrogenation and observed that conversion and oil yield increased as the mineral matter content (Fe, Ti) increased. They also showed that kaolinite minerals in coal could be used as a catalyst during DCL. They demonstrated this by studying the correlation between kaolinite concentration and total carbon conversion during DCL and found that an increase in the concentration of kaolinite in coal led to an increase in carbon conversion and oil yield. To further illustrate the catalytic effect of kaolinite, Gray[142] impregnated kaolinite in a coal sample before liquefaction. Results of this study showed that there was an increase in the total carbon conversion and oil yield. Based on this observation, it was established that the inherent mineral matter in coal could contribute to the breakdown of the coal structure, facilitate carbon conversion, and increase oil yield during DCL.

Although mineral matter in coal could influence the product yields during liquefaction, it can also have a negative influence on DCL, for instance, it could have a catalytic poisoning effect and ash-related issues.

- **Macerals and coal rank**

The rank of coal and maceral content plays a significant role in the conversion and yield obtained during direct liquefaction of coal.[146-148] As the coal rank increases, the solubility of coal in a solvent decreases, as carbon content increases from 85 to 89% (dry-ash-free-basis) regardless of temperature and solvent used.[149] Low-rank (lignite, sub-bituminous and bituminous) coals have been shown to exhibit higher yields of oil and conversion during the liquefaction process when compared to anthracite coal. Similarly, the petrographic nature of the coal has been shown to have a vital influence on the product yields during liquefaction.

Various researchers[150-153] have demonstrated that there is a direct correlation between the dissolution of coal in a solvent and the petrographic properties of the coal. Other investigators have shown that liptinite and vitrinite macerals in coal contain the majority of the extractable fractions, while the inertinite macerals in coal have a lower proportion of extractables.[4,149,154] The effectiveness of direct coal liquefaction significantly depends on the thermoplastic and dissolution properties of the reactive macerals.[152]

2.3.5 Products from direct coal liquefaction

The products obtained from direct coal liquefaction include mixed oils, which are the most wanted products, gases, asphaltenes, pre-asphaltenes and solid residues. A discussion of the various liquefaction products and some previous researches on liquefaction products are presented in this section.

The carbon conversion and oil yields generated during coal liquefaction are dependent on parameters such as the petrographic of the coal, heating rate, temperature, etc. This study focuses specifically on the residues generated during the direct liquefaction of coal. A summary of previous studies conducted using direct coal liquefaction is presented in Table 2.1.

Table 2-1: Operating conditions, coal types, solvents used, carbon conversion, and oil yields during direct coal liquefaction.

Solvent	Temperature (°C)	Coal type	Carbon conversion (%wt.)	Oil yield (%wt.)	Particle size	Reference
Phenanthrene	400	Float fraction of bituminous coal Vitrinite, liptinite and inertinite UK	86.7–92	–	0.5–1.0 mm	Cloke et al.[17]
Tetralin	385–445	Elkhorn coal	34–84.4	5–33.7	100 µm	Keogh et al.[154]
Tetralin	350–425	Chinese brown coal	70–80	30–60	154 µm	Yan et al.[155]
Recycle oil	400–460	Chinese bituminous coal	65 – 90	30 – 65	–	Li et al .[156]
Tetralin	200–400	Australian brown coal	65 – 80	25 – 40	-	Miura et al.[92]
Tetralin	380–420	Sub-bituminous coal	51 – 70.2	17.6 – 32.7	-	Shui et al.[157]
Methylnaphthalene	360	Bituminous coal	60 – 80	48.5 – 57.6	150 µm	Yoshida et al. [158]
Anthracene oil	380–420	Bituminous coal	70 – 80	-	75 µm	Barraza et al. [143]
Tetralin	200–350	Chinese lignite	20.6 – 70.2	51.69	-	Hao et al.[159]
Phenol	320–360	Waterberg bituminous	49.5	26.3	150 µm	Sehume et al.[92]
Tetralin	380–430	Three Chinese coals (ranks)	79 – 87.1	54 – 76.4	212 µm	Wang et al.[160]

- **Mixed oil**

Mixed oils are the preferred products during direct coal liquefaction. The mixed oils produced during liquefaction need refining before they can be used as a transportation fuel. A summary of previous studies conducted using direct coal liquefaction and the resulting oil yields is presented in Table 2.1. Sehume et al.[91] showed that an increase in liquefaction temperature led to an increase in the oil yield. The increase in the oil yield was attributed to the activation of the solvent at a higher temperature which produced a substantial amount of hydrogen atoms (hydrogen radicals - H^*). Jin et al[150] and Wang et al[160] showed that there was a direct correlation between vitrinite macerals in coal and high oil yields. This indicates that a higher amount of vitrinite in coal results in a higher amount of oil when compared to coals with higher amounts of inertinite. [150]

- **Gaseous products**

Gases are one of the groups of products obtained during coal liquefaction. These gases originate from molecular fragments that are weakly bonded to the coal matrix. The gaseous compounds are liberated at temperatures ranging from 200 to 375°C. The DCL process at elevated temperature produces high gas yields, as a result of the rupture of lighter hydrocarbons and secondary reactions, such as cracking, methanation and steam reforming.[161,162] The primary liquefaction gaseous compounds include H_2, CO, CO_2 and some hydrocarbon compounds (C_mH_n), such as methane, ethane, and propane.

- **Liquefaction residues**

Some estimations have shown that after the separation of liquefaction products, about 60% is mixed oil, 15% are gases, and solid residues represent approximately 25% of the liquefaction products.[149,164] The product yields obtained after coal liquefaction are, as previously discussed, dependent on the physical, chemical and mineralogical properties of the parent coal. In liquefaction technology, solid residues generated after the liquefaction process, are generally regarded as waste. These residues, if not used, may cause environmental problems, such as dust, spontaneous combustion, acid mine drainage, etc.

The useful utilisation of the solid residues produced after liquefaction will improve the economy of the process and decrease environmental pollution that would have been associated with the disposal of these residues. Converting coal liquefaction residues (CLR) to useful products and having an insight in the molecular, structural, chemical and physical compositions of the thermal processing products generated (liquid (tar) and solid (residue char)) from the residues are essential to understand the effective utilisation of CLR. Cui et al.[165] investigated the relationship between operating conditions and properties of residues and observed that

temperature and residence time are the key factors that could influence these properties. Residue products from liquefaction processes and feed coal may have certain similarities in terms of carbon content, calorific value, and a low H/C atomic ratio. The residue's composition may be different from coal due to the slightly higher concentration of asphaltenes adhering to the surface and mineral matter content when compared to the feed coal.[166]

Table 2.2 summarises some of the proximate and ultimate analyses results for the residues produced from liquefaction of coal as reported by different researchers.[91,164,165,172-178] This table shows that the coal liquefaction residues have a relatively high percentage of carbon, hydrogen, oxygen, slightly lower H/C atomic ratios and slightly lower percentages of organic sulphur when compared to their starting material. Proximate analysis also shows that the residues have a lower percentage of moisture, higher percentages of volatile matter and higher ash yields than those of the feed coal before liquefaction. The chemical properties such as fixed carbon content, volatile matter content and ash yields of these residues are similar to those of the feed material used for thermochemical processes.

Chu et al.[164] reported that liquefaction residues contained some quantity of organic matter with high boiling points similar to heavy oil and asphaltenes, and another quantity of a carbon-rich fraction, such as unreacted coal, minerals, high polymeric compounds and the remaining liquefaction catalysts. These residues thus contained a slightly higher amount of C, H, N, O and S, and mineral matter.[165] Based on the chemical properties highlighted by other investigators (Table 2.2), these residues may be a suitable feedstock for further thermochemical processing (pyrolysis and gasification).

Due to the high organic matter content, various investigators[166,167,168] have conducted studies on the utilisation of the residue produced from the coal liquefaction process. Other investigators[169-173] have studied the use of coal liquefaction residues focusing on the hydrogenation, synthesis and preparation of carbon nanofiber/carbon foam composite material.[169-173] In spite of these studies, not much research has been done on the use of these residues for pyrolysis and gasification. Studies done on the utilisation of liquefaction residues during thermochemical processing (pyrolysis and gasification) are discussed in Section 2.4.

Table 2-2: Summary of reported proximate and ultimate analyses results and H/C atomic ratios of coal liquefaction residues

	Proximate analysis (%wt.)			Ultimate analysis (%wt., daf)						
Sample	TM_{adb}	Ash_{daf}	VM_{daf}	C	H	N	S	O(diff.)	H/C	References
DCLR (DCL pilot plant Shenhua)	0.1	14.9	36.9	89.8	5.2	1.0	2.3	1.7	0.7	Xu et al.[172]
DLR (Shenhua 100 kg/day unit)	0.1	11.6	47.7	84.4	6.4	1.5	0.2	7.5	0.9	Chu et al.[164]
DLR from Huolinhe lignite coal	3.7	9.1	43.4	67.4	4.7	1.2	0.3	26.4	0.8	Zou et al. [173]
DLR from Xilinguole lignite coal	0.2	15.8	40.8	61.7	3.8	0.7	0.8	33.0	0.7	Zou et al. [173]
DLR (0.1T/day DCL unit using SH coal)	0.4	11.9	50.8	84.5	5.7	1.2	1.7	6.9	0.8	Li et al. [174]; Li et al. [176]
DLR (Chinese coal)	0.1	18.5	33.4	84.1	4.8	1.1	3.1	6.9	0.7	Xiao et al. [170]
DCLR (6 t/d DCL using Shenhua coal)	0.1	12.5	45.2	89.8	5.2	1.0	2.3	1.7	0.7	Xu et al. [175]; Lv et al.[176]
DLR (Using Wyoming sub-bituminous coal)		27.0		85.8	5.3	1.0	2.8	5.1	0.7	Sugano et al.[178]
Chinese bituminous coal (Yanzhou) residue	0.8	12.7	33.0	75.4	3.7	1.4	3.8	15.7	0.6	Cui et al.[165]
Chinese bituminous coal (Fenxi) residue	0.7	15.1	24.6	86.7	4.6	1.5	0.8	6.4	0.6	Cui et al. [165]
Bituminous South African coal residue	2.6	20.6	28.5	82.2	4.8	2	1.1	9.9	0.7	Sehume et al. [91]

2.4 The utilisation of liquefaction derived residues in thermochemical conversion processes

This section focuses on previous studies regarding the utilisation of liquefaction residues for pyrolysis and gasification processes.

2.4.1 Summary of previous studies on the use of liquefaction residues for pyrolysis

Luo et al.[179] studied the effect of pyridine extraction on the tar properties during pyrolysis of a solvent extracted bituminous coal. In their study, the bituminous coal was first demineralised, and extraction was performed on the acid-treated bituminous coal sample using pyridine as a solvent. The pyrolysis of the coal and the solvent extracted residue was studied using a thermogravimetric (TG) analyser and a fixed bed reactor. Results of their study indicated that the pyrolysis tar yield of the residue was lower when compared to those obtained from the feed coal samples. When the samples were treated under H_2 atmosphere, the residue's tar yield was doubled in comparison to those obtained when N_2 was used. Luo et al.[179] attributed the increase in tar yield under N_2 atmosphere to pore growth during pyridine extraction. The pyridine liquefaction assisted in the faster diffusion of the hydrogen gas into the pore structure of the coal residue matrix and decreased the formation of polycondensation reactions.

Zou et al.[173] studied the influence of tetrahydrofuran extraction on a lignite coal sample during pyrolysis. In their study, the pyrolysis of two lignite coal samples and their tetrahydrofuran extracted residues at 450–700°C was investigated. Their results showed that the tetrahydrofuran derived residues exhibited higher gas and char yields with a lower pyrolytic water and tar yield when compared to the feed coal samples. Also, results from their GC-MS and the solid-state ^{13}C NMR analyses of the tars revealed that the tars generated from the residues contained more mononuclear aromatic, oxygen-containing groups, such as phenol, and higher aromaticity factors when compared to the feed coal samples.

Zhu et al.[180] examined the effect of the solvent extraction on the structure and pyrolysis behaviour of two Xinjiang coal samples. Before pyrolysis, pyridine solvent extraction was conducted on lignite and bituminous coal samples. Pyrolysis experiments were performed using a fixed bed reactor on the raw coal samples and their pyridine solvent extracted residues. It was observed from their structural analysis results that the pyridine-extracted residues' char samples showed an increase in pore volume and improved porosity in comparison to the feed coal chars. Results obtained from the pyrolytic product distribution of their samples showed that the pyridine derived residues exhibited higher gas yields and significantly lower tar yields when compared to the feed coal samples. They ascribed the increase in the pore volume of the residues to the removal of extractable organics in the pores.

These organics may be transformed into volatiles and colloidal products during pyrolysis. They concluded from their study that the liquefaction process assisted in increasing the number of active pores that were formed in the solvent extracted residues.

Xu et al.[181] studied the pyrolysis characteristics and kinetics of residues from the China Shenhua direct liquefaction plant. The pyrolysis tests were performed using TGA equipment. Results from their investigation showed that the residues from the plant exhibited catalytic behaviour under pyrolysis conditions. Kinetic analysis was performed on data obtained from their experiments using the distributed activation energy model (DAEM). The activation results derived from their model showed that the residues' samples followed a Gaussian distribution pattern with a pyrolysis activation energy of 87.6 kJ/mol.

Various investigators[172,175,177,182] have described co-pyrolysis of the liquefaction residues and coal. The liquefaction residues may act as a catalyst, an inhibitor, or show synergetic properties during co-pyrolysis.

Li et al. [177] investigated the properties of semi-coke from co-pyrolysis of lignite and direct liquefaction residues produced from Shandong coal. The pyrolysis study was conducted in a fixed-bed reactor under atmospheric pressure. Results from their study showed that the liquefaction semi-coke residues and the lignite semi-coke bonded to each other during the co-pyrolysis. The bonding of the two samples were ascribed to the melting and softening of the liquefaction residue during co-pyrolysis. It was also observed that the surface area and pore volume of the co-pyrolysed char samples increased when compared to the lignite semi-coke char sample. The co-pyrolysed samples showed an improved reactivity when compared to the lignite sample.

Xu et al.[172] investigated the effect of liquefaction residues on the physicochemical structure and combustion properties of chars obtained from co-pyrolysis of lignite with direct coal liquefaction residues (DCLR). Char samples of different proportions of lignite and DCLR were heated in a fixed bed reactor at 550°C. Results of their investigation revealed that the residues and lignite coal samples interacted, and both the yield of char and combustion reactivity of the co-pyrolysis samples were improved. The results of the char generated from the lignite samples, and the samples with added residues were compared. The results from the comparative method of studying showed that the dosing of the samples resulted in a higher aromaticity and ordered structure of the co-pyrolysis char than the lignite char. They also observed from their study that the reactivity of the residues improved when lignite samples were blended with the coal liquefaction residues. The improvement in the reactivity of the blended samples was attributed to the co-pyrolysis char having a unique structure which was different from the char obtained from the lignite.

Xu et al.[175] examined the interaction and kinetics during co-pyrolysis of derived liquefaction residues with lignite coal. Different ratios (10:0, 8:2, 6:4, 2:8, and 0:10) of liquefaction residues to lignite were used in their investigation. Results from their experiments revealed that the volatile matter contents of the co-pyrolysed samples increased at lower temperatures (200–500°C) and reduced at higher temperatures. The increase in the volatile matter contents of the co-pyrolysed samples was attributed to heavy oil molecules, and some of the asphaltenes were adhering to the surface of the liquefaction residue. They concluded in their study that the reactivity of the co-pyrolysed samples increased through the addition and mixing of the residues with the lignite samples.

Li et al.[177] examined the co-pyrolysis of lignite and Shandong coal liquefaction residues. Their study was aimed at increasing the tar yield and quality of the tars generated. Their co-pyrolysis experiments were conducted under atmospheric pressure using a fixed-bed reactor with residue dosages of 4, 7, and 15%wt. at 550°C. Results showed that there was an interaction between the residues and the lignite coal samples. This interaction aided in increasing the tar yields of the co-pyrolysed samples when compared to the lignite coal samples. They concluded from their investigation that the increase in the tar yield of the co-pyrolysed samples was attributed to a mass transfer process and hydrogenation of the organic constituents in the residues during the co-pyrolysis.

2.4.2 Summary of previous studies on the use of liquefaction residues for gasification.

Chu et al.[164] studied the steam gasification properties of residues obtained after liquefaction of coal, and the solvent extracted residue chars were compared with the char from the feed coal. Results from their study show that the liquefaction residue char has a lower gasification reactivity when compared to the feed coal char. The lower reactivity of the char from the residue was attributed to the unreacted coal, heavy oil, and condensation products during liquefaction.

Yan et al.[155] investigated the direct liquefaction of Chinese brown coal (Yannan), and subsequent CO_2 gasification of the residue under moderate conditions in a laboratory-scale autoclave. The effect of H_2 pressure, temperature, and product distribution were studied. A thermogravimetric analyser (TGA) was used to study the CO_2 gasification reactivity of the residues obtained from the liquefaction process. Results obtained from their liquefaction experiments showed that oil yield and carbon conversion increased as the temperature of liquefaction increases. The gasification results of the residue samples showed a higher reactivity during CO_2 gasification when compared to the raw coal under the same conditions. The higher reactivity of the residue samples was attributed to the alkaline elements'

enrichment. They concluded that their study would serve as an efficient way of improving the economy of direct coal liquefaction plants.

Chu et al.[183] examined the gasification reactivity of Shenhua liquefaction residues using steam and CO_2. In their study, the reactivity of Shenhua coal char and Shenhua liquefaction residues was compared in two different gasification atmospheres (CO_2 and steam) using a fixed-bed reactor. Their results showed that the reactivity of the coal char was higher in steam gasification when compared to the solvent extracted residue chars. The residue chars showed higher gasification reactivity in the CO_2 atmosphere. They reported that the difference in the reactivities in the two atmospheres could be attributed to the fact that the reactivity in steam was influenced by coal rank, and the CO_2 gasification reactivity of the residue chars was affected by the catalytic effect of the mineral matter.

Liu et al.[184] investigated the gasification and kinetics of char residues, extracted from the Shenhua direct liquefaction plants. A thermogravimetric analyser was used in examining the gasification kinetics. The gasification experiments were carried out on three coal residue chars using steam and CO_2. Results from their investigation revealed that temperature played a vital role in the gasification of the residue chars. They reported that the gasification reactivity of the char residues was improved in comparison to that of the coal sample. This could be attributed to the reduction in the carbon content and an increase in the pore volume of the residues from solvent extraction. Results of their gasification kinetics study showed that the shrinking core model adequately fitted the reactivity data. The authors concluded that the experimental results from the CO_2 and steam gasification of char residues could be well described by the shrinking core model.

Liu et al.[185] investigated the CO_2 gasification of liquefaction residues and petroleum coke while varying parameters such as temperature (900–1050˚C) and residue loading during co-gasification. A kinetic study was undertaken to understand the influence of residue loading on the gasification reactivity of the petroleum coke. Results of their study showed that the gasification reactivity was improved by the addition of residue to the petroleum coke. The catalytic influence was enhanced when the gasification temperature was increased. They concluded that a high temperature under the condition of chemical kinetic control increased the catalytic effect of the coal liquefaction residue, and the influence increased as residue addition increased.

Solvent extracted residues can also be used during hydrogenation. Li et al.[168] studied the hydro-treatment of a direct coal liquefaction residue and its components. Results revealed that a significant proportion of heavy liquid was found in the residue. Their results also indicated that hydro-treatment of the solvent extracted residue resulted in more of the lighter products

and less of the heavy products being extracted during the hydrothermal treatment process. FTIR and ^{13}C NMR analyses results showed an increase in hydrogen content and a decrease in the oxygen content of the hexane soluble fraction of the residue after hydro-treatment.

In a similar study, Li et al.[186] investigated the hydrogenation of heavy liquid from a DCLR produced from the Shenhua DCL plant using the Shenhua coal. They firstly investigated the stimulation of coal liquefaction in the presence of a Fe-based catalyst, and secondly, the online hydro-thermal treatment in the presence of a $NiMo/Al_2O_3$ catalyst. Results of their investigation indicated that the heavy liquids from DCLR could be hydrogenated using these two sets of experimental parameters, with the online hydro-treatment being more effective than the stimulated coal liquefaction. They suggested that hydrogenation of the toluene soluble and tetrahydrofuran soluble fraction of DCLR under the two conditions was possible, but the conversion to lighter products was undetectable under the coal liquefaction conditions.

2.5 Chapter 2 references

1. Ward, C.R. Coal Geology. *Encyclopedia of Physical Science and Technology,* 3rd ed.; Meyers R.A.; Ed.; Academic Press: New York, 2003; pp 45–77.

2. Ward, C.R. Coal Geology. In *Reference Module in Earth Systems and Environmental Sciences*; Elias, S.A., Alderton, D.H.M., Cochran, J.K., DellaSala, D.A., Faccenna, C., Goldstein, M.I., Lajtha, K., Marshall, S.J., Mather, T., Nehrenheim E., Schoof, J., Sinclair, H.D., Smith, P.N., Eds.; Elsevier, 2013; pp 1-30.

3. Meyers, R.A., Ed. *Coal Handbook*; Marcel Dekker: New York, 1981.

4. Schobert, H.H. *Chemistry of Fossil Fuels and Biofuels*; Cambridge University Press: Cambridge, New York, 2013; pp 396-413.

5. Speight, J.G. *The Chemistry and Technology of Coal*, 2nd ed.; Marcel Dekker: New York, 1994; Chapter 10, 12; pp 233-246; 277-294.

6. Matjie, R.H. Sintering and Slagging of Mineral Matter in South African Coals During the Coal Gasification Process. Ph.D. Thesis [Online], University of Pretoria, 2008. http://www.upetd.up.ac.za/thesis/available/etd-11112008-1259131/ (accessed April 30, 2018).

7. Ward, C.R. Analysis and Significance of Mineral Matter in Coal Seams. *Int. J. Coal Geol*. **2002,** *50*, 135-168.

8. Mastral, A.M.; Callén, M.; Mayoral, C.; Galbán, J. Polycyclic Aromatic Hydrocarbon Emissions from Fluidised Bed Combustion of Coal. *Fuel*. **1995**, *74*, 1762-1766.

9. Liu, G.; Niu, Z.; Van Niekerk, D.; Xue, J.; Zheng, L. Polycyclic Aromatic Hydrocarbons (PAHs) from Coal Combustion: Emissions, Analysis, and Toxicology. In *Reviews of Environmental Contamination and Toxicology;* Springer: New York, NY, 2008; pp 1-28.

10. Miller, B.G. *Coal Energy Systems*; Elsevier, 2004.

11. Benfell, K.E.; Liu, G.S.; Roberts, D.G.; Harris, D.J.; Lucas, J.A.; Bailey, J.G.; & Wall, T.F. Modelling Char Combustion: The Influence of Parent Coal Petrography and Pyrolysis Pressure on the Structure and Intrinsic Reactivity of its Char. *Proceedings of the Combustion Institute*, **2000**, *28*(2), 2233-2241.

12. Everson, R.C.; Neomagus, H.W.J.P.; Kaitano, R.; Falcon, R.; Van Alphen, C.; & Du Cann, V.M. Properties of High Ash Char Particles Derived from Inertinite-Rich Coal: 1. Chemical, Structural and Petrographic Characteristics. *Fuel*. **2008**, *87*, 3082-3090.

13. Falcon, R.M.S.; Snyman, C.P. *An Introduction to Coal Petrography: Atlas of Petrographic Constituents in the Bituminous Coals of Southern Africa*; Johannesburg: The Geological Society of South Africa, 1986; p 27.

14. International Committee for Coal Petrology (ICCP). The New Inertinite Classification (ICCP System, 1994), *Fuel*. **2001**, *80*, 459–471.

15. Tsai S.C. *Fundamentals of Coal Beneficiation and Utilisation*; Elsevier: Amsterdam, 1982.

16. Jones, R.B.; McCourt, C.B.; Morley, C.; King K. Maceral and Rank Influences on the Morphology of Coal Char. *Fuel*. **1985**, *64*, 1460-1467.

17. Cloke, M.; Clift, D.A.; Gilfillan, A.J.; Miles, N.J.; Rhodes, D. Liquefaction of Density Separated Coal Fractions. *Fuel Process Technol*. **1994**, *38*,153-63.

18. International Committee for Coal Petrology (ICCP). The New Vitrinite Classification (ICCP System, 1994), *Fuel*. **1998**, *77*, 349-358.

19. Taylor, G.H.; Teichmüller, M.; Davis, A.C.F.K.; Diesel, C.F.K.; Littke, R.; Robert, P. *Organic Petrology*; Borntraeger: Berlin-Stuttgart, 1998.

20. Sýkorová, I.; Pickel, W.; Christanis, K.; Wolf, M.; Taylor, G.H.; Flores, D. Classification of Huminite: ICCP System 1994. *International Journal of Coal Geology*, **2005**, *62*, 85-106.

21. Pickel, W.; Kus, J.; Flores, D.; Kalaitzidis, S.; Christanis, K.; Cardott, B.J.; Misz-Kennan, M.; Rodrigues, S.; Hentschel, A.; Hamor-Vido, M.; Crosdale, P. Classification of Liptinite: ICCP System 1994. *Int. J. Coal Geol*. **2017**, *169*, 40-61.

22. Dyrkacz, G.R.; Horwitz, E.P. Separation of Coal Macerals. *Fuel*. **1982**, *61*, 3-12.

23. Thomann, H.; Silbernagel, B.G.; Jin, H.; Gebhard, L.A.; Tindall, P.; Dyrkacz, G.R. Carbon Radical Spin Dynamics in Isolated Vitrinite Coal Macerals. *Energy & Fuels*. **1988**,*1*,333-339.

24. Choi, C.Y.; Muntean, J.V.; Thompson, A.R.; Botto, R.E. Characterisation of Coal Macerals Using Combined Chemical and NMR Spectroscopic Methods. *Energy & Fuels*. **1989**, *3*, 528-533.

25. Choi, C.Y.; Dyrkacz, G.R.; Stock, L.M. Density Separation of Alkylated Coal Macerals. *Energy & Fuels*. **1987**, *1*, 280-6.

26. Benson, S.A.; Holm, P.L. Composition of Inorganic Constituents in Three Low-Rank Coals. *Ind. Eng Chem Prod Res Dev*. **1985**, *24*,145-149.

27. Benson, S.A. Laboratory Studies of Ash Deposit Formation During the Combustion of Western U.S. Coals, Ph.D. Thesis, The Pennsylvania State University, Pennsylvania, US, 1987.

28. Ward, C.R. Ed., *Coal Geology and Coal Technology*; Blackwell Scientific Publications: London, 1984; pp 40-113.

29. Ward C.R.; French, D. *Analysis and Significance of Mineral Matter in Coal, The Society for Organic Petrology, Short Course Notes*; The University of New South Wales, Sydney, NSW, Australia, 2004; pp 7-68.

30. Ahmad T.; Awan, I.A.; Nisar, J.; Ahmad, I. Influence of Inherent Minerals and Pyrolysis Temperature on the Yield of Pyrolysates of Some Pakistani Coals. *Energ Convers Manage*. **2009**, *50*, 1163-1171.

31. Matjie, R.H.; French, D.; Ward, C.R.; Pistorius, P.C.; Li, Z. Behaviour of Coal Mineral Matter in Sintering and Slagging of Ash During the Gasification Process. *Fuel Process Technol.* **2011**, *92*, 1426-1433.

32. Xu, M.; Yan, R.; Zheng, C.; Qiao, Y.; Han, J.; Sheng, C. Status of Trace Element Emission in a Coal Combustion Process: A Review. *Fuel Proces Technol*. **2004**, *85*, 215-237.

33. Yi, H.; Hoo, J.; Duan, L.; Tang, X.; Ning, P.; Li, X. Fine Particle and Trace Element Emissions from an Anthracite Coal-Fired Power Plant Equipped with a Bag-House in China. *Fuel*. **2008**, *87*, 2050-2057.

34. Helble, J.J.; Srinivasachar, S.; Boni, A.A. Factors Influencing the Transformation of Minerals During Pulverised Coal Combustion. *Prog Energy Combust. Sci*. **1990**, *16*, 267-279.

35. Reifenstein, A.P.; Kahraman, H.; Coin, C.D.; Calos, N.J.; Miller, G.; Uwins, P. Behaviour of Selected Minerals in an Improved Ash Fusion Test: Quartz, Potassium Feldspar, Sodium Feldspar, Kaolinite, Illite, Calcite, Dolomite, Siderite, Pyrite and Apatite. *Fuel*. **1999**, *78*, 1449-1461.

36. Vassilev, S.V.; Menendez, R.; Alvarez, D.; Diaz-Somoano, M.; Martinez-Tarazona, M.R. Phase-Mineral and Chemical Composition of Coal Fly Ashes as a Basis for Their Multicomponent Utilisation. 1. Characterisation of Feed Coals and Fly Ashes. *Fuel*. **2003**, *82*, 1793-1811.

37. Vassileva, C.G.; Vassilev, S.V. Behaviour of Inorganic Matter During Heating of Bulgarian Coals: 2. Subbituminous and Bituminous Coals. *Fuel Process Technol*. **2006**, *87*, 1095-1116.

38. Waanders, F.B, Govender A. Mineral Associations in Coal and Their Transformation During Gasification. *Hyperfine Interactions*. **2005**, *166*, 687-691.

39. Grigore, M.; Sakurovs, R.; French, D.; Sahajwalla, V. Mineral Matter in Coals and Their Reactions During Coking. *Int. J. Coal Geol*. **2008**, *76*, 301-308.

40. Suárez-Ruiz, I.; Ward, C.R. Basic Factors Controlling Coal Quality and Technological Behaviour of Coal. In *Applied Coal Petrology*; Elsevier, 2008; pp 19-59.

41. Van Dyk, J.C.; Melzer, S.; Sobiecki, A. Mineral Matter Transformation During Sasol-Lurgi Fixed Bed Dry Bottom Gasification: Utilisation of HT-XRD and FactSage Modelling. *Miner. Eng*. **2006**, *19*, 1126-1135.

42. Van Dyk, J.C.; Keyser, M.J.; Coertzen, M. Syngas Production from South African Coal Sources Using Sasol–Lurgi Gasifiers. *Int. J Coal Geol*. **2006**, *65*, 243-253.

43. Matjie, R.H.; Van Alphen, C.; Pistorius, P.C. Mineralogical Characterisation of Secunda Gasifier Feedstock and Coarse Ash. *Minerals Engineering*. **2006**, *19*, 256-261.

44. Matjie, R.H.; Li, Z.; Ward, C.R.; French, D. Chemical Composition of Glass and Crystalline Phases in Coarse Coal Gasification Ash. *Fuel*. **2008**, *87*, 857-869.

45. Hlatshwayo, T.B.; Matjie, R.H.; Li, Z.; Ward, C.R. Mineralogical Characterisation of Sasol Feed Coals and Corresponding Gasification Ash Constituents. *Energy & Fuels*. **2009**, *23*, 2867-2873.

46. Hattingh, B.B. Product Evaluation and Reaction Modelling for the Devolatilisation of Large Coal Particles. Ph.D. Thesis, North-West University, Potchefstroom, 2012.

47. Chen, H.; Li, B.; Zhang, B. Effects of Mineral Matter on Products and Sulfur Distributions in Hydropyrolysis. *Fuel*, **1999**, *78*, 713-719.

48. McKee, D.W. Mechanism of the Alkali Metal Catalysed Gasification of Carbon. *Fuel*, **1983**, *62*, 170-175.

49. Bunt, J.R.; Neomagus, H.W.; Botha, A.A.; Waanders, F.B. Reactivity Study of Fine Discard Coal Agglomerates. *J. Anal Appl Pyrol*. **2015,** *113*, 723-728.

50. Wang, J.; Yao, Y.; Cao, J.; Jiang, M. Enhanced Catalysis of K_2CO_3 for Steam Gasification of Coal Char by Using Ca $(OH)_2$ in Char Preparation. *Fuel*. **2010**, *89*, 310-317.

51. Zhang, L.X.; Kudo, S.; Tsubouchi, N.; Hayashi, J.I.; Ohtsuka, Y.; Norinaga, K. Catalytic Effects of Na and Ca from Inexpensive Materials on In-Situ Steam Gasification of Char from Rapid Pyrolysis of Low-Rank Coal in a Drop-Tube Reactor. *Fuel Process Technol*. **2013**, *113*, 1-7.

52. Sakawa, M.; Sakurai, Y.; Hara, Y. Influence of Coal Characteristics on CO_2 Gasification. *Fuel*, **1982**, *61*, 717-720.

53. Ye, D.P.; Agnew, J.B.; Zhang, D.K. Gasification of a South Australian Low-Rank Coal with Carbon Dioxide and Steam: Kinetics and Reactivity Studies. *Fuel*. **1998**, *77*, 1209-1219.

54. Hattingh, B.B.; Everson, R.C.; Neomagus, H.W.; Bunt, J.R. Assessing the Catalytic Effect of Coal Ash Constituents on the CO_2 Gasification Rate of High Ash, South African Coal. *Fuel Process Technol*. **2011**, *92*, 2048-2054.

55. England, T.; Hand P.E.; Michael, D.C.; Falcon, L.M.; Yell, A.D. *Coal Preparation in South Africa: The South African Coal Processing Society*; Natal Witness Commercial Printers: Pietermaritzburg, 2002.

56. Suárez-Ruiz, I.; Crelling, J.C., Eds. *Applied Coal Petrology: The Role of Petrology in Coal Utilisation*; Academic Press, 2008.

57. Van Krevelen, D.W. *Coal: Typology, Physics, Chemistry, Constitution,* 3rd ed; Elsevier: Amsterdam, 1981; pp 58-88, 111-126, 160-174, 309-341.

58. Okolo, G.N.; Neomagus, H.W.; Everson, R.C.; Roberts, M.J.; Bunt, J.R.; Sakurovs, R.; Mathews, J.P. Chemical–Structural Properties of South African Bituminous Coals: Insights from Wide-Angle XRD–Carbon Fraction Analysis, ATR–FTIR, Solid-State 13C NMR, and HRTEM Techniques. *Fuel*. **2015**,*158*, 779-792.

59. Borrego, A.G.; Marbán, G.; Alonso, M.J. G.; Alvarez, D.; Menéndez, R. Maceral Effects in the Determination of Proximate Volatiles in Coals. *Energy & Fuels*, **2000,** *14*, 117-126.

60. Gavals George, R.A. Random Capillary Model with Application to Char Gasification at Chemically Controlled Rates. *AIChE Journal*, **1980**, *26*, 577-585.

61. Maroto-Valer, M. M.; Love, G. D.; Snape, C. E. Relationship Between Carbon Aromaticities and HC Ratios for Bituminous Coals. *Fuel*, **1994**, *73*, 1926-1928.

62. Bell, D.A, Towler, B.F.; Fan, M. *Coal Gasification and Its Applications*; Elsevier: Amsterdam, 2010.

63. Ledesma, E.B.; Kalish, M.A.; Nelson PF, Wornat MJ, Mackie JC. Formation and Fate of PAH During the Pyrolysis and Fuel-Rich Combustion of Coal Primary Tar. *Fuel*. **2000**, *79*, 1801-1814.

64. Borah, D.; Barua, M.; Baruah, M.K. Dependence of Pyrite Concentration on Kinetics and Thermodynamics of Coal Pyrolysis in Non-Isothermal Systems. *Fuel Process Technol*. **2005**, *86*, 977-993.

65. Leckel, D. Diesel Production in Coal-Based High-Temperature Fischer–Tropsch Plants Using Fixed Bed Dry Bottom Gasification Technology. *Fuel Process Technol*. **2011**, *92*, 959-969.

66. Schobert, H.H. *The Chemistry of Hydrocarbons Fuel*; Butterworths: Cornwall, 1990.

67. Gavalas, G.R. *Coal Science and Technology 4: Coal Pyrolysis*; Elsevier: Amsterdam, 1982**.**

68. Jiang, J.; Wang, Q.; Wang, Y.; Tong, W.; Xiao, B. GC/MS Analysis of Coal Tar Composition Produced from Coal Pyrolysis. *B. Chem Soc Ethiopia*. **2007**, *21*, 229-240.

69. Menéndez, R.; Blanco, C.; Santamaria, R.; Domínguez, A.; Blanco, C.G.; Suelves, I.; Herod, A.A.; Morgan, T.G.; Kandiyoti, R. Effects of Air-Blowing on the Molecular Size and Structure of Coal-Tar Pitch Components. *Energy & Fuels*. 2002,*16*,1540-1549.

70. Schosberg, R.H. *Chemistry of Coal Conversion*; Plenum Press: New York, 1985.

71. Reichel, D.; Klinger, M.; Krzack, S.; Meyer, B. Effect of Ash Components On Devolatilization Behavior of coal in Comparison with Biomass: Product Yields, Composition, and Heating Values. *Fuel*. **2013**,*114*, 64-70.

72. Neves, D.; Thunman, H.; Matos, A.; Tarelho, L.; Gómez-Barea, A. Characterization and Prediction of Biomass Pyrolysis Products. *Prog Energy Combust. Sci*. **2011,** *37*, 611-30.

73. Hayashi, J.I.; Nakagawa, K.; Kusakabe, K.; Morooka, S.; Yumura, M. Change in Molecular Structure of Flash Pyrolysis Tar by Secondary Reaction in a Fluidized Bed Reactor. *Fuel Process Technol*. **1992**, *30*, 237-248.

74. Chen, H.K.; Li, B.Q.; Yang, J.I.; Zhang, B.J. Transformation of Sulfur during Pyrolysis and Hydropyrolysis of Coal. *Fuel*. **1998**, *77*, 487-493.

75. Longwell, J.P.; Rubin, E.S.; Wilson, J. Coal: Energy for the Future. *Progress in Energy and Combustion Science*. **1995**, *21*, 269-360.

76. Roets, L.; Strydom, C.A.; Bunt, J.R.; Neomagus, H.W.; Van Niekerk, D. The Effect of Acid Washing on the Pyrolysis Products Derived from a Vitrinite-Rich Bituminous Coal. *J. Anal Appl Pyrol*. **2015**, *116*, 142-151.

77. Roets, L.; Bunt, J.R.; Neomagus, H.W.; Strydom, C.A.; Van Niekerk, D. The Effect of Added Minerals on the Pyrolysis Products Derived from a Vitrinite-Rich Demineralised South African Coal. *J. Anal Appl Pyrol*. **2016**, *121*, 41-49.

78. Pretorius, G.N.; Bunt, J.R.; Gräbner, M.; Neomagus, H.; Waanders, F.B.; Everson, R.C.; Strydom, C.A. Evaluation and Prediction of Slow Pyrolysis Products Derived from Coals of Different Rank. *J. Anal Appl Pyrol*. **2017**, *128*, 156-167.

79. Minchener, A.J. Coal Gasification for Advanced Power Generation. *Fuel*. **2005**, *84*, 2222-2235.

80. Smith, P.J.; Smoot, L.D. *Coal Combustion and Gasification*; Plenum Press: New York, 1985.

81. Hebden, D.; Stroud, H.J.F. Coal Gasification Processes. In Elliot, M.A., Ed. *Chemistry of Coal Utilisation, Second Supplementary Vol*; Wiley-Interscience, 1981; pp 665-784.

82. Williams, R.H.; Larson, E.D. A Comparison of Direct and Indirect Liquefaction Technologies for Making Fluid Fuels from Coal. *Energy Sustain Dev*. **2003**, *7*, 103-29.

83. Mochida, I.; Okuma, O.; Yoon, S.H. Chemicals from Direct Coal Liquefaction. *Chemical Reviews*. **2014**, *114*, 1637-1672.

84. Höök, M.; Aleklett, K. A Review on Coal-To-Liquid Fuels and its Coal Consumption. *Int. J Energy Res*. **2010**, *34*, 848-864.

85. Vietor, R.H. The Synthetic Liquid Fuels Program: Energy Politics in the Truman Era. *Bus. Hist. Rev*. **1980**, *54*, 1-34.

86. Gibson, P. Coal to Liquids at Sasol, Presented at Kentucky Energy Security Summit, 2007.

87. Zhang, Y. Shenhua Coal Conversion Technology and Industry Development. In Proceedings of Global Climate and Energy Project International Workshop on Exploring the Opportunities for Research to Integrate Advanced Coal Technologies with CO_2 Capture and Storage in China, Stanford University: Palo Alto, 2005, pp 21-50.

88. Kabe, T.; Ishihara, A.; Qian, E.W.; Sutrisna, I.P.; Kabe, Y. *Coal and Coal-Related Compounds: Structures, Reactivity and Catalytic Reactions*; Elsevier, 2004, pp 269-301.

89. Kristiansen, A. *Understanding Coal Gasification*. IEA Coal Research: London, 1996.

90. Spath, P.; Dayton, D. *Preliminary Screening: Technical and Economic Assessment of Synthesis Gas to Fuels and Chemicals with Emphasis on the Potential for Biomass-Derived Syngas* [Online]; National Renewable Energy Laboratory: Golden, CO, USA, 2003; http://www.nrel.gov/docs/fy04osti/34929.pdf (accessed February 25, 2020).

91. Sehume, T.Z.; Strydom, C.A.; Bunt, J.R.; Schobert H.H. Effectivity of Phenol During Solvent Extraction of a South African Bituminous Coal Under Mild Conditions. *Energy & Fuels*. **2017**, *31*, 13655-13665.

92. Miura, K.; Shimada, M.; Mae, K.; Sock, H.Y. Extraction of Coal Below 350°C in Flowing Non-Polar Solvent. *Fuel*. **2001**, *80*, 1573-1582.

93. Oviawe, A.P.; Nicole, D. Ranking of Hydrogen Donor Reactivity by Model Acceptor and by Coal Conversion. *Trends Appl. Sci Res*. **2006**, *1*, 301-308.

94. Li, X.; Hu, H.; Jin, L.; Hu, S.; Wu, B. Approach for Promoting Liquid Yield Indirect Liquefaction of Shenhua Coal. *Fuel Process Technol*. **2008**, *89*, 1090-1095.

95. Shui, H.; Cai, Z.; Xu, C. Recent Advances in Direct Coal Liquefaction. *Energies*. **2010**, *3*, 155-70.

96. Johannes, I.; Tiikma, L.; Luik, H.; Tamvelius, H.; Krasulina, J. Catalytic Thermal Liquefaction of Oil Shale in Tetralin. *ISRN Chemical Engineering*. **2012**, 1-12.

97. Liu, Z.; Shi, S.; Li, Y. Coal Liquefaction Technologies: Development in China and Challenges in Chemical Reaction Engineering. *Chem Eng Sci*. **2010**, *65*, 12-17.

98. Deutsche Bank China's Alternative Energy Landscape: A Strategic Imperative, 2007. http://www.fullermoney.com/content/2007-12-04/chinaaltenergy.pdf (accessed April 18, 2019).

99. Uwaoma, R.C.; Strydom, C.A.; Matjie, R.H.; Bunt, J.R. Influence of Density Separation of Selected South African Coal Fines on the Products Obtained During Liquefaction Using Tetralin as a Solvent. *Energy & Fuels*. **2019**, *33*, 1837-1849.

100. Flatman-Fairs, D.P.; Harrison, G. Suitability of UK Bituminous and Spanish Lignite Coals, and Their Blends for Two-Stage Liquefaction. *Fuel*. **1999**, *78*, 1711-1717.

101. Cai, J.; Wang, Y.; Huang, Q. Rapid Liquefaction of Longkou Lignite Coal By Using a Tubular Reactor Under Methane Atmosphere. *Fuel*. **2008**, *87*, 3388-3392.

102. Song, C.; Schobert, H.H.; Hatcher, P.G. Temperature-Programmed Liquefaction of a Low-Rank Coal. *Energy & Fuels*. **1992**, *6*, 326-328.

103. De Marco Rodriguez, I.; Chomon, M.J.; Caballero, B.; Arias, P.L.; Legarreta, J.A. Liquefaction Behaviour of a Spanish Sub-Bituminous A Coal Under Different Conditions of Hydrogen Availability. *Fuel Process Technol*. **1998**, *58*, 17-24.

104. Huang, L.; Schobert, H.H. Comparison of Temperature Conditions Indirect Liquefaction of Selected Low-Rank Coals. *Energy & Fuels*. **2005**, *19*, 200-207.

105. Masaki, K.; Yoshida, T.; Li, C.; Takanohashi, T.; Saito, I. The Effects of Pre-Treatment and the Addition of Polar Compounds on the Production of “HyperCoal” from Sub-Bituminous Coals. *Energy & Fuels*. **2004**, *18*, 995-1000.

106. Kashimura, N.; Takanohashi, T.; Saito, I. Upgrading the Solvent Used For the Thermal Extraction of Sub-Bituminous Coal. *Energy & Fuels*. **2006**, *20*, 2063-2066.

107. Sakanishi, K.; Hasuo, H.U.; Kishino, M.; Mochida, I. Solvent-Free Liquefaction of Brown and Sub-Bituminous Coals Using Nimo Sulfide Catalyst Supported on Carbon Nanoparticles. *Energy & Fuels*. **1998**, *12*, 284-288.

108. Kuznetsov, P.N.; Bimer, J.; Salbut, P.D.; Korniyets, E.D.; Kuznetsova, L.I.; Snape, C.E. The Nature of the Synergistic Effect of Binary Tetralin-Alcohol Solvents in Kansk-Achinsk Brown Coal Liquefaction. *Fuel Process Technol*. **1997**, *50*, 139-152.

109. Tagaya, H.; Takahashi, K.; Hashimoto, K.; Chiba, K. Coal Liquefaction by Binary Solvent Systems Composed of Tetralin and Reducible Compounds. *Energy & Fuels*. **1989**, 345-350.

110. Chiba, K.; Tagaya, H.; Kobayashi, T.; Shibuya, Y. Solvent Extract Liquefaction of Coal with Fractionated Anthracene Oil and Recycle Solvent. *Ind. Eng Chem Res*. **1987**, *26*, 1329-1335.

111. McMillen, D.F.; Malhotra, R.; Tse, D.S. Interactive Effects Between Solvent Components: Possible Chemical Origin of Synergy in Liquefaction and Co-Processing. *Energy & Fuels*. **1991**, *5*, 179-187.

112. Mochida, I.; Takayama, A.; Sakata, R.; Sakanishi, K. Hydrogen-Transferring Liquefaction of an Australian Brown Coal with Polyhydrogenated Condensed Aromatics: Roles of Donor in the Liquefaction. *Energy & Fuels*. **1990**, *4*, 81-84.

113. Mochida, I.; Takayama, A.; Sakata, R.; Sakanishi, K. Liquefaction of Australian Brown Coal with Mixed Solvents of Different Qualities and Reactivities of Transferable Hydrogens. *Energy & Fuels*. **1990**, *4*, 398-401.

114. Sakata, R.; Takayama, A.; Sakanishi, K.; Mochida, I. Roles of nondonor solvent in the hydrogen-transferring liquefaction of Australian brown coal. *Energy & Fuels*. **1990**, 4,585-588.

115. Song, C.; Saini, A.K.; Yoneyama, Y. A New Process for Catalytic Liquefaction of Coal Using Dispersed MoS2 Catalyst Generated In Situ with Added H_2O. *Fuel*. **2000**, *79*, 249-261.

116. Song, C.; Saini, A.K. Strong Synergistic Effect Between Dispersed Mo Catalyst and H2O for Low-Severity Coal Hydroliquefaction. *Energy & Fuels*. **1995**, *9*, 188-189.

117. Mikita, M.A.; Bockrath, B.C.; Davis, H.M.; Friedman, S.; Illig, E.G. Water and Nondonor-Vehicle-Assisted Liquefaction of Illinois Bituminous Coal. *Energy & Fuels*. **1988**, *2*, 534-538.

118. Mochida, I.; Sakanishi, K. Catalysis in Coal Liquefaction. In *Advances in Catalysis;* Eley, D.D.; Pines, H.; Haag, W.O., Eds; Academic Press, 1994; Vol.40, pp 39-85.

119. Skowronski, R.P.; Ratto, J.J.; Goldberg, I.B.; Heredy, L.A. Hydrogen Incorporation During Coal Liquefaction. *Fuel*. **1984**, *63*, 440-448.

120. Whitehurst, D.D.; Mitchell, T.O.; Farcasiu, M. Coal *Liquefaction: the Chemistry and Technology of Thermal Processes*. Academic Press: New York, 1980.

121. Comolli, A.G.; Lee, T.L.; Popper, G.A.; Zhou P. The Shenhua Coal Direct Liquefaction Plant. *Fuel Process Technol*. **1999**, *59*, 207-215.

122. Kouzu, M.; Koyama, K.; Oneyama, M.; Aramaki, T.; Hayashi, T.; Kobayashi, M.; Itoh, H.; Hattori, H. Catalytic Hydrogenation of Recycle Solvent in a 150t/d Pilot Plant of the NEDOL Coal Liquefaction Process. *Fuel*. **2000**, *79*, 365-371.

123. Robinson, K. Reaction Engineering of Direct Coal Liquefaction. *Energies*. **2009**, *2*, 976-1006.

124. Okuma, O. Liquefaction Process with Bottom Recycling for Complete Conversion of Brown Coal. *Fuel*. **2000**, *79*, 355-364.

125. Hata, K.A.; Watanabe, Y.; Wada, K.; Mitsudo, T.A. Iron Sulfate/Sulfur-Catalyzed Liquefaction of Wandoan Coal Using Syngas-Water as a Hydrogen Source. *Fuel Process Technol*. **1998**, *56*, 291-304.

126. Sun, Q.; Fletcher, J.J.; Zhang, Y.; Ren, X. Comparative Analysis of Costs of Alternative Coal Liquefaction Processes. *Energy & Fuels*. **2005**, *19*, 1160-1164.

127. Shui, H.F.; Liu, J.L.; Wang, Z.C.; Zhang, D.X. Preliminary Study on Liquefaction Properties of Xiaolongtan Lignite under Different Atmospheres. *J. Fuel Chem Technol*. **2009**, *37*, 257-261.

128. Watanabe, Y.; Hata, K.A.; Kawasaki, N.A.; Wada, K.; Mitsudo, T.A. Synthetic Pyrite-Catalysed Coal Liquefaction in Syngas-Water Systems. *Energy & Fuels*. **1994**, *8*, 806-807.

129. Watanabe, Y.; Yamada, H.A.; Kawasaki, N.A.; Hata, K.A.; Wada, K.; Mitsudo, T.A. Fe (CO) 5-Sulfur-Catalysed Coal Liquefaction in H2O-CO Systems. *Fuel*. **1996**, *75*, 46-50.

130. Yang, K.; Batts, B.D.; Wilson, M.A.; Gorbaty, M.L.; Maa, P.S.; Long, M.A.; He, S.X.; Attalla, M.I. Reaction of Methane with Coal. *Fuel*. **1997**, *76*, 1105-1115.

131. Ikenaga, N.; Kan-nan, S.; Sakoda, T.; Suzuki, T. Coal Hydroliquefaction Using Highly Dispersed Catalyst Precursors. *Catal. Today*. **1997**, *39*, 99-109.

132. Hirano, K.; Kouzu, M.; Okada, T.; Kobayashi, M.; Ikenaga, N.; Suzuki, T. Catalytic Activity of Iron Compounds for Coal Liquefaction. *Fuel*. **1999**, *78*, 1867-1873.

133. Liu, Z.; Yang, J.; Zondlo, J.W.; Stiller, A.H.; Dadyburjor, D.B. In Situ Impregnated Iron-Based Catalysts for Direct Coal Liquefaction. *Fuel*. **1996**, *75*, 51-57.

134. Dadyburjor, D.B.; Fout, T.E.; Zondlo, J.W. Ferric-Sulfide-Based Catalysts Made Using Reverse Micelles: Effect of Preparation on Performance in Coal Liquefaction. *Catal. Today*. **2000**, *63*, 33-41.

135. Pinto, F.; Gulyurtlu, I.; Lobo, L.S.; Cabrita, I. Effect of Coal Pre-Treatment with Swelling Solvents on Coal Liquefaction. *Fuel*. **1999**, *78*, 629-634.

136. Kaneko, T.; Tazawa, K.; Koyama, T.; Satou, K.; Shimasaki, K.; Kageyama, Y. Transformation of Iron Catalyst to the Active Phase in Coal Liquefaction. *Energy & Fuels*. **1998**, *12*, 897-904.

137. Hulston, C.K.; Redlich, P.J.; Jackson, W.R.; Larkins, F.P.; Marshall, M. Nickel Molybdate-Catalysed Hydrogenation of Brown Coal Without Solvent or Added Sulfur. *Fuel*. **1996**, *75*, 1387-1392.

138. Wang, Z.; Shui, H.; Zhang, D.; Gao, J. A. Comparison of FeS, FeS+ S and Solid Superacid Catalytic Properties for Coal Hydro-Liquefaction. *Fuel*. **2007**, *86*, 835-842.

139. Wang, Z.; Shui, H.; Zhu, Y.; Gao, J. Catalysis of SO42-/ZrO2 Solid Acid for the Liquefaction of Coal. *Fuel*. **2009**, *88*, 885-889.

140. Garg, D.; Givens, E.N. Pyrite Catalysis in Coal Liquefaction. *Ind Eng Chem Process Des. Dev*. **1982**, *21*,113-117.

141. Kou, J.; Bai, Z.; Li, W.; Bai, J.; Guo, Z. Effects of Mineral Matters and Hydrogen Bonding on Rheological Behaviours of Brown Coal-Oil Slurries. *Fuel*. **2014**, *132*, 187-193.

142. Gray, D. Inherent Mineral Matter in Coal and Its Effect Upon Hydrogenation. *Fuel*. **1978**, *57*, 213-216.

143. Barraza, J.; Coley-Silva, E.; Piñeres, J. Effect of Temperature, Solvent/Coal Ratio and Beneficiation on Conversion and Product Distribution From Direct Coal Liquefaction. *Fuel*. **2016**, *172*, 153-159.

144. Mukherjee, D.K, Chowdhury PB. Catalytic Effect of Mineral Matter Constituents in a North Assam Coal on Hydrogenation. *Fuel*. **1976**, *55*, 4-8.

145. Gözmen, B.; Artok, L.; Erbatur, G.; Erbatur, O. Direct Liquefaction of High-Sulfur Coals: Effects of the Catalyst, the Solvent, and the Mineral Matter. *Energy & Fuels*. **2002**, *16*, 1040-1047.

146. Kiebler, M.W. In *Chemistry of Coal Utilisation: The Action of Solvent on Coal;* Lowry, H.H., Ed.; John Wiley: New York, 1945.

147. Fisher, C.H.; Sprunk, G.C.; Eisner, A.; O'Donnell, H.J.; Clarke, L.; Storch, H.H. *Hydrogenation and Liquefaction of Coal: Part 2. Effect of Petrographic Composition and Rank of Coal*; US Bureau of Mines Technical Paper 642: Washington, DC, 1942.

148. Vorres, K.S. *Users' Handbook for the Argonne Premium Coal Sample Program. Argonne National Laboratory, Argonne, IL*; National Technical Information Service United State Department of Commerce: Springfield, VA, 1993.

149. Speight, J.G. Thermal Reactivity. In *The Chemistry and Technology of Coal*, 3rd ed.; CRC Press: Boca Raton, FL, 2012; pp 391-422.

150. Jin, L.; Han, K.; Wang, J.; Hu, H. Direct Liquefaction Behaviors of Bulianta Coal and Its Macerals. *Fuel Process Technol*. **2014**, *128*, 232-237.

151. Barraza, J.; Portilla, A.; Piñeres, J. Direct Liquefaction of Vitrinite Concentrates Obtained by Column Flotation. *Fuel Process Technol*. **2011**, *92*, 776-779.

152. Bürküt, Y.; Suner, F.; Nakhla, F.M. Thermal Properties of Coal. In *Coal: Resource, Properties, Utilisation, Pollution*; Kural, O., Ed.; Istanbul Technical University: Istanbul, Turkey, 1994; Chapter 6.

153. Mitchell, G.D. Direct Coal Liquefaction, In *Applied Coal Petrology: The Role of Petrology in Coal Utilisation*; Suarez-Ruiz, I.; Crelling, J.C., Eds.; Academic Press, 2008; Chapter 6.

154. Keogh; R.A.; Taulbee, D.N.; Hower, J.C.; Chawla, B.; Davis, B.H. Liquefaction Characteristics of the Three Major Maceral Groups Separated From Single Coal. *Energy & Fuels*. **1992**, *6*, 614-618.

155. Yan, J.; Bai, Z.; Li, W.; Bai, J. Direct Liquefaction of a Chinese Brown Coal and CO_2 Gasification of the Residues. *Fuel*. **2014**, *136*, 280-286.

156. Li, X.; Hu, H.; Jin, L.; Hu, S.; Wu, B. Approach for Promoting Liquid Yield Indirect Liquefaction of Shenhua Coal. *Fuel Process Technol*. **2008**, *89*, 1090-1095.

157. Shui, H.; Li, H.; Chang, H.; Wang, Z.; Gao, Z.; Lei, Z.; Ren, S. Modification of Sub-Bituminous Coal By Steam Treatment: Caking and Coking Properties. *Fuel Process Technol*. **2011**, *92*, 2299-2304.

158. Yoshida, T.; Li, C.; Takanohashi, T.; Matsumura, A.; Sato, S.; Saito, I. Effect of Extraction Condition on “HyperCoal” Production (2)—Effect of Polar Solvents Under Hot Filtration. *Fuel Process Technol*. **2004**, *86*, 61-72.

159. Hao, P.; Bai, Z.Q.; Zhao, Z.T.; Yan, J.C.; Li, X.; Guo, Z.X.; Xu, J.L.; Bai, J.; Li, W. Study on the Preheating Stage of Low-Rank Coals Liquefaction: Product Distribution, Chemical Structural Change of Coal and Hydrogen Transfer. *Fuel Process Technol*. **2017**, *159*, 153-159.

160. Wang, S.; Tang, Y.; Schobert, H.H.; Guo, Y.; Su, Y. Petrology and Structural Studies in Liquefaction Reactions of Late Permian Coals From Southern China. *Fuel*. **2013**, *107*, 518-524.

161. Maroto-Valer, M.M.; Taulbee, D.N.; Andrésen, J.M.; Hower, J.C.; Snape, C.E. Quantitative 13C NMR Study of Structural Variations Within the Vitrinite and Inertinite Maceral Groups for a Semifusinite-Rich Bituminous Coal. *Fuel*. **1998**, *77*, 805-813.

162. Görling, M.; Larsson, M.; Alvfors, P. Bio-Methane Via Fast Pyrolysis of Biomass. *Appl. Energy.* **2013**,*112*, 440-447.

163. Wang, N.; Chen, D.; Arena, U., He, P. Hot Char-Catalytic Reforming of Volatiles From MSW Pyrolysis. *Appl. Energy*. **2017**, *191*, 111-124.

164. Chu, X.J.; Li, W.; Li, B.Q.; Chen, H.K. Gasification Property of Direct Coal Liquefaction Residue With Steam. *Process Saf Environ Prot*. **2006**, *84*, 440-445.

165. Cui, H.; Yang, J.; Liu, Z.; Bi, J. Characteristics of residues from thermal and catalytic coal hydroliquefaction. *Fuel*. **2003**, 82, 1549-56.

166. Uwaoma, R.C.; Strydom, C.A.; Matjie, R.H.; Bunt, J.R.; Okolo, G.N.; Brand, D.J. Pyrolysis of Tetralin Liquefaction Derived Residues From Lighter Density Fractions of Waste Coals Taken From Waste Coal Disposal Sites in South Africa. *Energy & Fuels*. **2019**, *33*, 9074-86.

167. Khare, S.; Dell'Amico, M. An Overview of Conversion of Residues From Coal Liquefaction Processes. *Can J Chem Eng*. **2013**, *91*, 1660-1670.

168. Li, J.; Yang, J.; Liu, Z. Hydro-Treatment of a Direct Coal Liquefaction Residue and Its Components. *Catal Today*. **2008**, *130*, 389-394.

169. Sugano, M.; Mashimo, K.; Wainai, T. Upgrading Reactions of Coal Liquefaction Residue With Basic Coal Liquid Related Model Compounds. *Fuel*. **1998**, *77*, 447-451.

170. Xiao, N.; Zhou, Y.; Qiu, J.; Wang, Z. Preparation of Carbon Nanofibers/Carbon Foam Monolithic Composite from Coal Liquefaction Residue. *Fuel.* **2010**, *89*, 1169-1171.

171. Xiao, N.; Zhou, Y.; Ling, Z.; Qiu, J. Synthesis of a Carbon Nanofiber/Carbon Foam Composite from Coal Liquefaction Residue for the Separation of Oil and Water. *Carbon* **2013**, *59*, 530-536.

172. Xu, J.; Bai, Z.; Bai, J.; Kong, L.; Lv, D.; Han, Y.; Dai, X.; Li W. Physico-Chemical Structure and Combustion Properties of Chars Derived From Co-Pyrolysis of Lignite With Direct Coal Liquefaction Residue. *Fuel*. **2017,** *187*,103-110.

173. Zou, L.; Jin, L.; Li, Y.; Zhu, S.; Hu, H. Effect of Tetrahydrofuran Extraction on Lignite Pyrolysis Under Nitrogen. *J. Anal Appl Pyrol*. **2015**, *112*,113-120.

174. Li, J.; Yang, J.; Liu, Z. Hydrogenation of Heavy Liquids From a Direct Coal Liquefaction Residue for Improved Oil Yield. *Fuel Process Technol*. **2009**, *90*, 490-495.

175. Xu, J.; Bai, Z.; Li, Z.; Guo, Z.; Hao, P.; Bai, J.; Li, W. Interactions During Co-Pyrolysis of Direct Coal Liquefaction Residue With Lignite and the Kinetic Analysis. *Fuel*. **2018**, *215*, 438-445.

176. Lv, D.; Bai, Z.; Yuchi, W.; Bai, J.; Kong, L.; Guo, Z.; Li, X.; Xu, J.; Li, W. Properties of Direct Coal Liquefaction Residue Water Slurry: Effect of Treatment By Low-Temperature Pyrolysis. *Fuel*. **2016**, *179*, 135-140.

177. Li, X.H.; Xue, Y.L.; Li, W.Y. Properties of Semi-Coke From Co-Pyrolysis of Lignite and Direct Liquefaction Residue of Shendong Coal. *J. Fuel Chem Technol*. **2015**, *43*, 1281-1286.

178. Sugano, M.; Tamaru, T.; Hirano, K.; Mashimo, K. Additive Effect of Tyre Constituents On the Hydrogenolyses of Coal Liquefaction Residue. *Fuel*. **2005**, *84*, 2248-2255.

179. Luo, A.Q.; Zhang, D.; Ping, Z.H.; Xuan, Q.U.; Zhang, J.L.; Zhang, J.S. Effect of Pyridine Extraction On the Tar Characteristics During Pyrolysis of Bituminous Coal. *J. Fuel Chem Technol*. **2017,** *45*, 1281-1288.

180. Zhu, P.; Luo, A.; Zhang, F.; Lei, Z.; Zhang, J.; Zhang, J. Effects of Extractable Compounds On the Structure and Pyrolysis Behaviours of Two Xinjiang Coal. *J. Anal. Appl Pyrol*. **2018**, *133*, 128-135.

181. Xu, L.; Tang, M.; Liu, B.; Ma, X.; Zhang, Y.; Argyle, M.D.; Fan, M. Pyrolysis Characteristics and Kinetics of Residue From China Shenhua Industrial Direct Coal Liquefaction Plant. *Thermochimica Acta*. **2014**, *589*, 1-10.

182. Li, X.; Xue, Y.; Feng, J.; Yi, Q.; Li, W.; Guo, X.; Liu, K. Co-Pyrolysis of Lignite and Shendong Coal Direct Liquefaction Residue. *Fuel*. **2015**, *144*, 342-348.

183. Chu, X.J.; Li, W.; Bai, Z.Q.; Li, B.Q.; Chen, H.K. Gasification Reactivity of Shenhua Direct Liquefaction Residue with Steam and CO_2. *J Fuel Chem Technol*. **2010**, *38*, 1-5.

184. Liu, P.F.; Zhang, Y.Q.; Fang, Y.T. Gasification Kinetics of Extraction Residue Char From Shenhua Direct Liquefaction Residue. *J Fuel Chem Technol*. **2012**, *40*, 1281-1288.

185. Liu, X.; Zhou, Z.J.; Hu, Q.J.; Dai, ZH, Wang FC. Experimental Study on Co-Gasification of Coal Liquefaction Residue and Petroleum Coke. *Energy & Fuels*. **2011**, *25*, 3377-3381.

186. Li, J.; Yang, J.; Liu, Z. Hydrogenation of Heavy Liquids from a Direct Coal Liquefaction Residue for Improved Oil Yield. *Fuel Process Technol*. **2009**, *90*, 490-495.

CHAPTER 3: INFLUENCE OF DENSITY SEPERATION OF SELECTED SOUTH AFRICAN COAL FINES ON THE PRODUCTS OBTAINED DURING LIQUEFACTION USING TETRALIN AS A SOLVENT.

R.C. Uwaoma, C.A. Strydom, R.H. Matjie, J.R. Bunt

In this chapter, the density separation of coal fines, liquefaction of the coal fines and their float fractions as well as all the results of the analyses that were obtained from the liquefaction experiments of the samples using tetralin as a solvent at mild conditions are reported.

The content of this paper was published in Energy & Fuels. **2019**, 33(3):1837-49.

Abstract

The liquefaction of two South African discarded coal fines and their density separated (float) fractions were carried out under moderate conditions in a laboratory autoclave. Liquefaction tests were carried out on both discarded coal fines and their float fraction samples at temperatures ranging between 380 and 420˚C using tetralin as a solvent and an initial nitrogen pressure of 3 MPa and a final pressure of 12 MPa. Oil samples produced from the liquefaction of coal fine discards and their float fractions were further characterised using Gas Chromatography-Mass Spectroscopy (GC-MS) and Nuclear Magnetic Resonance. The liquefaction tests results showed that the carbon conversion and oil yields were higher for the float fractions when compared to the discarded coal fines samples. The oils yields ranged from 24.4–37.2% (daf) for the oil produced from the float fractions of the coal fines and 19.1–29.3% for oils produced from the coal fines (daf). The oil and the gas yields of the float fraction samples were higher when compared to those of the coal fine discards. The higher carbon conversion and higher oil yields obtained from the float fractions demonstrated that density separation of the coal fine discards improved the overall carbon conversion and liquefaction yields. Coal fines discard and float fractions achieved 8%wt. (daf) and 10%wt. (daf) PAA yields at 420˚C respectively. The Waterberg and Highveld coal float fractions had carbon conversions of 50.7%wt. (daf) and 52.7%wt. (daf) respectively, in comparison to less than 42%wt. (daf) carbon conversion of the initially discarded coal fines. GC-MS results for the oil samples derived from coal fine discards and their float fractions showed that these oils contained 72 and 81%wt. naphthalene, respectively. Density separation of discarded coal fines is beneficial to produce a float fraction that may be used as feedstock for direct coal liquefaction. The analytical results indicate that density separation of the coal fines may be used to reduce high costs and volumes of discarded coal fines associated with the disposal and handling of discarded coal fines. Environmental problems are also addressed if discarded coal fines are utilised as a feedstock in industrial processes.

Keywords: liquefaction, float fraction, reactive macerals, oil yield, discarded coal fines, density separation

3.1 Introduction

South Africa is a developing country with abundant coal reserves but with a limited amount of crude oil reserves. Statistics from the Total petroleum company and other liquid production energy information,[1] estimates that South Africa has crude oil production of approximately 15 million barrels per year.[1] More than 160,000 barrels of fuel per day is produced by Sasol to meet the South African local demand.[2] Sasol uses indirect coal liquefaction for the production of synthetic fuels.[2] The proposed study will focus on direct liquefaction of discarded coal fines and their float fractions. The direct liquefaction process was chosen to investigate the possible application thereof to utilise waste material such as discarded coal fines.

The South African coal mining industry produced about 310 million tons of bituminous coal in 2016.[2] Thermochemical processes utilise some of the coal for oil, petrochemicals and steam generation. More than 60 million tons are discarded coal fines per annum, which are unavoidable by-products of the mining of South African coals. The discarded coal fines chemical and mineralogical properties are consistent with those of South African feed coals utilized in thermo-chemical processes.[3,4] These coals are low-rank coals that contain high ash percentage with the poor quality when compared with high-rank coals. Costs that are associated with the disposal and handling of the coal fine discards exceed the fuel value of these fines.[4] In addition, the discarded coal fines have negative environmental impacts that include dust, spontaneous combustion and acid mine drainage. This paper deals with utilisation of the float fractions produced from discarded coal fines in the direct liquefaction process in order to produce fuels. Density separation of the discarded coal fines may enrich some of the fractions in terms of their appropriate chemical properties for direct coal liquefaction (DCL). Should density separation of discarded coal fines be of a benefit for liquefaction, the environmental impacts of coal fines may be reduced.

Most South African coals are classified as low-rank bituminous coals. Density separation of, especially, lower-grade coal will enhance the properties by reducing the mineral matter contents and subsequently increasing the fixed carbon contents, calorific values and reactive macerals in the float fractions of the coal. These density separated fractions differ from each other and the parent coal in chemical, structural and physical properties such as maceral content, reflectance, density, hydrogen content, heteroatom content, and aromaticity. During DCL, it has been shown that coal-rich in vitrinite and liptinite provides higher carbon conversion than those rich in inertinite macerals.[5] The influence of maceral groups during DCL processes have been reported by various researchers.[5-7]

Thermochemical conversion of coal to liquid hydrocarbons can be achieved through liquefaction. Thermochemical processes include pyrolysis, solvent extraction, gasification, DCL and indirect coal liquefaction.[8, 9] Direct liquefaction is the conversion of coal to liquids by the dissolution of coal in a donor solvent (usually an organic hydrogen donor), or hydrogen as an atmosphere, in the presence or absence of a catalyst under mild temperature and pressure.[9] During direct liquefaction of coal, most of the chemical structures present in coal are retained. During the indirect liquefaction process, organic structures are destroyed to produce a gaseous mixture of CO and H_2. The products obtained during the direct liquefaction process include liquids (mixed oils), gases and residues. The dissolved hydrocarbon part (oil yield) can be further upgraded by thermal and catalytic cracking to naphtha, kerosene, vacuum gas oil, diesel, and these products are similar to crude petroleum oil. A high oil yield during the DCL process would make the process economically viable.

For this investigation, the liquefaction process consists of mixing the coal samples with a hydrogen-rich solvent. The process is performed under mild temperatures and pressures. During the process, hydrogen is transferred from the solvent to the coal to obtain the products. During the liquefaction of coal, the extraction yield not only depends on the rank of the coal but also on the solvent type and extraction temperature[10,11]. Tetralin has been demonstrated as a useful solvent to convert bituminous coal into valuable products via liquefaction, although most of these studies were done on a laboratory scale.[12-14] Tetralin is rich in hydrogen and can be converted to naphthalene during liquefaction.[14]

Previous direct liquefaction studies using tetralin as a solvent were performed with coals from the Northern Hemisphere countries.[5] Reactivities and yields differ during the different liquefaction processes.[5,7] In a recent study done with South African Waterberg coal, phenol was used as a solvent during extraction experiments.[15] The investigators used a beneficiated Waterberg coal that is vitrinite rich and had a low ash yield. A carbon conversion of 51.2 %wt. (daf) was reported. Other researchers studied the catalytic liquefaction of Waterberg coal using a mixture of hydrosulphide, sulphur and a coal/CO/H_2O mixture.[17] There is no literature on the direct liquefaction, using tetralin as a solvent, of South African discarded coal fines and their density separated float fractions.

The DCL products formed from the float fraction after density separation of South African bituminous discarded coal fines may indicate the potential for utilisation of this fraction. The objectives of this paper are: (1) to produce float fractions from Waterberg and Highveld fine coal discards; (2) To characterise the coal fine discards and float fractions; (3) to perform DCL on

discarded coal fines and their float fractions; and (4) to characterise and compare the different products (oil, PAA, residues) obtained after the DCL tests.

3.2 Experimental procedures

3.2.1 Materials

A bituminous coal sample was collected from the dumping sites of discarded coal fines originating from the Highveld coalfield. This coalfield is situated in the Mpumalanga Province in the Republic of South Africa. A Waterberg bituminous coal sample used was obtained from stockpiles of discarded coal fines originating from the Waterberg coalfield in the Limpopo Province of the Republic of South Africa. Particle sizes of the coal samples ranged from a fine powder to approximately 20 mm. The samples were sieved to obtain the >0.5 mm coal particles for density separation. The coal samples were oven-dried and stored under nitrogen to prevent oxidation before density separation. Tetralin, n-hexane and tetrahydrofuran with a purity of >99.5% were used for liquefaction and the separation processes, respectively.

3.2.2 Density separation

The density separation experiments were conducted at Bureau Veritas Testing and Inspection and SGS inspection, verification, testing and certification laboratories in South Africa using mixtures of benzene, perchloroethylene and TBE (tetrabromoethane). The density separation was done with two coal fines samples to produce a float fraction (<1.5 $g \cdot cm^{-3}$), a middlings fraction (1.5–1.8 $g \cdot cm^{-3}$) and a sink fraction (> 1.8 $g \cdot cm^{-3}$). The density separation was performed using the procedure described by SANS/ISO 7936. The samples to be used in the liquefaction experiments were referred to as the Highveld coal fines (HR), Highveld float fraction (<1.5 $g \cdot cm^{-3}$) (HF), Waterberg coal fines (WR), and Waterberg float fraction (<1.5 $g \cdot cm^{-3}$) (WF). The middlings and sink fractions were not subjected to the liquefaction experiments in this study due to their lower macerals contents and relatively high ash percentages in comparison to the original coal fine discards and the float fractions.

3.2.3 Liquefaction experiments

Before performing the liquefaction experiments, the coal fine discards, and their float fractions were pulverised to obtain 100% particles passing 212 µm. The pulverised samples were dried in an oven at 80°C for 24 hours to reduce the inherent moisture contents. The direct liquefaction experiments were carried out in an ASS316 high-pressure stainless steel autoclave system (300

mL capacity, 90 mm diameter and 150 mm height) under an N_2 atmosphere. The solvent used was tetralin (THN, purity ≥ 99.5%), which is a hydrogen donor solvent.[5] A mass ratio of 3:1 solvent to coal was used in the experiments. The reactor was purged, sealed and pressurised with N_2 to an initial pressure of 3 MPa. The autoclave was heated to the operational temperature (380, 400, and 420°C) using a heating rate of approximately 4.0°C/min and kept for a holding time of 20 min. The solid-liquid mixture (consisting of the coal residue, extract and solvent) were collected from the autoclave. The mixture was subsequently weighed (to calculate the yield of gaseous products), and then vacuum filtered to separate the coal residue from the organic liquid phase.

A series of solvent extractions were carried out on the liquid mixture using a reflux system at 85 °C for 1 hour, using a solvent/liquid product ratio of 1:1. The experimental procedure involves the extraction with tetrahydrofuran (THF) and n-hexane in sequence, in order to separate the products from the organic liquids.[15] The THF-insoluble part of the liquid residue was labelled THFI and represented the unreacted coal residue. The THF-soluble part of the liquid residue (THFI) was further extracted with hexane. The hexane-soluble (HS) product contained the oil part of the products and the solvent. The hexane-insoluble (HI) part of the extraction was labelled pre-asphaltenes (PAA) products. All the product yields were calculated on a dry ash-free basis (daf). The unreacted coal residues (THFI) and PAA products were washed with a low-boiling point organic solvent (acetone), to remove the residual solvent. The solvent extraction products were then dried under vacuum at 80°C for 24 hours.

The carbon conversions of the coal fines discard and float fraction samples during the solvent extraction processes were calculated as follows (all values indicated are masses):

$$W_s = \frac{W_1}{W_C} \times 100\% \qquad 3.1$$

$$W_p = \frac{W_2}{W_c} \times 100\% \qquad 3.2$$

$$C = \frac{W_c - W_1}{W_C} \times 100\% \qquad 3.3$$

where:

W_s = Solid yield (%wt., daf)

W_p = PAA yield (%wt., daf)

C = Conversion

W_1 = mass of (THF) insoluble fraction in g (daf)

W_2 = mass of (hexane) insoluble fraction in g (daf)

W_c = mass of coal fines or density separated fraction in g (daf).

Oil % = (Conversion – W_p – G)×100%. 3.4

The masses of the coal fines or density separated fractions (daf) are the masses of the dry, ash-free coal samples. G is the yield (%wt.) of the gaseous products which were obtained after the solvent extraction using a mass balance. The carbon conversion or extraction yields and intermediate products yields (PAA) are determined gravimetrically from the solvent-free dried residues.

3.2.4 Analysis of coal fines, float fractions and extracted products after the liquefaction

3.2.4.1 Coal fines discard, float fractions and extracted products compositions

The proximate analyses of the coal fine discards, their float fractions, PAAs and residues obtained after the liquefaction experiments, were conducted using a U-Therm FC-TGA-D automatic proximate analyser. The ISO standard methods are given in Table 3.1. Ultimate and total sulphur content analyses for the oil samples were done at the coal laboratory of the Council for Geosciences (CGS), Silverton, Pretoria. Analyses of the solid samples (discarded coal fines, float fractions, residue, and the pre-asphaltenes) were conducted at the laboratory of Bureau Veritas Testing and Inspections SA (Pty) Ltd, Pretoria. Ultimate analysis data for the coals and the density separated-fractions were obtained using a CE 440 analyser. The ultimate and proximate analyses for each sample were done in triplicate, and the average values are reported in this paper.

3.2.4.2 CO_2 low-pressure gas adsorption analysis

The CO_2 low-pressure adsorption analysis (CO_2-LPGA) was conducted using a Micrometics ASAP 2010 instrument. The discarded coal fines' samples and their float fractions were dried in a vacuum oven at 105°C for approximately 3 hours. Approximately 0.3 g of each sample was placed in a sample tube. Before the CO_2-LPGA analysis de-gassing of the samples were conducted at a temperature of 60°C and a pressure of 10 µm Hg for 48 hours. Carbon dioxide was used as the adsorbate gas, and an ice-water bath was used to keep the analysis temperature at 0°C. The isotherm data were acquired using ASAP 2020 v4.0 software in a relative pressure range of $0< P/P_0 \leq 0.032$. The CO_2 adsorption data was used to calculate the porosity of the

samples. All the adsorption experiments were repeated three times, and the final results are averages of three independent measurements from which experimental errors were calculated at a 95% confidence interval**.** Carbon dioxide low-pressure gas adsorption was done to determine the surface area of and the porosity of the discarded coal fines and their float samples.

3.2.4.3 Petrographic analyses

Petrographic analyses of the coal fines discard, and their float fractions were conducted at Bureau Veritas Testing and Inspection South Africa. The petrographic analysis was done according to the standard ISO 7404-2:2009. Maceral composition was determined using a Zeiss Axio Imager M2m with a magnification of ×50 under oil immersion, according to the ISO 7404-3 method. The coal rank determination was based on the ISO 11760 classification of coal. The group macerals in the coal fines discard and float fractions were measured by a 500-point count method following the ISO standard 7404-3:2009. The mass fraction of the mineral matter in the coal macerals is calculated using the following equation:

Mineral matter = (1.08×ash yield %wt.) + (0.55×sulphur %wt.) 3.5

3.2.4.4 X-ray diffraction (XRD) and X-ray fluorescence (XRF) analyses

The mineralogical and the chemical analyses of the coal fine discards and float fraction samples were conducted in the laboratories of North-West University (NWU) using XRD and XRF techniques. The discarded coal fines samples, along with the residues from the liquefaction experiments were subjected to mineralogical analysis using an X'Pert PRO PANalytical (Philips) – Unit 2 XRD instrument with anode material cobalt and Rietveld-based X'Pert HighScore Plus Software.[17,18] Each solid sample was spiked with 20% Si (Aldrich, 99.9% purity) and was micronised in a McCrone micronising mill.

Coal fines discard and float fraction samples were also subjected to XRF analysis. The solids were fused into a borosilicate disk[19] and analysed using a PANalytical (Axios Max) WD-XRF spectrometer equipped with a 50 kV Rh-anode X-ray tube, six filters, a P10 gas purge facility and a high-resolution silicon drift detector.

3.2.4.5 Inductively coupled plasma-optical emission spectrometry (ICP-OES) analysis

An Agilent 725 Radial ICP-OES instrument was used to measure concentrations of elements in samples before and after liquefaction experiments. This was done to investigate the effect of

inherent mineral matter on the conversion efficiency. The analysis methods were described elsewhere.[20]

3.2.4.6 Gas chromatography-mass spectrometry (GC-MS) analyses

The oily liquid products (HS) from the coal fine discards and their float fractions extracted during the liquefaction experiments were characterised by GC-MS using an Agilent 6890N gas chromatograph (GC) coupled with an Agilent 5975 mass detector. The GC was equipped with an Agilent 19091S column (30 m length, 0.25 mm diameter, 0.25 µm film). The column was heated to 290°C at a heating rate of 5°C/min for 30 min and kept isothermally until all the components of the samples have evolved. The National Institute of Standards and Technology (NIST) database was used for peak identification.

3.2.4.7 Nuclear magnetic resonance (NMR) of HS products

^{1}H NMR measurements of the HS products were conducted at the Central Analytical Facility of Stellenbosch University (Republic of South Africa). The ^{1}H NMR spectra were measured on an Agilent PUnityP Inova 400 MHz spectrometer at ambient temperature using deuterated chloroform (d-$CDCl_3$) as a solvent. For the ^{1}H spectra, a 60 s relaxation time was used for quantitative conditions. The tetrakis-(trimethylsilyl)-silane (TKS) peak was used as an internal reference. ^{1}H NMR analyses were performed on the HS oil samples to determine the relative amounts of hydrogen-bonded to aliphatic carbon chains and aromatic rings.

3.2.4.8 Solid-state ^{13}C NMR analyses

The CP-MAS ^{13}C NMR analytical method was conducted at the Central Analytical Facility of Stellenbosch University (Republic of South Africa). The solid-state ^{13}C NMR spectra were obtained from a Varian VN MRS 500 MHz two-channel spectrometer using 4 mm zirconia rotors and a 4 mm Chemagnetics™ T3 HX MAS probe. The power parameters were optimised for Hartmann-Hahn matches, and the radiofrequency fields were γCB1C= γHB1H≈ 56 kHz. The chosen contact time for cross-polarisation was 2 ms. A method described by other investigators were used for the Magic-Angle-Spinning (MAS), and Dipolar dephasing experiments.[21,22]

The integration reset points and calculations were taken from other investigators.[23,24] A combination of magnetic-angle spinning and cross-polarisation (CP-MAS ^{13}C NMR) was employed during the analysis. The Mestrenova 11.0.2 software package was used to process the spectra, and integral pre-set tables are set up to ensure that the same regions are integrated

reproducibly.[21,22] A correction factor of 1.3 was derived from the publication and used to correct the intensity of the bridgehead aromatic carbons (peak 135–90ppm for dipolar dephasing experiment) for the loss in magnetisation during the interrupted decoupling.[23]

3.3 Results and discussion

3.3.1 Coal composition

The results of the proximate and ultimate analyses of the two discarded coal fines samples and their float fractions are presented in Table 3.1. The HR and WR samples exhibited slightly lower volatile matter contents and fixed carbon contents in comparison with other South African coals.[4] As expected, the ash yields of the two discarded coal fines samples were higher in comparison to their parent coal samples. The carbon and hydrogen concentrations of the discarded Highveld and Waterberg coal fines samples are similar to those described by Matjie et al.[3] The calorific value of the coal fines was 17.7 MJ/kg for HR and 21.6 MJ/kg for WR.

As expected, the float fractions from the density separated coal fines samples showed a slight increase in the volatile matter and carbon contents and the calorific values from the values for the coal fines (Table 3.1). The lower ash yields for the float fractions indicate that some of the excluded mineral matters reported to the sink and middlings fractions. There were not much differences in the moisture contents of the coal fine discards and the float fractions of both coal samples. The middlings and the sink fractions of both coals were thus less suitable for the liquefaction experiments, due to their relatively higher ash yields, lower volatile matter contents and lower calorific values. Detailed analyses of the middlings and the sink fraction samples were therefore not performed at this stage.

The results of ultimate analyses are summarised in Table 3.1. Data in this Table show that the two coal fine discards (Highveld and Waterberg) and their float fractions contained relatively higher percentages of elemental carbon with lower nitrogen and sulphur contents. As expected, the oxygen contents of the float fraction samples were slightly higher when compared to the discarded coal fines samples. The ultimate analysis results for the samples evaluated in this study are in good agreement with those for other South African coals that were previously reported.[3] The sink fractions had relatively high sulphur and oxygen contents and lower proportions of carbon. The float fractions of the two coal samples showed lower sulphur contents when compared to the middlings and the sink fractions. This could imply that a high sulphur content in

the middling and sink fractions are associated with a high proportion of excluded pyrite contained in the rock fragments present in the sink fractions.

Table 3-1: Proximate, ultimate, calorific value, H/C, O/C, mass, and density separation yield results of coal fines and their density separated fractions

Sample ID/Properties	**Method of Analysis**	**HR**	**HF<1.50**	**HF1.5-1.80**	**HS> 1.80**	**WR**	**WF<1.50**	**WF1.5-1.80**	**WS> 1.80**
Mass (g)		65000	25250	18750	21000	104020	47560	38360	18100
Yield (%)		100	38.9	28.9	32.3	100	45.7	36.9	17.4
Calorific value HHV (MJ/kg)	ISO 1928:2009	17.7	25.7	21.0	8.5	21.6	27.2	19.9	10.8
Proximate Analysis (%wt., ad)									
Inherent moisture	ISO11722:1999	3.0	4.1	4.2	2.1	3.1	3.4	1.9	1.4
Ash yield	ISO1171:2010	42.0	11.8	27.7	65.8	30.2	13.4	34.2	55.6
Volatile matter yield	ISO:562:2010	17.7	29.4	19.3	13.7	25.7	31.2	24.2	17.9
Fixed carbon	(by difference)	37.3	54.7	48.8	18.4	41.0	52.0	39.7	25.1
Ultimate Analysis (%wt., daf)									
Carbon	ISO17247:2013	75.5	75.6	78.7	68.5	77.2	77.7	77.4	64.7
Hydrogen	ISO17247:2013	5.9	5.7	5.0	6.7	5.4	5.1	5.3	5.3
Nitrogen	ISO17247:2013	2.1	2.6	1.7	2.4	1.5	1.5	1.7	1.6
Total sulphur content	ISO 19579:2006	1.8	1.3	1.7	3.0	1.9	1.2	1.4	11.4
Oxygen	(by difference)	14.9	14.7	12.9	19.4	14.0	14.5	14.3	17.0
H/C atomic ratio		0.94	0.90	0.76	1.17	0.84	0.79	0.82	0.98
O/C atomic ratio		0.15	0.15	0.12	0.21	0.14	0.14	0.14	0.20

HR= Highveld raw, HF<1.5= Highveld float, HF1.8= Highveld middling, HS>1.8= Highveld sink; WR= Waterberg raw, WF<1.5= Waterberg float, WF1.8= Waterberg middling, WS>1.8= Waterberg sink.

3.3.2 CO_2 low-pressure gas adsorption analysis

A summary of the surface areas and porosity properties of the samples as determined from the low-pressure CO_2 adsorption analyses are given in Table 3.2. The different analytical methods and models used to obtain the results are also summarised in Table 3.2. As shown in this Table, the Dubinin-Radushkevich (D-R) micropore surface areas and the Brunauer-Emmet-Teller (BET) surface areas of the coal fine discards were found to be lower when compared to the surface areas of the float fractions. The increase in the surface area of the float fractions could be attributed to the removal of some of the minerals in the float fraction. The microporosities of the coal fine discards calculated from the CO_2 adsorption data were also lower compared to those of the float fractions. There were no significant differences in the average micropore volumes of the coal fine discards and their float fractions. Due to the higher porosity and the surface area values for the float fractions in comparison to the discarded coal fines and the other density separated fractions, it is expected that the solvent will penetrate the structure of the float fraction more efficiently, leading to higher extraction efficiencies during the liquefaction experiments.

Table 3-2: CO_2 low-pressure gas adsorption analysis results of coal fines and their float fractions

	HR	HF<1.50	WR	WF<1.50
CO_2 low-pressure gas adsorption analysis results				
BET surface area (m^2/g)	61.8 ± 3.0	76.8 ± 1.9	66.0 ± 1.0	86.4 ± 1.2
H-K average micropore diameter (Å)	3.870 ± 0.044	3.893 ± 0.014	3.859 ± 0.012	3.837 ± 0.011
D-R micropore volume (cm^3/g)	0.0396 ± 0.002	0.0525 ± 0.002	0.0418 ± 0.003	0.0561 ± 0.001
Porosity (%) (3 Å ≤ d_p ≤ 5 Å)	3.70 ± 0.36	4.24 ± 0.10	3.97 ± 0.15	5.26 ± 0.03
D-R micropore surface area (m^2/g)	98.7 ± 5.5	131.0 ± 5.2	104.3 ± 7.4	140.0 ± 2.4

Note: D-R - Dubinin-Radushkevich; BET - Brunauer-Emmet-Teller; H-K - Horvath-Kawazoe; CO_2 ads data - CO_2 adsorption data.

3.3.3 Petrographic analyses

The petrographic analysis results in Table 3.3 revealed that the two coal fine discards were inertinite-rich, with relatively lower vitrinite contents. The petrography analysis also reveals that the coal fine discards contained low percentages of liptinite. Comparing the petrographic analysis results for HR and WR samples with those for the float samples, it was observed that there was a slight increase in the vitrinite contents of the float fractions with a corresponding decrease in the

inertinite content. The liptinite contents of the float fractions also do not show much difference with that in the coal fine discards. The total volume of reactive (TV+TL+RSF) in the HR and WR samples were 59.6 vol.% (mmb) and 65.4 vol.% (mmb), respectively. As expected, these values slightly increased for the HF and WF samples as they have values of 74 vol.% (mmb) and 70 vol.% (mmb) respectively. The higher value of reactive macerals of the float fractions is a good indication that the float fractions may be a better feedstock for utilisation in the liquefaction experiments than the original coal fine discards. The petrographic analysis indicates that these coal fine discards samples may be classified as a typical medium rank C bituminous coal according to the ISO-11760:2005 method. Wang et al.[25] stated in their study that liquefaction conversion decreases with an increase in coal rank, indicating that coal rank influences the performance of coal during the liquefaction process.

Table 3-3: Petrographic analysis results of the HR and WR, and their float fractions (%vol., mmb)

Sample Identification	HR	HF<1.5	WR	WF<1.5
Total vitrinite (TV)	34.9	58.4	39.3	51.6
Total liptinite (exinite) (TL)	0.9	3.8	3.3	1.5
Total inertinite (calculated) (TI)	41.8	24.7	40.7	37.8
Reactive semifusinite (RSF)	23.8	11.8	22.8	17.7
Inert semifusinite (ISF)	15.3	10.8	14.2	13.2
Fusinite + secretinite	2.2	2.1	3.7	6.9
Mineral matter (calculated)	22.9	13.1	16.7	9.1
Total reactives (TV+TL+RSF)	59.6	74.0	65.4	70.8
Total inerts (calculated)	40.4	26.0	34.6	29.2

Note: HR= Highveld coal fines, HF<1.5= Highveld float, WR= Waterberg coal fines, WF<1.5= Waterberg float.

3.3.4 XRF analysis results

XRF results (elemental composition reported as oxides) for the HR, WR samples and their respective float fractions (see Table 3.4) show that SiO_2, Al_2O_3, CaO and Fe_2O_3 were the most abundant in the coal fine discards and their different float fractions. MgO and K_2O were found to be present in smaller proportions. The XRF results obtained in this study are in a good agreement with the XRD results reported in Table 3.5. The significant difference between the coal fine discards and their float fractions is a relative increase in the CaO contents in the float samples. The higher Ca content in the coal float fractions can be attributed to the presence of the calcite

and dolomite cleats, and organic calcium in macerals in these samples.[26] The base/acid (B/A) ratios of the coal fines samples are found to be smaller when compared to the float fractions.

Table 3-4: Normalised XRF analysis results based on loss on ignition and B/A (base/acid) ratios for the HR and WR and their density separated float fractions (%wt.)

Compound	HR	HF	WR	WF
SiO_2	50.4	51.6	63.0	52.0
Al_2O_3	29.1	26.2	26.7	24.2
Fe_2O_3	4.8	3.0	3.1	7.7
TiO_2	0.8	1.5	1.5	1.7
P_2O_5	0.2	0.7	0.2	1.0
CaO	3.9	12.6	2.5	9.0
MgO	1.2	3.3	0.8	1.5
Na_2O	nd	nd	nd	nd
K_2O	0.4	0.9	1.9	0.9
MnO	0.1	0.1	0.0	0.2
SO_3	0.5	0.2	0.3	1.8
B/A ratio	0.12	0.24	0.07	0.24
$SiO_2 + Al_2O_3 + Fe_2O_3$	84.3	80.7	92.8	83.9

Note: HR= Highveld coal fines, HF<1.5= Highveld float, WR= Waterberg coal fines, WF<1.5= Waterberg float.

3.3.5 XRD analysis results

The XRD analysis results of the coal fine discards and their float fractions are presented in Table 3.5. The major crystalline minerals in the coal fines and their float fractions were kaolinite, quartz, and dolomite, with smaller proportions of gypsum, pyrite, muscovite, anatase, calcite and rutile. As expected, the concentrations of the amorphous phase (mostly organic carbon) of the float fractions were higher when compared to the coal fine discards.

The presence of included clay minerals and clay mineral cleats in the float fractions may enhance the liquefaction process. Clay minerals, including kaolinite, have been shown by various investigators to act as a catalyst during coal liquefaction.[27,28] The XRD results also showed the presence of pyrite (FeS_2) in the coal fine discards and their float fractions. The pyrite mineral in the coal may show a catalytic effect during the liquefaction process, as a catalytic activity has been reported by other investigators.[29,30] Some studies have shown that pyrite could decompose to pyrrhotite ($Fe_{1-x}S$) during direct liquefaction, and that pyrrhotite is involved in the processes during the hydrogenation of coal.[31]

Table 3-5: XRD results of the coal fines and their float fraction (as % crystalline and amorphous phases) (%wt.)

Mineral phases	WR	WF<1.5	HR	HF<1.5
Quartz	11.2	5.50	11.5	1.72
Kaolinite	16.2	9.2	20.3	8.15
Dolomite	3.2	0.01	5.5	0.48
Calcite	1.3	0.17	-	0.25
Pyrite	0.3	0.2	0.3	0.13
Anatase	0.2	0.0	0.4	0.1
Graphite	0.5	0.3	0.1	0.4
Muscovite	0.9	-	-	0.1
Gypsum	0.6	0.1	0.9	0.2
Periclase	0.2	0.1	-	-
Microcline	-	-	0.8	0.2
Amorphous/organic carbon	65.4	84.42	60.2	89.23

Note: HR= Highveld coal fines, HF<1.5= Highveld float, WR= Waterberg coal fines, WF<1.5= Waterberg float.

3.4 Effect of coal maceral composition on liquefaction

The liquefaction product distribution, which includes oil, gas, PAA and residues, obtained from the liquefaction tests of the discarded coal fines and their float fractions are given in Table 3.6 and Figure 3.1. The results are reported on a 95% confidence intervals based on three repeats at each liquefaction temperature (380, 400 and 420°C). The oil yields and the carbon conversion under N_2 atmosphere (Figure 3.1) decreased in the samples in the order HF>WF>WR>HR. These values may be correlated with the maceral compositions of the discarded coal fines and their float fractions (Table 3.3). Vitrinite was enriched in the WF and HF float fraction samples, making up 51.6% and 58.4% respectively (Table 3.3) of macerals. The inertinite content slightly decreased in the WF and HF float fraction samples to 24.7% and 27.8%, respectively (Table 3.3). The lower oil yields of the coal fine discards may be explained by the higher amounts of inertinite in the coal fine discards (Table 3.3).

Figure 3.1(d) summarises the results of carbon conversion for all the samples at 380 and 420°C liquefaction temperatures. Figure 3.1(d) shows that the float fractions gave higher carbon conversions when compared to the coal fine discards, due to the increase in vitrinite and total reactive macerals of the float fractions when compared to the coal fine discards (Table 3.3). As stated by other researchers,[31] vitrinite usually has a higher amount of extractable aliphatic hydrocarbons, which are more easily broken during heat treatment than for the inertinite macerals. The oil yields and carbon conversions obtained from this study were lower when compared to values from the literature.[33] The higher values of the oil yields that were reported by other

researchers could be attributed to the maceral composition, as the coal sample used by these authors contained vitrinite contents of close to 93.0%vol.[32]

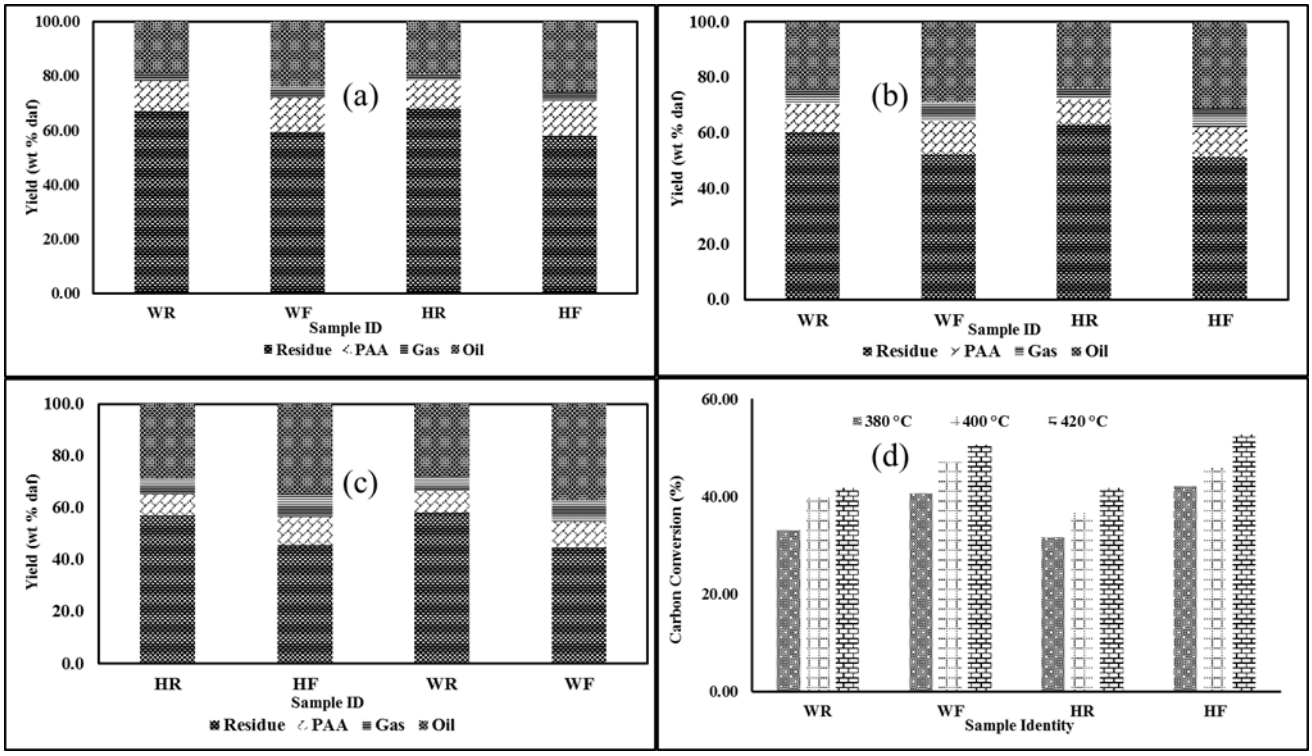

Figure 3-1: Percentage products distribution of coal fines and density separation fractions at (a) 380°C, (b) 400°C, (c) 420°C, (d) Coal conversion at different temperatures. Note: HR= Highveld coal fines, HF<1.5= Highveld float fraction, WR= Waterberg coal fines, WF<1.5= Waterberg float fraction.

Figure 3.2 shows the correlation between the surface areas, total reactive macerals, and conversion. It is observed that there is a positive correlation between the surface areas, total reactive macerals, and conversion. This indicates that an increase in the surface area or the total reactive macerals as observed for the float fractions in comparison to the coal fine discards leads to an increase in conversion.

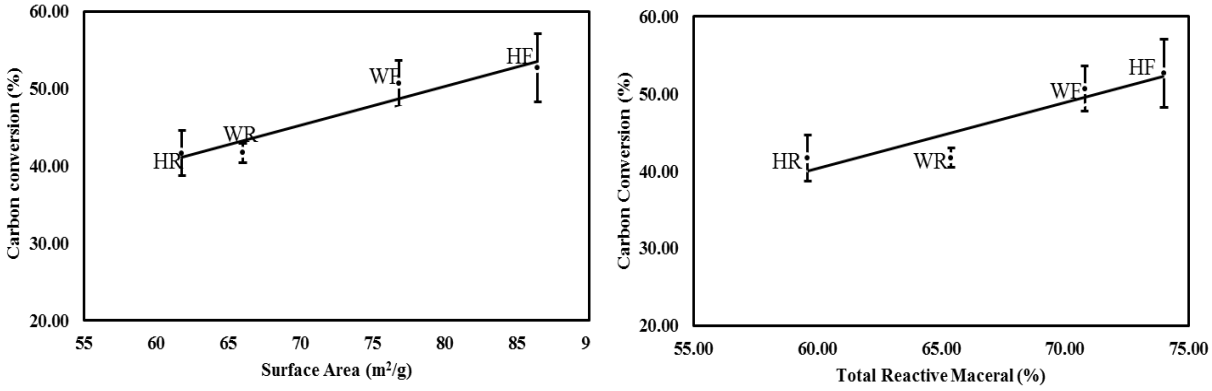

Figure 3-2: Correlation of (a) surface area vs carbon conversion, (b) Total reactive macerals vs conversion Note: HR= Highveld coal fines, HF<1.5= Highveld float fraction, WR= Waterberg coal fines, WF<1.5= Waterberg float fraction

Table 3-6: Percentages products distribution of coal fine discards and float fractions at 380°C, 400°C, 420°C, and coal conversion

		380°C		
	WR	WF	HR	HF
Residue	67±3.2	59.3±2.4	68.0±2.0	58.0±2.2
PAA	11.2±0.7	12.8±0.8	10.3±0.7	12.5±0.3
Gas	2.70±0.5	3.8±0.5	2.3±0.1	3.7±0.5
Oil	19.1±1.6	24.4±2.7	19.4±1.9	25.8±2.4
Conversion	33.00±2.8	40.70±3.5	31.60±3.0	42.00±3.9
		400°C		
Residue	60.5±2.4	52.60±2.3	63.1±2.0	51.5±2.9
PAA	10.2±0.5	11.9±0.9	9.0±0.9	10.5±0.5
Gas	5.0±0.3	6.7±0.5	4.0±0.6	6.8±0.6
Oil	24.3±1.7	28.8±1.3	23.9±1.3	31.2±1.5
Conversion	39.70±2.4	47.00±3.5	37.00±4.2	46.00±3.5
		420 °C		
Residue	57.0±2.1	45.70±3.3	58.30±2.8	44.8±1.2
PAA	8.00±0.7	10.80±0.6	8.30±0.6	9.8±0.3
Gas	6.00±0.6	8.7±0.5	5.5±0.3	8.2±0.6
Oil	29.00±1.1	34.8±1.1	27.9±1.5	37.2±1.2
Conversion	41.70±4.0	50.70±3.5	41.30±2.8	52.60±4.4

3.5 Effect of temperature on the product distribution

3.5.1 Effect of temperature on carbon conversion

The amounts of the direct liquefaction products of South Africa bituminous coal fine discards and their float fractions, using tetralin as solvent under N_2 at temperatures between 380 and 420°C are presented in Figure 3.1. As expected, carbon conversion increased with an increase in temperature. This trend is consistent with the data from previously reported studies.[15,16,33] The carbon conversion increased for the float fraction when compared to coal fine discards. This could be attributed to the higher vitrinite contents and low ash yields in the float fractions when compared to the coal fine discards. Barraza et al. [33] obtained a higher carbon conversion of about 85%wt. (daf) for density separated samples (float fraction) when compared to carbon conversion of the parent coal. They used bituminous coal from South America, which contained 92. 9%vol. vitrinite. Sofianos et al.[16] obtained a carbon conversion 93.3%wt. (daf) using a higher vitrinite rich (84.9%vol.) beneficiated Waterberg coal and water as a solvent in the DCL experiments.

3.5.2 Effect of temperature on products yields during the liquefaction tests

The oil yield increased as the temperature of the liquefaction increased (Figure 3.1). The increase in the oil yield could be as a result of the further breaking down of the pre-asphaltenes and residue parts of the products at higher temperatures leading to the formation of more oil and gases. The oil production efficiencies of the float fraction samples were higher when compared to the coal fine discards. The increase in oil yield agrees with the decrease in the PAA as the temperature of the liquefaction increased.

The PAA contents decreased with an increase in the liquefaction temperature (Figure 3.1). As described above, there was an increase in the percentage of oil at a higher temperature, with the corresponding decrease in amounts of PAA.

The amounts of residue decreased as the temperature of the liquefaction increased (Figure 3.1). For instance, the HF residue reduced from 58% at 380°C to 45.7% at 420°C. The residue from the WF reduced from 59% at 380°C to 50% at 420°C. Comparing the values of the residues of the coal fine discards and their corresponding float fractions, it was observed that the float samples have lower amounts of residue than the coal fine discards. This follows the same trend as for the carbon conversions, amounts of oil and gases that were obtained from the coal fine

discards. As temperature increases, the coal macromolecular structure further depolymerises, producing more oil and gases with a corresponding decrease in the amounts of the residues.

Figure 3.1 presents the gas yield results from the liquefaction experiments. During the liquefaction process, it has been observed by other investigators that the major liquefaction gas components include H_2, CO, CO_2 and some hydrocarbon compounds (C_mH_n) such as methane, ethane, and propane.[15,32] The gas yield increased from 4.0%wt. (daf) at 380 °C to 6.7% (daf) at 420 °C for the WF sample, and 3.8%wt. (daf) at 380°C to 6.0%wt. (daf) at 420 °C for the HF sample. The higher temperatures cause rupture of lighter hydrocarbons. Secondary reactions, such as cracking, methanation and steam reforming, will subsequently result in higher gas yields. [34,35]

3.6 Analysis of liquefaction products

3.6.1 Proximate, ultimate and ICP-OES analyses of residues, PAA and oils extracts

The proximate and ultimate analyses results of the PAA and oil extracts and the residues from the liquefaction experiments are shown in Table 3.7. An increase in the volatile matter, moisture and oxygen contents of the float fractions' residues and PAA extracts in comparison to those of the coal fine discards was observed. As expected, the float fractions residues showed relatively higher values of fixed carbon, volatile matter content and lower ash yields when compared to the residues obtained from the coal fine discards. The contents of fixed carbon and volatile matter in the residues from the float fractions and the coal fine discards were found to be lower than in the samples before liquefaction (Table 3.1). The low percentages of fixed carbon and volatile matter in the residues were attributed to the removal of organic matter in the coal matrix during liquefaction. The residue produced from coal fine discards contains a higher ash yield when compared to the float fraction residues, as expected. The PAAs produced from float samples showed a slight increase in fixed carbon, volatile matter and moisture contents in comparison to the PAA values for the coal fines samples.

During liquefaction, some minerals such as pyrite may be transformed to form other compounds.[36] Alkali and alkaline element-bearing minerals were detected in the liquefaction product residues using mineralogical analysis. These minerals may act as catalysts during the gasification process.[37] The ICP-OES analysis results for the residues and PAA parts of the liquefaction products are presented in Table 3.8. This Table indicates that the PAAs and residues produced from the liquefaction of the coal fine discards and their float fractions contained low amounts of Ca, Al, P, Mg, Mn, Ti and Fe compounds.

The calorific values (CVs) of the liquefaction residues from the float fractions were found to be higher than for the residues derived from the coal fine discards (see Table 3.7). The HS and PAA samples produced from all the samples had higher CVs compared to those of the residues. The O/C and H/C atomic ratios of the liquefaction residues from the coal fines and the float fractions do not show much difference. The H/C ratios of the HS oil products ranged from 1.03–1.08. The values of H/C of the HS products were higher when compared to those of the PAA and residue products. This could be attributed to the percentages of hydrogen that were extracted from the carbon matrix of the coal samples to form HS products during the liquefaction experiments.

The HS fractions from the liquefaction of the coal fine discards and their corresponding float fractions were similar in terms of their ultimate and proximate analyses. The oil (HS) fractions obtained from this study were carbon-rich fuels containing a low amount of nitrogen and a trace amount of sulphur. The density of the oily products (HS products) at 20 °C varied between 0.83 and 0.87 g/cm^{-3}, while the viscosity ranged from 1.5 to 2.08 mPas at 20°C. The flashpoints of the derived oil products ranged from 20.9–24.2°C.

Table 3-7: Proximate and the ultimate analyses results of DCL products (HS, PAAs and residues)

Residue					
Proximate Analysis (%wt. air-dry basis)	Standard method	HR	HF	WR	WF
% Inherent moisture content	ISO 11722: 1999	2.5	2.0	2.8	2.1
% Ash yield	ISO 1171: 2010	48.7	25.7	37.0	26.9
% Volatile Matter (VM)	ISO 5621: 2010	15.6	25.2	19.7	25.6
% Fixed carbon (FC)	(by difference)	33.2	47.1	40.5	45.4
Fuel ratio (FC/VM)		2.1	1.9	2.1	1.8
Calorific Value (MJ/kg)		15.6	22.7	16.8	25.7
Ultimate Analysis (%wt.daf) ISO 29541: 2010					
Carbon		82.9	85.4	81.9	85.3
Hydrogen		4.7	5.2	5.4	5.0
Nitrogen		2.0	1.8	1.7	2.0
Sulfur	ISO 19579: 2006	2.3	2.3	2.2	2.0
Oxygen	(by difference)	8.03	4.3	8.8	5.6
H/C (atomic ratio)		0.69	0.72	0.78	0.70
S/C		0.01	0.01	0.01	0.009
O/C		0.02	0.019	0.019	0.017
PAA					
Proximate Analysis (%wt. air-dry basis)	Standard method	HR	HF	WR	WF
% Inherent moisture content	ISO 11722: 1999	4.2	4.0	3.8	3.2
% Ash yield	ISO 1171: 2010	1.0	1.2	1.0	1.0
% Volatile Matter (VM)	ISO 5621: 2010	48.9	53.2	49.7	54.2
% Fixed carbon (FC)	(by difference)	45.9	41.6	45.5	40.0
Fuel ratio (FC/VM)		0.9	0.8	0.9	0.7

Calorific Value (MJ/kg)		34.5	33.6	33.8	34.8
Ultimate Analysis (%wt. daf) ISO 29541: 2010					
Carbon		86.4	87.4	86.1	87.7
Hydrogen		6.2	5.91	6.0	6.24
Nitrogen		2.0	2.1	1.9	1.7
Sulfur	ISO 19579: 2006	0.4	0.47	0.52	0.53
Oxygen	(by difference)	5.2	4.13	5.48	5.3
H/C (atomic ratio)		0.9	0.8	0.8	0.8
S/C		0.002	0.002	0.002	0.002
O/C		0.045	0.035	0.048	0.045
	HS				
Proximate Analysis (%wt. air-dry basis)	Standard method	HR	HF	WR	WF
% Inherent moisture content	ISO 11722: 1999	8.7	8.7	8.7	8.7
% Ash yield	ISO 1171: 2010	0.0	0.0	0.0	0.0
% Volatile Matter	ISO 5621: 2010	92.3	92.3	92.3	92.3
%Fixed carbon	(by difference)	0.0	0.0	0.0	0.0
Calorific Value (MJ/kg)		41.5	43.4	41.2	41.1
Ultimate Analysis (%wt. air-dry basis) ISO 29541: 2010					
Carbon		86.2	88.6	85.5	87.8
Hydrogen		7.8	7.9	7.4	7.6
Nitrogen		0.06	0.17	0.09	0.14
Sulfur	ISO 19579: 2006	0.2	0.21	0.17	0.2
Oxygen	(by difference)	5.7	3.2	6.8	4.4
H/C (atomic ratio)		1.08	1.06	1.03	1.03
Viscosity at 20°C (mPas)	ASTM D7806	1.5	1.9	2.0	2.1
Density (built-in u-tube cell) gcm^{-3}	ASTM D7777	0.83	0.87	0.83	0.83
Flashpoint (°C)	ASTM D7806	21.5	24.2	20.9	21.8

Table 3-8: Trace and lighter elements contents as determined by ICP-OES analyses in the float fractions, and their liquefaction products: PAAs and residues

Sample:	HR	HR-R	HF Raw	HF-R	HF-PAA	WR	WR-R	WF-Raw	WF-R	WF-PAA
					ppm					
B	33.0	50.0	49.0	71.0	17.0	10.0	14.0	13.0	7.0	2.0
Na	1161.0	1228.0	132.0	162.0	77.0	124.0	176.0	65.0	86.0	32.0
Mg	2650.0	3581.0	409.0	642.0	39.0	2393.0	2644.0	614.0	653.0	48.0
Al	11770.0	13540.0	2178.0	3248.0	53.0	7027.0	9586.0	1581.0	2102.0	108.0
P	1650.0	1470.0	844.0	1123.0	59.0	1300.2	1523.0	479.5	799.0	65.0
K	843.5	1991.0	286.0	400.2	63.1	798.0	1218.0	157.1	270.0	60.0
Ca	14390.0	22190.0	6530.0	7430.0	365.4	11780.0	12380.0	5066.0	6556.0	252.0
Ti	2300.0	2724.8	559.3	347	94.7	1054.0	1320.0	554.7	771.0	241.0
Cr	230.0	280.2	66.7	149.2	55.9	250.2	265	55.3	124.2	45.1
Mn	620.0	750.0	150.4	411.1	21.6	280.5	328.5	54.25	72.5	9.9
Fe	5402.0	7221.0	2193.0	3340.0	266.0	14880.0	12880.0	1852.0	3224.0	222.4
Pd	5.3	6.5	2.6	4.5	0.1	3.0	3.8	0.73	1.091	0.1
Ag	17.2	20.2	3.2	5.2	1.2	5.0	6.4	3.93	4.395	1.0
Ba	1200.0	1325.0	528.2	855.2	23.3	591	620.4	376.5	491.7	35.8

3.6.2 GC-MS analyses of the oily (HS) part of the liquefaction product

The GC-MS results for the oil samples produced from the liquefaction experiments using the Waterberg and Highveld float fractions are given in Table 3.9. The GC-MS results show that these oil samples contained similar organic compounds. The oil samples produced from both the Waterberg float and Highveld float samples contained 76.5% and 82% naphthalene, respectively. As expected, the oil produced from the coal fine discards is characterised by a lower percentage of naphthalene when compared to those produced from the float fractions. The presence of naphthalene in the oil sample could be due to the dissolution of organic matter in tetralin during the liquefaction experiments of the coal fine discards and their float fractions, and due to the transformation of tetralin. Other compounds that were detected by the GC-MS analysis include decalin, butyl benzene, methyl indane, phenol, trimethyl phenol, and o-cresol. Egiebor and Gray[14] in their study on the liquefaction of Highvale coal using argon as a reaction gas and tetralin as a solvent reported 94.5%wt. naphthalene in the oil part of their products.

Table 3-9: The GC-MS analysis results for the oil samples derived from HR, HF WR and WF at 420°C

	Mass, %			
Component	WR oil	WF oil	HR oil	HF oil
2,2-Dimethyl butane	0.1	0.0	0.0	0.0
2-Methyl pentane	1.8	0.1	0.4	0.0
3-Methyl pentane	2.0	0.0	0.0	0.0
N-Hexane	3.0	2.7	7.5	1.1
2-Methyl hexane	0.3	0.0	0.1	0.0
Methyl cyclopentane	0.9	0.1	0.5	0.0
Acetone	0.9	1.0	2.5	0.5
t-Decalin	1.2	1.1	1.0	1.0
c-Decalin	1.1	1.3	1.2	0.6
N-Tridecane	0.3	0.4	0.3	0.2
Butyl benzene	2.5	2.4	2.1	1.9
Allyl benzene	0.2	0.2	0.1	0.2
Methyl indan	9.5	9.5	8.2	7.3
Ethyl indan	0.7	0.8	0.8	0.6
Cyclopentyl indan	0.2	0.3	0.2	0.2
Dimethyl indan	0.3	0.3	0.3	0.2
Ethyl tetralin	0.2	0.2	0.2	0.3
Naphthalene	72.1	76.5	71.0	81.9
Butylated hydroxyl toluene	0.1	0.1	0.2	0.3
Trimethyl phenol +O-cresol	0.8	1.0	1.0	0.8
Phenol	0.3	0.3	0.3	0.6
Trimethyl Phenol	0.2	0.2	0.2	0.1
O-ethyl phenol	0.0	0.1	0.1	0.1
2,5-Xylenol	0.1	0.1	0.1	0.1
2,4- Xylenol	0.2	0.2	0.2	0.2
P- cresol	0.2	0.3	0.4	0.5
M- cresol	0.2	0.2	0.2	0.3
Ethyl methyl phenol	0.5	0.5	0.6	0.5
2,3- Xylenol	0.0	0.0	0.0	0.1
P-Ethyl phenol + 3,5- Xylenol	0.2	0.2	0.2	0.3
M-Ethyl phenol	0.1	0.1	0.1	0.1
3,4- Xylenol	0.1	0.1	0.2	0.1
Total	100.0	100.0	100.0	100.0

3.6.3 ^{1}H nuclear magnetic resonance analysis results of oily (HS) liquefaction products

The ^{1}H NMR results are shown in Table 3.10. For quantification purposes, the spectra were divided into regions, as indicated in Table 3.10. The sharp peak at 2.7 ppm is assigned to naphthenic hydrogen, and the peak at 1.8 ppm represents the resonance peak from β-CH_2, which is as a result of a CH_2 proton from tetralin.[15] The peaks at 4.5 ppm and 9.5 ppm are assigned to the aromatic hydrogen.[14,38] It was observed that the H_{ar}/H_{al} ratios for the oil obtained from the Waterberg and Highveld float samples were 2.2 and 2.6, respectively. These values were slightly higher when compared to the oil obtained from the coal fine discards. This implies that relatively more aromatic hydrogen is present in oils derived from the float fractions when compared to those of the coal fine discards. Table 3.10 shows the quantitative results of the ^{1}H NMR. The oil sample produced from WF contained higher aliphatic and low aromatic hydrogen contents than those of oil from the HF sample. These results are in a good agreement with the GC-MS results for the float fractions when compared to those for the oil from the coal fine discards. The ^{1}H NMR results obtained in this study are comparable with the results obtained by other researchers [14] for the liquefaction of Highveld coal using tetralin as a solvent.

Table 3-10: Proton NMR results of the oil samples derived from HR, HF, WR and WF at 420°C (ppm)

	Symbol	Peaks	WR Oil	WF Oil	HR Oil	HF Oil	HC oil[15]
Aliphatic proton 0.5–4.5 ppm	H_{Al}		**36**	**30.9**	**39**	**27.5**	**28.5**
Aliphatic H γ to an aromatics	Hγ	0.5-1.00	1.6	2.2	0.8	1.5	1.3
Aliphatic methyl β to an aromatics	$H_{\beta1}$	1.0-1.6	2.9	3.4	3.5	2.4	4.4
Alicyclic H β to two aromatics (naphtenic, methylene)	$H_{\beta2}$	1.6-2.00	9.2	8.2	10.2	7.8	6.70
Aliphatic H in methyl or methylene to aromatic and possible attached to another ring	$H_{\alpha1}$	2.0-3.0	17.2	14.2	18.4	13.5	16.0
Aliphatic H in methylene to an aromatic ring and β to another or two rings	$H_{A,\ F}$	3.0-3.69	2.8	1.2	3.2	0.78	-
Aliphatic H in methyl or methylene to two aromatic rings	H_D	3.69-4.5	2.3	1.7	2.9	1.5	-
Olefinic protons (4.5–6.3 ppm)	H_{ol}	4.5-6.3	-	-	-	-	-
Aromatic protons (6.3–9.5 ppm)	H_{Ar}		**64**	**69.1**	**61**	**72.5**	**71.5**
Aromatic hydrogen	H_{ArUC}	4.5-6.3	60.8	66.8	56.5	71.3	71.5
Sterically hindered aromatic hydrogen (phenolic H)	H_{ArC}	6.3-8.36	3.2	2.3	4.5	1.2	-
		Total	**100**	**100**	**100**	**100**	**100**
H_{ar}/H_{al}			1.8	2.2	1.6	2.6	2.5

HC = values from oil obtained by Egiebor and Gray[14] on the liquefaction of Highvale coal[15]

3.6.4 Solid-state ^{13}C nuclear magnetic resonance results

The NMR spectra of the coal fines discard, float fractions samples, residue and PAA samples are presented in Figure 3.3. The coal structural parameters were calculated as described in the literature.[24,25] The spectra showed two distinct peaks with a pronounced peak in the region of 90–200 ppm, which indicates the aromatic peaks and an aliphatic peak in a region of 0–90 ppm. A small spin sideband with low intensity, which indicates an aromatic ring, was observed in the region of 200–240 ppm.[21] The aliphatic carbon has methyl groups at 0–25 ppm; methylene carbon appears within the region of 25–50 ppm, methoxyl groups resonates at 50–65 ppm, while the ester group appears at 65–80 ppm.[39,40] PAAs extracts of the float fractions and their residues gave similar spectra in the aromatic and the aliphatic regions. When comparing the peak intensities of the float fractions, residues and the PAAs, peak broadening was observed for the float fractions and the residues in the aromatic and the aliphatic regions.

The NMR structural parameter results are shown in Table 3.11. It was observed that there was a slight difference in the fraction of aromatics (f_a) between the coal fine discards and float fractions. The HF sample contained 76% aromatic carbon and 24% aliphatic carbon, while the WF contained 78% aromatic carbon and 22% aliphatic carbon respectively. When comparing the aromatic and aliphatic carbon of the float fractions to the coal fine discards, it was observed that the aromatic carbon of the coal fine discards was slightly higher than those of the float fractions. The HR and WR samples contained 80% and 82% respectively of aromatic carbon. The residues produced from the float fractions showed a slight increase in the aromatic carbon contents and a corresponding decrease in the aliphatic contents when compared to those of the coal fine discards.

The PAAs produced from the WF sample was made up of 74% aromatic and 26% aliphatic carbon. The PAAs produced from the HF contained 72% aromatic and 28% aliphatic. The PAAs of the WR was made up of 72% aromatic and 28% aliphatic. The PAAs produced from the HR contained 74% aromatic and 26% aliphatic. The NMR results indicated that the PAAs from the float fractions and the coal does not show much difference in the aromatic and the aliphatic carbon contents. Tetralin as a solvent during liquefaction of South African float fractions from the coal fine discards produced PAAs containing a higher proportion of aromatic carbon and a low percentage of aliphatic carbon. Similar results were reported by other researchers during solvent extraction of Canadian low-rank coal and Montana sub-bituminous coal using non-polar organic solvents.[41]

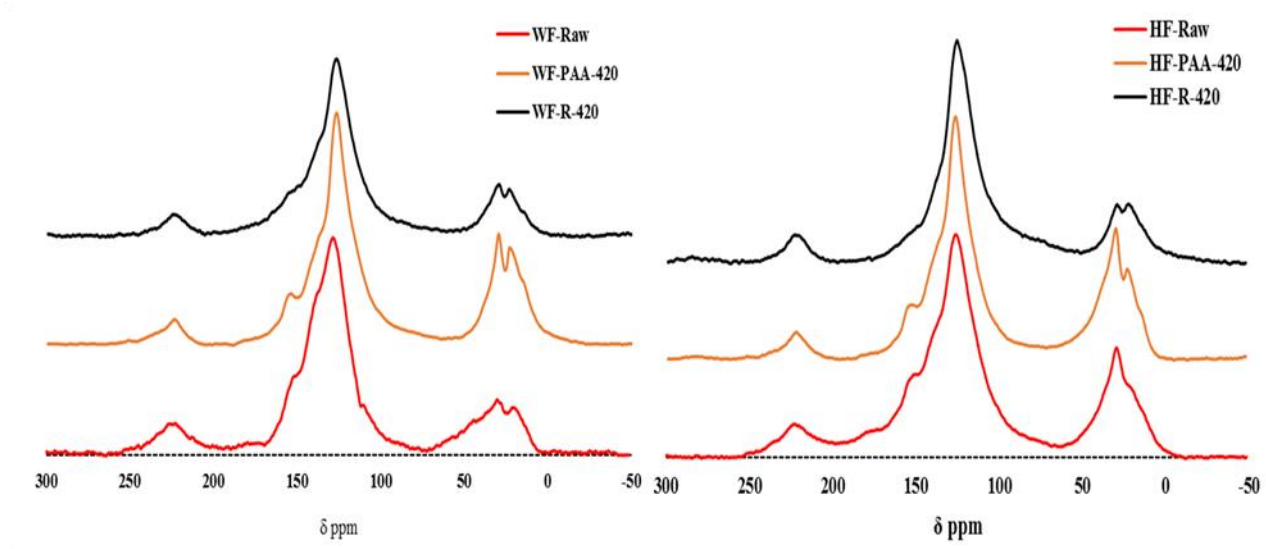

Figure 3-3: ^{13}C CP NMR spectrum of the float fractions and their liquefaction products: residues and PAAs

Table 3-11: Structural parameters from solid-state ^{13}C CP-NMR for the coal fines, float fractions and their liquefaction products: residues and PAAs

	WR	WR-PAA-420°C	WR-R-420°C	WF1.5	WF-PAA-420°C	WF-R-420°C	HR	HR-PAA-420°C	HR-R-420°C	HF1.5	HF-PAA-420°C	HF-R-420 ˚C
Fraction aromatic	0.80	0.72	0.82	0.73	0.74	0.86	0.81	0.77	0.82	0.78	0.72	0.84
Aromatic carbon	0.75	0.70	0.75	0.72	0.73	0.81	0.74	0.75	0.76	0.75	0.71	0.79
Fraction of aliphatic	0.20	0.28	0.18	0.27	0.26	0.14	0.19	0.23	0.18	0.22	0.28	0.16
Aliphatic carbons bonded to oxygen	0.05	0.04	0.07	0.03	0.03	0.02	0.042	0.03	0.06	0.038	0.04	0.05
Carbonyl/carboxyl and amide carbons	0.09	0.02	0.07	0.06	0.03	0.03	0.07	0.02	0.05	0.07	0.01	0.04
Fraction phenolics	0.10	0.06	0.09	0.08	0.06	0.02	0.10	0.07	0.09	0.09	0.06	0.04
Fraction alkylated aromatic	0.16	0.13	0.15	0.16	0.14	0.16	0.16	0.14	0.15	0.16	0.14	0.15
Fraction non-protonated aromatic carbons	0.50	0.51	0.50	0.54	0.51	0.56	0.56	0.55	0.51	0.54	0.51	0.62
Fraction protonated aromatic carbons	0.22	0.19	0.25	0.21	0.22	0.25	0.19	0.2	0.25	0.2	0.2	0.15
Aromatic bridgehead carbons	0.29	0.32	0.25	0.25	0.3	0.32	0.31	0.34	0.27	0.3	0.31	0.33
Fraction of methyl groups in aliphatic	0.06	0.10	0.05	0.08	0.12	0.06	0.05	0.08	0.05	0.07	0.14	0.06
Aliphatic CH and CH_2	0.13	0.18	0.08	0.41	0.16	0.08	0.11	0.14	0.05	0.31	0.18	0.1

Summary

This investigation studied the liquefaction of coal fine discards and their corresponding float fractions. Liquefaction was conducted using tetralin as a solvent under inert atmosphere (N_2). Results of the liquefaction tests revealed that the float fractions achieved higher carbon conversions, oil yields and gas yields when compared to the coal fine discards. The higher oil yields and carbon conversions of the float fractions were attributed to the higher concentrations of the vitrinite macerals, higher surface areas, porosity, organic carbon contents and alkaline indices (catalytic effect) of the float fractions in comparison to the coal fine discards. The effect of temperature revealed that as temperature increased the yields of oil and gas increased, with a corresponding decrease in the amounts of PAA and residue samples, as expected.

Analysis of the different liquefaction products were performed using traditional and advanced analytical techniques. The analytical results of the liquefaction products showed that the residues produced from the float fractions have lower contents of FC and VM and lower CV than those of the coal fine discards, indicating better conversion for the float fractions. The oil yields of all the samples showed a high relative heating rate and high amounts of volatile matter. The GC-MS results for the oil samples show that this oil contained mainly naphthalene with lower amounts of other aliphatic and aromatic compounds.

The oil produced from the float fractions contained higher contents of aromatic hydrogen and naphthalene when compared to the oil produced from the coal fine discards. The results obtained from the liquefaction test suggested that the beneficiated coal fine discards (density separated float fraction) will improve the carbon conversion and percentage oil yield during direct liquefaction processes. Also, the float fractions produced from the coal fine discards may be used as a feedstock for utilisation in the direct coal liquefaction process.

3.7 Conclusions

The direct liquefaction of South African coal fine discards and their float fractions were investigated with tetralin as a solvent, using a laboratory autoclave at a temperature ranging from 380–420°C under inert N_2 atmosphere, with an initial pressure of 3 MPa. The results showed that density separation of coal fine discards produced a float fraction beneficial for direct liquefaction. Density separation of the coal fine discards provides a float fraction with the following enhanced properties in comparison to the coal fine discards before beneficiation:

- The float fractions show higher calorific values, surface areas, vitrinite contents and reactive maceral contents with a reduction in ash yield. These characteristics render the float fractions more reactive and more suitable for utilisation in direct coal liquefaction processes.
- Higher carbon conversions were achieved from the float fractions with a corresponding decrease in the amounts of residues. An increase in liquefaction temperature increased the carbon conversion and the yield of oil. These are attributed to the increase in the vitrinite contents in the float samples.
- The oil produced from liquefaction of the float fractions contained a relatively higher amount of hydrogen-bonded to aromatic rings and a relatively higher percentage of naphthalene.
- Proximate and ultimate analyses indicated that the oil and the PAA parts of the liquefaction products have higher calorific values and higher fixed carbon contents when compared to the residues, which have higher ash yields. However, the residue samples from the float fractions could be suitable as feedstock for the utilisation in combustion and gasification processes, due to relatively high calorific values and fixed carbon contents and lower ash yields when compared to residues from the coal fines.
- Solid-state NMR results indicated that the Highveld float sample contained 76% aromatic and 24% aliphatic carbon respectively, while the WF contained 78% aromatic and 22% aliphatic carbon respectively. When comparing these to the coal fines, it was observed that the aromatic carbon of the coal fines was slightly higher than that of the float fractions, with the WF and HR samples having aromatic carbon contents of 80% and 82% respectively. Solid-state NMR results indicated that the HF sample contained 76% aromatic and 24% aliphatic carbon, while the WF sample contained 78% aromatic and 22% aliphatic carbon. When comparing these to the coal fines, it was observed that the aromatic carbon of the coal fines was slightly higher than that of the float fractions.

Density separation of coal fines is beneficial to produce a float fraction that may be used as feedstock for DCL. This paper showed that density separation of Highveld and Waterberg discarded coal fines leads to a float fraction that gave liquefaction products similar to that reported in the literature for other bituminous feed coals.[15,16] The volumes of fine coal and high costs associated with the disposal and handling thereof may be reduced by utilising density separation to obtain a feedstock for direct liquefaction. This utilisation will also assist in reducing environmental problems (dust, spontaneous combustion and acid mine drainage).

- **Acknowledgements**

The work presented in this paper is based on the research supported by the South African Research Chairs Initiative of the Department of Science and Technology and National Research Foundation of South Africa (Coal Research Chair Grant No.: 86880 and incentive grant No. 115228). Any opinion, finding or conclusion or recommendation expressed in this material is that of the author(s) and the NRF does not accept any liability in this regard. The XRD and XRF analyses done at North-West University laboratories (Mrs Belinda Venter) are acknowledged. Dr Kgutso Mokoena is also acknowledged for assisting with the GC-MS analysis of the oil samples. Bureau Veritas Testing and Inspection and SGS inspection, verification, testing and laboratories are acknowledged for assisting with the analytical methods. South African power stations (Highveld and Waterberg) are acknowledged for the supply of the coal samples used in this study.

3.8 Chapter 3 references

1. EIA: U.S. Energy Information and Administration, 2015 http://www.connaissancedesenergies.org/sites/default/files/pdf-pt-vue/south_africa.pdf.
2. Fossil fuel foundation: Unlocking the past for the future submission to the Department of Energy Re. IRP 2016. http://www.fossilfuel.co.za/wp-content/uploads/2017/06/FFF-response-to-IRP2016_Rev-5-003.pdf (accessed 20-02-2017).
3. Matjie, R.H.; Li, Z.; Ward, C.R.; Kosasi, J.; Bunt, J.B. and Strydom, C.A. Mineralogy of furnace deposit produced by South African coals during pulverized-fuel combustion tests. *Energy & Fuels* **2015**, 29, 8226- 8238.
4. Reddick, J.F.; Von Blottnitz, H.; Kothuis, B. A cleaner production assessment of ultra-fine coal waste generated in South Africa. *J. South. Afr*, **2007**, 107, 55-60.
5. Keogh, R. A.; Taulbee, D. N.; Hower, J. C.; Chawla, B.; Davis, B. H. Liquefaction characteristics of the three major maceral groups separated from a single coal. *Energy & Fuels* **1992**, 6, 614-618.
6. Dyrkacz, G.R.; Horwitz, E.P. Separation of coal macerals. *Fuel* **1982**, 61, 3-12.
7. Choi, C.Y.; Muntean, J.V.; Thompson, A.R.; Botto, R.E. Characterisation of coal macerals using combined chemical and NMR spectroscopic methods. *Energy & Fuels* **1989**, 3, 528-33.
8. Akash, B.A. Thermochemical liquefaction of coal. *Int. J. Therm. Environ. Eng*. **2013**, 5, 51-60.
9. Mochida, I.; Okuma, O.; Yoon, S.H. Chemicals from direct coal liquefaction. *Chem. Rev.,* **2013**, 114, 1637-72.
10. Masaki, K.; Yoshida, T.; Li, C.; Takanohashi, T.; Saito, I. The effects of pretreatment and the addition of polar compounds on the production of “HyperCoal” from sub-bituminous coals. *Energy & Fuels* **2004**, 18, 995-1000.
11. Kim, S.; Woo, K.J.; Jeong, S.K.; Rhim, Y.J.; Lee, S.H. Production of low ash coal by thermal extraction with N-methyl-2-pyrrolidinone. *Korean J. Chem. Eng.* **2008**, 25, 758-63.
12. Renganathan, K.; Zondlo, J.W.; Mintz, E.A.; Kneisl, P.; Stiller, A.H. Preparation of an ultra-low ash coal extract under mild conditions. *Fuel Process. Technol*. **1988**, 18, 273-8.

13. Wang, S.; Tang, Y.; Schobert, H. H.; Guo, Y.; Su, Y. Petrology and structural studies in liquefaction reactions of Late Permian coals from Southern China. *Fuel*, **2013**, 107, 518–524.

14. Egiebor, N. O.; & Gray, M. R. Evidence for methane reactivity during coal pyrolysis and liquefaction. *Fuel* **1990**, 69, 1276–1282.

15. Sehume, T. Z.; Strydom, C. A.; Bunt, J. R.; Schobert, H. H. Effectivity of Phenol during Solvent Extraction of a South African Bituminous Coal under Mild Conditions. *Energy & Fuels* **2017**, 31, 13655−13665.

16. Sofianos, A.C.; Butler, A.C.; Louwrens, H.B. Catalytic liquefaction of South African coals using the carbon Monoxide/Water system. Part 1: Pyrite Catalysis. *Fuel Process. Technol.* **1989,** 22, 175–188.

17. Speakman, S.A. Introduction to PANalytical X'Pert HighScore Plus v3.0, PhD MIT Center for Materials Science and Engineering, 2012, 1–107 [Web:], (http://prism.mit.edu/xray/tutorials.htm).

18. Rietveld, H.M. A profile refinement method for nuclear and magnetic structures. *J. Appl. Crystallogr.* **1969**, 2, 65–71.

19. Norrish, K.; Hutton, J.T. An accurate X-ray spectrographic method for the analysis of a wide range of geological samples. *Geochimi. Cosmochimica. Acta*. **1969**, 33, 431–453.

20. Uwaoma, R.C., Water leaching of inorganic species from coal ash and slag generated at typical Underground Coal Gasification (UGC) temperature, M.Sc. dissertation. North-West University, 2017, 77p.

21. Causemann S., Report on ss ^{13}C NMR characterisation of four coal samples. Central Analytical Facility (CAF), Stellenbosch University; 2012. 6p.

22. Okolo, G. N.; Neomagus, H. W.; Everson, R. C.; Roberts, M. J.; Bunt, J. R.; Sakurovs, R.; Mathews, J. P. Chemical–structural properties of South African bituminous coals: Insights from wide-angle XRD–carbon fraction analysis, ATR–FTIR, solid-state 13C NMR, and HRTEM techniques. *Fuel* **2015**, 158, 779–792.

23. Solum, M. S.; Pugmire, R. J.; Grant, D. M. Carbon-13 solid-state NMR of Argonne-premium coals. *Energy & Fuels* **1989**, 3,187–193.

24. Solum, M. S.; Sarofim, A. F.; Pugmire, R. J.; Fletcher, T. H.; Zhang, H. 13C NMR analysis of soot produced from model compounds and a coal. *Energy & Fuels*, **2001**, 15, 961–971.

25. Wang, S.; Tang, Y.; Schobert, H.H.; Guo, Y.; Su, Y. Petrology and structural studies in liquefaction reactions of Late Permian coals from Southern China. *Fuel*, **2013**,107, 518–524.

26. Ward, C. R. Analysis and significance of mineral matter in coal seams. *Int. J. Coal Geol.* **2002**, 50, 135–168.

27. Mukherjee, D. K.; Chowdhury, P. B. Catalytic effect of mineral matter constituents in a North Assam coal on hydrogenation. *Fuel,* **1976**, 55, 4–8.

28. Gözmen, B.; Artok, L.; Erbatur, G.; Erbatur, O. Direct liquefaction of high-sulfur coals: Effects of the catalyst, the solvent, and the mineral matter. *Energy & Fuels* **2002**, 16, 1040–1047.

29. Hirschon, A. S.; Wilson Jr, R. B. Highly dispersed coal liquefaction catalysts. *Fuel* **1992**, 71, 1025-1031.

30. Murakami, K.; Yokono, T.; Sanada, Y. An investigation of the role of hydrogen sulphide in coal liquefaction catalysis by high-temperature and high-pressure e.s.r. *Fuel* **1986**, 65, 1079-1080.

31. Kabe, T.; Ishihara, A.; Qian, E. W.; Sutrisna, I. P.; Kabe, Y. *Coal and coal-related compounds: structures, reactivity and catalytic reactions*, Elsevier: Tokyo 2004, vol. 150, Chapter 4, 181–266.

32. Jin, L.; Han, K.; Wang, J.; Hu, H. Direct liquefaction behaviors of Bulianta coal and its macerals. *Fuel Process. Technol.* **2014**,128, 232-237.

33. Barraza, J.; Portilla, A.; Piñeres, J. Direct liquefaction of vitrinite concentrates obtained by column flotation. *Fuel Process. Technol.* **2011**, 92, 776-779.

34. Görling, M.; Larsson, M.; Alvfors, P. Bio-methane via fast pyrolysis of biomass. *Appl. Eng.* **2013**,112, 440-447.

35. Wang, N.; Chen, D.; Arena, U., & He, P. Hot char-catalytic reforming of volatiles from MSW pyrolysis. *Appl. Eng.* **2017**, 191, 111-124.

36. Kotanigawa, T.; Yamamoto, M.; Sasaki, M.; Wang, N.; Nagaishi, H.; Yoshida, T. Active site of iron-based catalyst in coal liquefaction. *Energy & Fuels* **1997**, 11, 190-193.

37. Floess, J. K.; Longwell, J. P.; Sarofim, A. F. Intrinsic reaction kinetics of microporous carbons. 1. Noncatalysed chars. *Energy & Fuels* **1988**, 2, 18-26.

38. Allen, D. T.; Grandy, D. W.; Petrakis, L. Comparative structural profiles of heavy bitumens by a novel functional group analysis. In *Characterization of Heavy Crude Oils and Petroleum Residues;* Technip Paris, 1984, p 309.

39. Franco, D. V.; Gelan, J. M.; Martens, H. J.; Vanderzande, D. J. M. Characterization by 13C CP/MAS NMR spectroscopy of the structural changes in coals after chemical treatments. *Fuel* **1991**, 70, 811-817.

40. Song, C.; Hou, L.; Saini, A. K.; Hatcher, P. G.; Schobert, H. H. CPMAS 13C NMR and pyrolysis-GC-MS studies of structure and liquefaction reactions of Montana sub-bituminous coal. *Fuel Process. Technol.* **1993**, 34, 249-276.

41. Rahman, M.; Samanta, A.; Gupta, R. Production and characterization of ash-free coal from low-rank Canadian coal by solvent extraction. *Fuel Process. Technol*. **2013** *115*, 88-98.

CHAPTER 4: PYROLYSIS OF TETRALIN LIQUEFACTION DERIVED RESIDUES FROM LIGHTER DENSITY FRACTIONS PRODUCED OF WASTE COALS TAKEN FROM WASTE COAL DISPOSAL SITES IN SOUTH AFRICA.

R.C. Uwaoma, C.A. Strydom, R.H. Matjie, J.R. Bunt, G.N. Okolo, D.J. Brand

In this chapter, the pyrolysis of residues derived from tetralin liquefaction of the float fractions from the coal fines and the analysis of the different pyrolytic products (tar and char) are reported.

The content of this paper was published in Energy & Fuels. **2019**, 33(9):9074-86.

Abstract

The lighter density (<1.5 g/cm^3) fractions produced from two waste coals sampled from the waste coal disposal sites at thermochemical plants situated in South Africa were used as feed materials for liquefaction with tetralin. The liquefaction residues from the lighter density and untreated lighter density fractions were used in pyrolysis experiments. Pyrolysis of the lighter density fractions was carried out in a Fischer Assay oven at 750 and 920°C under an argon atmosphere. Advanced analytical techniques (gas chromatography−mass spectrometry and nuclear magnetic resonance (NMR) spectroscopy) were employed to characterise the pyrolysis products. Also, the lighter density fractions, liquefaction residues, and their chars were examined using conventional and advanced analytical techniques. The pyrolysis char yields of the liquefaction residues ranged between 74% and 76%, and those of the coal float fractions ranged between 67.0 and 71.5%. Gas pyrolysis yields ranged between 16.0% and 20.0% for the residues and between 14.5% and 18.4% for the lighter density fractions, while the pyrolytic water and the tar products of the lighter density fractions were slightly higher than those of the liquefaction-derived residues. The proton NMR analysis of the tars from the residues shows marginally higher amounts of aromatic protons than those of the lighter density fractions. Chars which were generated after pyrolysis of the liquefaction-derived residues show higher porosity values than those from the pyrolysis of the lighter density fractions. The differences in the porosities are attributed to the opening of pores and extraction of some lower molecular mass aliphatic species from the coal matrix during liquefaction. The pyrolysis products distribution and analysis of the products showed that the residues (waste material) generated after tetralin liquefaction of the float fractions from the float−sink experiments of waste coals may be utilised for thermochemical processes (pyrolysis).

Keywords: tetralin, coal float fraction, liquefaction residues, pyrolysis, density separation

4.1 Introduction

Liquefaction of the lighter density (<1.5 g/cm^3) fractions generated from the float−sink experiments of waste coal deals with the thermal degradation of coal organic matter in a hydrogen-rich solvent, under moderate temperature (<450°C) and pressure, to produce gases, mixed oil, and coal residues. Research studies have shown that residues produced during coal liquefaction contain a significant amount of organic matter. The high concentrations of carbon and hydrogen in these residues indicate a possibility for their utilisation for pyrolysis and gasification.[1-6]

The liquefaction-derived coal residues properties results obtained from waste coals and their <1.5 g/cm^3 lighter density fractions are similar to those of the feedstocks used during coal thermochemical processes.[7] Discarding coal residues from liquefaction processes may have negative environmental impacts, including health risks and generation of polluting gases. The utilisation of these residues as a starting material for pyrolysis, gasification, or combustion processes may present an opportunity to produce valuable products and to reduce the negative environmental impacts of the waste material.

Currently, the information with regards to the pyrolysis of coal residues produced from the liquefaction of density- separated fractions (<1.5 g/cm^3 floats) is limited. Previous studies on pyrolysis of coal and analysis of the pyrolytic products focused on the use of bituminous coal liquefaction of South African lighter density fractions from waste from South Africa as a feedstock.[8,9] Analysis of the pyrolytic products generated from the residues after coal liquefaction has not yet been reported in the literature.[7,10] The utilisation of the residues produced after liquefaction of lighter density fractions may assist in decreasing the amounts of this waste material.

This paper compares the pyrolysis products produced from the residues after liquefaction of the lighter density fractions (obtained from float−sink experiments of waste coals) to the pyrolysis products from the lighter density fractions. Analyses of the tars and chars were carried out using advanced and traditional techniques (solid-state ^{13}C and liquid-state nuclear magnetic resonance (NMR), gas chromatography−mass spectrometry (GC−MS), CO_2 low-pressure adsorption, Fourier-transform infrared (FTIR), proximate, and ultimate). Understanding the pyrolysis behaviour of the liquefaction residues with regards to different pyrolytic products (tars, water, gases, and chars) will give an insight into the usefulness of liquefaction-derived residues of the lighter density fractions from the waste coals for further thermochemical processing.

4.2 Experimental procedures and analytical methods

4.2.1 Material

The Highveld float (<1.5 g/cm^3) (HF) and Waterberg float (<1.5 g/cm^3) (WF) fractions were produced via float-sink experiments of Highveld and Waterberg coal wastes as described earlier.[7] The HF and WF samples stand for the lighter density fractions generated from the float-sink experiments of the waste coal according to the method described by Uwaoma et al.[7] The results of conventional analyses (proximate and ultimate) of these samples were presented and discussed in the recent article by Uwaoma et al. [7]

4.2.2 Pyrolysis

Pyrolysis of the samples was performed using two instruments: a thermogravimetric analyser (TGA) and in a modified Fisher Assay set-up, as described below.

4.2.2.1 Thermogravimetric analyses

The lighter float fractions and their liquefaction-derived residues were subjected to thermogravimetric analyses using an SDT Q600 TGA. The procedure which was used for the thermogravimetric experiment has been reported.[11]

4.2.2.2 Fisher Assay analyses

The liquefaction-derived residues and the waste coal float fractions were air-dried and screened to −212 μm particle size. The samples were thoroughly mixed three times using a standard cone and quartering method (DD CENT/ TS14780:2005). This method was employed in order to obtain a representative sample that will be used for pyrolysis test.

Pyrolysis of the samples was conducted using a modified Fisher Assay setup as described by Roets et al.[8] and shown in Figure 4.1. The Fisher Assay equipment was designed to carry out experiments at temperatures above the ISO 647 temperature. Pyrolysis tests were conducted on the float samples from the untreated waste coals, and their liquefaction-derived residues from the lighter density fractions in an ASS316 high-pressure stainless steel reactor (50 g capacity, 55 mm diameter, and 65 mm height). The pyrolysis method of waste coal is stated elsewhere.[8] The modified Fisher Assay setup can withstand temperatures up to 1000°C using stainless steel retorts. The equipment is also designed in such a way that the different fractions of the pyrolytic distribution products (char, tar, gas, and pyrolytic water) can be captured and quantified.[8,12] The condensed volatiles and pyrolytic water were trapped in a scrubber solution containing toluene. A Dean−Stark distillation setup was used to isolate the pyrolytic water and the condensed volatile fraction from the mixture of condensed volatiles and gas liquor captured

by toluene. After removal of the pyrolytic water, the toluene was removed in a rotary evaporation setup at 60°C and pressure of 27 mbar by heating it for 20 min. Tedlar bags were used to capture the gases from the solvent scrubbers.

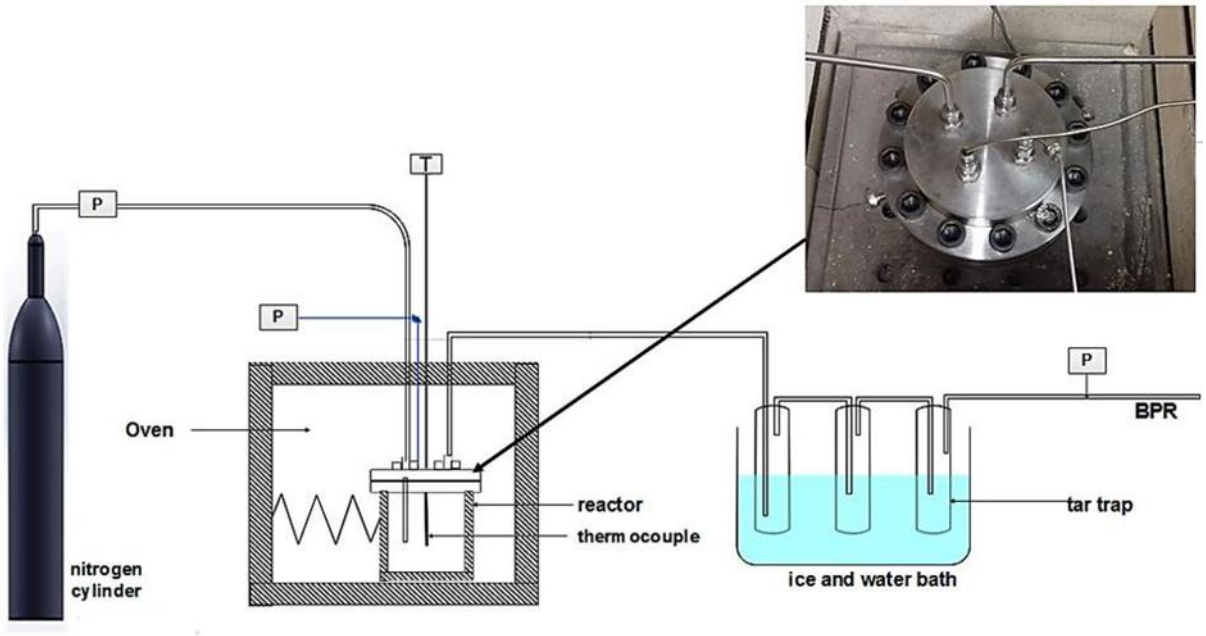

Figure 4-1: The Fisher Assay setup (adapted from Roet et al.[8])

The pyrolytic water, tar, char, and gas yields were evaluated on a dry basis using the following equations:

$$Pyrolytic\ water,\ \%\text{wt.}: \quad \frac{W_1 \times 100}{W_0} - M_{ad} \tag{4.1}$$

$$Tar,\ \%wt.: \quad \frac{W_2 \times 100}{W_0};\ W_2 = W_{RV,f} - W_{RV,i} \tag{4.2}$$

$$Char,\ \%wt. \quad \frac{W_3 \times 100}{W_0} \tag{4.3}$$

$$Gas, \%wt.: 100 - (char + tar + total\ water) \tag{4.4}$$

Where W_0 is mass of the coal (float fractions and residues) dry basis; W_1 is mass of total water; W_2 is mass of tar, which was calculated from the mass of the empty rotary evaporation flask ($W_{RV,\,i}$) and the mass of the rotary evaporation flask after toluene removal ($W_{RV,f}$); W_3 is mass of char; M_{ad} is moisture content, %wt., in the original sample on an air-dry basis (ad).

4.3 Analysis of pyrolysis products

4.3.1 Tar analysis

- **GC-MS and Gas Chromatography-Flame Ionisation Detection (GC-FID) Analyses**

GC−MS and GC−FID analyses of tars generated from the pyrolysis test were carried out by using an Agilent 7890 GC equipped with an FID and an Agilent 7890N GC connected to a mass selective detector (MSD). Only semi-quantitative results were obtained from the GC−FID and GC− MS techniques. GC−MS was used first for peak identification before performing GC−FID on the samples for quantification of different components in the tar. Before GC−MS analysis, approximately 200 mg of tar samples were dissolved in 2 cm^3 of dichloromethane (CH_2Cl_2). About 0.2 µL of the solution (tar and solvent) was inserted into the GC with a split ratio of 100:1. The procedure for the GC− MS analysis of the tar samples is reported in the literature.[7]

- **NMR analysis of tar**

An Agilent 600 MHz Inova spectrometer was used to conduct the liquid-state proton (^1H) and carbon-13 (^{13}C) NMR analyses using deuterated chloroform ($CDCl_3$) as a solvent. The standard pulse sequences were modified in VnmrJ 4.2 to obtain semiquantitative NMR spectra. The modifications are for proton (onepul, 60 s relaxation delay) and carbon (onepul, gated decoupling, 15 s relaxation delay), respectively. Before the liquid-state analysis, 20 mg of the tar sample was dissolved in the solvent ($CDCl_3$). Tetramethylsilane (TMS) was added to the samples and the signal used as the internal chemical shift reference and set to 0 ppm. The spectra were broadly divided into aliphatic and aromatic integral regions and further subdivided using the same reset points as set by other investigators.[13,14] For the proton NMR aliphatic functional groups analysis, chemical shift values were defined from 0.5 to 5 ppm and the aromatic functional groups from 6 to 9 ppm. For the ^{13}C NMR analysis, the spectral regions are respectively defined from 0 to 100 ppm (aliphatic compounds) and 100 to 160 ppm (aromatic compounds).

- **FTIR analysis of tar**

The FTIR spectra of the tars produced in this study were measured using a Spectrum 100 FTIR spectrometer (Perkin Elmer) with a Pike Miracle detector. The FTIR analysis of the tar samples is reported elsewhere.[15] A spectral resolution of 2 cm^{-1}, 32 scans, and a wavenumber range of 4000−400 cm^{-1} was used to obtain qualitative FTIR results.

4.3.2 Char composition

- **Proximate and ultimate analyses**

Proximate analysis was conducted on the lighter density fractions, their liquefaction residues and subsequent chars generated after the pyrolysis test, standard procedure was followed to obtained proximate results. The percentage inherent moisture content, ash yield, and volatile

matter content of all the samples were evaluated using the ISO standard methods reported in our previous study.[7] The fixed carbon content was evaluated by difference. The ultimate analysis of the same samples submitted for the proximate analysis following ISO 29541: 2010 standard procedure determines the percentages of C, H, S and N in these samples. The percentage of elemental oxygen was evaluated by difference. Chars were characterised using a CE 440 elemental analyser.

- **Solid-state ^{13}C NMR**

The coal analysis utilised ^{13}C CP and CP with Dipolar Dephasing (DD) NMR experiments (protonated carbon suppression) performed at 12kHz MAS as described elsewhere.[16,17] This method is very cost-effective and still relevant today and was subsequently reinstated at the Central Analytical Facility of the University of Stellenbosch (Republic of South Africa). The model used for the spectra acquisition and the conditions employed in recording the spectra of ^{13}C CP and CP DD has been reported in the literature.[7] The same amount of transients was used for both the ^{13}C CP and CP DD NMR experiments of a particular sample. These consisted of an HF char at 920°C, HF liquefaction residue char at 920°C, WF char at 920 °C and a WF liquefaction residue char at 920°C. The solid-state NMR experiments, processing and the calculation of different coal fractions have been reported extensively by the same investigators.[16,17]

- **CO_2 surface analysis**

Micromeritics ASAP 2010 instrument was employed to conduct the CO_2 low-pressure gas adsorption analysis (CO_2-LPGA). The lighter density fractions, liquefaction residues and their char samples were dried in an oven prior to the (CO_2-LPGA) analysis. A detailed description of the procedure, the software used in obtaining the data and the pressure ranges used for CO_2-LPGA analysis has been described elsewhere.[7,18] The Dubinin- Radushkevich (D-R), micropore surface areas and BET surface areas were evaluated from the isotherm CO_2 adsorption data.[19] The average micropore diameters and micropore volumes were deduced using the Horvart-Kawazoe (H-K) method.[19,20] The porosity of the samples was calculated using the cumulative amount of CO_2 adsorbed.

4.4 Results and discussion

4.4.1 TGA of coal float fractions and their liquefaction residues

The weight loss and DTG curves are provided in Figure 4.2. From this figure, it is clear that the sample DTG peaks indicated distinctive peaks when using inert (nitrogen) and oxidising (air) conditions. The small peaks were displayed between 100 and 200°C due to the

dehydration of moistures from the samples during the DTG analysis. The pronounced peaks within the range of 300−550°C for all samples can be attributed to the fragmentation of lighter density particles due to the volatility of lighter organic species and gases contained in these coals.[21] The lighter density fractions and their liquefaction-derived residue peak intensities differ in this region, with the lighter density fractions having higher peak intensities matching those of the liquefaction-derived coal residues. The lower peak intensity of the liquefaction residues in this region is ascribed to the removal of lighter organic species from the coal structure during the liquefaction tests. The third peak, occurring in the region of 800 °C, can be attributed to the partial transformation of inherent minerals (clays, carbonates, sulfides) contained in the coal chars due to the removal of hydration water and gases during pyrolysis.

Approximately 10%wt. more chars are produced during pyrolysis from the liquefaction residues (78.2% for HF-R and 79.1% for WF-R) than their float fractions (68.9% for HF and 69.8% for WF). This is expected as more of the smaller volatile compounds would have been extracted by liquefaction solvent, and the liquefaction-derived residues are thus likely to produce less volatile compounds during pyrolysis.

After combustion at 900°C, the ash yields were as follows: HF 12.2%, HF-R 27.0% and WF 15.0%, WF-R 24.6%). The results from TG analysis in air are consistent with the proximate analysis results reported in our previous study,[7] which give an ash yield of 11.4% for the Highveld float fraction and 13.8% for the Waterberg float fraction with 26.9% and 25.7% for the liquefaction residues HF and liquefaction WF residues, respectively.

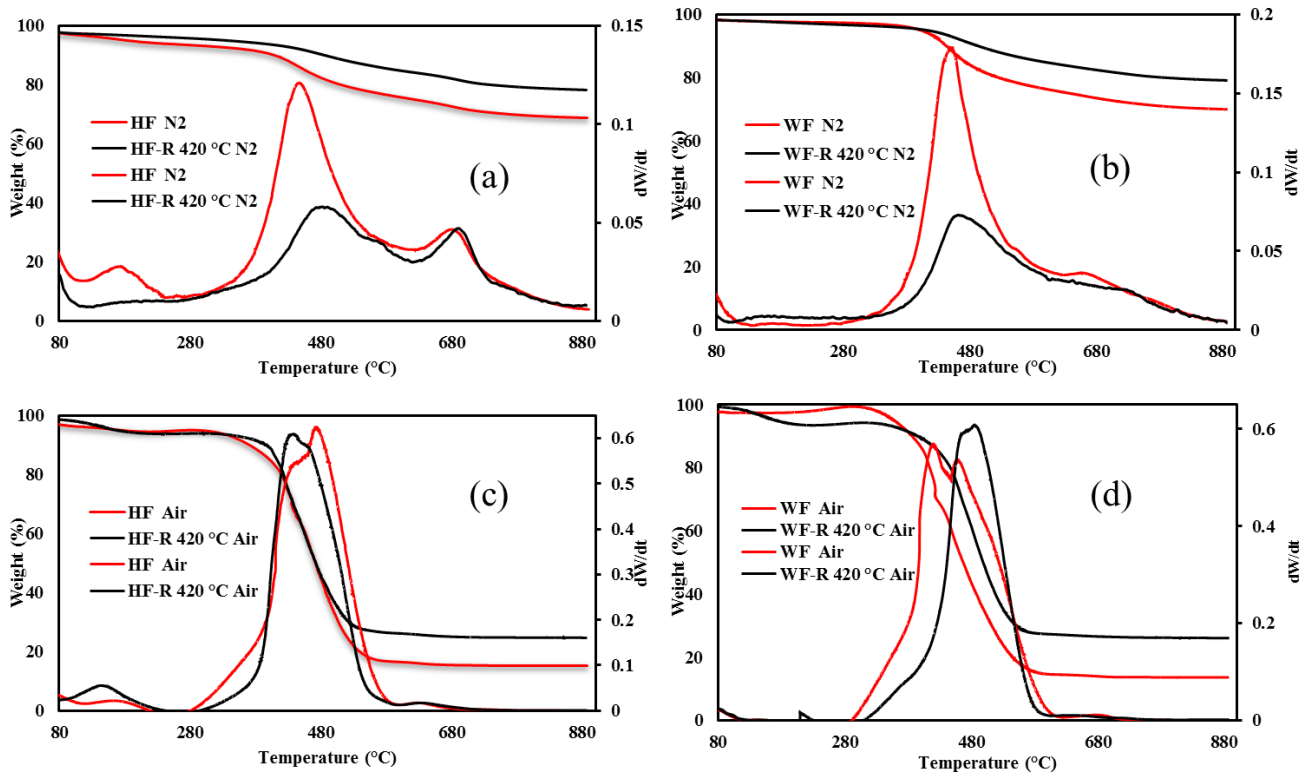

Figure 4-2: DTG and TG curves of (a) Highveld float fraction and residue in N_2; (b) Waterberg float fraction and residue in N_2; (c) Highveld float fraction and residue in air; (d) Waterberg float fraction and residue in air. HF N_2 = Highveld float under nitrogen; WF N_2 = Waterberg float under nitrogen; HF-R 420°C N_2 = Highveld float residue under nitrogen; WF-R 420°C N_2 = Waterberg float residue under nitrogen; HF Air = Highveld float under air; WF Air = Waterberg float under air; HF-R 420°C Air = Highveld float residue under air; WF-R 420°C Air = Waterberg float residue under air.

4.4.2 Distribution of pyrolytic products

The amounts of tar, pyrolytic water, gas and char generated during the pyrolysis of the lighter density fractions and their liquefaction-derived coal residues are given in Table 4.1 (results obtained from the Fisher Assay analyses). The results obtained from the three experimental repeats at 750 and 920°C used in this study are reproducible and accurate, with greater than 90% confidence intervals. Table 4.1 indicates that the amount of tar that was generated from the lighter density fractions are higher (11%) than those of liquefaction residues at 750°C than at 920°C. However, the two coal float fractions produced similar tar yields at 750°C; the HF fraction produced a tar yield of 10.8% at 750°C, while the WF fraction produced a tar yield of 10.5% at 750°C. Other investigators reported similar results for different coal samples.[22–24]

The HF and WF liquefaction-derived residues gave tar yields of 6.0 and 6.3%wt. at 750 °C after pyrolysis, respectively. At 950°C, the tar amounts were 3.8%wt. for the WF liquefaction-

derived residue and 3.2%wt. for the HF liquefaction-derived residue. As expected, the liquefaction-derived residues produced lower tar yields than those of the lighter density fractions. Tetralin liquefaction process removed smaller molecular compounds and some of the mobile phases in the coal samples. These compounds usually concentrated in the tar produced during pyrolysis, and thus less tar is expected for the liquefaction residues than for the float fraction samples after pyrolysis. Given et al.[25] stated that coal is made up of two phases, a mobile (extractable) and stationary phase. These two phases may be separated during the liquefaction process. Some researchers have shown that the extractable phase is comprised of hydrocarbon and oxygenated compounds that are entrenched or free in the molecular structure of coal, with the extracted compounds having molecular weights of less than 500 amu.[26,27]

Pyrolytic water yield: Water can be formed through various steps during pyrolysis: by internal moisture in coal which evaporates at 100°C; by inherent moisture associated with carbon matrix that the coal gives off at 130−200°C and water of hydration associated with clays in coal that starts to dehydroxylate at above 300°C.[28] Coal hydrolysis reactions may also occur at high temperatures. An increase in temperature from 750 to 920°C increased the yield of pyrolytic water by approximately 2%wt. (Table 4.1). This higher amount of water obtained at 920°C is attributed to dehydration of clay minerals above 700°C and the hydrolysis reactions of the coal matrix.[29] The coal float fractions showed higher pyrolytic water yields than the liquefaction-derived residue samples, suggesting that tetralin-extracted organic molecules undergo hydrolysis in the float fraction samples.

Table 4-1: Normalised pyrolytic products distribution of coal float fractions and their corresponding liquefaction residues at 750 and 920°C (%wt.)

Pyrolytic product distribution at 750°C				
Sample ID	**WF**	**HF**	**WF Residue**	**HF Residue**
Char	71.5 ± 0.2	67.0 ± 0.6	76.0 ± 1.2	74.0 ± 0.2
Pyrolytic water	3.5 ± 0.3	5.9 ± 0.2	1.6 ± 0.3	2.9 ± 0.5
Tar	10.5 ± 0.9	10.8 ± 1.4	6.3 ± 1.9	6.0 ± 2.0
Gas	14.5 ± 1.2	16.4 ± 1.2	16.0 ± 2.3	17.1 ± 1.6
Total Volatiles	28.8 ± 0.5	33.0 ± 1.5	24.0 ± 2.4	25.5 ± 1.2
Pyrolytic product distribution at 920°C				
Sample ID	**WF**	**HF**	**WF Residue**	**HF Residue**
Char	70.8 ± 0.2	66.0 ± 1.7	73.9 ± 0.5	73.3 ± 0.3
Water	5.5 ± 0.3	7.6 ± 0.4	4.4 ± 0.4	3.5 ± 0.1
Tar	7.5 ± 0.9	8.1 ± 1.4	3.8 ± 0.1	3.2 ± 0.7
Gas	16.25 ± 1.2	18.4 ± 0.1	18.0 ± 0.3	20.0 ± 0.8
Total Volatiles	29.6 ± 0.7	33.1 ± 0.6	25.0 ± 0.8	28.3 ± 0.7

Note: ID = identification; WF= Waterberg float (<1.5 g/cm^3), HF=Highveld float (<1.5 g/cm^3), WF Residue= Waterberg float liquefaction residue, HF residue = Highveld float liquefaction residue.

Gas yield: The gas yields for HF and WF were 18.4 and 16.3%wt. respectively, at 920°C (Table 4.1). These values increased for the liquefaction-derived residues with HF-residue producing 20.0%wt. and WF-residue 18.4%wt. of gas yields. The liquefaction residue samples generated gas yields approximately 2% higher than those produced from the lighter density fractions. The tetralin liquefaction process aided in creating a more porous surface, thus enabling better pyrolysis, with the result of more gaseous products being formed. The increased surface area will assist in the liberation of volatiles from the coal matrix during pyrolysis. This is indicated in the structural analysis results of the liquefaction residues (Section 4.4.4.3), where the physical properties of lighter density fractions and their liquefaction residues that are based on the measured porosity and surface area are presented and discussed. Similar results on the increase in porosity of the liquefied residues are reported for bituminous coal samples.[30]

Char yield: As expected, the small reduction in the char yields of the lighter density fractions and their residues was observed as pyrolysis temperature increased. The char produced from the lighter density fractions had between 3 and 8%wt. lower char yield when compared to those generated from the liquefaction residues samples. The liquefaction-derived residues contain less lower-molecular-weight compounds and more macromolecular weight compounds, resulting in less degradation and thus higher char yields for the liquefaction residues than those of the lighter density fractions.[28,31]

The XRD analysis[33] was followed to qualify and quantify the concentrations of crystalline and amorphous phases contained in the lighter density fractions and their corresponding liquefaction residues, and the mineralogical results are presented in Table 4.2. From the XRD

results, it is clear that the most predominate minerals contained in these samples are quartz and kaolinite with a smaller quantity of dolomite, calcite, and microcline. Also, a high proportion of amorphous material (organic carbon) is contained in these samples. Other researchers[15,35,33] found the presence of similar coal minerals in South African coals. The ash yields were higher for the liquefaction residues due to a decrease in organic matter, resulting in a relative decrease in the available volatile matter and fixed carbon. The mineralogical results of the 1.3 g/cm^3 float fraction and its char samples when using automated X- ray-based QEMSCAN indicate that kaolinite and fusinite, which are contained in these samples, did not transform or decompose at 550°C to form meta-kaolinite during pyrolysis.[33] Vitrinite and possibly carboxylic acid salts contained in these float fraction particles softened and formed agglomerates during the pyrolysis experiments.[33] The kaolinite particles contained in the heavy density (>1.9 g/cm^3) fraction undergo a partial transformation to produce meta-kaolinite and hydration water vapour. These transformation reactions caused bigger particles in this fraction to be cracked and broken into fragments during pyrolysis. High carbon concentration in the organic matter (macerals) in coals may contribute to the partial or no observed transformation of minerals during the pyrolysis of these coals.[34,35] Other Investigators have shown that the addition of minerals such as pyrite and clays including kaolinite and silica, do not catalyse the pyrolysis reactions during South African coals pyrolysis.[8] However, kaolinite may enhance the overall gas yield during pyrolysis.[8]

Minor proportions (<0.5%) of carboxylic acid salts may contribute to catalysing the pyrolysis reactions in South African coals.[32,33] The minor proportions of carboxylic acid salts, inherent minerals, and significant proportions of extraneous minerals contained in these coals do not contribute to the pyrolysis reactions at 450−550°C during pyrolysis of South African coals under an inert atmosphere. However, significant fractions of carboxylic acid salts contained in the overseas lignites may catalyse pyrolysis and gasification reactions.[36]

The tetralin liquefaction experiments somewhat changed the product distribution after pyrolysis compared to those of the lighter density fractions (Table 4.1). The liquefaction residue derived samples contained slightly higher gas and char yields than those obtained from the lighter density fractions. However, the proximate analysis obtained from the liquefaction samples indicates that it may be utilised for pyrolysis and further thermal processing.[7] The products obtained during pyrolysis were further characterised, and the results will be discussed in the next section. The results obtained from the pyrolysis study indicate that the liquefaction experiments help in the degradation and loosening of cross-link structure in coal, which resulted in more gases and chars from the liquefaction residues.

Table 4-2: Proportion of amorphous and total crystalline mineral phases of the float fractions, residues and their char samples from XRD analysis (%wt.).

	WF	WF-R	HF	HF-R
Quartz	5.8	9.2	1.7	3.1
Siderite	0.2	0.2	-	-
Kaolinite	9.4	14.3	8.2	15.3
Pyrite	0.9	-	1.2	-
Muscovite	-	0.4	-	-
Dolomite	-	0.1	0.5	1.1
Calcite	0.2	0.4	0.3	0.7
Magnetite	-	-	-	-
Pyrrhotite	-	0.4	-	0.3
Microcline	-	-	-	-
Amorphous/organic C	84.5	75.1	89.2	79.6

4.4.3 Tar analysis results

4.4.3.1 GC-MS analysis of tar samples

The GC−MS results of the tars produced at 750°C during pyrolysis of the lighter density samples and their liquefaction-derived residues are provided in Table 4.3. The results of the tars that were detected by GC−MS at 920°C are not presented in this study, as the qualitative results were similar to those of tars produced at 750°C. The major tar components are oxygen-containing monoaromatics, such as phenols, cresols, *m*, *p*-cresols, and polyaromatics (fluorine, methyl ethyl dibenzofuran, methyl fluorine, phenanthrene, and anthracene). All tars produced from the pyrolysis experiments contained methyl-substituted aromatics (significant components of the polyaromatics). Polyaromatic hydrocarbons (PAH) in tars are formed based on two models proposed by Frenklach and Wang.[37] Direct combination of two aromatic rings, such as two benzene rings, may form a biphenyl compound, which further undergoes a reaction to produce a PAH. The second model describes the abstraction of hydrogen, which aids in the activation of the aromatic rings, enabling acetylene addition reactions. This leads to the formation of cyclisation compounds. Apart from the phenolic compounds and PAHs, aliphatics such as alkanes and alkenes were also detected in the tars. Similar GC−MS results were obtained for tar samples generated from the pyrolysis of lignite tetrahydrofuran liquefaction-derived residues.[28] GC−MS results of the tars from the solvent liquefaction showed higher percentages of naphthalene, its compounds, and minor- aromatics compounds, such as phenolic groups favourably matching those of the tars generated from the lighter density fractions. The liquefaction process may assist in exposing latent oxygen in the coal structure, which may facilitate reactions to form oxygenated compounds, such as OH-containing compounds.[28,38] The GC−MS results matched those obtained from the ^{1}H NMR analysis of the tar, which will be discussed in the next section.

Table 4-3: The GC-MS analysis results of the tar samples generated from the pyrolysis of lighter density fractions and their corresponding liquefaction residues at 750°C (tetralin free basis)

	Mass %			
Component	HF	HF-Residue	WF	WF-Residue
N-Hexane	0.52	0.12	0.82	0.00
N-Octane	0.72	0.00	1.24	0.00
Acetone	0.52	0.00	0.62	0.22
THF	0.41	0.35	1.96	2.20
N-Nonane	0.83	0.12	1.93	0.00
1- Nonane	0.52	0.12	0.52	0.00
Benzene	0.52	0.00	0.62	0.00
N-Decane	0.52	0.12	0.52	0.22
1-Decene	0.62	0.12	0.82	0.11
N-Undecane	0.52	0.23	0.74	0.33
Methyl thiophene	0.31	0.46	0.72	0.00
Ethylbenzene	0.31	0.12	0.52	0.22
1-Undecene	0.52	0.23	0.72	0.22
Xylene	2.17	0.70	2.78	0.44
N-Dodecane + Xylene	1.34	0.58	1.44	0.55
C3 Benzene	2.58	0.93	2.99	1.21
1-Dodecene	0.72	0.12	0.82	0.22
N-Tridecane	1.14	0.23	1.24	0.44
1-Tridecene	0.62	0.12	0.72	0.22
Indan	0.72	0.23	0.72	0.33
N-Tetradecane	0.93	0.23	1.24	0.44
Methyl Indan	1.34	0.81	1.86	1.32
1-Tetradecene	0.41	0.12	0.72	0.33
N-Pentadecane	0.52	0.12	0.62	0.33
Indene	0.31	0.12	0.21	0.22
Benzofuran	0.21	0.00	0.21	0.33
N-Hexadecane	0.41	0.12	0.52	0.33
Methyl Indene	0.72	0.35	0.62	0.33
Methyl Benzofuran	0.31	0.12	0.21	0.44
Dimethyl Indan	0.41	0.23	0.31	4.41
1-Hexadecene	0.21	0.12	0.21	0.22
N-Heptadecane	0.52	0.12	0.52	0.33
Naphthalene	2.58	8.46	2.37	10.68
N-Octadecane	0.52	0.12	0.62	0.22
Benzothiophene	0.52	0.00	0.41	5.73
Methyl Naphthalene	2.37	3.36	2.27	0.00
N-Nonadecane	0.52	0.12	0.62	0.44
2,6-Xylenol	1.55	0.46	1.13	1.10
Ethyl methyl Phenol	7.22	8.46	5.26	5.62
Ethyl Naphthalene	0.72	0.46	0.52	0.88
N-Eicosane	0.62	0.12	0.72	0.33
O-Cresol	4.54	7.65	5.20	6.28
Phenol	7.53	9.62	6.39	8.37
Dimethyl Naphthalene	1.44	0.46	1.03	1.21
O-Ethyl Phenol	1.34	0.46	1.24	0.77

N-C21	0.10	0.00	0.10	0.11
2,5-Xylenol	2.99	4.87	2.06	1.87
2,4-Xylenol	7.84	7.18	9.28	4.41
P-Cresol	6.30	9.27	6.49	8.59
M-Cresol	5.37	10.78	6.39	6.17
2,3-Xylenol	1.14	8.46	0.72	0.88
P-Ethyl Phenol + 3,5-Xylenol	6.19	1.85	5.57	3.85
M-Ethyl Phenol	2.06	0.81	1.65	1.65
3,4-Xylenol	2.89	0.81	1.96	1.87
Dibenzofuran	0.72	0.35	0.52	0.55
Fluorene	1.24	0.70	0.62	1.54
Methyl Ethyl Dibenzofuran	2.99	0.70	2.17	1.10
Methyl Fluorene	1.55	0.58	1.65	1.21
Phenanthrene	1.14	0.46	1.20	0.88
Anthracene	0.72	0.35	0.62	0.55
Methyl Naphthalol	0.21	0.46	0.10	1.32
Methyl Phenanthrene	1.96	0.58	1.03	1.43
Methyl Anthracene	0.72	0.23	0.41	0.33
Naphthalol	0.00	4.52	0.00	4.07

4.4.3.2 NMR results of tar

The ^{1}H and ^{13}C NMR spectra of the tar generated at 750°C pyrolysis temperature are presented in Table 4.4 and Figure 4.3. ^{1}H NMR spectra in Figure 4.3(a) separates different types of proton functionalities in the tar, generated from the coal float fraction samples and their corresponding residues, according to their chemical shifts. The spectra are divided into two main chemical shift regions; the aromatic hydrogen (H_{ar}) (0.5–4.5 ppm) and the aliphatic proton (H_{al}) (6.3–9.5 ppm) regions. The H_{al} region is subdivided into H_{γ}, H_{β}, H_{α}, H_{δ} regions, representing the aliphatic hydrogen regions. The aromatics are also divided into condensable aromatic (H_{Arc}) and uncondensable aromatics (H_{UArc}).[39,40] The tar generated from the liquefaction residue shows two main peaks in the aliphatic region between 2.7 ppm and 1.8 ppm, whereas the tar produced from the lighter density fractions show one main peak (Figure 4.3(a)). These peaks are ascribed to the naphthenic methylene and to β-CH_2, which is assigned to the CH_2 protons from tetralin.[10]

Table 4.4 shows the quantitative distribution of proton classes in the tars produced during pyrolysis of the coal float fractions and liquefaction residues at 750°C. The calculated results from proton NMR analysis show that the percentage (normalised relative integral values) of aromatic protons were higher when compared to the aliphatic protons for all the samples, as is expected for a devolatilisation process because the aliphatic compounds combust before the aromatic compounds. The portion of uncondensable aromatics protons (H_{UArc}) for all tars was higher (48.5–55.5%) when compared to the condensable aromatics protons (H_{Arc}) (Table

4.4). The uncondensable aromatics protons are phenol and its related compounds, while condensable aromatics protons occur in naphthalene and its substituents, anthracene, xanthene, phenanthrene.[40] Similar compounds were observed during proton NMR analyses and GC-MS analyses of the samples. Proton NMR results of tars generated from the liquefaction residue showed a higher H_{ar} (< 60.5%) in comparison to those generated from the lighter density fractions H_{ar} (53.2–56.1%). The fractions of uncondensable aromatics proton and condensable aromatics protons of the liquefaction residues were observed to be more than those of the tars produced from the coal lighter density fractions. As expected, more of the aliphatic hydrogen-containing compounds are extracted from the coal matrix during liquefaction than aromatic hydrogen containing compounds.

Table 4-4: The liquid-state (^{1}H) and ^{13}C) NMR analysis results obtained from the pyrolysis of lighter density fractions and their liquefaction residues at 750°C (ppm). Integral areas in the NMR spectra are all normalised to 100 and thus expressed as a percentage of all integral areas within each NMR spectra.

Symbol	Integral reset points	WF	WF Residue	HF	HF Residue
		Aliphatic protons (0.5–6.3 ppm)			
H_{Al}		**46.8**	**38.7**	**43.9**	**38.0**
Hγ	0.5–1.00	3.9	0.9	3.2	0.0
$H_{\beta1}$	1.0–1.6	10.0	3.5	11.0	2.8
$H_{\beta2}$	1.6–2.00	2.4	5.2	2.3	5.02
$H_{\alpha1}$	2.0–3.0	27.6	29.0	26.3	29.2
$H_{\alpha2}$	3.0–3.69	0.9	0.03	0.2	0.1
H_D	3.69 – 4.5	0.01	0.01	0.0	0.02
H_{ol}	4.5 – 6.3	2.02	0.1	1.00	0.2
		Aromatic protons (6.3–9.5 ppm)			
H_{Ar}		**53.2**	**60.5**	**56.1**	**62.0**
H_{ArUC}	6.3 – 8.36	48.6	54.5	50.3	55.5
H_{ArC}	8.36 – 9.5	4.6	6.0	5.8	6.8
	Total	**100**	**100**	**100**	**100**
H_{Ar}/ H_{Al}		1.1	1.6	1.2	1.6
		Aliphatic carbons (13 ppm–49.3 ppm)			
C_{Al}		**25.9**	**21.5**	**25.4**	**21.5**
CH_3	13.0 – 23.0	15.8	5.0	14.4	5.0
CH_2	23.0 – 29.5	1.3	15.1	1.5	14.6
C_A	29.5 – 34.0	8.9	1.0	9.4	1.7
C_F	34.0 – 39.5	0.11	0.24	0.02	0.2
$C_{\alpha2}$	39.5 – 49.3	0.0	0.01	0.0	0.01
		Aromatic carbons (110 ppm–160 ppm)			
C_{Ar}		**74.1**	**78.5**	**74.6**	**78.5**
C_{ArP}	110.0 – 118	3.6	0.1	4.1	0.9
C_{Ar1}	118 – 122	1.1	0.1	1.4	0.4
C_{Ar2}	122 – 124	0.1	0.0	0.0	0.1
C_{Ar3}	124 – 133	56.5	65.3	57.0	61.8
C_{Ar4}	133 – 140	9.7	12.8	8.9	14.4
C_{ArC}	140 – 147	0.3	0.3	0.3	0.2
C_{Ar5}	147 – 167	2.9	0.1	2.8	0.8
Total		**100**	**100**	**100**	**100**
C_{Ar}/C_{Al}		2.9	3.7	2.93	3.7
$f_a = C_{Ar}/C_{Total}$		0.74	0.79	0.75	0.79

H_D = Aliphatic H in methyl or methylene attached to two aromatic rings, Hγ =Aliphatic Hγ to an aromatics, $H_{\alpha2}$=Aliphatic H in methylene attached to an aromatic ring and β to another or two rings, $H_{\beta1}$= Aliphatic methyl β to an aromatics, $H_{\alpha1}$=Aliphatic H in methyl and possible attached to another ring, $H_{\beta2}$=Alicyclic Hβ to two aromatics (naphtenic, methylene), H_{ol}= olefinic protons, $H_{\alpha2}$=aliphatic H in methylene to an aromatic ring and β to another or two rings, H_{ArUC} =aromatic hydrogen, H_{ArC} = sterically hindered aromatic hydrogen, CH_3 = methyl carbons, CH_2 =methylene (CH_2) and methine (CH) carbons or from aromatic ring (eg ethyl and propyl), C_A = methylene (CH_2) and methine (CH) carbons α to an aromatic ring and β to another, C_F= methylene (CH_2) and methine (CH) carbons α to two aromatic rings (fluorene type), $C_{\alpha2}$ = methylene (CH_2) and methine (CH) carbons α to two (disphenylmethane type), C_{ArP} =pericondensed aromatic- or protonated aromatic carbon, C_{Ar1}= C_{ar}-H ortho to C_{ar}-OH, C_{Ar2}= C_{ar}-H para to C_{ar}-OH; C_{ar}-CH_3 ortho to C_{ar}-OH, C_{Ar3}= quaternary aromatic carbons; C_{ar}-H meta to C_{ar}-OH, C_{Ar4}= C_{ar}-CH_3 para to C_{ar}-OH, C_{ArC} = CH or CH_2 meta to C_{ar}-OH, C_{Ar5}= C_{ar}-CH_3; CH_2 or CH para to C_{ar}-OH.[7]

The qualitative and quantitative ^{13}C NMR results of the tars produced at 750°C from the lighter density fractions and their liquefaction residues during pyrolysis are given in Figure 4.3(b) and Table 4.4. Two main regions (the saturated aliphatic region (13−49.3 ppm) and aromatics region (110−150 ppm)) were observed in the 13C NMR results, which are shown in Figure

4.3(b). The appearance of the peak at 77 ppm is as a result of the residual protonated $CHCl_3$ in the deuterated ($CDCl_3$) solvent utilised during the ^{13}C NMR analysis.[28] The aromatic carbon region can be subdivided into four parts (CH_2, C_A, C_F, C_α), while the aromatic region is divided into seven regions. The percentages of aromatic carbon of the different tars produced from this study were higher (74−78.5%) than the percentages of aliphatic carbon (Table 4.4). The results from the carbon NMR of the tars matched the GC−MS results (Table 4.3) and also the H NMR results.

Andrésen et al.[12] stated that tar generated at low pyrolysis temperatures are mainly made up of long aliphatic or acyclic chains, while those produced at 750°C are mainly characterised by smaller substituted branched aliphatics or alkyl-substituted aromatic carbon fractions. Results from Table 4.4, show that the percentage of aromatic carbons was higher when compared to the percentage of the aliphatic region in all the tars. Carbon NMR results of tars generated from the liquefaction residue showed a higher amount of C_{ar} (78.5%) in comparison to those generated from the lighter density coal fractions (74%). The fraction of aliphatic carbon (Table 4.4), of the lighter density fraction, were higher than those of the liquefaction residues. The lower aliphatic carbon percentages of the tars obtained from the residues indicate that the liquefaction experiments lead to the production of residues with less and smaller aliphatic side chains. The methyl carbon makes up the aliphatic region of the tar generated from the coal float fraction samples.

The aromaticity factors, $f_a = C_{ar}/C_T$, were calculated from the ^{13}C NMR data and were tabulated in Table 4.4. The f_a of all the samples ranged from 0.74–0.79 with f_a of the liquefaction residues were marginally higher when compared to those of the lighter density fractions. These results are in agreement with those of the samples previously presented and discussed in literature.[28,40]

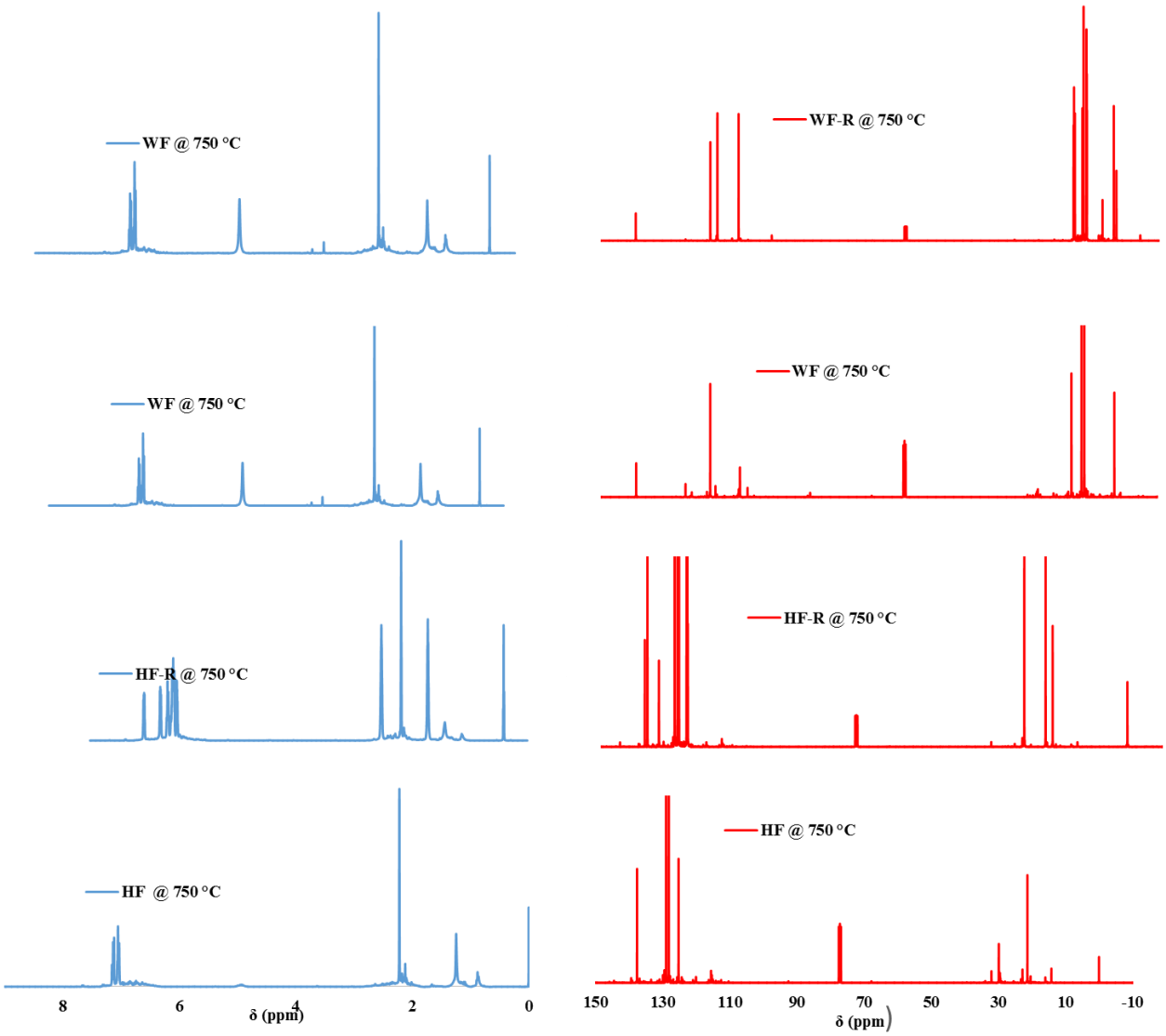

Figure 4-3: ^{1}H and ^{13}C NMR spectra of tars produced from lighter density fraction and their residues at 750°C pyrolysis temperature: (a) ^{1}H spectra, (b) ^{13}C spectra (The y-axis in all cases is Signal Intensity (Arbitrary units))

.

4.4.3.3 FTIR results of tar produced during pyrolysis at 750°C from coal lighter density fractions and their liquefaction residues.

The FTIR spectra of the tars that were generated at the devolatilisation temperature of 750 °C for all the tar samples under investigation are provided in Figure 4.4. Peak absorption values of the functional groups of interest were assigned as described elsewhere.[41] All the samples showed absorption peaks correlating to aromatic compounds at 750, 815, 3060, and 1600 cm^{-1}, and peaks corresponding to aliphatic compounds at 2850, 2922, and 2960 cm^{-1}. The ratio between the aliphatic C−H stretching peak area (2920 cm^{-1}) and the aromatic C−H

stretching peaks area (3040 cm^{-1}) indicates the degree of aromaticity for the tars produced from coal float samples when compared to those from their liquefaction-derived residues.

It was observed that in the aliphatic (2960, 2922, and 2850 cm^{-1}) regions, the liquefaction-derived residues' tars peaks were lower than the float fractions' peaks. The reduction in the peak heights of the liquefaction-derived residues' tars in the aliphatic region can be attributed to the extraction of some aliphatic compounds during the liquefaction treatment.

The phenoxyl ether stretching and carbonyl group peaks are assigned at 1100−1300 and 1700 cm^{-1} respectively.[41] The oxygen-containing functional compounds that were detected by the IR were given as C−O bands (1040 cm^{-1}), aryl ethers peaks (1262 cm^{-1}), and C=O peaks (1698 cm^{-1}). The peak intensities of tars generated from the liquefaction-derived residues were lower than those of the tars generated from the lighter density fractions in these peak regions. The moderately lower peak intensities of the tar produced from the liquefaction residues in these regions can thus be attributed to the loss of carbonyl compounds in the form of gases like CO_2 and CO during liquefaction.

The presence of alcohols and phenols in the tar samples is evidence of the shoulder peak at 3500 cm^{-1}, which corresponds to O−H stretching vibrations. The peaks from 700 to 900 cm^{-1} are assigned to out of plane aromatics C−H bending vibrations. These peaks indicate the existence of aromatics rings, which may be trans and cis saturated rings. The peaks of the tars produced from the coal float samples and their liquefaction-derived residues do not show much variation in the aromatic vibration regions. This indicates that the liquefaction mainly extracts the aliphatic components of the coal structure, with little influence on the aromatic part of the coal structure. FTIR analysis results for the tar samples matched the NMR and GC−MS results.

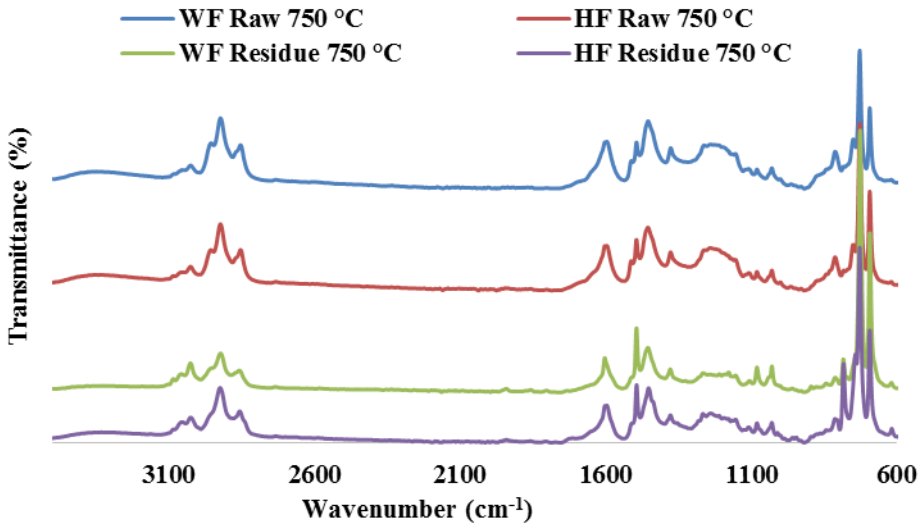

Figure 4-4: FTIR spectra of tars samples produced from the pyrolysis of lighter density fractions and liquefaction residues at 750°C charring temperature

In summary, the tars produced from the liquefaction-derived residues contained slightly more aromatic components when compared to the tars from float fraction tars. The tars generated from the liquefaction-derived residues are comparable to tars produced during pyrolysis of bituminous and lignite coals.[28,39–41] Regarding the tar composition, the liquefaction-derived residues thus seem to be suitable for further investigation as a starting material for gasification.

4.4.4 Chars composition

4.4.4.1 Proximate and elemental analyses

The proximate and ultimate analyses results for the lighter density fraction samples and their liquefaction-derived residues at devolatilisation temperatures of 750 and 920°C are given in Table 4.5. The proximate analysis results indicate that as pyrolysis temperature increases, the volatile matter content decreases with a corresponding increase in fixed carbon content and ash yields. Other researchers made similar observations with an increase in temperature.[42,43] The most significant differences between the chars produced from the lighter density samples and their liquefaction-derived residues were the percentage of ash yields and the fixed carbon content. The chars generated from HF and WF samples contain fixed carbon contents of 80.9%wt. (adb) and 75.5%wt. (adb) respectively at 920°C with ash yield of 14.6%wt. (adb) for the HF char and 21.0%wt. (adb) for the WF char. Their corresponding liquefaction-derived residue chars showed a lower fixed carbon content and higher percentage ash yields. The fixed carbon contents for the liquefaction-derived residue chars from HF and WF were 67.7%wt. (adb) and 69.20%wt. (adb) respectively, and an ash yield of 30.3%wt. (adb) was observed for the WF residue char and 29.8%wt. (adb) for the HF residue char. This can be attributed to the extraction of some aliphatic and aromatics components from the coal samples during the liquefaction experiments, leaving a lower initial carbon-based mass for pyrolysis. According to Suzuki al.[44], coal with ash yields in the range 14.7−28 (%wt., adb) and fixed carbon content values in the range 70−90 wt.% (adb) may be utilised for gasification. Researchers[45−47] reported that the ash yield in feed coals entering South African commercial gasifiers ranged between 22 and 30%. They indicated that the ash yield in feedstock for utilisation in South African commercial gasifiers must be less than 35%.[45−47] The liquefaction-derived residues thus show promise to be used as a feedstock for gasification.

The ultimate analysis of chars indicated that an increase in temperature leads to higher carbon contents. Also, there are decreases in the oxygen and hydrogen contents of all the chars, as expected. The reduction in these parameters was attributed to hydrogen abstraction and loss of some volatile components during the devolatilisation at a higher temperature. The primary source of the hydrogen released at temperatures above 700°C is the removal of hydrogen attached to aromatic rings and condensation of aromatics groups in coal.[48,49] The nitrogen contents of all the chars formed in this study do not show much difference before and after pyrolysis experiments. As expected, the sulphur contents decreased with increasing temperature from 750 to 920°C.

The chars from the lighter density fractions and their corresponding liquefaction residue chars do not show much variation with regards to ultimate analysis results, with the carbon contents differing by less than 2%. Results from this elemental analysis of all the chars generated during this investigation showed similar values to those described by other researchers.[43,50] The chars generated from all the samples in this investigation thus again compare favourably with those obtained from coal samples used for thermal processing.

Table 4-5: Proximate, ultimate, H/C, O/C, S/C analyses results of the lighter density fractions, liquefaction residues and char samples generated from the pyrolysis of coal float fractions and liquefaction residues at 750 and 920°C

	WF	WF-750 °C	WF-920 °C	HF	HF-750 °C	HF-920 °C	WF-R	WF-R750 °C	WF-R920 °C	HF-R	HF-R750 °C	HF-R920 °C
Proximate Analysis (%wt., air-dry basis)												
IM	3.4	1.7	1.7	4.1	2.6	2.6	2.1	1.5	1.4	2.0	2.1	2.0
Ash	13.4	20.5	21.0	11.8	15.0	14.6	26.9	29.3	30.9	25.7	29.3	29.8
VM	31.2	3.7	1.9	29.4	4.3	2.4	25.6	4.0	1.3	25.2	3.2	2.4
FC (by diff.)	52.0	74.6	75.8	54.7	78.7	80.9	45.4	65.7	66.4	47.1	65.4	69.2
Fuel ratio FC/VM	1.7	20.2	39.9	1.9	18.3	33.7	1.8	16.4	51.1	1.9	20.4	28.8
Ultimate Analysis (%wt., daf) ISO 29541: 2010												
C	77.7	93.4	94.2	75.6	93.4	95.0	85.3	93.8	94.5	85.4	92.8	93.7
H	5.1	1.5	1.2	5.7	1.2	1.0	5.0	0.8	0.8	5.2	0.9	0.7
N	1.5	1.8	1.4	2.6	2.2	1.7	2.0	1.8	1.2	1.8	1.7	1.5
S	1.2	1.0	1.2	1.3	0.8	0.5	2.0	1.2	1.2	2.3	2.4	2.6
O (by diff.)	14.5	2.3	2.0	14.7	2.7	2.1	5.8	2.4	2.3	4.3	2.1	2.5
H/C atomic ratio	**0.9**	**0.2**	**0.15**	**0.8**	**0.15**	**0.13**	**0.8**	**0.1**	**0.1**	**0.8**	**0.1**	**0.1**
O/C	**0.14**	**0.02**	**0.01**	**0.14**	**0.2**	**0.2**	**0.05**	**0.03**	**0.02**	**0.04**	**0.03**	**0.04**
S/C	**0.0058**	**0.004**	**0.005**	**0.01**	**0.005**	**0.002**	**0.002**	**0.0048**	**0.0047**	**0.002**	**0.003**	**0.0023**

WF =Waterberg Float, WF-750°C = Waterberg Float char at 750 ˚C, WF-920 ˚C = Waterberg Float Highveld Float char @920 ˚C, HF =Highveld Float, HF-750 ˚C = Highveld Float char @750 ˚C, HF-920 ˚C = Highveld Float char @920 ˚C, WF-R = Waterberg Float residue, WF-R750 ˚C = Waterberg Float residue char @750 ˚C, WF-R920 ˚C = Waterberg Float residue char @ 920 ˚C, HF-R = Highveld Float residue, HF-R750 ˚C = Highveld Float residue char @ 750 ˚C, HF-R920 ˚C = Highveld Float residue char @ 920 ˚C.

4.4.4.2 ^{13}C NMR analysis of the char produced during pyrolysis.

A comparison of the ^{13}C CP/MAS NMR spectra of the lighter density fraction samples, their liquefaction-derived residues, and their corresponding chars after pyrolysis is presented in Figure 4.5. The ^{13}C NMR results of the char generated from the lighter density fractions exhibited slightly higher signal area integral in the aliphatic region than those of their corresponding liquefaction-derived residue chars. As described previously, the extraction of some of the aliphatic compounds occurs during liquefaction. The peaks in the aliphatic region decreased for all the chars at 920°C in comparison to the lower temperature, with a corresponding increase in the aromatic peak heights. The aromatic peak region of all chars at 920°C shows peak broadening, consistent with results obtained by another investigator.[43] This is in line with the reduction in H/C ratios of the chars calculated from the ultimate analysis results (Table 4.5).

Table 4.6 indicates the calculated NMR structural parameters of the lighter density fractions, their liquefaction-derived residues, and their corresponding chars generated at 920 °C. The lighter density samples and their liquefaction-derived residues showed a decrease in the aliphatic carbon fractions and an increase in the aromatic carbon fractions. The lighter density fractions and their residue chars showed a minimal difference in the fraction of aromatics carbon (f_a). The Highveld lighter density fraction char contained 92% and 8% aromatic and aliphatic carbon contents respectively, while the Waterberg lighter density fraction contained 91% and 9% aromatic and aliphatic carbons, respectively. The fraction of aromatic carbons in the liquefaction residue chars had approximately 4% higher than those of the lighter density fraction chars. The ^{13}C NMR results are in line with the results of pyrolysis product distribution.

The fractions of carbonyl, phenolic, esters, and aliphatic oxygen carbons decreased in all chars produced at 920°C (Table 4.6) in comparison to the material before pyrolysis. The decrease in these functional group fractions was attributed to the evolution of gases, the abstraction of aliphatics, loss of some phenolics, and carbonyl functionalities during the pyrolysis as also reported for the tars.

The fractions of bridgehead carbons, non-protonated carbons and CH_3 groups in the aromatic region increased for all the chars of coal float fractions and residues after pyrolysis, while a portion of protonated carbons and CH_3 in the aliphatic region of all chars decreased. This happens because, protonated carbons have weaker C-C-bonds in comparison to non-protonated carbons, and these bonds are more easily broken during pyrolysis.[51] The fraction of carbons bonded to alkylated carbons do not show much change. The fraction of the bridgehead aromatic carbons increased for all chars after pyrolysis. The fraction of bridge aliphatic carbons decreased for all chars during pyrolysis.

The ^{13}C NMR results of the lighter density fractions and their liquefaction-derived residues, and their corresponding chars show similar results as the other analytical methods employed in this study.

Table 4-6: Structural and lattice results of ^{13}C NMR of the lighter density fraction, their residues and pyrolysis char samples (produced at 920°C)

Structural Parameter								
	WF<1.5	WF-R	WF-920 °C	WF-R-char-920°C	HF<1.5	HF-R	HF-920°C	HF-R-char-920°C
f_a	0.78	0.86	0.91	0.95	0.78	0.80	0.92	0.96
f_{al}	0.22	0.14	0.09	0.05	0.22	0.20	0.08	0.04
f_{al}^O	0.03	0.02	0.01	0.01	0.04	0.05	0.01	0.00
f_a^{CO}	0.06	0.03	0.02	0.01	0.07	0.04	0.01	0.00
f_a^P	0.08	0.02	0.04	0.03	0.09	0.04	0.04	0.02
f_a^S	0.16	0.16	0.15	0.16	0.16	0.15	0.14	0.16
f_a^N	0.54	0.56	0.76	0.80	0.54	0.62	0.72	0.80
f_a^H	0.21	0.25	0.04	0.03	0.20	0.15	0.03	0.02
f_a^B	0.25	0.32	0.36	0.40	0.30	0.33	0.30	0.40
f_{al}^{N*}	0.08	0.06	0.04	0.02	0.07	0.06	0.05	0.03
f_{al}^H	0.10	0.08	0.04	0.05	0.11	0.10	0.04	0.02
Lattice parameter								
	WF<1.5	WF R	WF-920 °C	WF-R-char-920°C	HF<1.5	HF-R	HF-920 °C	HF-R-char-920 ˚C
P_0	0.67	0.75	0.82	0.92	0.72	0.68	0.77	0.88
B.L	4.21	4.39	5.06	5.56	4.69	2.73	4.2	4.35
S.C	2.11	1.46	1.13	0.46	1.82	1.26	1.23	0.57
X_b	0.32	0.37	0.40	0.42	0.38	0.41	0.33	0.42
C	24.0	26.0	28.0	29.2	24.0	25.0	30.0	32.0
σ + 1	6.32	5.85	6.19	6.02	6.51	3.99	5.43	4.92
MW	475.6	425.7	389.6	390.6	488.8	439.5	412.5	429.3
M_G	0.27	0.29	0.11	0.09	0.26	0.19	0.1	0.06
M_δ	28.66	18.14	8.16	6.22	29.9	33.78	9.12	8.79

f_a^H = fraction of protonated carbons, f_{al}^O = aliphatic carbons bonded to oxygen, f_a = total fraction of aromatic carbons, f_{al}^H = fraction of protonated carbons and CH_3 in aliphatic region f_{al} = total fraction of aliphatic carbons, f_a^N = fraction of non-protonated carbons and CH_3 in aromatic region f_a^{CO} = fraction of carbons bonded to carbonyls, f_{al}^N = fraction of non-protonated carbons and CH_3 in aliphatic region, f_a^S = fraction of carbons bonded to alkylated carbons, f_a^P = fraction of carbons bonded to phenolic esters, f_a^B = fraction of bridgehead carbons, S.C.—number of side chains per cluster, M_G- fraction of aromatic ring carbons with a directly attached proton, *C*—average number of aromatic carbon atoms per cluster, MW—average molecular weight of the aromatic cluster, χ_b—mole fraction of aromatic bridgehead carbons, M_δ- average molecular weight of side chain or half-bridge mass, B.L.—number of bridges and loops per cluster, $\sigma + 1$—average number of attachments (bridges, loops and side chains) per cluster. [51]

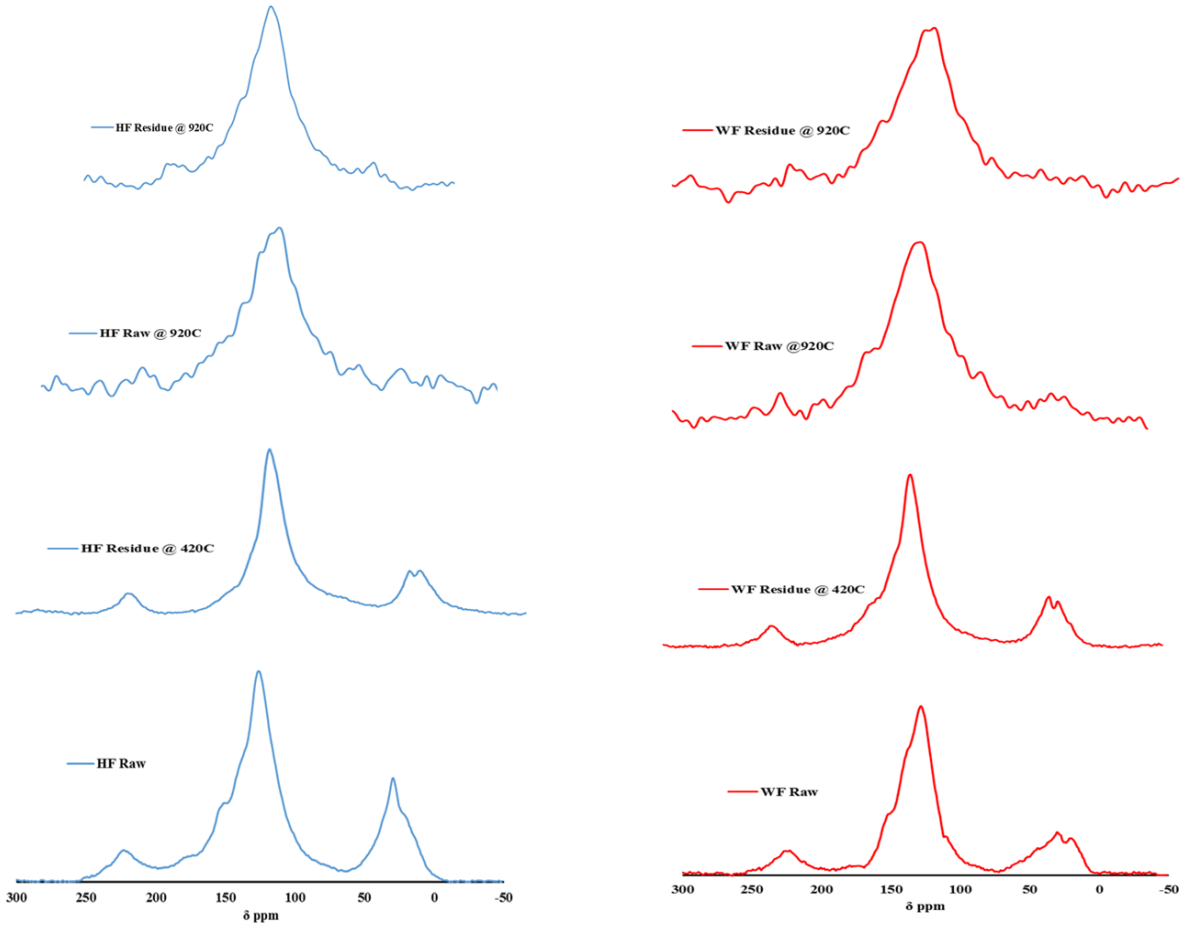

Figure 4-5: ^{13}C CP NMR spectra at 12 kHz MAS of the lighter density fractions, residues, and their corresponding char samples

4.4.4.3 Surface area analysis of samples

The surface area and porosity results obtained for the samples using a low-pressure CO_2 adsorption analysis are given in Table 4.7. The surface area values of the liquefaction-derived residues were lower than those of the lighter density fractions, while the porosity, micropore diameter, and D−R micropore volumes increased in the liquefaction-derived residues compared to those of the lighter density samples. An increase in the porosity values of the liquefaction-derived residues can be attributed to the dissolution of the lighter molecular structures contained in the coal in the tetralin during the liquefaction experiments. Some of the pores may be closed or blocked as a result of blockage by the organic components due to dredging during the extraction experiments. The orientation and rearrangements of the pores may be influenced during liquefaction, which may lead to lowering of the surface area.[52,53] The increased pore volumes for the liquefaction-derived residues show that new pores were developed during liquefaction.

The WF char had a D−R micropore surface area of 248.2 m^2/g and 13.9% porosity, while the HF char showed a D−R micropore surface area of 288.2 m^2/g and 15.9% porosity. The surface area of all chars increased with an increase in the pyrolysis temperature (Table 4.7). The increase in surface area as pyrolysis temperature increases could be attributed to the reduced volatile matter content and hydrogen abstraction volatilised at 920 °C. The softening, expansion and release of volatiles from coal matrix during devolatilisation resulted in the opening of closed pores and enlargement and transition of existing pores.[54,55]

Table 4-7: CO_2 low-pressure gas adsorption analysis results of the lighter density fractions, their corresponding liquefaction residues and chars samples generated from the pyrolysis of coal float fractions and their corresponding residues at 750 and 920°C charring temperature

	WF	WF-750 °C	WF-920 °C	HF	HF-750 °C	HF-920 °C	WF-R	WF-R750°C	WF-R920 °C	HF-R	HF-R750 °C	HF-R920 C
D-R micropore surface area (m^2/g)	140.0	233.2	248.2	131.0	276.9	288.1	89.3	265.3	274	88.9	300.9	311.7
BET surface area (m^2/g)	86.4	158.0	160.2	76.8	200.7	194.2	60.3	180.0	187.6	51.3	189.7	204.9
D-R micropore volume (cm^3/g)	0.06	0.10	0.06	0.05	0.11	0.04	0.06	0.09	0.052	0.06	0.08	0.05
H-K average micropore diameter (Å)	3.8	3.5	3.6	3.9	3.5	3.7	4.1	4.2	3.8	4.1	3.5	3.6
Porosity (%) (3 Å ≤ d_p ≤ 5 Å)	5.3	12.3	13.9	4.2	13.3	15.9	6.5	15.4	15.7	6.8	16.2	17.8

WF =Waterberg Float, WF-750°C = Waterberg Float char at 750 ˚C, WF-920 ˚C = Waterberg Float Highveld Float char @920 ˚C, HF =Highveld Float, HF-750 ˚C = Highveld Float char @750 ˚C, HF-920 ˚C = Highveld Float char @9200 ˚C, WF-R = Waterberg Float residue, WF-R750 ˚C = Waterberg Float residue char @750 ˚C, WF-R920 ˚C = Waterberg Float residue char @ 920 ˚C, HF-R = Highveld Float residue, HF-R750 ˚C = Highveld Float residue char @ 750 ˚C, HF-R920 ˚C = Highveld Float residue char @ 920 ˚C.

In summary, the chars produced from the liquefaction residues samples contained high values of surface area, porosity, and fraction of aromaticity values (from the solid-state NMR data). The results of the char obtained from the liquefaction-derived residues are similar to char produced by other investigators on pyrolysis of coal from South African bituminous coal.[36,46] Based on the char composition of the liquefaction-derived residues, the chars produced from these residues seem to be suitable as a starting material for further thermochemical process (gasification).

4.5 Conclusions

The lower density fractions produced by the float–sink separation of South African waste coals, and their tetralin liquefaction-derived residues were subjected to pyrolysis experiments at 750 and 920°C to investigate the possible utilisation of the liquefaction residues as starting material for further thermal processing (gasification). The amounts of char produced from the liquefaction residues were approximately 10% higher than the char produced from the lower density fractions (TG data). Under an oxidising atmosphere, the ash yields of the liquefaction samples were slightly higher than those of the lower density fractions, but that can be attributed to the loss of aliphatic compounds (see GC–MS, NMR, and FTIR results) from the coal structure during the liquefaction experiments. The pyrolysis product distribution of the liquefaction residues, as determined in the Fisher-Assay equipment, showed higher char and gas yields than those of the lighter density samples. The float fraction samples had more pyrolytic water and tar yields in comparison to the liquefaction residues. Again the lower tar yields observed for the liquefaction residues can be attributed to the loss of smaller organic molecules during the liquefaction experiments. CO_2 low-pressure adsorption methods showed that liquefaction experiments change the pore structure of the coal and open up pores within the coal structure, which may favour the diffusion of free radicals and assist in the reactivity of the liquefaction residues. The pyrolytic products' distribution and analysis results showed that the residues (waste material) generated after tetralin liquefaction of the float fractions from waste coals could be utilised during thermochemical processes (pyrolysis and gasification). The potential of utilisation of the coal liquefaction-derived residues in thermochemical processes may assist in decreasing both the amounts of waste coals and that of the residues from the liquefaction experiments.

- **Acknowledgements**

The authors of this manuscript acknowledge the following analysts from the different laboratories, plant and power station operators, and the funders of this project: Dr Kgutso Mokoena for his assistance in characterising the tar samples using a qualitative GC−MS analysis; Bureau Veritas Testing and Inspections South Africa laboratories for following the standard coal analyses to characterise coals, char, and liquefaction residues; the analysts at the Stellenbosch University, CAF, South Africa for using advanced analytical techniques (NMR analyses) to determine the proportions of organic compounds and protons and hydrogen in the coal, char, and liquid samples; Mrs Belinda Venter for using NWU XRD equipment to analyse coal, char, and liquefaction residue samples; South African power stations (Highveld and Waterberg) for providing the authors with the waste coal samples that were evaluated in this study; finally, the Department of Science and Technology and National Research Foundation of South Africa (Coal Research Chair Grant No. 86880 and Incentive Grant No. 115228) for funding this project throughout the study. DST and NRF of South Africa are not responsible for the contents of this paper.

4.6 Chapter 4 references

1. Cornils, B.; Hibbel, J.; Ruprecht, P.; Langhoff, J.; Dürrfeld, R. Gasification of hydrogenation residues using the Texaco coal gasification process. *Fuel Process. Technol.* **1984**, 9, 251-264.
2. Li, J.; Yang, J; and Liu, Z. Hydrogenation of heavy liquids from a direct coal liquefaction residue for improved oil yield. *Fuel Process. Technol.* **2009**, 90, 490-495.
3. Lv, D.; Yuchi, W.; Bai, Z.; Bai, J.; Kong, L.; Guo, Z.; Yan, J.; and Li, W. An approach for utilization of direct coal liquefaction residue: Blending with low-rank coal to prepare slurries for gasification. *Fuel* **2015**, 145,143-150.
4. Liu, X.; Zhou, Z.J.; Hu, Q.J.; Dai, Z.H.; Wang, F.C. Experimental study on co-gasification of coal liquefaction residue and petroleum coke. *Energy Fuels* **2011**, *25*, 3377-3381.
5. Yan, J.; Bai, Z.; Li, W.; Bai, J. Direct liquefaction of a Chinese brown coal and CO_2 gasification of the residues. *Fuel,* **2014**, *136*, pp.280-286.
6. Wang, Z.; Xue, W.; Zhu, J.; Chen, E.; Pan, C.; Kang, S.; Lei, Z.; Ren, S.; Shui, H. Study on the stability of hydro-liquefaction residue of Shenfu sub-bituminous coal. *Fuel* **2016**, *181*, 711-717.
7. Uwaoma, R. C.; Strydom, C. A.; Matjie, R. H.; Bunt, J. R. Influence of density separation of selected South African coal fines on the products obtained during liquefaction using tetralin as a solvent. *Energy Fuels* **2019**, 33, 1837-1849.
8. Roets, L.; Strydom, C.A.; Bunt, J.R.; Neomagus, H.W.; and van Niekerk, D. The effect of acid washing on the pyrolysis products derived from a vitrinite-rich bituminous coal. *J. Anal Appl Pyrol.* **2015**, *116*, 142-151.
9. Roets, L.; Bunt, J.R.; Neomagus, H.W.; Strydom, C.A.; Van Niekerk, D. The effect of added minerals on the pyrolysis products derived from a vitrinite-rich demineralised South African coal. *J. Anal Applied Pyrolysis*. **2016,**121:41-9.
10. Egiebor, N. O.; Gray, M. R. Evidence for methane reactivity during coal pyrolysis and liquefaction. *Fuel* **1990**, 69, 1276-1282.
11. Uwaoma, R.C.; Strydom, C.A.; Bunt, J.R.; Okolo, G.N.; Matjie, R.H. The catalytic effect of Benfield waste salt on CO_2 gasification of a typical South African Highveld coal. *J Therm. Anal. Calorim*. **2019**, 135, 2723-32.
12. Roets, L.; Bunt, J.R.; Neomagus, H.W.; Van Niekerk, D. An evaluation of a new automated duplicate-sample Fischer Assay setup according to ISO/ASTM standards and analysis of the tar fraction. *J. Anal Appl Pyrol.* **2014**, *106*, 190-196.
13. Andrésen, J.M.; Strohm, J.J.; Sun, L.; Song, C. Relationship between the formation of aromatic compounds and solid deposition during thermal degradation of jet fuels in the pyrolytic regime. *Energy Fuels* **2001**, *15*, 714-723.

14. Guillen, M.D.; Blanco, J.; Canga, J.S.; and Blanco, C.G. Study of the effectiveness of 27 organic solvents in the extraction of coal tar pitches. *Energy Fuels* **1991**, *5*, 188-192.
15. Uwaoma, R.C.; Strydom, C.A.; Matjie, R.H.; Bunt, J.R.; Van Dyk, J.C. The influence of the roof and floor geological structures on the ash composition produced from coal at UCG temperatures. *Int J Coal Prep Util*. **2018.** https://doi.org/10.1080/19392699.2018.1479260.
16. Solum, M. S.; Pugmire, R. J.; Grant, D. M. Carbon-13 solid-state NMR of Argonne-premium coals. *Energy Fuels* **1989**, 3,187-193.
17. Solum, M. S.; Sarofim, A. F.; Pugmire, R. J.; Fletcher, T. H.; Zhang, H. 13C NMR analysis of soot produced from model compounds and a coal. *Energy Fuels* **2001**, 15, 961-971.
18. Okolo, G.N.; Everson, R.C.; Neomagus, H.W.; Roberts, M.J.; Sakurovs, R. Comparing the porosity and surface areas of coal as measured by gas adsorption, mercury intrusion, and SAXS techniques. *Fuel* **2015**, *141*, 293-304.
19. Sobolik, J. L.; Ludlow, D. K. Parametric sensitivity comparison of the BET and Dubinin-Radushkevich models for determining char surface area by CO_2 adsorption. *Fuel* **1992**, 71, 1195-1202.
20. Horvath, G.; Kawazoe, K. Method for the calculation of effective pore size distribution in molecular sieve carbon. *J. Chem. Eng. Jpn.* **1983**, 16, 470-475.
21. Rahman, M.; Samanta, A.; Gupta, R. Production and characterization of ash-free coal from low-rank Canadian coal by solvent extraction. *Fuel Process. Technol*. **2013** *115*, 88-98.
22. Xu, W.C.; Tomita, A. Effect of temperature on the flash pyrolysis of various coals. *Fuel* **1987**, *66*, 632-636.
23. Soncini, R.M.; Means, N.C.; Weiland, N.T. Co-pyrolysis of low-rank coals and biomass: Product distributions. *Fuel* **2013**, *112*, 74-82.
24. Pretorius, G.N.; Bunt, J.R.; Gräbner, M.; Neomagus, H.; Waanders, F.B.; Everson, R.C.; Strydom, C.A. Evaluation and prediction of slow pyrolysis products derived from coals of different rank. *J. Anal Appl Pyrolysis*. **2017**,128,156-67.
25. Given, P.H.; Marzec, A.; Barton, W.A; Lynch, L.J.; Gerstein, B.C. The concept of a mobile or molecular phase within the macromolecular network of coals: a debate. *Fuel.* **1986**, 65,155-63.
26. Marzec, A. Towards an understanding of the coal structure: a review. *Fuel Process. Technol*. **2002,** 77, 25-32.

27. Sheng Q.T.; Shen, J.; Niu, Y.X.; Liu, G.; Ling, K.C. The effect of small molecular compounds in coal on quick, direct coal liquefaction at a high temperature. *Energy Sources,* Part A, **2015**, 37, 28-37.
28. Zou, L.; Jin, L.; Li, Y.; Zhu, S.; Hu, H. Effect of tetrahydrofuran extraction on lignite pyrolysis under nitrogen. *J. Anal Appl Pyrolysis*. **2015**, 112, 113-120.
29. Hu, H.; Zhou, Q.; Zhu, S.; Meyer, B.; Krzack, S.; Chen, G. Product distribution and sulfur behaviour in coal pyrolysis. *Fuel Process Technol*. **2004**, 85, 849-861.
30. Zhu, P.; Luo, A.; Zhang, F.; Lei, Z.; Zhang, J.; Zhang, J. Effects of extractable compounds on the structure and pyrolysis behaviours of two Xinjiang coal. *J. Anal Appl Pyrolysis*. **2018**,133, 128-135.
31. Luo, A.Q.; Zhang. D.; Ping. Z.H.; Xuan Q.U.; Zhang, J.L.; Zhang, J.S. Effect of pyridine extraction on the tar characteristics during pyrolysis of bituminous coal. *J.Fuel Chem Technol.* **2017**, *45*, 1281-8.
32. Rautenbach, R.; Strydom, C.A.; Bunt J.R.; Matjie, R.H.; Campbell, Q.P.; Van Alphen, C. Mineralogical, chemical, and petrographic properties of selected South African power stations' feed coals and their corresponding density separated fractions using float-sink and reflux classification methods. *Int J Coal Prep Util*. **2018**. https://doi.org/10.1080/19392699.2018.1533551.
33. Tsemane, M.M.; Matjie, R.H.; Bunt, J.R.; Neomagus, H.W.; Strydom, C.A.; Waanders, F.B.; Van Alphen, C.; Uwaoma R.C. Mineralogy and petrology of chars produced by South African caking coals and density separated fractions during pyrolysis and their effects on caking propensity. *Energy Fuels*. **2019**, 33, 7645-58.
34. Ma, Z.; Bai, J.; Li, W.; Bai, Z.; Kong, L. Mineral Transformation in char and its effect on coal char characterization reactivity at high temperatures part 1 Mineral transformation in char. *Energy Fuels* **2013**, 27, 4545−4554.
35. Ma, Z.; Jin Bai, J.; Bai, Z.; Kong, L.; Guo, Z.; Yan, J.; Wen, L. Mineral Transformation in Char and Its Effect on Coal Char Gasification Reactivity at High Temperatures, Part 2: Char Gasification. *Energy Fuels* **2014**, 28, 1846−1853
36. Quann, R.J.; Sarofim, A.F. A scanning electron microscopy study of the transformations of organically bound metals during lignite combustion. *Fuel*, **1986**, 65, 40-446, 1986.
37. Frenklach M.; Wang H. Detailed mechanism and modelling of soot particle formation. *In Soot formation in combustion;* Springer: Berlin, Heidelberg, 1994; pp165-192.
38. Shengyu, L. The fate of organic oxygen during coal pyrolysis. *Energy Sources*. **2003**, *25*, 479-488.
39. Zhao, Y.; Hu, H.; Jin, L.; Wu, B.; Zhu, S. Pyrolysis behavior of weakly reductive coals from northwest China. *Energy Fuels*. **2009**, *23*, 870-875.

40. Wang, P.; Jin, L.; Liu, J.; Zhu, S.; Hu, H. Analysis of coal tar derived from pyrolysis at different atmospheres. *Fuel* **2013**, *104*, 14-21.
41. Casal, M.D.; Díez, M.A.; Alvarez, R.; Barriocanal, C. Primary tar of different coking coal ranks. *International J. Coal Geol*. **2008,** *76*, 237-242.
42. Bunt, J.R.; Waanders, F.B. Pipe reactor gasification studies of a South African bituminous coal blend. Part 1–Carbon and volatile matter behaviour as function of feed coal particle size reduction. *Fuel*. **2009**, *88*, 585-594.
43. Roberts, M.J.; Everson, R.C.; Neomagus, H.W.; Okolo, G.N.; Van Niekerk, D.; Mathews, J.P. The characterisation of slow-heated inertinite-and vitrinite-rich coals from the South African coalfields. *Fuel* **2015,** *158*, 591-601.
44. Suzuki, T.; Mishima, M.; Kitaguchi, J.; Itoh, M.; Watanabe, Y. The catalytic steam gasification of one Australian and three Japanese coals using potassium and sodium carbonates. *Fuel Process Technol.* **1984**, 8, 205-212
45. Matjie, R.H. Sintering and slagging of mineral matter in South African coals during the coal gasification process. PhD thesis, University of Pretoria, Pretoria, South Africa, 2008; pp 128-132; 96-102.
46. Hlatshwayo, T.B.; Matjie, R.H.; Li, Z.; Ward, C.R. Mineralogical characterisation of Sasol feed coals and corresponding gasification ash constituents. *Energy Fuels* **2009**, 23, 2867-73.
47. Matjie, R.H.; Li, Z.; Ward, C.R.; Bunt, J.R.; Strydom, C. A. Determination of mineral matter and elemental composition of individual macerals in coals Highveld mines. *J. S Afr I Min Metall,* **2016**, 116, 169-180.
48. Jüntgen, H. Review of the kinetics of pyrolysis and hydropyrolysis in relation to the chemical constitution of coal. *Fuel*. **1984**, *63*, 731-737.
49. Porada, S. The reactions of formation of selected gas products during coal pyrolysis. *Fuel* **2004**, *83*, 1191-1196.
50. Everson, R.C.; Okolo, G.N.; Neomagus, H.W.; Dos Santos, J.M. X-ray diffraction parameters and reaction rate modelling for gasification and combustion of chars derived from inertinite-rich coals. *Fuel* **2013**, 109,148-56.
51. Malumbazo, N.; Wagner, N.J.; Bunt, J.R.; Van Niekerk D. Assumption H. Structural analysis of chars generated from South African inertinite coals in a pipe-reactor combustion unit. *Fuel Process Technol*. **2011,** 1; 92, 743-9.
52. Wang, F.; Zhang, D.J.; Li, X.P.; Yang, M.L. Adsorption behaviors for nitrogen by coal, its extract fractions, and residues. *J.Fuel Chem Technol.* **2003**, *31*, 395-399.
53. Zhang, D.J.; Wang, F.; Li, X.P.; Xian, X.F. Effect of solvent extraction on pore character and granularity of bituminous coal. *J.Fuel Chem Technol.* **2004**, *32*, 18-22.

54. Cloke, M.; Lester, E. Characterization of coals for combustion using petrographic analysis: a review. *Fuel*. **1994**, *73*, 315-320.
55. Laurendeau, N.M. Heterogeneous kinetics of coal char gasification and combustion. *Prog Energy Combust*. **1978**, *4*, 221-270.

CHAPTER 5: GASIFICATION OF CHARS FROM TETRALIN LIQUEFACTION OF <1.5 G/CM^3 CARBON-RICH RESIDUES DERIVED FROM WASTE COAL FINES IN SOUTH AFRICA.

R.C. Uwaoma, C.A. Strydom, R.H. Matjie, J.R. Bunt

In this chapter, the gasification of residues derived from the tetralin liquefaction of float fractions obtained from the coal fines, the reactivities of the derived residue chars and the float fraction chars as compared in this paper, are reported.

The content of this manuscript has been submitted to Journal of Thermal Analysis and Calorimetry. **Submission Number: JTAC-D-20-00049**

ABSTRACT: The float-sink density separation method was used to produce a <1.5 g/cm^3 coal density fraction. The sample was subjected to tetralin liquefaction and then pyrolysed to produce char samples. The <1.5 g/cm^3 coal density fraction and its liquefaction carbon-rich residue char samples produced during the pyrolysis experiments were subjected to CO_2 gasification tests. The chars were characterised using a thermogravimetric analyser by heating the samples at isothermal temperatures between 880–940°C under a CO_2 atmosphere. The results obtained from the gasification experiments revealed that the gasification reactivity values (R_i, R_s, R_{tf}, $R_{t/0.5}$) of the liquefaction carbon-rich residue chars were higher than those of the <1.5 g/cm^3 coal density fraction chars. Some inherent mineral matter in the residues may play a catalytic role during gasification of South African lower density waste coals and their derived liquefaction residue chars. The initial reactivity of the liquefaction residue chars was observed to be approximately double those of the <1.5 g/cm^3 coal density fraction chars. Significant increases in the number of pores were associated with the liquefaction experiments of these carbon-rich particles, which aided in the acceleration of the gasification reactions. The increases in the number of pores assisted the reduction of the gasification activation energy values. The random pore model (RPM) was shown to fit the experimental data the best and was used to determine kinetic parameters. The gasification activation energy of the <1.5 g/cm^3 coal density fraction chars was shown to be 190.5 kJ mol^{-1} and 236.7 kJ mol^{-1} for Highveld float (HF) and Waterberg float (WF) chars, respectively. The values of the activation energy for the liquefaction carbon-rich residues from the same two <1.5 g/cm^3 coal density fraction residue samples were 145.3 kJ mol^{-1} for the Highveld coal sample and 196.0 kJ mol^{-1} for the Waterberg coal sample. The gasification results obtained in this study indicate that there is a high possibility of utilising waste coal floats and their liquefaction carbon-rich residues during thermochemical processes (pyrolysis and gasification).

Keywords**:** CO_2 gasification, tetralin, <1.5 g/cm^3 coal density fractions, liquefaction carbon-rich residue, float-sink separation

5.1 Introduction

Liquefaction of coal is a process whereby the macromolecular structure of coal is broken down by the addition of a solvent under moderate temperature and pressure to produce clean liquid fuels[1]. These broken down and extracted molecules are subsequently used in the coal to liquid (CTL) process.[1] Liquefaction of the <1.5 g/cm^3 density fraction from discarded coal fines produces different products (oil, gases, pre-asphaltenes) and liquefaction residues (waste carbon-rich materials).[2,3,4] The distribution of the liquefaction products is found to be 60% mixed oils, 15% gas, and about 25% of liquefaction residues (waste by-product).[1,5,6] Researchers have also shown that liquefaction residues contain slightly higher percentages of C, H, N, O, S and some inherent inorganic matter.[1,2,3,7] Previous studies indicated that the calorific value and physical, chemical and mineralogical properties of the liquefaction carbon-rich residues are similar to those of raw coal utilised for thermochemical processes.[2,3] The residues produced from liquefaction do not only contain unreacted coal macerals and inherent mineral matter, but also some residual oil, asphaltenes, and pre-asphaltenes.[3,8]

Liquefaction derived residues of coal have been used as feedstock for gasification,[5,6,9] pyrolysis[10-13] and hydro-liquefaction.[14,15] Literature reported that coal liquefaction residues produced from Chinese Shenhua coal were utilised in the production of advanced materials, such as a carbon nanofiber/carbon foam material using an oxidation and carbonisation process.[16,17] Cui et al.[3] showed that residues produced from coal liquefaction had a higher reactivity during CO_2 gasification experiments in comparison to raw coal. Chu et al.[4] investigated the gasification properties of residues derived from liquefaction and found that the residue chars exhibited moderately higher reactivity in relation to the coal chars. Yan et al.[5] investigated the liquefaction of Chinese raw coal, and subsequent CO_2 gasification of the liquefaction residues obtained in H_2 atmosphere at 425°C in an autoclave. Results from their investigation showed that the feed coal chars had lower reactivity than those of the derived liquefaction residues, during similar CO_2 gasification conditions.

Kinetic models for carbon conversion under a carbon dioxide atmosphere have been established to quantify reactivity of coal.[18-21] Most of the kinetic gasification studies with South African feed coals were performed with coals that are rich in vitrinite and inertinite.[22,23] In a recent study,[7] the physical, mineralogical, chemical, and petrographic properties, as well as the calorific value, of the <1.5 g/cm^3 fraction and the liquefaction residues from this fraction were described for a South African discarded coal sample, and it was shown that these properties were similar to those of thermochemical process feed coals.

The gasification behaviour of liquefaction residues of South African coals has not yet been described. The CO_2 gasification of the char produced from a <1.5 g/cm^3 coal fraction and the liquefaction residues produced from the same fraction are compared in this paper. The <1.5 g/cm^3 coal fraction has been obtained from a South African discarded coal sample. The utilisation of residues from liquefaction of discarded coal may have economic benefits. Environmental issues that are associated with the disposal of significant amounts of waste coals may also be diminished if these discarded coals are utilised.

The gasification reactivity of the chars produced from <1.5 g/cm^3 coal density fractions and the carbon-rich char residues produced from liquefaction of the <1.5 g/cm^3 density coal fraction were obtained using different gasification reactivity models as will be described and discussed in this paper. The influence of parameters, such as the pore structure, and the inherent mineral matter, was taken into account and will be discussed.

5.2 Experimental procedures and analytical methods

5.2.1 Materials and sample preparation for experiments and analyses

The SANS/ISO 7936 method of the South African Bureau of Standards (SABS) was followed to recover the <1.5 g/cm^3 density fractions from discarded coal samples from the Highveld and the Waterberg areas in South Africa. These wastes were sampled by NWU students and operators from the mines using the ISO 1988:1975 and ISO 13909-4:2016 sampling methods. The <1.5 g/cm^3 density fractions (float fraction) were used in the liquefaction and pyrolysis experiments to produce liquefaction residues and pyrolysis chars at 920°C for the CO_2 gasification tests as described previously.[2,24] The liquefaction solid residues and <1.5 g/cm^3 density fraction char samples were homogenised separately (<75 µm) following a standard cone and quartering method (DD CEN/TS 14780:2005) to obtain a representative sample that was used for the CO_2 gasification experiments.[2]

Various analytical techniques, such as proximate and ultimate analyses, were performed, as previously described, with the samples and also the products of the gasification experiments.[2,24] The chars produced from the <1.5 g/cm^3 fraction of the Waterberg and the Highveld coal samples and their corresponding liquefaction residue samples were termed WF and HF, and WF-R and HF-R respectively.[2,24]

5.2.2 Demineralisation of liquefaction residue chars

The impact of mineral matter on the liquefaction residues in the CO_2 gasification reactions was investigated through demineralising the residues, using an extraction process with hydrochloric (HCl, 10.2 M) and hydrofluoric (HF, 22.6 M) acid, as reported elsewhere.[25,26] HCl

aids in the abstraction of some carbonates and acid-removable calcium, while HF removes most of the coal mineral matter (inherent mineral matter and extraneous minerals), including quartz and alumino-silicates.[26,27] After demineralisation, distilled water was used to wash the samples until no evidence of acids was observed in the samples using a pH meter. The demineralised residues were referred to as Highveld float demineralised residue (HF-DR) and Waterberg float demineralised residue (WF-DR). The efficiency of the demineralisation, E_d, was quantified using the following formula:

$$E_d = \left\{\frac{A_o - A_d}{A_o}\right\} \times 100 \qquad 5.1$$

where A_o denotes the % ash yield of the liquefaction carbon-rich residue before demineralisation and A_d is the % ash yield of the de-ashed residue (%w., db).

5.2.3 Composition of the chars of the <1.5 g/cm^3 coal and its liquefaction residue samples

All the char samples were analysed using proximate, ultimate, porosity and surface area analyses using the same equipment and under similar conditions, as described by Uwaoma, et al.[24] Some of the results reported in our previous paper have been repeated in this paper for comparison with the values for the demineralised samples.[24]

X-ray diffraction (XRD), as described previously[2], was used to evaluate fractions of minerals and amorphous phases contained in the samples. The X-ray fluorescence (XRF) was used to detect the inorganic elements in the ash samples of the <1.5 g/cm^3 coal density fractions, liquefaction carbon-rich residue, and char samples. All the analyses were performed as described previously.[2,24]

5.2.4 Char CO_2 gasification reactivity experiments.

The CO_2 gasification experiments with the chars from the <1.5 g/cm^3 coal sample and liquefaction carbon-rich residues were conducted in a TA Instruments SDT Q600 thermogravimetric analyser (TGA). Nitrogen gas was flushed through the set-up (furnace and sample) using a constant 100 cm^3/min flow for 25 minutes to create an inert atmosphere. For each gasification test, an approximately 15 ± 1 mg char sample was loaded into a 90 µL alumina crucible, and the furnace was heated to the desired isothermal reaction temperature (880, 900, 920 and 940°C) under a constant flow of N_2 gas (100 cm^3/min) with a ramp rate of 50°C/min. This was done to remove residual volatile matter before the gasification tests. Upon attaining the desired reaction temperature, CO_2 gas at a flow rate of 100 cm^3/min flushed the system until the reaction was completed. The experimental conditions were selected to ensure that the CO_2 gasification reaction rate followed regime 1 kinetics.[23]

To quantitatively investigate the chars' gasification reactivities, the fractional gasification conversion, *X*, of the fixed carbon in the residue chars, was evaluated using Equation 5.2.[22,23,29-32] The initial reactivity, R_i, and the specific or instantaneous reactivity, R_s, were deduced using Equations 5.3 and 5.4.[30,32,33]

$$X = \frac{m_o - m_t}{m_o - m_{ash}} \quad 5.2$$

$$R_i = \left.\frac{dX}{dt}\right|_{X=0} \quad 5.3$$

$$R_s = \frac{dM/dt}{M - m_{ash}} \quad 5.4$$

where: *X* is the fraction of gasification conversion; m_o is the original mass of the lighter density char or residue char before gasification; m_t is the remaining mass of char at time, *t*; m_{ash} is the mass of residual ash; *t* is experimental real-time; *M* is the mass of carbon that has reacted in the char at a specific reaction time t; m_{ash} is the mass of ash obtained after reaction.

5.2.5 Char CO_2 gasification kinetics

The kinetic modelling and calculation of kinetic parameters of the gasification process were carried out using different gasification reaction kinetic models. These models include the volumetric reaction model (VRM), the random pore model (RPM), and the shrinking core model (SCM). The shrinking core model assumes that the gasification reactions occur on the external char surface and then penetrate the internal surface of the char matrix. The details of the shrinking core model are described elsewhere, and the describe equation is given below.[34]

$$X = 1 - \left(1 - \frac{t_f}{3}\right) \quad 5.5$$

where: t_f is the time factor evaluated using the SCM.

The volumetric or homogenous reaction model assumes that the gasification reactions occur homogeneously throughout the outside and inside surfaces of the reaction environment. The homogenous equation is given, as postulated by Wen et al., below:[35]

$$X = 1 - exp(-t_f t) \quad 5.6$$

where: t_f is the time factor evaluated using the VRM. The time factor in the individual reaction models is evaluated using regression methods.

The random pore model (RPM) assumes a random pore size distribution and random orientation. The RPM is different from the other models because it explains changes in the structure of the char as the reaction proceeds. Liquefaction alters the pore structure of the coal matrix, and these structural changes will influence the reaction progress. The overall reaction rate using the RPM is given by Equation 5.7.[36] The influence of the operating condition is considered by the addition of the intrinsic reaction rate, r_s, to equation 5.7.[39] The differences in the structure of the char as the gasification reaction advances are described by the introduction of the RPM dimensionless structural parameter, ψ, which is determined by char properties (such as porosity) (Equation 5.8).[22,23,31,32,36]

$$\frac{dX}{dt} = \frac{r_s S_o (1-X)\sqrt{1-\psi \ln(1-X)}}{(1-\varepsilon_o)} \qquad 5.7$$

$$\psi = \frac{4\pi L_o (1-\varepsilon_o)}{S_o^2} \qquad 5.8$$

The RPM conversion, X, at the real-time, t, is given in Equation 5.9.[22,23]

$$X = 1 - \exp\left[-t_f t \cdot \left(1 + \frac{t_f t \psi}{4}\right)\right] \qquad 5.9$$

where t_f is the time factor evaluated using the RPM. The structural parameter, ψ, can be estimated by linear regression, following the method proposed in reference 22, using the dimensionless time, $t/t_{0.9}$ (Equation 5.10). $t_{0.9}$ is the time required to reach 90% conversion.

$$\frac{t}{t_{0.9}} = \frac{\sqrt{1-\psi \ln(1-X)} - 1}{\sqrt{1-\psi \ln(1-0.9)} - 1} \qquad 5.10$$

The activation energy, E_a, was calculated using the slope of the graphical plot of ln(t_f) against T^{-1}. The lumped pre-exponential factor, k_{so}, was estimated from the intercept of the plot of ln(t_f) versus T^{-1}. By plotting ln t_f against ln Y_{CO2} at a constant temperature, the reaction order with respect to CO_2 concentration, m, can be determined from the slope. The gas constant (R) is 8.314 J / mol·K. The kinetic parameters were determined using the initial reactivity, R_i, or the initial specific reactivity, R_s, by substituting the t_f term in Equation 5.11 with the appropriate reactivity term:

$$\ln(t_f) = -\frac{E_a}{RT} + m \ln(y_{CO_2}) + \ln(k'_{so}) \qquad 5.11$$

The quality of fit (QOF) was used to evaluate the fitting of the kinetic models. The QOF is defined by Equation 5.12 and has been used by other investigators to evaluate the kinetic models.[28]

$$QOF\ (\%) = 100\ \times \left(1 - \frac{\sum_1^N \frac{X_{cal} - X_{exp}}{X_{exp}}}{N}\right) \qquad 5.12$$

where X_{cal} and X_{exp} are the calculated conversions and experimental conversion obtained from the model, respectively, and the data points used for models are represented by N.

5.3 Results and discussion

5.3.1 Char analysis results

5.3.1.1 The compositions of the <1.5 g/cm^3 density fraction and liquefaction residue chars

The proximate, ultimate, and CO_2 adsorption results of the 1.5 g/cm^3 density fraction and liquefaction residue chars are given in Table 5-1 (the already reported results[2,24] obtained for the samples are repeated in the table to compare to those of the demineralised samples). The volatile matter contents of all the chars decreased after pyrolysis, as expected. The reduction in the volatile matter contents of these samples was attributed to the abstraction of hydrogen during the pyrolysis tests. The chars of the demineralised liquefaction residue showed a reduction in the ash yields and an increase in the fixed carbon contents, as expected. The demineralised liquefaction residue samples showed a similar demineralisation efficiency of 89.4% and 89.8% for the Waterberg liquefaction residue and the Highveld liquefaction residue, respectively.

The ash yield of the demineralised Highveld residue char was determined to be 3.0%wt., whilst that for the demineralised Waterberg residue char was determined to be 3.5 %wt. The fixed carbon contents of the demineralised chars were observed to increase slightly in comparison to the fixed carbon contents of the liquefaction carbon-rich residue chars. This increase in the fixed carbon contents of the demineralised chars was attributed to the removal of mineral matter from the samples. The proximate and ultimate analyses results for the chars produced in this study are similar to those of the coals, which are fed into South African gasifiers and boilers.[37,38,39]

The ultimate analysis results of the demineralised samples are presented in Table 5-1 along with a repeat of the relevant data from our previous paper.[24] It was shown that the <1.5 g/cm^3 coal density fraction, their liquefaction carbon-rich residue, and demineralised residue chars were rich in elemental carbon (>75 wt.%, daf), rending the lighter density coal fractions and their residue chars suitable feedstock for gasification reactions.[22,23] The ultimate analysis of the lighter fraction coals and their carbon-rich residues did not show much variation when compared to those of the demineralised carbon-rich residues. In essence, the only meaningful difference was in the sulphur contents. As expected, the demineralised carbon-rich residues showed a lower sulphur percentage when compared to the <1.5 g/cm^3 coal fraction and the carbon-rich liquefaction residue samples.

Table 5-1: Proximate and ultimate analyses results of the chars generated at 920°C from the <1.5 g/cm^3 coal samples, their liquefaction carbon-rich residues, and the demineralised samples

	WF char	HF char	WF-R char @	WF-R (D) char	HF-R char	HF-R (D) char
Proximate analysis data (%wt., air dry basis (adb))						
Inherent moisture	1.7	2.6	1.4	1.2	1.4	1.5
Ash yield	21.0	14.6	30.2	3.2	29.5	3.0
Volatile matter (VM)	1.9	2.4	1.3	1.5	2.4	2.0
Fixed carbon (FC) (by difference)	75.8	80.9	67.1	94.1	66.7	93.5
Fuel ratio (FC/VM)	39.9	33.7	51.6	62.7	27.8	46.7
E_d (%)	-	-	-	89.4	-	89.8
Ultimate analysis (%wt., dry ash-free basis (daf) ISO 29541: 2010						
Carbon	94.9	95.0	94.5	95.3	93.3	94.3
Hydrogen	0.8	0.7	0.8	0.6	0.7	0.8
Nitrogen	1.4	1.7	1.2	1.2	1.5	1.3
Sulphur	1.2	0.5	1.2	0.7	1.1	0.6
Oxygen (by difference)	1.8	2.1	2.3	2.2	3.4	3.0
H/C atomic ratio	0.1	0.09	0.11	0.08	0.09	0.1
O/C atomic ratio	0.01	0.2	0.02	0.012	0.04	0.24
S/C atomic ratio	0.005	0.002	0.0047	0.003	0.0023	0.0024

Note: (D)- demineralized residue; WF Char at 920°C= Waterberg <1.5 g/cm^3 coal density fraction pyrolysed at 920 ˚C; HF Char @920 °C = Highveld <1.5 g/cm^3 coal density fraction, pyrolysed at 920 ˚C; WF-R Char @920 ˚C= Waterberg liquefaction carbon-rich residue pyrolysed residue at 920 ˚C; HF-R Char @920 ˚C= Highveld liquefaction carbon-rich residue pyrolysed residue at 920 ˚C.

5.3.1.2 XRD analysis

Results from the XRD analysis of the <1.5 g/cm^3 coal density fractions, their liquefaction carbon-rich residues and the chars generated at 920°C are summarised in Table 5-2. Samples contained high amounts of amorphous phases, with only small proportions of crystalline phases. The XRD results obtained for the <1.5 g/cm^3 coal density fractions, liquefaction carbon-rich residues, and their char samples were consistent with values obtained by other researchers on South African coals.[37,38] As expected, the amorphous phase (organic carbon and alumino-silicate) results of the <1.5 g/cm^3 coal density fraction chars were higher (79.2–85.5%) in comparison to those of the liquefaction carbon-rich residue chars (70.3–74.5%). The lower amorphous phase percentages of the residues were ascribed to a reduction in organic matter, leading to a drop in the percentages of volatile matter and fixed carbon. This was consistent with the high % ash yield values obtained from proximate analysis of the chars (Table 5-1). The XRD results revealed that the demineralised residue samples contained 100% amorphous material, which mainly consisted of organic carbon.

The XRD results (Table 5-2) show that the most abundant crystalline minerals in the <1.5 g/cm^3 coal density fractions, their liquefaction carbon-rich residue and subsequent char samples were quartz (SiO_2), and kaolinite $Al_2[Si_2O_5](OH)_4$ with small amounts of siderite ($FeCO_3$), pyrite (FeS_2), dolomite ($CaMg(CO_3)_2$, and calcite (CaCO3). Kaolinite minerals were found in the Highveld <1.5 g/cm^3 coal fraction and the Waterberg <1.5 g/cm^3 coal fraction samples, but their mode of occurrence in these two fractions differed as described by other authors[38,39,40] that have investigated South African coals. The kaolinite contents decreased with an increase in temperature in all char samples produced in this study (Table 5-2). Kaolinite transformed at 400–528°C to form meta-kaolinite (amorphous phase) during the dehydration of kaolinite.[41] Microcline of <3.5% was found in all the char samples. The products from the disintegration of kaolinite could undergo further reactions with K_2O to generate microcline at around 500–800°C.[42] Taking into account the decreased organic matter in the liquefaction residue samples, the mineralogy of the chars produced from the coal density fractions <1.5 g/cm^3 and their liquefaction carbon-rich residues did not differ significantly from each other. The only significant difference observed was the presence of pyrite in the <1.5 g/cm^3 density fraction and pyrrhotite in the liquefaction residue samples. Pyrite transforms to pyrrhotite ($Fe_{1-x}S$) under inert atmosphere during liquefaction and pyrolysis.

Table 5-2: XRD analysis results of the chars generated at 920°C of the <1.5 g/cm^3 coal samples, their liquefaction carbon-rich residues, and the demineralised samples (%wt.)

Mineral phases	WF	WF char	WF-R	WF-R char	WF-R (D)	HF	HF char	HF-R	HF-R char	HF-R (D) char
Quartz	5.8	13.3	9.2	21.3	-	1.7	4.1	3.1	9.2	-
Siderite	0.2	0.1	0.2	-	-	-	0.2	-	0.4	-
Kaolinite	9.4	4.4	14.3	5	-	8.2	7	15.3	8.4	-
Pyrite	0.9	-	-	-	-	1.2	-	-	0.1	-
Muscovite	-	-	0.4	-	-	-	-	-	-	-
Dolomite	-	-	0.1	-	-	0.5	0.5	1.1	1.1	-
Calcite	0.2	0.3	0.4	0.2	-	0.3	0.3	0.7	0.4	-
Magnetite	-	-	-	-	-	-	-	-	0.1	-
Pyrrhotite	-	0.8	0.4	0.9	-	-	0.7	0.3	1.7	-
Microcline	-	1.5	-	2.4	-	-	1.6	-	3.2	-
Amorphous phase/organic C	84.5	79.2	75.1	70.3	100	89.2	85.5	79.6	74.5	100

5.3.1.3 XRF analysis

The XRF analysis results of the ash samples are presented in Table 5-3. The ash samples of the <1.5 g/cm^3 coal density fraction, their liquefaction carbon-rich residues and their subsequent chars consisted mainly of Si, Al, Ca, and Fe and minor proportions of P, Mg, T, Na, and K which were all reported as elemental oxides. The XRF results obtained in this study compared well with those of the ash samples of South African coals and chars.[38,39,40] There were no significant differences between the XRF results of the ash samples of the <1.5 g/cm^3 coal density fractions and their liquefaction carbon-rich residues.

Table 5-3: XRF results of the ash samples of coal density fractions of <1.5 g/cm^3 and their liquefaction carbon-rich residue chars on LOI free basis (%wt. lfb)

Elements	WF	WF char at 920 °C	WF-R	WF-R char at 920°C	HF	HF char at 920°C	HF-R	HF-R char at 920 °C
Fe_2O_3	5.0	4.8	5.2	5.2	5.6	4.7	5.4	5.2
SiO_2	57.6	56.3	57.3	58.2	40.7	44.9	42.8	44.5
Al_2O_3	26.2	25.5	26.3	26.3	29.5	31.4	28.8	29.2
K_2O	0.7	0.8	0.7	0.8	0.5	0.6	0.5	0.6
P_2O_5	1.6	1.4	1.5	1.5	1.4	1.4	1.3	1.3
MnO	0.1	0.1	0.1	0.1	0.1	0.2	0.3	0.2
CaO	5.1	4.6	5.4	5.2	12.3	10.1	12.0	11.6
MgO	0.6	0.7	0.8	0.8	2.3	2.8	3.4	3.5
TiO_2	1.6	1.5	1.6	1.6	1.5	1.6	1.4	1.5
Na_2O	0.1	0.1	0.1	-	0.4	0.4	0.6	0.6
SO_3	1.4	4.3	1.1	0.3	5.7	1.9	3.3	1.8
Total (*wt.%,lfb*)	100.0	100.1	100.1	100.0	100.0	100.0	99.8	100.0

5.4 Char-CO_2 gasification results

Figure 5-1 presents the mass loss curves obtained from the CO_2 gasification experiments for the Highveld <1.5 g/cm^3 density fraction, the Waterberg <1.5g/cm^3 density fraction, and their liquefaction residue chars at 940°C. A rapid reduction in mass was observed in the early stage of the gasification reaction for all the char samples, until an equilibrium point with no further mass loss. The final equilibrium mass corresponded to the remaining ash and a small percentage of carbon that was not converted during the gasification steps. The remaining mass percentages in all cases were less than 5% more than the ash yields determined for the samples (Table 5-1), and the value of 23% was close to the % mass loss observed during the CO_2-gasification experiments, which indicated that the % carbon conversion efficiency of the <1.5 g/cm^3 density fraction chars and the liquefaction residue chars, differed from each other. The difference in the carbon conversion efficiency of the samples was accredited to the liquefaction test abstracting some organic components of coal moiety.

The Highveld and Waterberg <1.5 g/cm^3 density fractions achieved 81.2% and 78.1% mass loss efficiencies respectively, while their corresponding residues achieved 69.6% mass loss for the Highveld residue char and 67.4% mass loss for the Waterberg residue char. Similar trends were observed for the liquefaction residue samples. The time needed for mass losses of the residues chars to stop (completed reactions) was nearly doubled when compared to that of the <1.5 g/cm^3 density fraction chars, under the same gasification conditions of the experiments.

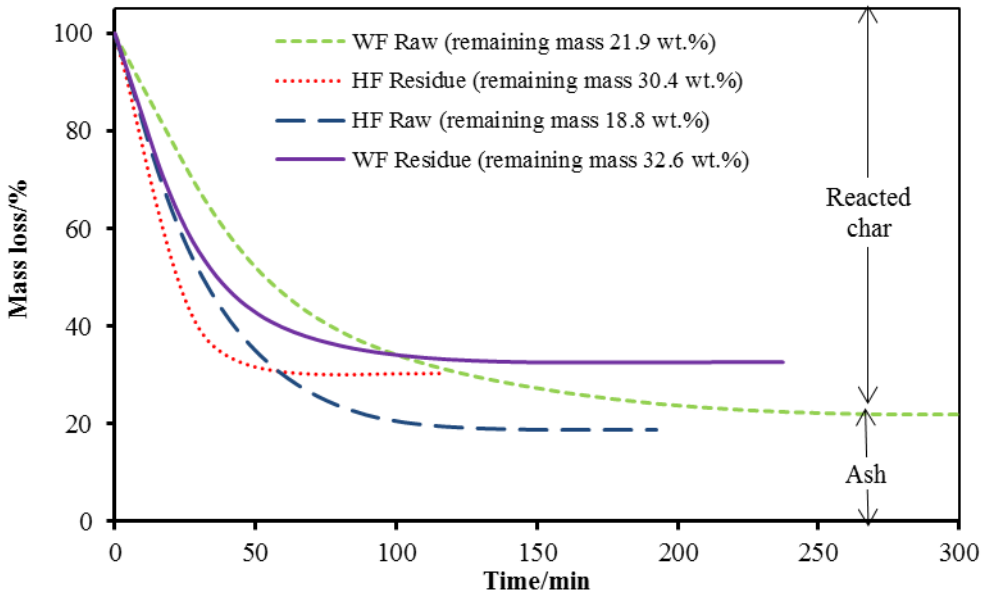

Figure 5-1: Char-CO_2 isothermal gasification mass loss results for the char samples at 940°C

The data obtained from the TGA experiments were normalised to exclude the ash yields. It was assumed that no gaseous products were produced from the mineral decomposition reaction with CO_2 according to Equation 5.3.[22,23,29-32] The fraction conversion plots using the normalised results obtained from the TGA experiments are presented in Figure 5-2.

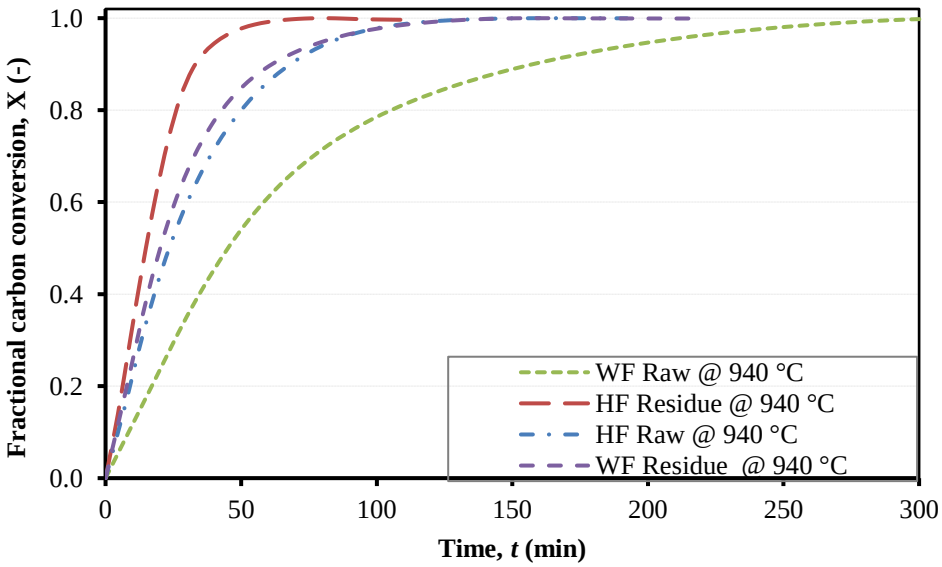

Figure 5-2: Normalised gasification fractional carbon conversion curve of the char–CO_2 gasification experiments at 940°C for WF, HF, and their liquefaction carbon-rich residues

5.5 Effect of temperature on the gasification conversion

Figure 5.3 indicates that the gasification reactions followed Arrhenius type reactions, where a rise in gasification temperature increased the conversion. Other investigators have reported similar trends on the effect of temperature during gasification of South African coals.[22,23,43] The increase in the rates of reaction as temperature increased showed that the reactivities increased with temperature.

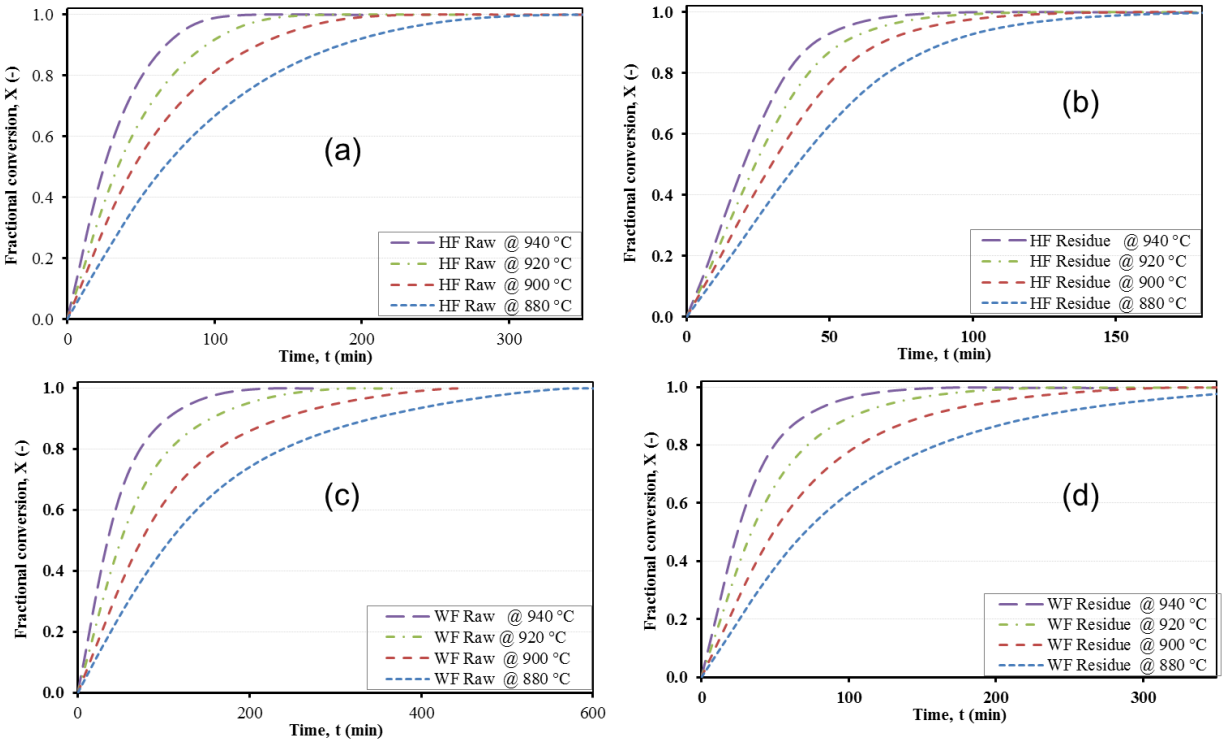

Figure 5-3: Effect of temperature on fractional conversion for: (a) Highveld coal density fractions <1.5 g/cm^3, (b) Highveld liquefaction carbon-rich residue, (c) Waterberg coal density fractions <1.5 g/cm^3, (d) Waterberg liquefaction carbon-rich residue sample

5.6 CO_2 gasification reactivity of the chars

As presented in Table 5-4, at a lower gasification temperature of 880°C, the HF raw and the WF raw chars showed 90% carbon conversion after 189.2 min and 467.2 min, respectively. The liquefaction residue chars reached 90% carbon conversion faster when compared to the <1.5 g/cm^3 density fractions, with the HF residue char reaching 90% carbon conversion after 69.9 min and the WF residue char reaching 90% conversion after 203.8 min at 880°C gasification temperature. Table 5-4 also shows that as the temperature of gasification rose, the time for 90% conversion of all the samples decreased. The observed faster gasification rate of the liquefaction residue chars could be attributed to: (1) the influence of the surface

area and porosity, which were altered during the gasification process – the surface area and porosity of the chars used in this study were reported in our previous paper[24]; and (2) the inherent mineral matter in the residues could have played a catalytic role during the gasification test.

The gasification reactivities of the lighter density float chars and the liquefaction residue chars were established using the initial reactivities (R_i) of the samples (Equation 5.4),[30,32,33] while the specific or instantaneous reactivities (R_s) of the samples were calculated using Equation 5.5.[32,33] The determination of R_i was attained by plotting a graph of the rate of reaction, dX/dt, against the gasification fractional carbon conversion, X. The initial reactivities of the <1.5 g/cm^3 coal density fractions and their liquefaction carbon-rich residue chars were obtained from the carbon conversion versus time plots at time t = 0. A plot showing the different reactivity values of the lighter density fraction and their residue chars are presented in Figure 5.4. The times for attaining 50% ($t_{0.5}$), and 90% ($t_{0.9}$) carbon conversion are listed and used as indicators of the reactivity.

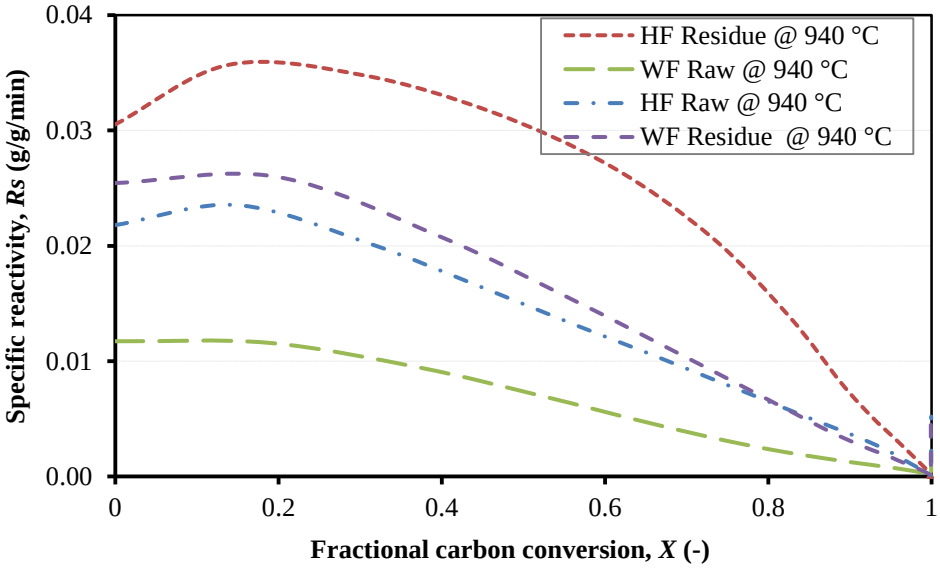

Figure 5-4: Comparison of the reactivities of the four samples: dX/dt as a function of carbon conversion at 940°C

It is evident from Table 5-4 that the <1.5 g/cm^3 density fraction char samples exhibited lower reactivity than those of their corresponding liquefaction residue char samples. Both the $t_{0.5}$ and $t_{0.9}$ of the liquefaction residue char samples were observed to be significantly higher than those of the lighter density fraction char samples by a factor ≤ 2.2 for WF-R and ≤ 3.5 for WF-R.

Table 5-4: Gasification reactivities of the char samples from the <1.5 g/cm^3 coal density fractions and their liquefaction carbon-rich residue samples

Temp.	Sample ID	$t_{0.5}$,(min)	$t_{0.9}$, (min)	$R_{t0.9}$	$R_{t0.5}$	R_i, (min^{-1})	R_s,(g/g·min)
880°C	HF Raw	62.69	189.16	0.0048	0.0080	0.0087	0.0087
	HF Residue	30.97	69.90	0.0129	0.0161	0.0148	0.0148
	WF Raw	131.53	467.20	0.0019	0.0038	0.0039	0.0040
	WF Residue	57.85	203.77	0.0044	0.0086	0.0097	0.0097
900°C	HF Raw	45.00	137.55	0.0065	0.0111	0.0120	0.0120
	HF Residue	23.93	54.28	0.0166	0.0209	0.0188	0.0188
	WF Raw	84.32	298.35	0.0030	0.0059	0.0064	0.0064
	WF Residue	41.31	138.78	0.0065	0.0121	0.0131	0.0131
920°C	HF Raw	31.40	93.46	0.0096	0.0159	0.0171	0.0171
	HF Residue	18.41	41.43	0.0217	0.0272	0.0244	0.0244
	WF Raw	56.65	197.88	0.0045	0.0088	0.0093	0.0093
	WF Residue	29.26	93.23	0.0097	0.0171	0.0178	0.0178
940°C	HF Raw	23.48	68.19	0.0132	0.0213	0.0218	0.0218
	HF Residue	14.88	33.15	0.0271	0.0336	0.0305	0.0305
	WF Raw	37.88	128.09	0.0070	0.0132	0.0139	0.0139
	WF Residue	20.13	61.41	0.0147	0.0248	0.0254	0.0254

The reactivities of the chars produced from the <1.5 g/cm^3 coal density fractions and their liquefaction carbon-rich residue samples increased with temperature, as expected. The liquefaction carbon-rich residue chars showed significantly higher reactivities in comparison to those of the <1.5 g/cm^3 density fraction samples in all investigated cases. The higher reactivity values of the liquefaction carbon-rich residue chars may have been due to an increase in porosity during liquefaction. The liquefaction process creates a larger surface area and consequently produce more active carbon sites. Inherent minerals in the residues may also have had a catalytic effect on gasification (especially alkali compounds).

5.7 Effect of porosity on gasification reactivity of <1.5 g/cm^3 density fraction and carbon-rich residue chars

The relationship between the D-R micropore surface area and the porosities were compared to the initial CO_2 reactivity of the <1.5 g/cm^3 density fraction chars and liquefaction residue chars and are presented in Figure 5.5. The detailed surface analyses of the char samples have been reported in our previous study.[24] The initial reactivity of all the chars increased with an increase in porosity at the different gasification temperatures used in this investigation. The liquefaction residue chars had higher reactivity than those of the lighter density coal chars, as already described, and they also had larger surface area and porosity than those of the <1.5 g/cm^3 coal density fractions. More new pores were formed during liquefaction, as some micro

and macromolecular fractions were abstracted from the coal matrix. Similar results were obtained by Liu et al.[9] from the gasification tests of residue chars from the Shenhua direct liquefaction plant. They suggested that the reactivity improvement of the residue chars may be ascribed to the reduction in the amount of carbon and an increasing number of new pores that were formed in the residue during liquefaction.

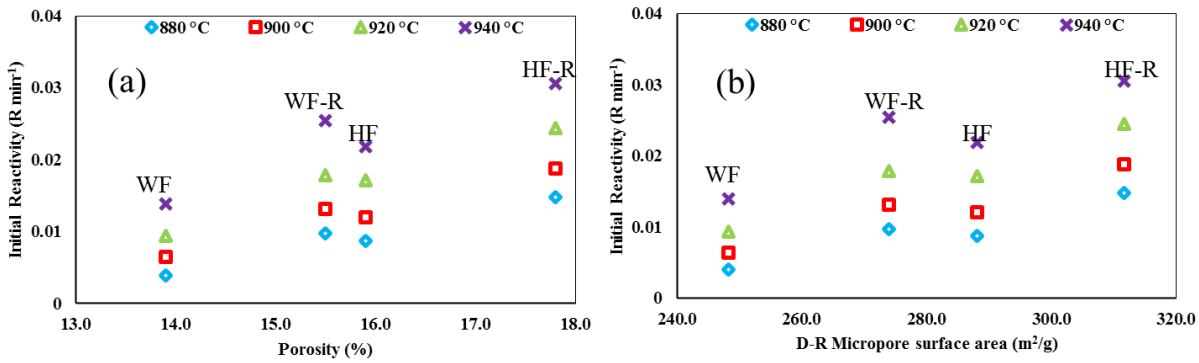

Figure 5-5: Influence of some surface parameters on the initial reactivity of the samples: (a) Influence of porosity; (b) Influence of micropore surface area. (WF= Waterberg float char, HF= Highveld float char, WF-R= Waterberg float residue char, HF-R= Highveld float residue char

5.8 Influence of mineral matter on gasification reactivity of lighter density fraction and residue chars

During the liquefaction of coal, the inherent mineral matter was enriched in the liquefaction residues. This was due to the extraction of organic matter during the liquefaction tests. The coal liquefaction carbon-rich residue chars were demineralised, and the proximate analysis results of the liquefaction residue chars before and after demineralisation are reported in Table 5-1. As established in the char reactivity tests (Table 5.4), the char reactivity of the liquefaction residues was higher than this of the <1.5 g/cm^3 density fraction chars. A part of the increase in the reactivity of the liquefaction residue chars could be attributed to the inherent mineral matter enrichment in the residues. The inherent minerals in the liquefaction residues may have interacted and transformed during the CO_2 char gasification experiments. The interaction of the salts of carboxylic acid and the transformation of the included minerals may have catalysed the pyrolysis and gasification reactions.[44] To investigate these claims further, the liquefaction residue chars were demineralised. The CO_2 gasification results of the residue chars and the demineralised residue chars are given in Figure 5.6. The weight loss percentages of the demineralised residue char samples showed a mass loss to less than 3.0 wt.% (ad). This implied that the inherent mineral matter in the liquefaction residue chars was minimal due to the demineralisation experiments. The demineralised liquefaction residues showed a reduction in the char-CO_2 gasification reactivity. The initial reactivity of the Highveld

demineralised liquefaction residue char and Highveld liquefaction residues (HF-R) coal were 0.0148 min^{-1} and 0.0026 min^{-1}, respectively at 880°C. The Waterberg liquefaction residue chars and the demineralised Waterberg residue chars achieved reactivity of 0.0097 min^{-1} and 0.0024 min^{-1} at 880°C, respectively. As expected, the reactivity of the demineralised liquefaction carbon-rich residue chars, was lower than that of the liquefaction residue chars. Similar results for the demineralised chars of residues generated from the liquefaction of Shenhua feed coal were reported by other researchers.[9]

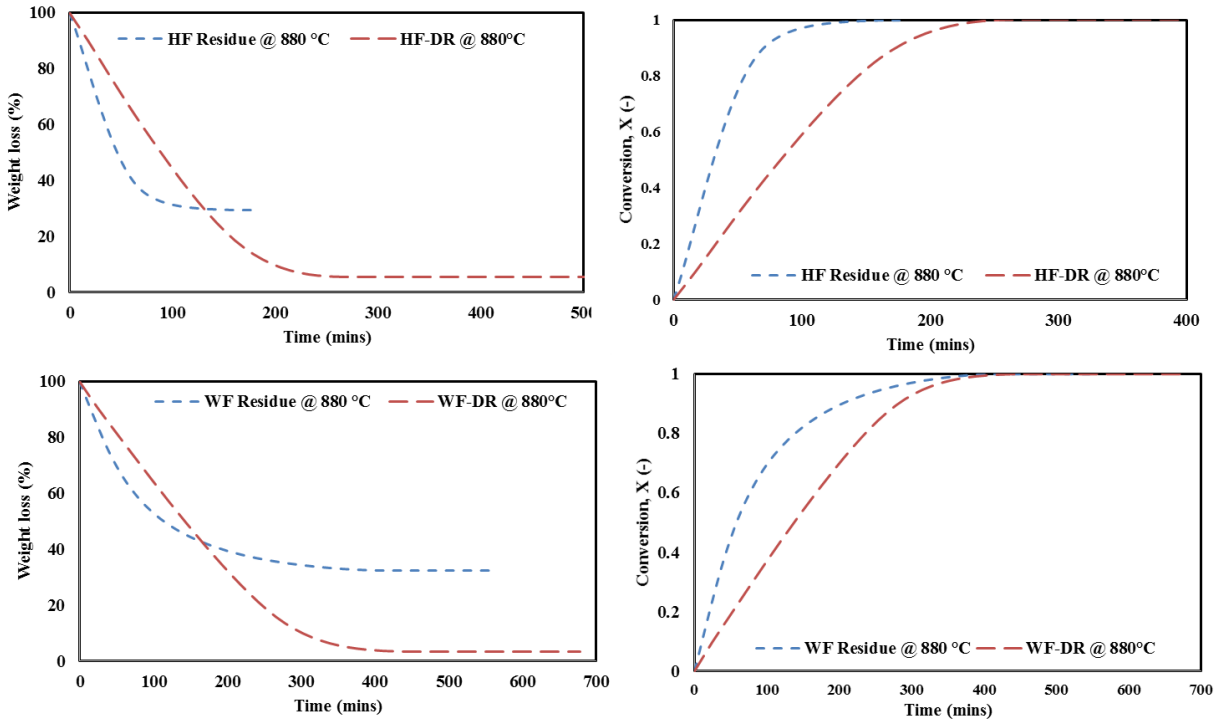

Figure 5-6: Mass loss and carbon conversion of the chars from the liquefaction residues and demineralised liquefaction residues during CO_2 gasification at 880°C

5.9 Kinetic modelling using the random pore model volumetric reaction model

The random pore model and the volumetric reaction model were employed to determine parameters such as the time factors, t_f, (using regression method) and the structural parameters, ψ (Equations 5.6 and 5.9 respectively). The shrinking core model was not reported in this investigation because it did not fit to the experimental data. Uncertainty parameters were used to evaluate the accuracy of the two models used in this investigation. These parameters, which are the quality of fit (Equation 5.12) and error sum of squares (ESS), were determined from the model fitting as presented in Figure 5.7.

The summary of the RPM and VRM determined time factors and the structural parameters at different temperatures for the <1.5 g/cm^3 coal density fraction and their liquefaction carbon-

rich residue char samples are presented in Table 5-5. From the determined RPM and the VRM reactivity values, t_f, reactivities for the <1.5 g/cm^3 density fraction and liquefaction residue chars favourably compared with the initial reactivity and the specific reactivity values. The structural parameters, ψ, of the <1.5 g/cm^3 coal density fraction chars and their liquefaction carbon-rich residue chars were found to increase with an increase in isothermal experimental temperature, similar to the data of other investigators.[22,23] As expected, the time factors obtained for the <1.5 g/cm^3 coal density fraction chars, and their liquefaction carbon-rich residue chars were also observed to increase with an increase in the isothermal experimental temperature. These results are comparable to data previously published for South African bituminous coals.[22,23] The structural parameter, ψ, for the lighter density fraction chars indicated that only pore coalescence occurred during the early phase of the gasification reaction, with $\psi < 2$. Hence, the surface areas of the chars of the <1.5 g/cm^3 coal density fractions decreased with increasing carbon conversion. The residue chars, however, underwent pore growth ($\psi > 2$) at the initial stages of the gasification reaction, which was characterised by increasing surface area with increasing carbon conversion.

Fitting experimental conversion data to the RPM and VRM models gave a satisfactory fit for the <1.5 g/cm^3 density fraction chars and their liquefaction carbon-rich residue chars (Figure 5.7). The RPM, however, gave a better fit for all the samples used in this investigation when compared to VRM. The RPM gave a QOF of 97–98%, while the VRM gave a QOF of 87–94% for all samples. The evaluated uncertainty parameters in Table 5 showed that the RPM exhibited a higher QOF and a lower ESS for all the samples when compared to a lower QOF and higher ESS obtained when using the VRM. The fitting of the data obtained during the experiment to the RPM and VRM models indicated that the CO_2 gasification reactivity of the chars from the <1.5 g/cm^3 density fractions and their liquefaction carbon-rich residue were under chemical reaction control (Regime I).

Table 5-5 RPM and VRM determined time factors, $t_{f,}$ structural parameter, ψ, quality of fit, and error sum of squares

Temperature	Sample ID	RPM t_f (min^{-1})	RPM ψ (-)	QOF_{RMP}	ESS_{RMP}	VRM t_f (min^{-1})	QOF_{VRM}	ESS_{VRM}
880°C	HF Raw	0.01003	0.512	98.91	0.00082	0.01160	92.74	0.01225
	HF Residue	0.01250	3.650	99.40	0.00044	0.02122	92.50	0.04722
	WF Raw	0.00620	0.196	98.73	0.00143	0.06672	94.20	0.00915
	WF Residue	0.00950	0.712	98.34	0.00138	0.00994	95.02	0.00652
900°C	HF Raw	0.01330	0.844	98.68	0.00093	0.01603	94.92	0.01803
	HF Residue	0.15780	4.140	99.30	0.00740	0.02770	90.16	0.06324
	WF Raw	0.08940	0.237	98.09	0.00250	0.00820	95.06	0.01882
	WF Residue	0.01350	0.82	98.15	0.00211	0.14670	94.02	0.0823
920°C	HF Raw	0.01670	1.209	98.46	0.00095	0.20560	94.69	0.01379
	HF Residue	0.01850	4.920	98.73	0.00114	0.34160	87.18	0.07942
	WF Raw	0.01290	0.380	97.30	0.00352	0.01430	95.68	0.00882
	WF Residue	0.01900	1.152	97.72	0.00323	0.02130	93.42	0.01023
940°C	HF Raw	0.02260	1.420	98.50	0.00082	0.03058	92.61	0.03178
	HF Residue	0.02197	5.440	98.95	0.00011	0.04178	87.95	0.07804
	WF Raw	0.01842	0.510	97.30	0.00343	0.02118	95.49	0.01113
	WF Residue	0.02557	1.354	97.43	0.00422	0.03061	95.33	0.01441

RPM t_f = random pore model time factor, *RPM* ψ = random pore model structural parameters, QOF_{RMP} =random pore model quality of fit, ESS_{RMP} = random pore model error sum of square, VRM t_f = volumetric Reactive model time factor, QOF_{VRM} = volumetric Reactive model quality of fit, ESS_{VRM} = volumetric Reactive model error sum of square

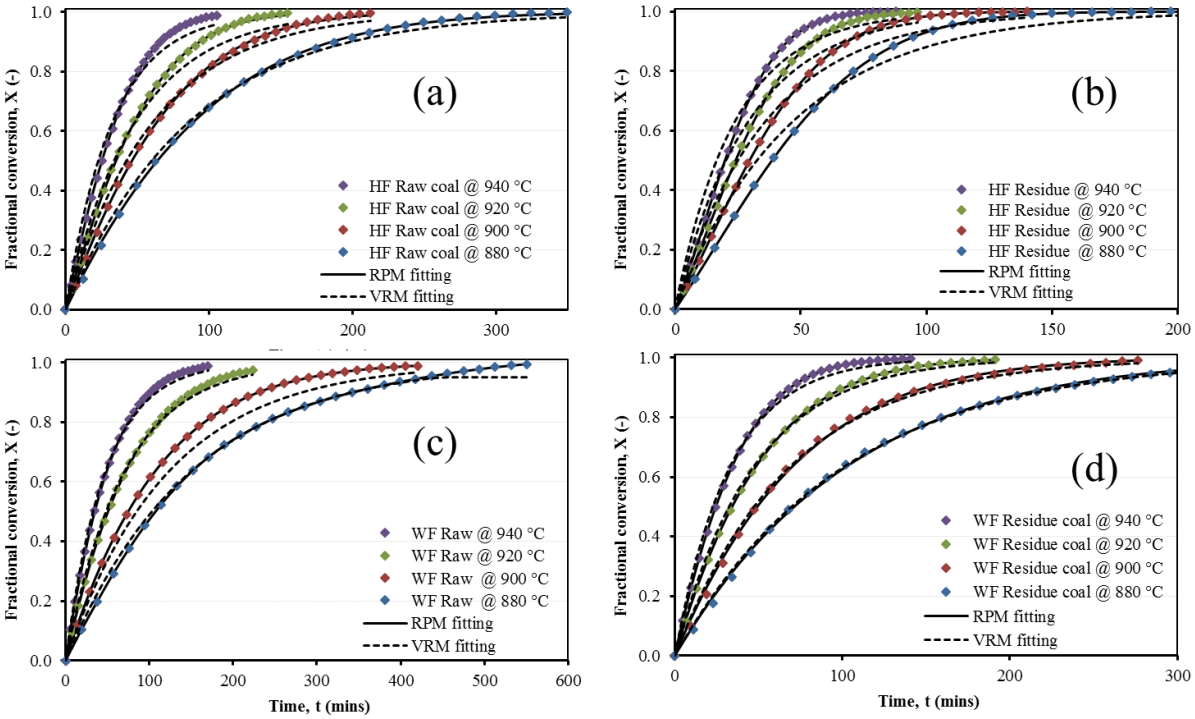

Figure 5-7: RPM and VRM fitting to experimental data of (a) Highveld <1.5 g/cm^3 density fraction, (b) Highveld <1.5 g/cm^3 density fraction residue, (c) Waterberg carbon-rich residue, (d) Waterberg carbon-rich residue sample

5.10 Determination of activation energy and pre-exponential factor

Using the $R_{t0.5}$, R_i, $R_{s,}$ RPM t_f, and the VRM t_f, Arrhenius plots were constructed to estimate the apparent activation energy and the lumped pre-exponential factor of the gasification reactivity of the different samples following Equation 5.11. The Table 5-6 present the parameters from the grapy that was used to obtain the activation energy and the pre-exponential factor values (linear equation used in obtaining the activation energy, R^2, slope and intercept) for the five reactivity model during CO_2 gasification of all the char samples.

Table 5-6 Activation energies (kJ/mol) and lumped pre-exponential factors (min^{-1}) for CO_2 gasification as determined from the various reaction reactivity models

Reactivity model	Equation	R^2	Slope	Intercept	Ea	k_{so}
HF Raw						
$R_{t0.5}$	y = -23136x + 15.232	0.999	-23136	15.232	196.0	4.12E+06
$t_{f(RPM)}$	y = -22459x + 14.821	0.997	-22459	14.821	192.0	2.73E+06
$t_{f(VRM)}$	y = -21922x + 14.55	0.995	-21922	14.55	182.3	2.08E+06
R_s	y = -21759x + 14.132	0.996	-21759	14.132	190.0	1.37E+06
R_i	y = -21770x + 14.142	0.996	-21770	14.142	190.5	1.39E+06
HF Residue						
$R_{t0.5}$	y = -17230x + 10.82	0.999	-17230	10.82	147.4	5.00E+04
$t_{f(RPM)}$	y = -16732x + 10.253	0.999	-16732	10.253	141.6	2.84E+04
$t_{f(VRM)}$	y = -16752x + 9.7715	0.998	-16752	9.7715	139.3	1.75E+04
R_s	y = -16983x + 10.511	0.999	-16983	10.511	145.3	3.67E+04
R_i	y = -16982x + 10.511	0.999	-16982	10.511	145.3	3.67E+04
WF Raw						
$R_{t0.5}$	y = -28911x + 19.505	1.000	-28911	19.505	234.4	2.96E+08
$t_{f(RPM)}$	y = -27885x + 18.841	1.000	-27885	18.841	235.0	1.52E+08
$t_{f(VRM)}$	y = -27953x + 19.157	0.999	-27953	19.157	232.4	2.09E+08
R_s	y = -28917x + 19.567	0.998	-28917	19.567	236.0	3.15E+08
R_i	y = -29122x + 19.738	0.997	-29122	19.738	236.7	3.73E+08
WF Residue						
$R_{t0.5}$	y = -24557x + 15.531	0.998	-24557	15.531	205.0	5.56E+06
$t_{f(RPM)}$	y = -24952x + 16.056	0.997	-24952	16.056	207.6	9.40E+06
$t_{f(VRM)}$	y = -23547x + 15.024	0.998	-23547	15.024	195.8	3.35E+06
R_s	y = -22340x + 14.722	0.997	-22340	14.722	196.6	2.48E+06
R_i	y = -22339x + 14.722	0.997	-22339	14.722	196.0	2.48E+06

Table 5-6 shows the activation energies of all the reactivity models used in this study. From Table 5-6 it was observed that the activation energies obtained for all the reactivity models showed the same trends, with the residue char showing lower activation energy values when compared to the higher activation energies for the float fraction samples. For instance, the estimated apparent activation energy of the gasification reaction evaluated when using R_i was 190.5 kJ/mol for the HF char; 145.3 kJ/mol for HF residue char; and 236.0 kJ/mol for the WF char and 196.6 kJ/mol for WF residue char. The reported activation energy values of the lighter density fractions are comparable to values obtained for CO_2 gasification of coal chars by other investigators.[23,24,33,36] The liquefaction residue chars had lower activation energy than that of the lighter density fraction chars. This follows the same trend and reasoning as that for the gasification reactivity as described earlier in the article.

The activation energy, which was calculated using the initial reactivity, R_i, and the initial specific reactivity, R_s, was similar for all the chars described in this investigation. The lumped

pre-exponential factors were lower for the residue chars than for the <1.5 g/cm^3 density fraction chars. However, the lumped pre-exponential factor for the <1.5 g/cm^3 density fraction char was comparable to those stated by other investigators.[23,24]

The experimental data and the predicted model data (from the RPM) were compared using a dimensionless plot of the carbon conversion, *X,* versus reduced time, $t/t_{0.9}$, for the lighter density fraction and residue chars (Figure 5-8). Reduced time values were calculated from the RPM equation. The results obtained from the comparative study showed that the estimated structural parameter values were suitable to describe the data obtained from the CO_2 gasification experiments of the lighter density fraction chars and their residue chars.

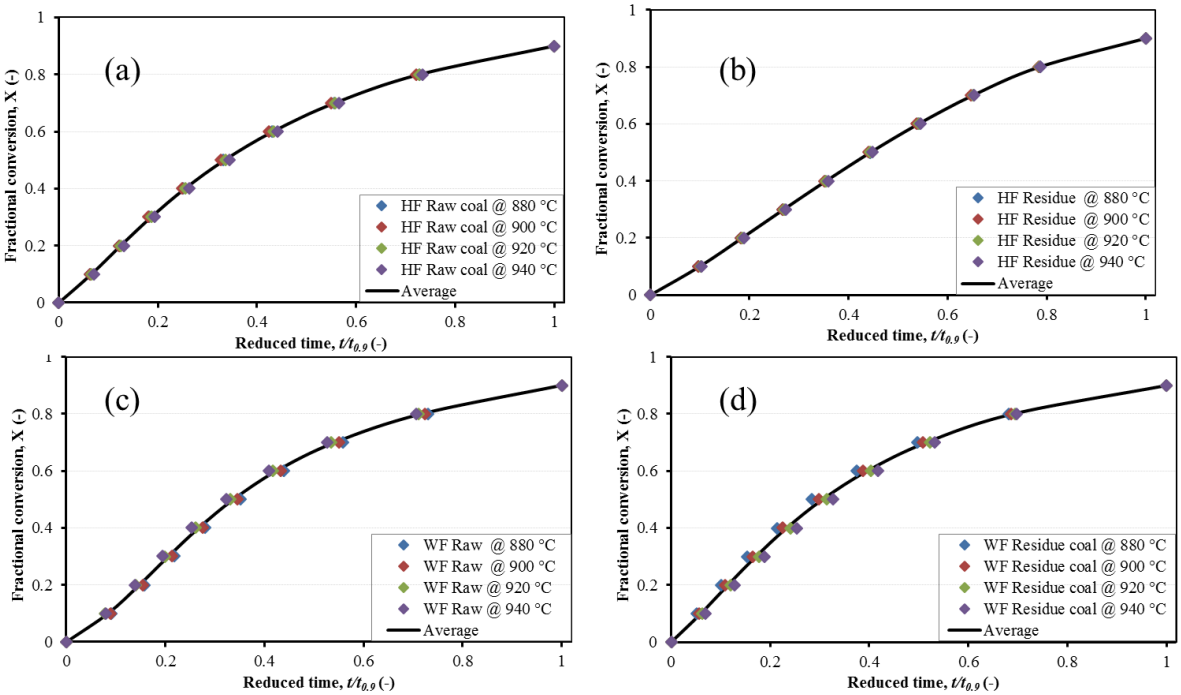

Figure 5-8: Carbon fractional conversions as a function of reduced time for chars from (a) Highveld <1.5 g/cm^3 density fraction, (b) Highveld residue, (c) Waterberg <1.5 g/cm^3 density fraction, (b) Waterberg residue

5.11 Conclusions

In this study, <1.5 g/cm^3 coal density fractions generated from the float-sink density separation method applied to South African discard coals and the liquefaction carbon-rich residue of the <1.5 g/cm^3 density fractions were subjected to CO_2 gasification at 880–940°C. Reactivity and kinetic analysis results showed that the liquefaction of the discard coal samples influenced the gasification results significantly. Based on the gasification results, the following conclusions were deduced:

- The liquefaction residue chars showed higher reactivity than those of the <1.5 g/cm^3 coal density fraction chars using all the reactivity parameters (R_i, R_s, R_{tf}, $R_{t/0.5}$).
- The apparent activation energy values for the gasification reactions of the liquefaction residue chars were lower than those of the <1.5 g/cm^3 density fraction chars. The activation energy of the <1.5 g/cm^3 density fraction chars were 190.5 kJ·mol^{-1} and 236.7 kJ·mol^{-1} for the Highveld and the Waterberg coals, respectively, while the activation energy for the liquefaction residue chars were 145.3 kJ·mol^{-1} for the Highveld coal and 196.0 kJ·mol^{-1} for the Waterberg coal.
- After demineralisation of the liquefaction residue chars, the demineralised chars showed lower reactivity values than those of liquefaction residue chars, indicating an influence caused by the inorganic compounds in the samples.
- The higher porosities of the liquefaction residue chars in comparison to the chars from the float fractions coal samples aided in increasing the reactivity values (for all the models used) of the residue chars.
- The experimental data for both the waste <1.5 g/cm^3 density fraction chars, and their corresponding liquefaction carbon-rich residue chars satisfactorily agreed with the RPM and VRM model predictions, with the RPM giving the best fit for all samples used in this investigation. This implies that the gasification reactions were under regime I (chemical control regime).
- The liquefaction residue chars exhibited a relatively higher RPM structural parameter than those of the <1.5 g/cm^3 density fraction chars.

The chars from liquefaction derived residues of the <1.5 g/cm^3 coal density fractions generated from South African discard coal fines may be utilised for CO_2 gasification. Utilising the liquefaction waste material may decrease the costs that are linked to the handling and disposal of coal waste material and improve the adverse health and environmental issues associated with the waste materials.

- **Acknowledgements**

The authors of this manuscript give thanks to the analysts, researchers and funders of the following laboratories and the Department of Science and Technology and National Research Foundation of South Africa: Mrs Belinda Venter of NWU geology laboratories, Bureau Veritas laboratories; SGS laboratories for their assistance in the analyses of the coal, char and residue; Dr Gregory Okolo for surface area analysis of the solid samples; and DST and NRF for the schemes offering financial assistance to the South African Research Chairs Initiative

of the (Coal Research Chair Grant No.: 86880 and incentive grant No. 115228). DST and NRF departments are not responsible for the manuscript contents.

5.12 Chapter 5 references

1. Khare, S.; Dell'Amico, M. An Overview of Conversion of Residues from Coal Liquefaction Processes. *Can J Chem Eng*. **2013**, *91*, 1660-1670.

2. Uwaoma, R.C.; Strydom, C.A.; Matjie, R.H.; Bunt, J.R. Influence of Density Separation of Selected South African Coal Fines on the Products Obtained During Liquefaction Using Tetralin as a Solvent. *Energy Fuels*. **2019**, *33*, 1837-1849.

3. Cui, H.; Yang. J.; Liu, Z.; Bi, J. Characteristics of Residues from Thermal and Catalytic Coal Hydroliquefaction. *Fuel* **2003,** *82*, 1549-1556.

4. Vasireddy, S.; Morreale, B.; Cugini, A.; Song, C.; Spivey, J.J. Clean Liquid Fuels from Direct Coal Liquefaction: Chemistry, Catalysis, Technological Status, and Challenges. *Eng. Environ Sci*. **2011**, *4*, 311-345.

5. Chu, X.J.; Li, W.; Li, B.Q.; Chen, H.K. Gasification Property of Direct Coal Liquefaction Residue with Steam. *Process Saf Environ*. **2006**, *84*, 440-445.

6. Yan, J.; Bai, Z.; Li, W.; Bai, J. Direct Liquefaction of a Chinese Brown Coal and CO_2 Gasification of the Residues. *Fuel* **2014**, *136*, 280-286.

7. Itoh, H.; Hiraide, M.; Kidoguchi, A.; Onozaki, M.; Ishibashi, H.; Namiki, Y.; Ikeda, K.; Inokuchi, K.; Morooka, S. Simulator for Coal Liquefaction Based on the NEDOL Process. *Ind. Eng. Chem. Res*. **2001**, *40*, 210-217.

8. Xu, L.; Tang, M.; Liu, B.; Ma, X.; Zhang, Y.; Argyle, M.D.; Fan, M. Pyrolysis Characteristics and Kinetics of Residue from China Shenhua Industrial Direct Coal Liquefaction Plant. *Thermochim. Acta*. **2014**, *589*, 1-10.

9. Chu, X.; Li, W.; Li, B.; Chen, H. Sulfur Transfers from Pyrolysis and Gasification of Direct Liquefaction Residue of Shenhua Coal. *Fuel* **2008**, *87*, 211-215.

10. Li, J.; Yang, J.L.; Zhou, S.F.; Li, Y.M. Pyrolysis Property of Solvent Extracts from a Direct Coal Liquefaction Residue. *J. Fuel Chem. Technol*. **2010,** *38*, 647-651.

11. Li X.H.; Xue, Y.L.; LI, W.Y. Properties of Semi-Coke from co-Pyrolysis of Lignite and Direct Liquefaction Residue of Shendong Coal. *J. Fuel Chem. Technol*. **2015**, *43*, 1281-1286.

12. Zhu, P.; Luo, A.; Zhang, F.; Lei, Z.; Zhang, J; and Zhang, J. Effects of Extractable Compounds on the Structure and Pyrolysis Behaviours of Two Xinjiang Coal. *J. Anal Appl Pyrolysis.* **2018**, *133*, 128-135.

13. Zou, L.; Jin, L.; Li, Y.; Zhu, S. and Hu, H. Effect of Tetrahydrofuran Extraction on Lignite Pyrolysis under Nitrogen. *J. Anal Appl Pyrolysis.* **2015**, *112*, 113-120.

14. Li, J.; Yang, J.; Liu, Z. Hydro-Treatment of a Direct Coal Liquefaction Residue and Its Components. *Catal. Today*. **2008**, *130*, 389-394.

15. Sugano, M.; Mashimo, K.; Wainai, T. Upgrading Reactions of Coal Liquefaction Residue with Basic Coal Liquid Related Model Compounds. *Fuel*. **1998**, *77*, 447-451.

16. Xiao, N.; Zhou, Y.; Qiu, J.; Wang, Z. Preparation of Carbon Nanofibers/Carbon Foam Monolithic Composite from Coal Liquefaction Residue. *Fuel*. **2010**, *89*, 1169-1171.

17. Xiao, N.; Zhou, Y.; Ling, Z.; Qiu, J. Synthesis of a Carbon Nanofiber/Carbon Foam Composite from Coal Liquefaction Residue for the Separation of Oil and Water. *Carbon*. **2013**, *59*, 530-536.

18. Ergun, S. Kinetics of the Reaction of Carbon Dioxide with Carbon. *J Phys Chem*. **1956**, *60*, 480-485.

19. Koening, P.; Squires, R.; Laurendeau, N. Char Gasification by Carbon Dioxide. *Fuel* **1986**, *65*, 412-416.

20. Radovic, L.; Jiang, H.; Lizzio, A. A Transient Kinetics Study. References of Char Gasification in Carbon Dioxide and Oxygen. *Energy Fuels*. **1991**, *5*, 68–74.

21. Chen, S.; Yang, R.; Kapteijn, F.; Moulijn, J. A New Surface Oxygen Complex on Carbon: Toward a Unified Mechanism for Carbon Gasification Reactions. *Ind Eng Chem*. **1993**, *32*, 2835-2840.

22. Everson, R.C.; Neomagus, H.W.; Kaitano, R.; Falcon, R.; Du Cann, V.M. Properties of High Ash Coal-Char Particles Derived From Inertinite-Rich Coal: II. Gasification Kinetics with Carbon Dioxide. *Fuel.* **2008**, *87*, 3403-3408.

23. Everson, R.C.; Okolo, G.N.; Neomagus, H.W.; Dos Santos, J.M. X-ray Diffraction Parameters and Reaction Rate Modelling for Gasification and Combustion of Chars Derived From Inertinite-Rich Coals. *Fuel*. **2013**, *109*, 148-156.

24. Uwaoma, R.C.; Strydom, C.A.; Matjie, R.H.; Bunt, J, Okolo, G.N.; Brand, D.J. Pyrolysis of Tetralin Liquefaction Derived Residues from Lighter Density Fractions of Waste Coals Taken from Waste Coal Disposal Sites in South Africa. *Energy Fuels*. **2019**, *33*, 9074-9086.

25. Roberts, M.J.; Everson, R.C.; Neomagus, H.W.; Van Niekerk, D.; Mathews, J.P.; Branken, D.J. Influence of Maceral Composition on the Structure, Properties and Behaviour of Chars Derived From South African Coals. *Fuel.* **2015**, *142*, 9-20.

26. Önal, Y.; Ceylan, K. Effects of Treatments on the Mineral Matter and Acidic Functional Group Contents of Turkish Lignites. *Fuel*. **1995**, *74*, 972-977.

27. Wijaya, N.; Zhang, L. A Critical Review of Coal Demineralization and Its Implication on Understanding the Speciation of Organically Bound Metals and Submicrometer Mineral Grains in Coal. *Energy Fuels*. **2011**, *25*, 1-6.

28. Okolo, G.N.; Everson, R.C.; Neomagus, H.W.; Roberts, M.J.; Sakurovs, R. Comparing the Porosity and Surface Areas of Coal as Measured by Gas Adsorption, Mercury Intrusion and SAXS Techniques. *Fuel*. **2015**, *141*, 293-304.

29. Molina, A & Mondragón, F. Reactivity of Coal Gasification with Steam and CO_2. *Fuel*. **1998**, *77*, 1831-1839.

30. Liu, G.; Benyon, P.; Benfell, K.E.; Bryant, G.W.; Tate, A.G.; Boyd, R.K.; Harris, D.J.; Wall, T.F. The Porous Structure of Bituminous Coal Chars and Its Influence on Combustion and Gasification under Chemically Controlled Conditions. *Fuel*. **2000**, *79*, 617-626.

31. Meng, L.; Wang, M.; Yang, H.; Ying, H.; Chang, L. Catalytic Effect of Alkali Carbonates on CO_2 Gasification of Pingshuo Coal. *Int. J. Min. Sci. Technol*. **2011**, *21*, 587-590.

32. Cetin, E.; Moghtaderi, B.; Gupta, R.; Wall, T.F. Biomass Gasification Kinetics: Influences of Pressure and Char Structure. *Combust. Sci. Technol*. **2005,** *177*, 765-791.

33. Roberts, D.G & Harris DJ. Char Gasification with O_2, CO_2, and H_2O: Effects of Pressure on Intrinsic Reaction Kinetics. *Energy Fuels.* **2000**,*14*, 483-489.

34. Levenspiel, O. *Chemical Reaction Engineering*., 2nd ed, Wiley Eastern Ltd: New Delhi, India, 1972; pp 357-408.

35. Wen CY. Noncatalytic Heterogeneous Solid-Fluid Reaction Models. *Ind. Eng. Chem. Res*. **1968**, *60*, 34-54.

36. Bhatia, S.K.; Perlmutter, D.D. A Random Pore Model for Fluid-Solid Reactions: I. Isothermal, Kinetic Control. *AIChE J.* **1980**, *26*, 379-386.

37. Matjie, R.H.; French, D.; Ward, C.R.; Pistorius, P.C.; Li, Z. Behaviour of Coal Mineral Matter in Sintering and Slagging of Ash during the Gasification Process. *Fuel Process. Technol*. **2011,** *92*, 1426-1433.

38. Spears, D.A.; Duff, P.D.; Caine, P.M. The West Waterberg Tonstein, South Africa. *Int. J. Coal Geo*. **1988**, *9*, 221-233.
39. Tsemane, M.M, Matjie, R.H.; Bunt, J.R.; Neomagus, H.W.; Strydom, C.A.; Waanders, F.B.; Van Alphen, C.; Uwaoma R. Mineralogy and Petrology of Chars Produced by South African Caking Coals and Density Separated Fractions during Pyrolysis and Their Effects on Caking Propensity. *Energy Fuels*. **2019**, *33*, 7645-7658.
40. Rautenbach, R.; Strydom, C.A.; Bunt J.R.; Matjie, R.H.; Campbell, Q.P.; Van Alphen, C. Mineralogical, Chemical, and Petrographic Properties of Selected South African Power Stations' Feed Coals and Their Corresponding Density Separated Fractions Using Float-Sink and Reflux Classification Methods. *Int J Coal Prep Util*. **2019**, *39*, 421-446.
41. Heller-Kallai L. Reactions of Salts with Kaolinite at Elevated Temperatures. *I. Clay Minerals*. **1978**, *2*, 221-235.
42. Zogała, A.; Janoszek, T. CFD Simulations of Influence of Steam in Gasification Agent on Parameters of UCG Process. *J. Sustain. Min*. **2015**, *14*, 2–11.
43. Uwaoma, R.C.; Strydom, C.A.; Bunt, J.R.; Okolo, G.N.; Matjie, R.H. The catalytic Effect of Benfield Waste Salt on CO_2 Gasification of a Typical South African Highveld Coal. *J. Therm. Anal. Calorim*. **2019,** *135*, 2723-2732.
44. Mangena, S.J. Fuel Evaluation and Coal Properties Transformation in a Sasol-Lurgi Fixed Bed Dry Bottom Gasifier Operating on North Dakota Lignite. Ph.D. Thesis, North-West University: Potchefstroom, 2008.

CHAPTER 6 CONCLUSIONS AND RECOMMENDATIONS

This chapter contains a summary of significant findings and conclusions of the experimental results obtained from this investigation, as well as some recommendations for future studies based on the thermochemical utilisation of South African coal fines and its density separated fractions.

6.1 Introduction

The efficiency of beneficiating South African coal discards and utilisation of the float fractions generated from density separation during a thermochemical process (liquefaction, pyrolysis and gasification) were investigated in this study. The main aims and objectives of this investigation were outlined in Chapter 1 and are compared to the outcomes of the investigation in this chapter.

6.2 Conclusions regarding the objectives of the study

The objectives of this study, as outlined in Chapter 1, are given below with the conclusions made regarding the objectives.

- Determine the physical, chemical and structural properties of the coal and its density-separated fractions, and subsequently evaluate the suitability of this feedstock for a coal liquefaction process.

Two samples of coal fine discards from the Highveld and Waterberg coalfields were beneficiated using a density separation technique. Three fractions were obtained: float (<1.5 g/cm^3), middlings (1.5 > x < 1.9 g/cm^3) and sink (>1.9 g/cm^3). The analysis of the different density fractions and the feed material showed that the float fraction had more fixed carbon and volatile matter, higher calorific value, porosity, and surface area than the other fractions. The float fractions also exhibited lower ash yields compared with the middlings and the sink fractions. Petrographic results of the samples revealed that the float fractions were richer in vitrinite and total reactive macerals when compared with the raw coal fines. These results for the float fraction rendered it more reactive and suitable for further utilisation than the original coal fines samples.

- Estimate the influence of the liquefaction operating temperature on the production efficiency during liquefaction using tetralin.

Liquefaction tests were conducted with fine coal discards, and their float fractions at 380–420°C in an autoclave. The starting materials (float fractions and coal fines) were compared to investigate the influence of their physical and chemical properties on the liquefaction products at various temperatures. Results from the liquefaction tests showed that as the temperature of liquefaction increased, carbon conversions and oil yields increased, with a subsequent reduction of the liquefaction residues. The float fractions showed higher oil yields and conversion at elevated liquefaction temperature when compared to the coal fine discards at the same temperatures. This was attributed to the relatively higher vitrinite and reactive macerals in the float fractions compared with those found in the coal fines.

- Determine and compare the chemical composition of the liquid products from tetralin coal liquefaction of the float fractions and the coal fines using different advanced and traditional analytical methods.

Liquid-state NMR results of the oils obtained from the liquefaction study revealed that the float fraction samples contained a relatively higher amount of hydrogen-bonded to the aromatic rings and a higher proportion of naphthalene when compared with the coal fines.

- Determine the composition of the tetralin liquefaction residues produced from the coal fines and the float fractions.

The solid-state ^{13}C NMR analysis results of the liquefaction residues from the coal fine discards and the float fractions indicated that the float fraction residues contained 78% aromatic carbon and 22% aliphatic carbon. In contrast, a slight increase in the aromatic carbon was observed for the coal fines. The composition of the residues was established and described in detail using techniques such as CO_2 low-pressure adsorption NMR, proximate and ultimate analyses.

- Compare the liquefaction products of the coal fine discards, and its low density separated samples.

The liquefaction product yields obtained from the coal fines and the float fractions were compared, and the residues from the float fractions showed higher carbon conversion and oil yields compared with the coal fines. While the oil yields of the float fraction ranged from 24.4–37.2%wt. (daf), 19.1–29.3%wt. (daf) were obtained from the coal fine discards. Carbon conversion of 50.7–52.7%wt. (daf) was achieved for the float fraction in comparison with < 42%wt. (daf) for the coal fines. The coal float fractions achieved higher carbon conversion and oil yields due to the higher percentage of vitrinite and reactive macerals in these samples, and lower ash yields.

- Investigate and compare the different product yields from the float fraction samples, and their liquefaction derived residues.

Proximate and ultimate analyses of the liquefaction product generated after the heat treatment revealed that the oil and the pre-asphaltene products had higher fixed carbon contents, higher calorific values and significantly lower ash yields in comparison with the liquefaction residues that

contained less fixed carbon, and had higher ash yields in comparison to the liquid products. Comparing the fixed carbon contents and ash yields of the liquefaction residues derived from the float fractions and the coal fines samples, it was observed that the float fractions contained more fixed carbon (HF-R- 47.1%wt. (daf) and WF-R- 45.4%wt. (daf)) and had lower ash yields (HF-R- 25.7%wt. (daf) and WF-R- 26.9%wt. (daf)). The coal fines residues contained less fixed carbon (HF-R- 33.2%wt. (daf) and WF-R- 39.5%wt. (daf)), and more ash (HF-R- 25.7%wt. (daf) and WF-R- 26.9%wt. (daf)) when compared with the residues from the float fractions. In general, the chemical properties of the liquefaction residues obtained from the float fraction were found to be close to those of the fines coal samples. The float fraction residues thus may be suitable as a starting material for pyrolysis and gasification processes.

- Measure and compare the chemical, physical and structural changes of the subsequent chars after pyrolysis.

The pyrolysis product distribution of the float fraction and liquefaction residues as determined from the Fisher–assay analyses showed that the char yields of the liquefaction residues ranged from 74.0–76.0% and that of the coal float fractions were between 67.0% and 71.5% at 750 °C. Gas pyrolysis yields ranged from 16.0–20.0% for the residues and 14.5–18.4% for the coal float fractions. Higher char and gas yields obtained from the liquefaction residues in comparison to the float fraction samples were attributed to the changes in the pore structures and decreased in ash and volatile matter contents of the liquefaction residues. The pyrolytic water and the tar yields of the coal float fractions were slightly higher compared with those of the liquefaction residues.

Proton (^{1}H) NMR analyses of the tar produced at a pyrolysis temperature of 750°C, showed a higher amount of aromatic protons, ranging from 60.5–62.0 ppm for the liquefaction residues in comparison with < 56.0 ppm for the coal float fractions. The amounts of aliphatic protons of the tars generated from the coal float fractions were higher when compared to those of the liquefaction residues. It was also observed from the GC-MS analysis data that the residues contained more phenolics and monoaromatics when compared to the tars from the coal float fractions. This was attributed to the liquefaction process aiding in ring-opening, which assisted in exposing oxygen that facilitated the reaction between ether and –O–, making it possible to be converted to OH during pyrolysis.

The chars produced after pyrolysis of the liquefaction residues showed higher porosities when compared with those from pyrolysis of the coal float fractions. The porosities of the chars produced from the liquefaction residues ranged from 15.5–16.3%, in comparison with <14% after

pyrolysis of the coal float fractions. CO_2 low-pressure adsorption methods showed that the liquefaction process changed the pore structure of the material and opened up pores within the coal structure, which may have favoured the diffusion of free radicals and assisted in the reactivity of the liquefaction residues.

- Conduct CO_2 gasification reactivity experiments with the produced char samples on a laboratory scale at temperatures similar to those prevailing in fluidised-bed gasification and investigate the influence of the chemical, physical and structural changes of the chars on the observed char–CO_2 gasification reactivity of the density separated float fractions and the coal fines liquefaction residue char samples.

Results from the char–CO_2 gasification experiments showed that the liquefaction residues had higher reactivities for all the reactivity models (R_i, R_s, R_{tf} and $R_{t/0.5}$) used in this study when compared with the float fraction chars. The reactivities of all the samples were observed to increase as gasification temperatures increased, as expected.

The estimated activation energies of the liquefaction residue chars were observed to be lower than those of the float fraction chars. The activation energy of the liquefaction residue chars were found to be between 145.3 kJ·mol^{-1} and 196.0 kJ·mol^{-1}; whereas the float fraction chars' activation energy values were between 190.5 kJ·mol^{-1} and 236.7 kJ·mol^{-1}. The lower activation energy values of the residue chars were attributed to slightly higher inherent mineral matter contents and also to liquefaction opening up pores, which increased the reactivity of the liquefaction residues during gasification.

- Apply the resulting gasification experimental data to already existing gasification kinetic models.

The experimental data were compared to those obtained from the random pore model (RPM) and volumetric reaction model (VRM), and both models gave satisfactory agreements, with the RPM being better. The results obtained from the model fitting of the liquefaction residues' chars and the float fractions' chars indicated that the gasification reactions were under a chemically controlled regime (Regime I).

6.3 Conclusions regarding the hypotheses of the study

Some hypotheses were formulated for the study in Chapter 1 and are now evaluated as follows:

- Density separation of the coal fines will assist in beneficiation of the coal fines, and the float fraction will be enriched with more reactive macerals and lower ash yields.

  This hypothesis was proven. The coal fines were density separated, and the float (<1.5 g/cm^3) fractions showed higher fixed carbon and vitrinite macerals contents and lower ash yields than for the coal fines samples.

- During liquefaction of coal fines and their density separated fractions (float fractions), organic species may dissolve in the selected solvent at different temperatures.

  This hypothesis was proven. The solvent, tetralin, a suitable hydrogen-rich solvent, dissolved some of the coal molecular structure and facilitated good extraction yield efficiencies at the temperatures used during the liquefaction experiments.

- Higher extraction efficiencies may be achieved from the float fraction after density separation in comparison to the coal fines samples that were not density separated.

  This hypothesis was proven. Higher carbon conversion and oil yields were achieved from the float fractions (<1.5 g/cm^3) at tetralin liquefaction temperatures between 380–420°C.

- The oil yields produced during liquefaction can be improved by using density-separation methods to increase the percentage of reactive macerals in the starting material.

  The float fractions (<1.5 g/cm^3) contained higher contents of vitrinite and total reactive macerals and lower amounts of inertinites. These resulted in higher carbon conversion and oil yields during tetralin liquefaction when compared with the coal fines.

- During liquefaction, the coal matrix undergoes dredging, which could lead to an increase in porosity. The larger porosity of the residues will influence the gasification reactions.

  This hypothesis was proven. The liquefaction process opened closed pores and may have created new pores, as the porosities of the liquefaction residue samples were increased in comparison to the coal fines samples. The increase in the porosity as a result of liquefaction process enhanced the gasification reactivity of the residue chars.

- Coal liquefaction residues that contain more fixed carbon and hydrogen and have higher calorific values may be used for coal gasification processes.

  The residues contained a reasonably high percentage of fixed carbon and had relatively high calorific values. Literature indicated that the proximate analysis results and the calorific values

of the liquefaction residues were comparable to those of coal used for thermochemical processes (gasification and pyrolysis).

- The liquefaction process of the coal may improve the reactivity of the coal residues and may have an impact on the activation energy of the gasification reactions.

  This hypothesis was proven. The liquefaction residue chars had higher gasification reactivities and lower activation energies when compared to the coal fines float fraction (< 1.5 g/cm^3) chars.

6.4 General contributions of the study

- This investigation provides useful information for the separation of South African coal fine discards using float-sink density separation techniques. It also provides a comparison of the chemical, mineralogical, structural and physical analyses of the coal fine discards, and their density separated fractions.

- This study contributes to research and development of the effective utilisation of coal fine discards, and their density separated float fraction (<1.5 g/cm^3) during coal liquefaction to produce liquid fuel and other value-added chemicals.

- The study provides valuable insight into the influence of different parameters, such as temperature and petrographic structure, during liquefaction of the coal fine discards, and their density separated float (<1.5 g/cm^3) fractions.

- The study provides an understanding of the use of different analytical techniques such as CPMAS ^{13}C NMR, proximate, ultimate and low-pressure gas adsorption analytical methods to track the effect of liquefaction on the generated residues.

- The study shows that the residues (waste) generated after liquefaction can be used further to generate pyrolytic products. Waste utilisation is essential to decrease the impact on the environment.

- This research helps in providing a comparison of the chemical and physical analysis of the tars produced during pyrolysis of the float fractions and their liquefaction residues using ^{1}H and ^{13}C liquid and solid-state NMR, GC-MS and FTIR analytical techniques.

- A comparison of the gasification reactivity of the float fraction chars and their liquefaction residues chars was described in this study.

- A correlation of different parameters such as surface area and porosity on the gasification reactivity of the float fraction chars and their residue chars was accomplished in this investigation.

- This investigation provides useful insight into the use of the random pore model and the volumetric reaction model into simulation of the CO_2 gasification process of liquefaction residues.

- The investigation contributes to the effective utilisation of carbon-rich residues generated from the liquefaction of density separated coal fine discards as a suitable feedstock for coal utilisation processes (pyrolysis and gasification). Beneficiating and using the coal float fractions for liquefaction and subsequently using the residues from the liquefaction for pyrolysis and gasification purposes will help in closing the liquefaction process gap and improve the economy of the liquefaction process and value chain.

- The utilisation of coal fine discards will assist in reducing the volume of coal fines and the high cost associated with handling and disposal of these fines. The utilisation of coal fines will assist in minimising environmental problems, such as dust, spontaneous combustion and acid mine drainage, caused by discarded coal fines.

6.5 Recommendations for future research

The results obtained in this investigation lead to the following recommendations for future investigations:

- The middlings and sink fractions produced after density separation of the coal fine discards could be further demineralised and investigated for suitability for further thermochemical processes. Should this be possible, all waste from coal fines will be utilised. Valuable minerals may also be extracted from these fractions. These materials could also be evaluated for the production of aluminium sulphate using the sulphuric acid leaching technology.

- The liquefaction product yields obtained from the float fractions may be improved through the use of liquefaction catalysts and other hydrogen-rich solvents or a blend of hydrogen-rich solvents.

- Economical and feasibility studies on the liquefaction of density separated float fractions may be investigated.

- The influence (possible catalytic activity) of inherent mineral matter and extraneous minerals on the liquefaction and pyrolysis processes of the float fraction and the liquefaction residues

needs to be investigated. This will give an insight into the specific mineral matter in the coal matrix that may enhance the product distribution yields during liquefaction, pyrolysis and gasification.

- Investigation of the gasification of the residues using a combination of gases such as H_2O, O_2, H_2, CO_2, and air may benefit the industry. This may clarify the effect of the gasifying agent either as an inhibitor or a promoter during the gasification of residues produced after liquefaction of the float fractions generated from density separation of South Africa coal fines.

- Economic and feasibility studies on the utilisation of liquefaction residues for combustion and gasification processes may be undertaken. This will aid in the understanding of the industrial applicability of the processes to utilise the liquefaction residues.

- Co-pyrolysis and co-gasification studies of the carbon-rich residues and coal fines may be investigated. This will assist in understanding if the residues have synergistic effects on coal utilisation processes.

- The economic feasibility of density separation and the subsequent use of the liquefaction residues for pyrolysis and gasification need to be investigated. This will aid in understanding the financial aspects and potential economic advantages and disadvantages of the proposed processes.